

Laser Induced Linear and Nonlinear Optical Studies on Certain Metal Halides and Tartrate Crystals for Photonic Applications

Ph. D. Thesis submitted to

Cochin University of Science and Technology

In partial fulfillment of the requirements for the award of the Degree of

Doctor of Philosophy

by

Rejeena.I

Reg. No: 3704

**International School of Photonics
Cochin University of Science and Technology
Cochin -682022, Kerala, India**

April 2015

Laser Induced Linear and Nonlinear Optical Studies on Certain Metal Halides and Tartrate Crystals for Photonic Applications

Ph D thesis in the field of Photonics

Author:

Rejeena.I

Research Fellow

International School of Photonics

Cochin University of Science & Technology

Cochin -682022, Kerala, India

rejeenanaufal@gmail.com

Research Advisor:

Dr. P. Radhakrishnan

Professor

International School of Photonics

Cochin University of Science & Technology

Cochin -682022, Kerala, India

radhak@cusat.ac.in, padmanabhan.radhak@gmail.com

International School of Photonics

Cochin University of Science & Technology

Cochin -682022, Kerala, India

www.photonics.cusat.edu

April 2015

Cover image: *Fluorescence emission of magnetic field applied Cadmium Tartrate and Z-scan trace of Lead Chloride.*

***Dedicated to my loving husband and children,
My mothers and teachers.....***

INTERNATIONAL SCHOOL OF PHOTONICS
COCHIN UNIVERSITY OF SCIENCE AND TECHNOLOGY
COCHIN -682022, KERALA, INDIA

Dr. P. Radhakrishnan
Professor

 **Certificate**

This is to certify that the thesis entitled “**Laser Induced Linear and Nonlinear Optical Studies on Certain Metal Halides and Tartrate Crystals for Photonic Applications**” submitted by **Mrs. Rejeena. I.**, is an authentic record of research work carried out by her under my guidance and supervision in partial fulfillment of the requirement of the degree of Doctor of Philosophy of Cochin University of Science and Technology, under the Faculty of Technology and has not been included in any other thesis submitted previously for the award of any degree.

Kochi-682022
23 - 04- 2015

Dr. P. Radhakrishnan
(Supervising guide)

Phone: +91 484 2575848 Fax: 0091-484-2576714.
Email: radhak@cusat.ac.in, padmanabhan.radhak@gmail.com

**INTERNATIONAL SCHOOL OF PHOTONICS
COCHIN UNIVERSITY OF SCIENCE AND TECHNOLOGY
COCHIN -682022, KERALA, INDIA**

Dr. P. Radhakrishnan
Professor

Certificate

This is to certify that the thesis entitled “**Laser Induced Linear and Nonlinear Optical Studies on Certain Metal Halides and Tartrate Crystals for Photonic Applications**” submitted by **Mrs. Rejeena. I.**, has incorporated all the relevant corrections and modifications suggested by the audience during the pre-synopsis seminar and recommended by the Doctoral Committee.

*Kochi-682022
23- 04- 2015*

Dr. P. Radhakrishnan
(Supervising guide)

Declaration

I, Rejeena.I., do hereby declare that the thesis entitled “**Laser Induced Linear and Nonlinear Optical Studies on Certain Metal Halides and Tartrate Crystals for Photonic Applications**” is a genuine record of research work done by me under the supervision of Dr. P. Radhakrishnan, Professor, International School of Photonics, Cochin University of Science and Technology, Kochi–22, India and it has not been included in any other thesis submitted previously for the award of any degree.

Kochi- 682022
23- 04- 2015

Rejeena.I

Acknowledgements

Thanks God, the creator, for the blessings through out my life...

I am thankful to many individuals who have supported me during the period of this research.

Foremost, I would like to express my sincere gratitude to my supervisor Dr. P. Radhakrishnan, Professor, International School of Photonics (ISP), to select me as a student to work under his guidance. The sincere support and valuable suggestions from him have gone a long way in the completion of my work. His patience and constant support are ever remarkable .

I would like to thank very much to Prof. V. P. N. Nampoori, Professor Emeritus, International School of Photonics, for his sincere suggestions throughout my research work. His inspiration and encouragement are always valuable.

My sincere thanks goes to Dr. M. Kailasnath, Director, ISP and Dr. Sheenu Thomas, Assistant Professor, ISP for their wholehearted support and advice during my doctoral work,

I sincerely acknowledge Dr. Lillibai , my research collaborator during the early stage of my research work. I thank her for gave me some samples.

I am so much indebted to Dr. Vinoy Thomas, Asst.Prof. at Christian College, Chengannur for his close companion and suggestions to make this thesis a fruitful one.

*I owe so much to Prof. Sheik Ahammed, the Principal, M.S.M.College, Kayamkulam for his constant support and inspiration. His kind consideration is always memorable especially in the period of writing the thesis. **I always thankfully remember Prof. Cherian Mathew, the man behind my success, unfortunately he is not with us.***

I am thankful to Prof.C.Mathew, Prof. Sherlykutty, Dr.M.H.Rahimkutty, Dr.S.Jayakumar(HOD of Physics Dept, M.S.M.College), Dr.S.Bhadrakumari, Dr.D.Suhama, Mr.Anilkumar, Jyothi, Anjana, Sefeena, Ajeena, Smitha,

Saranya, Deepthi, Jaleel Ikka, Sivadasan chettan and Ravi chettan of Physics Dept, M.S.M.College for their support.

I am always thankful to Dr.Reena of chemistry Dept. for her inspiring words and a good companion.

Sincere thanks go to my colleagues of M.S.M.College, Kayamkulam.

I would like to acknowledge Dr.Nithyaja, the person who helped me a lot at the initial stage of my research. I thank Libeesh Sir, Dr.Geetha, Dr.Santhi, Dr.Rajesh, Dr.Roseleena, Misha, Sreeja.S, Dr.Tintu, Linesh, Indu, Divya, Musfir, Manju, Suneetha, Sreelekha, Sabitha, Susmitha, Ajna, Nitheep, Bobby Sir, Bejoy, Dr. Sony T George, Linslab, Ratheesh, Jaison, Aldrin, Aparna and Sr.Anju for all their support and for creating a very vibrant environment.

I am always indebted to Mathew and Pradeep for their constant support during Sundays and holidays. The time with Mathew is memorable for me because of his sincerity that showed towards me during the experimentation in laser lab.

I would like to thank Lab, library and administrative staff of the ISP for the assistance extended during the tenure. I acknowledge KSCSTE and UGC for the financial support.

I gratefully acknowledge Samad Ikka, Jasmin Itha, Hiba and Diya for their kind hospitality during the writing time of the thesis. No words are enough to thank them.

I am also grateful to my parents, brothers, sister and in-laws for their prayers and inspiration throughout my research work. Special thanks goes to my mothers Aisha and Arifa for their help and adjustments with my kids.

Finally, I would like to express my indebtedness to my ever-loving and always supporting husband Mr. Naufal and my kids Ishan and Rihan for their company and love that makes the thesis fruitful.

Rejeena.I

“Curiosity has its own reason for existing. One cannot help but be in awe when he contemplates the mysteries of eternity, of life, of the marvelous structure of reality”.

Albert Einstein

Preface

Nonlinear optics is a broad field of research and technology that encompasses subject matter in the field of Physics, Chemistry, and Engineering. It is the branch of Optics that describes the behavior of light in nonlinear media, that is, media in which the dielectric polarization P responds nonlinearly to the electric field E of the light. This nonlinearity is typically only observed at very high light intensities. This area has applications in all optical and electro optical devices used for communication, optical storage and optical computing. Many nonlinear optical effects have proved to be versatile probes for understanding basic and applied problems. Nonlinear optical devices use nonlinear dependence of refractive index or absorption coefficient on the applied field. These nonlinear optical devices are passive devices and are referred to as intelligent or smart materials owing to the fact that the sensing, processing and activating functions required for optical processes are inherent to them which are otherwise separate in dynamic devices.

The large interest in nonlinear optical crystalline materials has been motivated by their potential use in the fabrication of all-optical photonic devices. Transparent crystalline materials can exhibit different kinds of optical nonlinearities which are associated with a nonlinear polarization. The choice of the most suitable crystal material for a given application is often far from trivial; it should involve the consideration of many aspects. A high nonlinearity for frequency conversion of ultra-short pulses does not help if the interaction length is strongly limited by a large group velocity mismatch and the low damage threshold limits the applicable optical intensities. Also, it can be highly desirable to use a crystal material which can be critically phase-matched at room temperature.

Among the different types of nonlinear crystals, metal halides and tartrates have attracted due to their importance in photonics. Metal halides like lead halides have drawn attention because they exhibit interesting features from the stand point of the electron-lattice interaction .These materials are important for their luminescent properties. Tartrate single crystals show many interesting physical properties such as ferroelectric, piezoelectric, dielectric and optical characteristics. They are used for nonlinear optical devices based on their optical transmission characteristics. Among the several tartrate compounds, Strontium tartrate, Calcium tartrate and Cadmium tartrate have received greater attention on account of their ferroelectric, nonlinear optical and spectral characteristics. The present thesis reports the linear and nonlinear aspects of these crystals and their potential applications in the field of photonics.

Chapter 1 will mainly focus on the optical nonlinear crystals and the various optical nonlinear processes .Different types of nonlinear optical processes like Second Harmonic Generation, Optical Kerr effect, Self-phase modulation, Two photon absorption etc. are explained in this chapter .The experimental techniques used to identify these nonlinearities are discussed in detail. The theory of open aperture Z-scan technique is described. Relevant aspects of the choice of a nonlinear crystal and their various applications are mentioned. The peculiarities of the lead halides and metal tartrates crystals used in the present studies are also explained. The advantage of gel method for the preparation of these crystalline materials and the role of X-ray diffraction in the characterization of the samples are also discussed in this chapter. The theory and experimental methods of Thermal lensing for the non radiative decay studies are also explained in detail .

Chapter 2 discusses the synthesis of Lead Bromide (PbBr_2) crystals by solution-gel technique. Gels are formed from the suspension of the solution by the establishment of a three-dimensional system of cross linkages between the molecules of one component. The structural characterization of PbBr_2 by X-ray diffraction studies is also mentioned in this chapter. Optical absorption studies are carried out using linear absorption measurements on these crystalline material. The details of determination of the optical band gap is also discussed. Photoluminescence studies on these PbBr_2 samples show the emission characteristics at different excitations. Non radiative emissions are also possible from these crystal samples which are identified using thermal lens experiment. Nonlinearity of the material is studied using the highly sensitive Z-scan experimental technique. The absorptive nonlinear measurements are used for optical limiting studies on PbBr_2 is also described in this section.

In **Chapter 3**, the spectral and optical nonlinear studies carried out on Lead Chloride (PbCl_2) crystals are discussed. PbCl_2 is the model material from heavy element halogenide group since it satisfies high birefringence, low attenuation coefficient and wide transparency range. Silica hydrogel is used to grow good quality single crystals of PbCl_2 because of its better suitability compared to other organic gels. Five different types of PbCl_2 sample crystals are prepared employing ultraviolet, infrared radiations, electric and magnetic fields. Optical characteristics including absorption and fluorescence emissions on these materials are also studied. Open aperture Z-scan measurements of transmittance reveal the reverse saturable absorption behaviour of the five PbCl_2 samples in solution phase. Thermal diffusivity studies are also carried out and the results are discussed in detail.

The main focus of **chapter 4** is on the studies of Lead Fluoride (PbF_2) crystals. It discusses the synthesis, linear and nonlinear measurements on three types of PbF_2 crystal samples. The samples PbF_2 -UV and PbF_2 -IR are synthesized by irradiating with UV and IR radiations. The structural studies confirm the

crystallinity and the spectral characteristics are also investigated. Fluorescence spectroscopy reveals the luminescence aspects of the sample crystals. Bahae's method illustrates the optical nonlinearity in the respective samples which is also described in this section. The lens like characteristics of the samples are exploited using mode matched thermal lensing technique.

Chapter 5 describes the synthesis and characterizations of gel derived Calcium Tartrate crystals. Calcium Tartrate (CaTT) crystals belonging to the orthorhombic system exhibit different kinds of optical nonlinearities which are associated with a nonlinear polarization. The CaTT crystals are synthesized using electric and magnetic fields and their structural characteristics are given in this chapter along with that of the pure sample. Band gap plots of these crystals are explained in detail and the direct gap values are tabulated. Heat transfer mechanism on the electric and magnetic field applied samples are described in this section. The positive and negative values of nonlinear absorption coefficients are measured and discussed. The peak response of transmittance curve for these CaTT crystals show saturable absorption behaviour.

Chapter 6 explains the synthesis, optical, non-radiative decay and nonlinear studies of Strontium Tartrate (SrTT) crystals. The emission studies against different excitations are carried out by taking the room temperature fluorescence spectra of these SrTT samples using a Cary Eclipse fluorescence spectrophotometer. Two photon absorption mechanism of these crystalline materials are studied using a Q-switched laser of 532 nm through a method based on the principle of spatial beam distortion. The SrTT samples have smaller thickness compared to the diffraction length of the focused beam. Nonlinearity of these crystals are measured at different laser powers and the values of nonlinear absorption coefficients are calculated. The switching and limiting responses are also described here.

Chapter 7 presents the linear and nonlinear studies on Cadmium Tartrate (CdTT) crystals prepared by solution–gel method. It also gives the details of temperature rise produced in the sample as a result of non radiative relaxation of the energy absorbed from a laser .This is studied using the dual beam mode matched thermal lens technique. This section presents the small-volume sample capability and dependency on thermo-optic properties of solvents. Thermal diffusivity of CdTT crystals are determined employing a TEM₀₀ Gaussian laser beam as the excitation source. The Z-scan experimental traces without an aperture on these samples exhibit the response of transmittance and hence the limiting thresholds are evaluated.

The general conclusions of the present work and future prospects are discussed in **chapter 8**.

List of Publications

International Journals

1. **I.Rejeena**, B.Lillibai, B.Nithyaja, V.P.N.Nampoori, and P.Radhakrishnan “Optical Studies on Sol-Gel derived Lead Chloride crystals “*Journal of Engineering, Computers & Applied Sciences (JEC & AS)* 4(2013) 5-9.
2. **I.Rejeena**, B.Lillibai, Roseleena Toms, B.Nithyaja, V.P.N.Nampoori, and P.Radhakrishnan “Optical Non-linear Studies on Sol-gel Derived Lead Chloride Crystals Using Z-scan Technique” *Journal of Engineering, Computers & Applied Sciences (JEC&AS)* 4 (2014), 46-50
3. **I. Rejeena**, M. H. Rahimkutty, V. P. N. Nampoori, and P. Radhakrishnan. "Effect of nonlinear absorption on electric field applied lead chloride by Z-scan technique." In *Light and its interactions with matter*, AIP Publishing 1620, no. 1(2014): pp. 422-425.
4. **I.Rejeena**, B.Lillibai, Roseleena Toms, V.P.N.Nampoori, and P.Radhakrishnan “Optical Nonlinearity in Lead Iodide Di Hydrate grown with UV and IR radiations using Z-scan Technique” *AIP- 1391*, (2011) 691-693
5. **I.Rejeena**, B.Lillibai, V.P.N.Nampoori, and P.Radhakrishnan “Optical limiting and switching responses of gel grown calcium tartrate crystals by nonlinear measurements” (Communicated)
6. **I.Rejeena**, B.Lillibai, V.P.N.Nampoori, and P.Radhakrishnan “Spectral and Non radiatedecay studies of Lead di bromide single crystals by mode matched Thermal Lens Technique”(communicated)

7. **I.Rejeena**, B.Lillibai, V.P.N.Nampoori, and P.Radhakrishnan “Spectral and Lensing characteristics of Gel-derived Strontium Tartrate Single Crystals using Dual-Beam Thermal Lens Technique”(Communicated)
8. Raneesh, **I.Rejeena**, Rehana P. Ummar, Nandakumar kalarikkal, P.Radhakrishnan “Nonlinear optical absorption studies of sol - gel derived Yttrium Iron Garnet (Y₃Fe₅O₁₂) nanoparticles by Z-scan technique “(*Elsevier, Ceramics International*, 38 (2012) 1823–1826
9. Rose Leena Thomas, Vasuja , Misha Hari,Nithyaja B, Mathew S, **Rejeena I** , Sheenu Thomas , V P N Nampoori ,P Radhakrishnan “Optical Nonlinearity in TteO₂-ZnO Glass from Z-scan technique”,*Journal of Nonlinear Optical Physics & Materials*. 3 (2011) 351–356
10. G.Lillibai, **I.Rejeena**, Rose Leena Thomas, B.Nithyaja,, M.H.Rahimkutty ,V.P.N.Nampoori, P.Radhakrishnan “Nonlinear Optical Investigation on Lead Iodide Di Hydrate using Open aperture Z-scan Measurement” (in press)

Conference Proceedings

1. **I.Rejeena**; Lillibai, B. Nithyaja, Misha Hari, Indu Sebastian, V.P.N.Nampoori, P. Radhakrishnan “NonlinearOptical Investigation on Lead Iodide Di Hydrate using Open aperture Z-scan Measurement “, proceedings of International conference of Contemporary trends in Optics and Opto Electronics, Thiruvanan- thapuram, India P-574. January 17-19, 2011
2. **I.Rejeena**,B.Lillibai, Rose Leena Thomas, V.P.N.Nampoori, P.Radhakrishnan “Optical Nonlinearity in Lead Iodide Di Hydrate grown with UV and IR radiations using Z-scan Technique”

(Proceedings of OPTICS'11: International Conference on Light Calicut, Kerala India.) O-NLO-175 2011 May23- 25

3. **I.Rejeena**, B. Raneesh, Nandakumar kalarikkal ,V.P.N.Nampoori and P.Radhakrishnan Nonlinear Optical Absorption Studies on Sol - gel derived Yttrium Iron Garnet (Y₃Fe₅O₁₂) Nanoparticles by Z-scan Technique, Cochin Nano 2011 August 14-17
4. **I.Rejeena**, G.Lillibai², S.Mathew, V.P.N.Nampoori and P.Radhakrishnan Optical Characterization of Lead Iodide di Hydrate grown by Gel method International Conference on “Nano science, Engineering & Advanced Computing (ICNEAC-2011)” Narsapur, Andhra Pradesh, India, July 2011, 8-10
5. **I.Rejeena**, B.Lillibai, V.P.N.Nampoori, and P.Radhakrishnan Spectral and Optical limiting applications of sol-gel derived lead chloride crystals xxxvi OSI Symposium on Frontiers in Optics and Photonics, IIT Delhi, 5 December2011
6. **I.Rejeena**. Lillibai.B, Pradeep Chandran, Ca, Mathew.Ca, V.P.N.Nampoori and P.Radhakrishnan Sol-gel derived Lead Chloride Crystals for optical limiting Applications Proceedings of xx1v Kerala science congress.Rubber Board Kottayam January 29-31, 2012
7. **I.Rejeena** Lillibai, M. H. Rahimkutty, V.P.N.Nampoori, P. Radhakrishnan Effect of Nonlinear absorption on Electric field applied Lead chloride by Z-scan Technique OPTICS'14: International Conference on Light at NIT Calicut, Kerala India 2014 March19 to 21(**Best paper award**)
8. Rose Leena Toms, Vasuja, **Rejeena**, Misha Hari, Nithyaja, V.P.N.Nampoori, P.Radhakrishnan, Sheenu Thomas Optical Nonlinearity in ZnO- TeO₂ Glass from Z-scan technique, proceedings of International conference of Contemporary trends in Optics and Opto Electronics, Thiruvananthapuram, India, P- 565 January 17-19, 2011

Contents



1	Nonlinear Crystals and Optical Nonlinear Processes.....	1
1.1	Introduction.....	2
1.1.1	Relevant Aspects for the Choice of Nonlinear Crystals.....	2
1.2	Lead Halide Nonlinear crystals	4
1.2.1	Metal Tartrate Crystals.....	5
1.3	Growth Mechanism -Gel Technique	5
1.3.1	Advantage of Gel method	6
1.3.2	Applications of the Gel-grown crystals.....	7
1.4	Structural Characterization by X-ray Diffraction Studies	7
1.5	Optical Linear Studies	8
1.5.1	Optical Absorption Spectroscopy	8
1.5.2	Optical Band gap.....	9
1.5.3	Photoluminescence Studies.....	10
1.5.4	Heat transfer mechanism in crystals by Thermal lens Technique....	10
1.6	Nonlinear optical processes	12
1.6.1	Second harmonic Generation	13
1.6.2	Sum and Difference Frequency Generation	14
1.6.3	Optical Parametric Oscillation	15
1.6.4	Optical Parametric Amplification	16
1.6.5	Third Harmonic Generation	16
1.6.6	Optical Kerr Effect.....	16
1.6.7	Self-phase modulation.....	17
1.7	Optical Nonlinear Measurements	17
1.7.1	Measurement of Nonlinear Absorption.....	17
1.7.2	Z-Scan Technique	18

1.7.3	Open aperture Z-scan experiment	19
1.7.4.	Theory of Open aperture Z-scan experiment	20
1.7.5.	Closed aperture Z-scan experiment.....	22
1.8.	Nonlinear Absorption –Mechanism by Two-photon absorption	23
1.9	Scope of the thesis	25
	Conclusions	25
	References	26
2	Spectral and Optical Nonlinear studies on Lead Bromide (PbBr₂) crystals	35
2.1	Introduction	36
2.2	Synthesis.....	37
2.2.1	Structure of Hydro Silica gel	38
2.2.2.	Preparation of PbBr ₂ single crystals.....	39
2.3	Structural Characterization by X-ray Diffraction studies	40
2.4	Optical Characterizations	41
2.4.1.	Linear Absorption studies of PbBr ₂ in solution phase	41
2.4.2	Optical band gap studies	42
2.4.3	Fluorescence emission characteristics of PbBr ₂ from photo luminescence studies	44
2.5.	Thermal lensing in PbBr ₂ crystal.....	45
2.5.1.	Thermal diffusivity measurements.....	46
2.6.	Measurement of optical nonlinearity	48
2.6.1.	Open aperture Z-scan experiment on lead bromide crystal.....	48
2.7	Optical Limiting in PbBr ₂ crystal	53
	Conclusions	55
	References	56

3	Spectral and Optical nonlinear studies on lead Chloride (PbCl₂) crystals.....	61
	3.1 Introduction	62
	3.2 Synthesis.....	64
	3.3 X-ray Diffraction studies	65
	3.4 Spectral studies on Lead chloride crystals.....	66
	3.4.1 Optical absorption studies	67
	3.4.2 Bangap determination from Linear Absorption Spectra	68
	3.4.3. Flourescence Studies.....	71
	3.5 Thermal diffusivity studies of PbCl ₂	74
	3.6 Nonlinear optical Studies on PbCl ₂	76
	3.7 Optical limiting Studies on PbCl ₂	82
	Conclusions	84
	References	85
4	Linear and Nonlinear optical studies on lead Fluoride (PbF₂) Crystals.....	89
	4.1 Introduction	90
	4.2 Lead Fluoride sample preparation	92
	4.2.1 Preparation of hydro silica gel	92
	4.2.2 Lead Fluoride crystals from gel	92
	4.2.3 Ultra Violet irradiated PbF ₂	92
	4.2.4 Infrared Irradiated PbF ₂	93
	4.3 Structural studies	93
	4.4 Linear optical Measurements.....	94
	4.4.1. Absorption	94
	4.4.2 Optical band gap of PbF ₂ crystals	96
	4.4.3 Flourescence Emission Studies	97
	4.5. Thermal Diffusivity Measurements in PbF ₂ crystal.....	100

4.6. Nonlinear optical Studies on PbF ₂ crystals using Z-scan Experiment.....	103
4.7 PbF ₂ as an optical limiter.....	106
Conclusions	110
References	111
5 Spectral and Nonlinear optical studies on Calcium Tartrate (CaTT) crystals	115.
5.1 Introduction	116
5.2. Preparation of sample crystal	117
5.2.1. Preparation of Electric field applied calcium tartrate crystal CaTT-ELE	118
5.2.2. Preparation of Magnetic field applied calcium tartrate crystal- CaTT-MAG	118
5.3. Structural study using XRD.....	119
5.4 Linear Optical Characteristics	120
5.4.1 Absorption Studies.....	120
5.4.2. Optical Band gap of CaTT.....	122
5.4.3. Fluorescence Emission studies on CaTT	124
5.4.4 Luminescence Mechanism in CaTT.....	130
5.4.5.Non radiative decay mechanism in CaTT.....	133
5.5. Nonlinear optical studies on CaTT	136
5.6.Optical limiting Studies on CaTT.....	141
Conclusions	142
References	143
6 Linear and Nonlinear optical studies on Strontium Tartrate (SrTT) crystals	147
6.1 Introduction	148
6.2. Preparation of SrTT crystals.....	149
6.3. Structural study using XRD.....	149
6.4. Optical Linear Studies on SrTT.....	150

6.4.1 Linear Absorption Studies	151
6.4.2 Optical Band gap studies.....	152
6.4.3 Fluorescence spectral studies.....	154
6.4.4 Mechanism of photoluminescence in SrTT	158
6.4.5. Thermal diffusivity Measurements	161
6.5 Optical Nonlinear Studies on SrTT	163
6.6. Optical limiting Studies on SrTT.....	167
Conclusions	169
References	170
7 Linear and Nonlinear optical studies on Cadmium Tartrate (CdTT) crystals.....	173
7.1 Introduction	174
7.2 CdTT sample Synthesis.....	175
7.3 Structural Characteristics.....	176
7.4. Linear Optical Characterizations	177
7.4.1 Absorption Measurements	177
7.4.2. Optical Band gap of CdTT.....	179
7.4.3 Photoluminescence studies	181
7.4.4 Mechanism of photoluminescence in CdTT	185
7.4.5 Non radiative decay mechanism in CdTT.....	188
7.5. Nonlinear optical studies on CdTT.....	190
7.6. Optical limiting Studies on CdTT.	193
Conclusions	195
References	196
8 General Conclusions and future suggestions.	199
8.1. General Conclusions.....	200
8.2 Future Suggestions	204
Appendix- Published Articles	

List of Figures



Figure 1.1	:	A typical crystal for stimulated Raman scattering	3
Figure.1.2	:	Schematic of Direct and Indirect band gaps of a crystalline material	9
Figure.1.3	:	A schematic diagram of Fluorescence emission	10
Figure.1.4	:	Thermal lens experimental set up.	12
Figure.1.5	:	Schematic of second harmonic generation.....	14
Figure.1.6	:	Optical parametric oscillator	15
Figure.1.7	:	Schematic of Third harmonic generation	16
Figure.1.8	:	Open aperture Z-scan experimental set-up.....	18
Figure.1.9	:	Open aperture z-scan trace	20
Figure 1.10	:	Closed aperture z-scan plot	23
Figure.1.11	:	TPA Energy level diagram.....	24
Figure2.1	:	XRD of gel derived PbBr ₂ crystal	40
Figure.2.2	:	Linear absorption spectrum of PbBr ₂	41
Figure.2.3	:	Direct band gap plot of PbBr ₂ sample	43
Figure.2.4	:	Indirect band gap plot of PbBr ₂ sample	43
Figure2.5	:	Fluorescence emission spectra of PbBr ₂ at an excitation wavelength (a) 240 nm (b) 250 nm	44
Figure.2.6	:	A thermal lens signal of Rh-PbBr ₂ at a power of 50 mW	47
Figure.2.7	:	Time dependent TL plot of PbBr ₂	47
Figure.2.8	:	Open aperture z-scan plot of PbBr ₂ . at different laser powers, (a)100 MW/cm ² , (b)150 MW/cm ² and (c) 200 MW/cm ²	50
Figure.2.9	:	The response of an optic limiter.....	53
Figure.2.10	:	Optical limiting response of PbBr ₂ at a laser power density of (a) 100 MW/cm ² (b) 150 MW/cm ² and (c) 200 MW/cm ²	54

Figure.3.1	:	Crystal structure of PbCl ₂	63
Figure3.2	:	XRD of gel derived PbCl ₂ crystal	66
Figure .3.3	:	Room temperature absorption spectra of five PbCl ₂ crystal samples at concentrations (a) c1 and (b) c2.....	67
Figure.3.4	:	Optical band gap plot of (a) pure (b) UV (c) IR (d) electricfield and (e) magneticfield applied PbCl ₂ samples at c1.....	69
Figure 3.5	:	Fluorescence emission spectra of PbCl ₂ at an excitation wavelength 270 nm for (a) pure (b) UV (c) IR (d) electric field and (e) magnetic field applied samples	72
Figure.3.6	:	TL plot of PbCl ₂ (a) pure (b) UV (c) IR (d) electric field and (e) magnetic field applied samples	75
Figure.3.7(a)	:	Open aperture z scan plot of pure PbCl ₂ at a laser power 100 MW/cm ²	77
Figure.3.7(b)	:	Open aperture z scan plot of UV irradiated PbCl ₂ at a laser power 100 MW/cm ²	88
Figure.3.7(c)	:	Open aperture z scan plot of IR irradiated PbCl ₂ at a laser power 100 MW/cm ²	78
Figure.3.7(d)	:	Open aperture z scan plot of electric field applied PbCl ₂ at a laser power 100 MW/ cm ²	79
Figure.3.7(e)	:	Open aperture z scan plot of magnetic field applied PbCl ₂ at a laser power 100 MW/cm ²	79
Figure 3.8	:	Combined z scan trace of PbCl ₂ at I ₀ =100 MW/cm ²	80
Figure 3.9	:	Combined z scan trace of PbCl ₂ at I ₀ =125 MW/cm ²	80
Figure 3.10	:	Optical limiting response of PbCl ₂ (a) pure ,(b) UV irradiated, (c) IR irradiated, (d) electric field and (e) magnetic field applied samples	83
Figure.4.1	:	Crystal structure of orthorhombic α-PbF ₂	91
Figure.4.2	:	Powder X-ray diffraction pattern of PbF ₂ crystal.....	93
Figure 4.3	:	UV/VIS absorption spectra of pure, UV irradiated and IR irradiated PbF ₂ crystals.....	94
Figure.4.4	:	Optical band gap plot of (a) pure (b) UV irradiated and (c) IR irradiated PbF ₂ samples.	96

Figure.4.5.(a)	:	Emission spectra of pure PbF ₂ at an excitation wavelength of 250 nm.	97
Figure.4.5.(b)	:	Emission spectra of pure PbF ₂ at an excitation wavelength of 260 nm.	98
Figure.4.5.(c)	:	Emission spectra of ultra violet (UV) irradiated PbF ₂ at an excitation wavelength of 230 nm.....	98
Figure.4.5.(d)	:	Emission spectra of ultra violet (UV) irradiated PbF ₂ at an excitation wavelength of 250 nm.	99
Figure.4.5.(e)	:	Emission spectra of infrared (IR) irradiated PbF ₂ at an excitation wavelength of 250 nm.....	99
Figure.4.6.(a)	:	Thermal lens plot of pure Rh-PbF ₂	101
Figure.4.6.(b)	:	Thermal lens plot of ultra violet irradiated Rh-PbF ₂	101
Figure.4.6.(c)	:	Thermal lens plot of infrared irradiated Rh-PbF ₂	102
Figure.4.7.	:	Open aperture z-scan plot of pure PbF ₂ . at different laser powers, (a)100 MW/cm ² , (b)150 MW/cm ² and (c) 200 MW/cm ²	103
Figure.4.8.	:	Open aperture z-scan plot of UV irradiated PbF ₂ . at laser powers, (a)100 MW/cm ² , (b)150 MW/cm ² and (c) 200 MW/cm ²	104
Figure.4.9.	:	Open aperture z-scan plot of IR irradiated PbF ₂ . at laser powers, (a)100 MW/cm ² , (b)150 MW/cm ² and (c) 200 MW/cm ²	105
Figure.4.10	:	Optical limiting response of pure PbF ₂ at a laser power density of (a) 100 MW/cm ² (b) 150 MW/cm ² and (c) 200 MW/cm ²	107
Figure.4.11	:	Optical limiting response of UV irradiated PbF ₂ at a laser power density of (a) 100 MW/cm ² (b) 150 MW/cm ² and (c) 200 MW/cm ²	108
Figure.4.12	:	Optical limiting response of IR irradiated PbF ₂ at a laser power density of (a) 100 MW/cm ² (b) 150 MW/cm ² and (c) 200 MW/cm ²	109
Figure.5.1	:	Structure of calcium tartrate crystal	116
Figure.5.2	:	Schematics of crystal preparation of CaTT.....	119
Figure 5.3	:	XRD of CaTT crystal.....	120

Figure.5.4	:	UV/VIS absorption spectra of CaTT crystal.....	121
Figure5.5	:	Optical band gap plot of (a) pure (b) electric field applied and (c) magnetic field applied CaTT samples...	123
Figure.5.6	:	Emission spectra of pure CaTT at an excitation wavelength of (a) 230 nm (b) 240nm (c)260 nm and (d) 280 nm	125
Figure.5.7	:	Combined fluorescence emission spectra of pure CaTT crystal.....	125
Figure.5.8	:	Fluorescence emission from electric field applied CaTT (CaTT-ELE) at an excitation wavelength of (a) 230 nm, (b) 240 nm and (c) 260 nm.....	126
Figure.5.9	:	Combined fluorescence Emission spectra of CaTT-ELE	127
Figure.5.10	:	Emission spectra of CaTT-MAG at an excitation wavelength of (a) 230 nm (b) 240 (c) 250 nm (d) 260 nm and (e) 280 nm	129
Figure.5.11	:	Combined fluorescence Emission spectra of CaTT-MAG	129
Figure.5.12	:	FTIR spectra of CaTT [20]	130
Figure 5.13.	:	Schematic of the energy levels involved in the fluorescence spectra of CaTT based on combinations and overtones of various modes.....	133
Figure.5.14(a)	:	Thermal lens plot of Rh-CaTT- pure	134
Figure.5.14(b)	:	Thermal lens plot of Rh-CaTT- ELE	134
Figure.5.14(c)	:	Thermal lens plot of Rh-CaTT- MAG	135
Figure.5.15	:	Figure.5.15: Z- scan plot of pure CaTT (a) at various laser power densities	137
Figure.5.16	:	Open aperture Z-scan plot of CaTT-ELE.....	138
Figure.5.17	:	combined Z scan plot of CaTT-MAG.....	138
Figure 5.18	:	Optical limiting response of (a) CaTT-pure and (b) CaTT-ELE.....	141
Figure 6.1.	:	XRD of SrTT crystal.....	150
Figure.6.2	:	UV/VIS absorption spectra of SrTT solution.....	151

Figure 6.3	:	Optical band gap plot of (a) pure (b) electric field applied and (c) magnetic field applied SrTT samples....	153
Figure.6.4	:	Emission spectra of pure SrTT at an excitation wavelength of (a) 230 nm (b) 240nm (c)250 nm and (d) Combined fluorescence emission spectra of pure SrTT...	155
Figure.6.5	:	Fluorescence emission from electric field applied SrTT (SrTT-ELE) at an excitation wavelength of (a) 230 nm, (b) 250 nm , (c) 260 nm,(d) 270 nm and (e) combined spectra	156
Figure.6.6	:	Emission spectra of SrTT-MAG at an excitation wavelength of (a) 230 nm (b) 240 (c) 250 nm (d) 280 nm and (e) combined emission spectra	157
Figure 6.7	:	FTIR spectrum of SrTT.....	158
Figure 6.8.	:	Schematics of the energy levels involved in the fluorescence spectra of SrTT based on combinations and overtones of various modes	160
Figure.6.9	:	Thermal lens plot of (a) Rh-SrTT- pure (b) Rh-SrTT-ELE and (c) Rh-SrTT- MAG	162
Figure.6.10(a)	:	Combined Z-scan plot of SrTT- pure.....	164
Figure 6.10(b)	:	Combined Z-scan plot of SrTT- pure.....	164
Figure 6.10(c)	:	Combined Z-scan plot of SrTT-MAG.....	165
Figure 6.11(a)	:	Optical limiting response of SrTT-pure	168
Figure 6.11(b)	:	Optical limiting response of SrTT-ELE.....	168
Figure 7.1	:	Schematic of crystal preparation of CdTT	176
Figure 7.2	:	XRD of CdTT crystal.....	176
Figure.7.3 (a,b)	:	Linear absorption spectra of CdTT –pure and (b) CdTT-MAG	177
Figure.7.3 (c)	:	combined Linear absorption spectra	178
Figure 7.4	:	Optical direct band gap plot of (a) pure and (b) magnetic field applied CdTT samples.....	180
Figure 7.5	:	Optical Indirect band gap plot of (a) pure and (b) magnetic field applied CdTT samples.....	181

Figure 7.6	:	Emission spectra of pure CdTT at an excitation wavelength of (a) 230 nm (b) 240nm (c)250 nm and (d) 260 nm(e) 280 nm and(f) combined emission spectra	182
Figure.7.7	:	Emission spectra of CdTT-MAG at an excitation wavelength of (a) 230 nm (b) 240 (c) 250 nm (d) 260 nm , (e) 270 nm (f) 280 nm and (g) combined emission spectra	184
Figure 7.8	:	FTIR spectrum of CdTT	186
Figure 7.9.	:	Schematics of the energy levels involved in the fluorescence spectra of CdTT based on combinations and overtones of various modes	188
Figure.7.10	:	Thermal lens plot of (a) Rh-CdTT- pure and (b) Rh-CdTT- MAG	189
Figure.7.11 (a)	:	Combined z scan plot of pure CdTT at three laser powers ($P_1=75 \text{ MW/cm}^2$, $P_2=163 \text{ MW/cm}^2$ and $P_3=251 \text{ MW/cm}^2$)	191
Figure.7.11(b)	:	Combined z scan plot of CdTT-MAG at two laser powers 75 MW/cm^2 and 251 MW/cm^2	192
Figure 7.12(a)	:	Optical limiting response of CdTT-pure at (a) 163 MW/cm^2 and (b) 251 MW/cm^2	193
Figure 7.12(b)	:	Optical limiting response of CdTT-MAG at (a) 75 MW/cm^2 and (b) 251 MW/cm^2	194

List of Tables



Table 1.1	:	Laser and Crystal parameters for the selection of a suitable crystal.....	3
Table.2.1	:	Measured values of D , θ , and t_c for Rhodamine -6G incorporated lead bromide solution	48
Table.2.2	:	Measured values of nonlinear absorption coefficient, $\text{Im}(\chi^{(3)})$ and optical limiting threshold for PbBr_2	52
Table 3.1	:	Properties of PbCl_2 from literature	64
Table.3.2	:	Measured values of linear absorption coefficient α for the five different PbCl_2 crystals.....	68
Table 3.3	:	Measured values of optical band gap of PbCl_2 at two concentrations c_1 and c_2	70
Table 3.4	:	Measured values of emission peaks for PbCl_2 at concentrations c_1 and c_2 (gm/ml)	73
Table.3.5	:	Measured values of D , θ , and t_c for rhodamine incorporated lead chloride solution	76
Table 3.6	:	Measured values of nonlinear absorption coefficient and optical limiting threshold for PbCl_2 samples	81
Table.4.1	:	Properties of lead fluoride from literature	91
Table.4.2	:	Measured values of α and λ_{Peak} for the three different PbF_2 crystals.....	95
Table.4.3	:	Measured values of D , θ , and t_c for Rhodamine-6G incorporated lead Fluoride solution.....	102
Table.4.4	:	Measured values of nonlinear absorption coefficient and imaginary part of third order susceptibility for PbF_2	106
Table.4.5	:	Measured values optical limiting threshold for PbF_2 sample solutions	110
Table 5.1	:	Properties of calcium tartrate from literature	117
Table.5.2	:	Measured values of α and λ_{Peak} for the three different CaTT crystals	122

Table 5.3	:	Measured values of optical band gap of CaTT.....	124
Table 5.4.	:	FTIR band assignments of CaTT	131
Table.5.5	:	Details of fluorescence bands and assignments of CaTT ..	132
Table 5.6	:	Values of ν taken from FTIR spectra of CaTT.....	132
Table.5.7	:	Measured values of D , θ ,and t_c for rhodamine incorporated CaTT solution.....	135
Table 5.8	:	Measured values of nonlinear absorption coefficient, saturation intensity and optical limiting threshold for CaTT.....	140
Table 5.9	:	Measured value of $\text{Im}(\chi^{(3)})$ of CaTT at three different input fluencies.....	140
Table.6.1	:	Measured values of α and λ_{Peak} for the three different SrTT crystals	152
Table 6.2	:	Measured values of optical band gap of SrTT.....	154
Table.6.3	:	Details of fluorescence bands and assignments of SrTT...	158
Table 6.4	:	Values of ν taken from FTIR spectra of SrTT.....	160
Table.6.5	:	Measured values of D , θ ,and t_c for Rhodamine incorporated SrTT solution	163
Table 6.6	:	Measured values of nonlinear absorption coefficient and imaginary part of third order susceptibility [Im $(\chi^{(3)})$] of SrTT	166
Table.6.7	:	Observed values of limiting threshold for SrTT.....	169
Table.7.1	:	Measured values of α and λ_{Peak} for the two different CdTT samples	179
Table 7.2	:	Measured values of optical band gap of CdTT	180
Table 7.3	:	The emission peaks of CdTT pure sample at five different excitations.....	183
Table 7.4	:	The emission peaks of CdTT -MAG sample at six different excitations	185
Table7.5	:	Values of ν taken from FTIR spectra of CdTT	187
Table7.6	:	Details of fluorescence bands and assignments of CdTT ..	187

Table.7.7	:	Measured values of D, θ , and t_c for Rhodamine-6G incorporated CdTT solution	190
Table 7.8	:	Measured values of nonlinear absorption coefficient and imaginary part of third order susceptibility [$\text{Im}(\chi^{(3)})$] of CdTT	192
Table.7.9	:	Observed values of limiting threshold for CdTT	194

Chapter 1

Nonlinear Crystals and Optical Nonlinear Processes

Abstract

This chapter gives a general introduction to the different types of optical nonlinear processes. The peculiarities of nonlinear crystals and their selection criteria have also been discussed. A nonlinear optical crystal can be selected for a frequency conversion depending upon its ability to obtain high conversion efficiency. The importance of lead halides and metal tartrate crystals in the field of photonics is also presented in this chapter. The relevance of solution-gel method for the preparation of these crystalline materials and the role of X-ray diffraction in the structural characterization of the samples are also discussed. The experimental methods of Thermal lensing for the non radiative decay studies are explained. The theory and experimental method of optical nonlinear measurements by z-scan technique have been discussed.

1.1 Introduction

A nonlinear crystal is an optical material that possesses a strong nonlinear dielectric response function to optical radiation. The large interest in nonlinear optical crystalline materials has been motivated by their potential use in the fabrication of all-optical photonic devices [1]. Transparent crystalline materials can exhibit different kinds of optical nonlinearities which are associated with a nonlinear polarization [2]. Crystalline materials with second order nonlinearity are mainly used for parametric nonlinear frequency conversion. The frequency doublers and optical parametric oscillators belong to this category. Crystals exhibiting a third order nonlinearity via Kerr effect are well suited for electro-optic modulators. The choice of the most suitable crystalline material for a given application should involve the consideration of many aspects. For example, a high nonlinearity for frequency conversion of ultra-short pulses does not help if the interaction length is strongly limited by a large group velocity mismatch and the low damage threshold limits the applicable optical intensities. Also, it can be highly desirable to use a crystalline material which can be critically phase-matched at room temperature, because noncritical phase matching often involves the operation of the crystal in a temperature-stabilized crystal oven [3].

1.1.1 Relevant Aspects for the Choice of Nonlinear Crystals

Many different properties of a nonlinear crystal can be important for an application [4-7]. A nonlinear optical crystal can be selected for a frequency conversion depending upon its ability to obtain high conversion efficiency. The conversion efficiency is related to the effective nonlinear coefficient (d_{eff}), crystal length (L), input power density (P) and phase mismatch. In general, higher power density, longer crystal length, larger nonlinear coefficients and smaller phase mismatch will result in higher conversion efficiency. However, there is always some limitation coming from nonlinear crystals and lasers. For example, the d_{eff} is determined by the nonlinear crystal itself and the input power

density have to be lower than the damage threshold of crystal. Therefore, it is important to select a right crystal for our applications. In the following table we list the laser and crystal parameters for selecting the right crystals for NLO processes[1-7].



Figure 1.1: A typical crystal for stimulated Raman scattering

The figure 1.1 shows a crystal of Barium Nitrate - $Ba(NO_3)_2$ and undoped potassium gadolinium tungstate $KGd(WO_4)_2$ or KGW which have attracted much interest as most suitable for stimulated Raman scattering (SRS). Among the different types of nonlinear crystals, metal halides and tartrates have attracted due to their importance in photonics.

Table 1.1 Laser and Crystal parameters for the selection of a suitable crystal

Parameter for NLO Crystal Selection	
Laser Parameters	Crystal Parameters
NLO Process	Phase-Matching Type and Angle, d_{eff}
Power or Energy, Repetition Rate	Damage Threshold
Divergence	Acceptance Angle
Bandwidth	Spectral Acceptance
Beam Size	Crystal Size, Walk-Off Angle
Pulse Width	Group Velocity Mismatching
Environment	Temperature Acceptance, Moisture

1.2 Lead Halide Nonlinear Crystals

Lead Halides have drawn attention of many workers because they exhibit interesting features from the stand point of the electron-lattice interaction [8-21]. These materials are important for their luminescent properties [22]. Nonlinear optical (NLO) materials like lead halides have enormous potential applications on the technological front which include optical limiting, optical switching, optical data processing and optoelectronic device fabrication [23]. They have also been used as bistable devices and are good candidates for making prototype detectors for x-ray imaging [24-25]. The second order NLO effect in the molecules originates from a non-centro symmetric structure. Among several compounds reported for NLO property, Lead derivatives are noticeable materials for their excellent crystallizability. Large magnitude of third order nonlinearity and ultrafast response are required to make ultrafast optical switches. Recent device modeling suggests that heavy atom materials can be optimized for optical limiter designs [26]. The comparatively large nonlinearity of these materials can also be exploited for all optical switching applications, quantum information processing and integrated all optical signal processing due to their instantaneous nonlinear response with light interactions [27]. Compared to dynamic devices these NLO materials are passive devices and are referred to as intelligent or smart materials owing to the fact that the sensing processing and activating functions required for optical limiting or switching actions are inherent to them which are otherwise separate in dynamic devices [28-30]. The low threshold of these materials for nonlinear response is of much importance as they could be used for the protection of human eye from the laser effects.

1.2.1. Metal Tartrate Crystals

Tartrate single crystals show many interesting physical properties such as ferroelectric, piezoelectric, dielectric, optical and other pertinent

characteristics [31-34]. They are used for nonlinear optical devices based on their optical second harmonic generation, optical transmission characteristics, fabrication of crystal oscillators and resonators and controlled laser emission [35-37]. Among the several tartrate compounds, Strontium Tartrate, Cadmium Tartrate and Calcium Tartrate have received greater attention on account of their ferroelectric, nonlinear optical and spectral characteristics [38-39]. Calcium tartrate crystals are well known for their ferroelectric properties in pure as well as doped forms [40]. Strontium tartrate is an important member of the tartrate family having device applications [40-42]. Growth of mixed crystals of various compositions is a fast growing field of research because of the great need of such crystals for several applications. Recent focus is on tartrate mixed crystals which constitute a very interesting system for academic and research studies. M. Mary Freeda et al reported the growth of mixed crystals of Strontium Calcium Barium (SCBT) tartrate by gel method[37]. The structural, spectral, optical, chemical, dielectric and mechanical characterization of the grown crystals by single crystal and powder XRD studies, FTIR, optical absorption studies, SHG efficiency measurement, energy dispersive analysis, dielectric and micro hardness studies are also reported[43-50].

1.3 Growth Mechanism -Gel Technique

A gel may be defined as a two component system of a semi-solid nature rich in liquid. Gels and gelatin are very important in medicine, biology etc., because plants and animals are mainly composed of gels. A gel can also be regarded as a loosely interlinked polymer. Silica hydrogel, gelatin gel, agar, clay gel, soap fluid, polyacrylamide, dense solution of metal hydroxides, poly vinyl alcohol, oleates, sterates, aluminates etc. are materials that can be categorized as gels and a sol subjected to a number of treatments such as warming, cooling, chemical reaction, addition of external reagents can be used for gelation [51-55].

Henisch explained the use of gel to grow the crystals. Chemical reaction, chemical reduction, complex dilution and reduction of solubility are the popular methods of crystal growth in gel. The crystals of sulphates, tartrates, molybdates, barium oxalates and iodates were grown by chemical reaction method [56-59]. KDP and ADP crystals were grown by reduction of solubility method. Günter P. et al reported non centro symmetry in $\text{CaC}_4\text{H}_4\text{O}_6 \cdot 4\text{H}_2\text{O}$ crystals by nonlinear optical measurements [60].

1.3.1 Advantage of Gel method

The gel technique is in fact, the method of growing crystals when the material decomposes at temperature below their melting points and also for those not having suitable solvents for crystallization. The gel method has unique characteristic of suppression of nucleation centers [57]. The main advantage of this method lies in the simplicity with which strain-free perfect crystals can be obtained at low temperatures. For a certain class of substances which have very slight solubilities in water and enormously high melting points or which decomposes on heating, and cannot be satisfactory grown from the melt or from the vapour, the gel method offers a reasonable prospect, of success. The gel method is ideally suited for doping studies. The classical gel method is usually useful for substances having low solubility and low dissociation temperature. Crystals which are grown in gels can be easily observed if the gel is transparent. The gel method also offers possibilities for studies on the dependence of polytypism on the parameters of crystal growth. However the quality of crystals grown in gel is good but the size is invariably small compared to other methods.

1.3.2 Applications of the Gel-grown crystals

The technique is widely used by several investigators to grow crystals having a variety of properties. Gel-grown crystals are used to study new research applications such as electron spin resonance measurement of Mn^{2+} in calcium

tartrate. A lot of work has been done on gel grown lead iodide to clarify its complicated band and defective structures and also polytypism. The gel method is capable of yielding crystals of high optical perfection and wide morphology [59-60]. The growth of crystals for ferroelectric and laser applications is one of the important uses of the gel technique.

The gel method has proved to be an aid in the success of research in crystal physics. A factor to be inquired into is the chemical role played by internal gel surfaces and the extent to which it is governed by the structure of the gel. Various applications that single crystals find in modern devices, from miniature transistors to massive computers, have created new demands for perfect crystals. The gel method is capable of yielding such single crystals. The realization of the scope and utility of the gel method is growing in the field of medical sciences. Facts about polytypism can easily solve problems of crystal structure. The gel method offers new possibilities of such studies.

1.4 Structural Characterization by X-ray Diffraction Studies

X-ray diffraction has provided a wealth of important information to science and industry. For example X-ray diffraction technique was employed to identify the crystal growth. The X-ray diffraction provides sufficient information in determining the dimension of the unit cell of the crystal lattice and the atomic arrangement within the cell. X-ray diffraction provides a convenient and practical means for the qualitative identification of crystalline compounds. This application is based on the fact that the X-ray diffraction pattern is unique for each crystalline substance. The basic X-ray diffractometer consists of an X-ray generator including a tube for deriving necessary radiations [61].

The phenomenon of X-ray diffraction by crystals results from a scattering process in which X-rays are scattered by constituent atoms without change in wavelength. Further analysis leads to knowledge of the size, shape and orientation for the unit cell. Out of the various possible XRD methods, the

powder method is of special importance since it is the only technique which is readily applicable to all crystalline materials. A powder pattern is obtained when X-rays are diffracted by a sample consisting of very large number of randomly oriented crystalline particles, i.e., a powder sample.

The powder method is the only technique which can be used with that large class of substances which cannot be obtained easily in the form of perfect crystal of appreciable size. In this method a monochromatic X-ray beam is used and instead of using a single crystal, fine powder having random chaotic characterization are used. Such a powder requires no rotation because every atomic plane is present in every possible orientation and hence the diffraction depends upon the fact that in a fine powder the grains are arranged in an entirely chaotic manner. The crystal was identified by comparing the inter planar spacing and intensities of the powder pattern with the pattern in JCPDS index file.

1.5 Optical Linear Studies

1.5.1 Optical Absorption Spectroscopy

The optical absorption measurements are governed by the Beer- Lambert Law and the absorbance is given as[62]

$$A = \log(I_0/I) = \epsilon cl \text{ for a given wavelength}$$

$$A = \text{absorbance}$$

$$I_0 = \text{intensity of light incident upon a sample cell}$$

$$I = \text{intensity of light leaving the sample cell}$$

$$C = \text{molar concentration of the solute}$$

$$l = \text{length of sample cell (cm)}$$

$$\epsilon = \text{molar absorptivity}$$

1.5.2 Optical Band gap

The band gap is the energy difference between the lowest point of the conduction band and the highest point of the valance band. The band gap in materials can be direct or indirect [63]. The threshold of the optical absorption determines the band gap. In the direct absorption process a photon is absorbed by the crystal with the creation of an electron and a hole. But in the indirect absorption process the minimum energy gap involves electrons and holes separated by a substantial wave vector. The materials for which the valence band maximum and the conduction band minimum correspond to the same momentum are called direct band gap materials. Materials for which this is not the case are known as indirect band gap materials. A transition between the top of the valance band and bottom of the conduction band in an indirect band gap material requires a substantial change in the electron's momentum [63-65]. This has important consequences for optical transitions between these two bands induced by absorption or emission of photons. Direct band gap materials are efficient light emitters compared to indirect band gap ones.

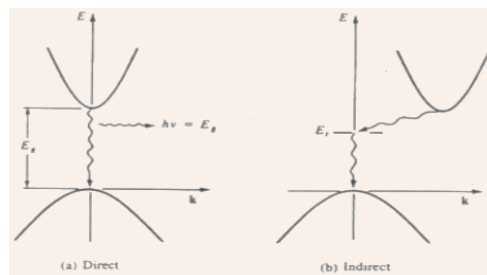


Figure.1.2 Schematic of Direct and Indirect band gaps of a crystalline material

1.5.3 Photoluminescence Studies

Photoluminescence is the phenomena which involves the absorption of energy and subsequent emission of light. If the time delay between absorption and re emission is less than 10^{-8} s, the material is fluorescent in nature. In luminescence,

the exciting photons have generally greater energy than the emitted photons [61]. Fluorescence occurs when an orbital electron of a molecule, atom or nanostructure relaxes to its ground state by emitting a photon of light after being excited to a higher quantum state by some type of energy. The specific frequencies of excited and emitted light are dependent on the particular system. [61,63]. The efficiency of luminescence is closely related to the de excitation dynamics of atoms[66].The luminescence is down shifted in frequency related to the absorption through an effect known as Stokes shift. Figure 1.3 represents a schematic representation of fluorescence emission process.

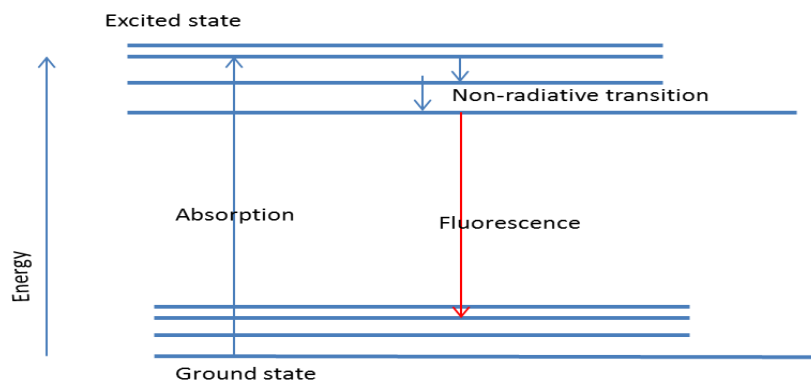


Figure.1.3: A schematic diagram of Fluorescence emission

1.5.4 Heat transfer mechanism in crystals by Thermal lens Technique

Photo thermal spectroscopy is a group of high sensitivity spectroscopic techniques used to measure optical absorption and thermal characteristics of a sample. The basis of photo thermal spectroscopy is the change in thermal state of the sample resulting from the absorption of radiation [67]. Light absorbed and not lost by emission results in heating. The heat rises temperature thereby influencing the thermodynamic properties of the sample or of a suitable material adjacent to it. Measurements of the temperature, pressure, or density changes that occur due to optical absorption are ultimately

the basis for the photo thermal spectroscopic measurements [68]. There are several methods and techniques used in photo thermal spectroscopy. Each of these has a name indicating the specific physical effect measured.

The thermal lens technique is based on measurement of the temperature rise that is produced in an illuminated sample as a result of non radiative relaxation of the energy absorbed from a laser. Because the technique is based on direct measurement of the absorbed optical energy, its sensitivity is higher than conventional absorption techniques [69]. However, advantages of the thermal lens technique are not only limited to its ultra-sensitivity but also include other unique characteristics such as small-volume sample capability and dependency on thermo-optical properties of solvents. The main focus is, however, on the instrumentation and applications based on unique characteristics of the technique. Specifically, the discussion begins with a description of different types of thermal lens configurations for e.g., the single-beam and double-beam instruments, differential, multi wavelength, thermal lens-circular dichroism instruments, and thermal lens microscope [70]. A detailed description of various applications including applications based on its ultra-sensitivity (eg; applications in environment, agriculture and food science, biochemistry and biomedicine, measurements in the near- and middle-infrared region, and kinetic determination), applications based on its small-volume capability (eg; microfluidic devices, detection for capillary electrophoresis), and applications based on exploitation of its dependency on thermo-physical properties of solvents to either determine physical properties of the solvent or to further enhance the sensitivity of the technique are available in the literature [71].

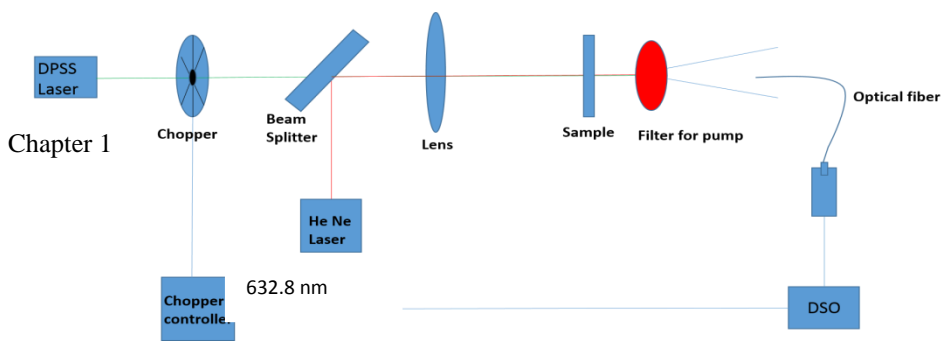


Figure.1.4:Thermal lens experimental set up.

The experimental set up of TL is as shown in the above figure 1.4. A 532 nm diode pumped solid state laser, (DPSS) with a maximum power of 150 mW is used as the excitation source. A 2mW He–Ne laser used as the probe is arranged to be collinear with the pump using a dichroic beam splitter. A chopper is used to modulate the pump beam intensity. The pump beam passing through the chopper is focused using an achromatic lens. The two beams are focused into the sample cell such that the beam area at the sample plane is the same for both pump and probe resulting in a mode matched TL configuration. The thermal lens is detected by coupling to a detector system through an optical fiber. The output signal from the detector is processed using a digital storage oscilloscope (DSO).

Theory

The relative change in the beam intensity is proportional to the relative changes in power of the beam reaching the detector and hence is a direct measure of the thermal lens signal. If the beam is suddenly turn on at time $t=0$, the lens effect builds up with time so that the focal length follows the relation[71].

$$F(t) = f_{\infty} \left[1 + \frac{t_c}{2t} \right]$$

Where t_c is the thermal time constant and f_{∞} is the focal length of the equivalent lens in a steady state determined by radial heat conduction given by

$$f_{\infty} = \frac{\pi k \omega^2}{PA \left(\frac{dn}{dT} \right)}$$

Where k is the thermal conductivity, ω is the spot size, P is the laser power, A is the sample absorbance and $\frac{dn}{dT}$ is the refractive index change with temperature.

The time constant t_c relates to the thermal diffusivity D by

$$t_c = \frac{\omega^2}{4D}$$

The thermal diffusivity in the sample is detected by the effect on propagation of the probe beam aligned with the centre of the lens. The relation connecting intensity as a function of time is given by

$$I(t) = I(0) \left[1 - \frac{\theta}{1 + t_c/2t} + \frac{\theta^2}{2 \left(1 + \frac{t_c}{2t} \right)^2} \right]$$

Where I_0 is the initial intensity and the parameter θ is related to the thermal power radiated as heat P_{th} through the relation given as

$$\theta = \frac{P_{th}}{\lambda k} \left(\frac{dn}{dt} \right)$$

where λ is the laser wavelength, k is the thermal conductivity and dn/dt is the refractive index gradient.

1.6 Nonlinear optical processes

The behavior of light in a nonlinear medium is described by a branch of optics which is known as nonlinear optics. In a nonlinear medium the dielectric polarization P depends nonlinearly on the electric field E of the light. This nonlinearity is observed at very high light intensities such as those from a pulsed laser in order to provide the electric field comparable to interatomic fields, typically 10^8 V/m. Nonlinear optics deals with the nonlinear interaction of light with matter and also describes the problems of light induced changes of the optical properties of a medium[72-74].

The observation of nonlinearity requires the application of lasers. Nonlinear optical effects are analyzed by considering the response of the

dielectric material at the atomic level to the electric fields of an intense light beam [75]. The propagation of a wave through a material produces changes in the spatial and temporal distribution of electrical charges as the electrons and atoms interact with the electromagnetic fields of the wave. A parametric non-linearity is an interaction in which the quantum state of the nonlinear material is not changed by the interaction with the optical field [76-77].

Each nonlinear optical process consists of two parts. The first part gives the induction of a nonlinear response in the medium by the intense light. The second part is the modification of optical fields by the reaction of the medium in a nonlinear way. Nonlinear properties in optical region are demonstrated by the harmonic generation of light observed for the first time by Franken and coworkers in 1961[78].The major nonlinear optical processes involve the following.

1.6.1 Second harmonic Generation

When an intense laser beam travels through a nonlinear optical medium, a frequency doubling occurs. Thus a polarization oscillating at frequency 2ω radiates an electromagnetic wave of the same velocity as that of the incident wave. This wave has the same characteristics of directionality and monochromaticity as the incident wave and is emitted in the same direction. This phenomenon is known as the second harmonic generation (SHG) [78]. The nonlinear polarizability $\chi^{(2)}$ of the crystalline materials depends on the direction of propagation, polarization of the electric field and the orientation of the optic axis of the crystal. Schematic of second harmonic generation is illustrated in the figure 1.5 [79].

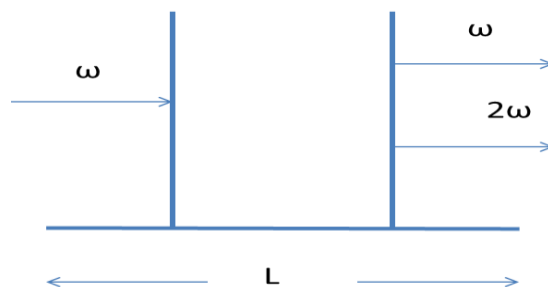


Figure.1.5. Schematic of second harmonic generation

In a nonlinear media the relation connecting the polarization P and the electric field E is given as follows [78-79]

$$P = \epsilon_0 [\chi^{(1)}E + \chi^{(2)}E^2 + \chi^{(3)}E^3 + \dots]$$

where $\chi^{(1)}$ is linear optical susceptibility and $\chi^{(2)}, \chi^{(3)} \dots$ represent the nonlinear susceptibilities.

Centro-symmetric crystals and isotropic medium like liquids or gases do not possess second harmonic generation. Anisotropic crystals such as uniaxial crystals possessing non-centro symmetry give second harmonic generation.

If the medium exhibits a second order nonlinearity, then the relation between P and E can be written as

$$P = \epsilon_0 \chi^{(1)}E + \epsilon_0 \chi^{(2)}E^2$$

1.6.2. Sum and Difference Frequency Generation

If two light waves having different frequencies ω_1 and ω_2 enter into a nonlinear medium and generate a light of frequency which is the sum of the two incident frequencies, then the process is termed as a sum frequency generation. The generation of light with a frequency which is the difference between the incident frequencies is known as difference frequency generation [79].

Suppose there are two distinct frequency components incident on a nonlinear medium ,

then
$$E(t) \propto E_1 \exp(i\omega_1 t) + E_1^* \exp(-i\omega_1 t) + E_2 \exp(i\omega_2 t) + E_2^* \exp(-i\omega_2 t)$$

Therefore

$$\begin{aligned}
 E(t)^2 \propto & E_1^2 \exp(2i\omega_1 t) + E_1^{*2} \exp(-2i\omega_1 t) \\
 & + E_2^2 \exp(2i\omega_2 t) + E_2^{*2} \exp(-2i\omega_2 t) \\
 & + 2E_1 E_2 \exp(i[\omega_1 + \omega_2]t) + 2E_1^* E_2^* \exp(-i[\omega_1 + \omega_2]t) \\
 & + 2E_1 E_2 \exp(i[\omega_1 - \omega_2]t) + 2E_1^* E_2^* \exp(-i[\omega_1 - \omega_2]t) \\
 & + 2|E_1|^2 + 2|E_2|^2
 \end{aligned}$$

} →	Second harmonic generation
→	Sum frequency generation
→	Difference frequency generation
→	DC rectification

1.6.3. Optical Parametric Oscillation

The generation of a signal and idler waves using a parametric amplifier in a resonator is called optical parametric oscillation. In this process, a nonlinear crystal is placed in an optical resonator which is tunable because any frequency ω_2 taken as the signal can satisfy the condition $\omega_2 + \omega_3 = \omega_1$ for frequency ω_3 . Here ω_3 represents the idler wave and ω_1 is the pump frequency[79]. The application of optical parametric oscillators includes light detection and ranging (LIDAR), high-resolution spectroscopy, medical research, environmental monitoring, display technology, and precision frequency metrology.



Figure.1.6. Optical parametric oscillator

1.6.4. Optical Parametric Amplification

Optical parametric amplification is the amplification of a signal input in the presence of a high frequency pump wave and can be considered as a difference frequency generation. Optical parametric amplification is initiated by a single pump beam [73]. An optical parametric amplifier consists of both the signal and idler waves coupled through a nonlinear crystal. This process can be treated as a three wave mixed amplifying process.

1.6.5. Third Harmonic Generation

Third harmonic generation is possible in crystals that exhibit inversion symmetry. In this case the polarization vector P is related to the field strength E as follows [78]

$$P = \epsilon_0 \chi^{(1)} E + \chi^{(3)} E^3 + \dots$$

or in vector notation

$$P = \epsilon_0 \chi^{(1)} \mathbf{E} + \epsilon_0 \chi^{(3)} E^2 \mathbf{E} + \dots$$



Figure.1.7. Schematic of Third harmonic generation

1.6.6. Optical Kerr Effect

The polarization of a beam propagating in the medium can be changed by the optical field induced birefringence [79]. If a medium of asymmetric molecules is placed in an electric field, the molecules are aligned parallel to the field direction. This parallel alignment creates birefringence thereby changing the refractive index of the medium. The change in refractive index has a quadratic dependence on the electric field. Thus the Kerr effect can be treated as an intensity dependent refractive index or a $\chi^{(3)}$ effect.

1.6.7. Self-phase modulation

The optical Kerr effect can produce a variation of refractive index in a medium by passing a very short pulse through it. A change in the frequency is obtained by a phase shift produced by the refractive index variation. Normal dispersion regions give redder portions of the pulses with very high velocity thereby causing the broadening of the pulse. This effect can be used for pulse compression. It is caused by the temporal variation in the intensity creating a temporal variation in the refractive index [73]

Self-focusing - an effect due to the Optical Kerr effect and possibly higher order nonlinearities caused by the spatial variation in the intensity creating a spatial variation in the refractive index., Kerr-lens mode locking - the use of Self-focusing as a mechanism to mode lock laser, Optical phase conjugation, Stimulated Brillouin scattering, interaction of photons with acoustic phonons, Multi-photon absorption-simultaneous absorption of two or more photons, transferring the energy to a single electron and multiple photo ionization, near-simultaneous removal of many bound electrons by one photon etc. are other nonlinear processes[78-79].

1.7 Optical Nonlinear Measurements

1.7.1.Measurement of Nonlinear Absorption

Bahae described a method by which the Z-scan technique can be used to determine both the nonlinear refractive index and the nonlinear absorption coefficient for materials that show such nonlinearities simultaneously [80]. Large refractive nonlinearities in materials are commonly associated with a resonant transition which may be of single or multi photon nature. The nonlinear absorption in such materials arising from either direct multi photon absorption, saturation of the single photon absorption, or dynamic free-carrier absorption have strong effects on the measurements of nonlinear refraction using the Z-scan technique. Z-scan with a fully open aperture is insensitive to nonlinear

refraction. Such Z- scan traces with no aperture are expected to be symmetric with respect to the focus at $z = 0$ where they have either a minimum transmittance or a maximum transmittance. The coefficients of nonlinear absorption can be easily calculated from such transmittance curves. In this case, the Z-scan transmittance is insensitive to beam distortion and is only a function of the nonlinear absorption.

1.7.2 Z-Scan Technique

M.S.Bahae et al demonstrated a single-beam technique that is sensitive to less than $\lambda/300$ nonlinearly induced phase distortion [80]. Several papers report the measurement of nonlinear refraction and transmittance using a variety of techniques including nonlinear interferometry, degenerate four-wave mixing, nearly degenerate three-wave mixing, ellipse rotation and beam distortion measurements [81-87]. The first three methods, namely, nonlinear interferometry and wave mixing, are potentially sensitive techniques, but all require relatively complex experimental apparatus. Beam distortion measurements, on the other hand, are relatively insensitive and require detailed wave propagation analysis. The technique reported by M.S.Bahae here is based on the principles of spatial beam distortion, but offers simplicity as well as very high sensitivity [80].

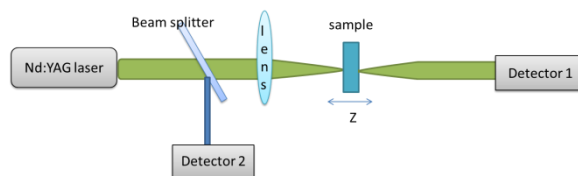


Figure.1.8: Open aperture Z-scan experimental set-up

Using a single Gaussian laser beam in a tight focus geometry, as depicted in the figure.1.8, the transmittance of a nonlinear medium was measured through a finite aperture in the far field as a function of the sample position z measured with respect to the focal plane. A material with a negative nonlinear refractive index and a thickness smaller than the diffraction length of

the focused beam can be regarded as a thin lens of variable focal length. The scan is started from a distance far away from the focus i.e.; a negative z , the beam irradiance is low and negligible nonlinear refraction occurs; hence, the transmittance remains relatively constant. As the sample is brought closer to focus, the beam irradiance increases, leading to self-lensing in the sample. A negative self-lensing prior to focus will tend to collimate the beam, causing a beam narrowing at the aperture which results in an increase in the measured transmittance. As the scan in z continues and the sample passes the focal plane to the right (positive z), the same self-defocusing increases beam divergence, leading to beam broadening at the aperture, and thus a decrease in transmittance. This suggests that there is a null as the sample crosses the focal plane. Induced beam broadening and narrowing have been reported [87-88].

1.7.3 Open aperture Z-scan experiment

Measurement of light transmittance without an aperture is termed as open aperture z-scan technique. Nonlinear absorption of a sample is manifested in the open aperture z-scan measurements. If nonlinear absorption like two photon absorption is present, it is indicated by the transmission minimum at the focal point. If the transmission increases with the increase in intensity, this results in a transmission maximum at the focal region. The transmission minimum gives a valley and transmission maximum gives a peak in the transmittance traces. The valley nature of transmittance indicates the reverse saturable absorption (RSA) behaviour and the transmission peak shows the saturable absorption (SA).

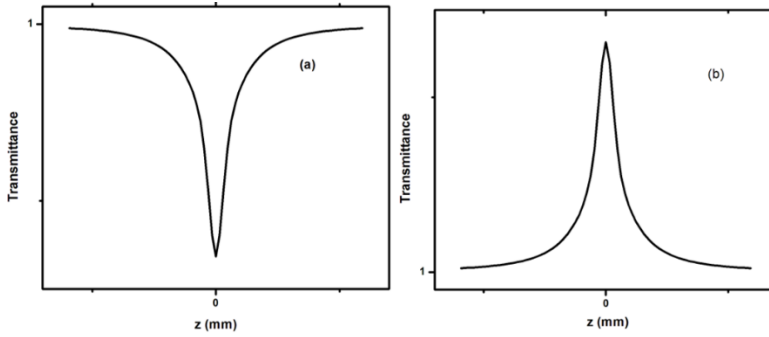


Figure.1.9 : (a) Reverse saturable absorption curve and (b) Saturable absorption curve of open aperture Z-scan

1.7.4 Theory of Open aperture Z-scan experiment

In the absence of an aperture, transmitted light measured by the detector in a Z-scan experiment is not sensitive to phase variations of the beam and hence it can be neglected. The intensity dependent nonlinear absorption coefficient [80]

$$\alpha(I) = \alpha + \beta I \longrightarrow (1)$$

The irradiance distribution at the sample is given as

$$I_z(z, r, t) = \frac{I(z, r, t)e^{-\alpha l}}{1 + q(z, r, t)} \longrightarrow (2)$$

where

$$q(z, r, t) = \beta I(z, r, t)L_{eff} \longrightarrow (3)$$

L_{eff} is the effective thickness of the sample which is related to the linear absorption coefficient α and the sample length L as

$$L_{eff} = \frac{1 - e^{-\alpha L}}{\alpha} \longrightarrow (4)$$

The total transmitted power,

$$P(z, t) = P_I(t)e^{-\alpha l} \frac{\ln[I + q(z, t)]}{q_0(z, t)} \longrightarrow (5)$$

where
$$P_t(t) = \frac{\pi\omega_0^2 I_0(t)}{2} \longrightarrow (6)$$

and

$$q_o(z, t) = \frac{\beta I_0 L_{eff} z_0^2}{z^2 + z_0^2} \longrightarrow (7)$$

For a temporally Gaussian pulse, the time integration of the transmitted power $P(z,t)$ gives the normalized energy transmittance $T(z)$ as follows

$$T(z) = \frac{1}{q_0 \sqrt{\pi}} \int_{-\infty}^{\infty} \ln(1 + q_0 e^{-t^2}) dt \longrightarrow (8)$$

Nonlinear absorption coefficient is obtained from the fitting of the experimental results to equation (8). Nonlinear absorption coefficient β is inversely proportional to the incident laser intensity which is cleared from equation (7).

If $q_0 < 1$, the equation of energy transmittance can be simplified as

$$T(z) = \sum_{m=0}^{\infty} \frac{[-q_0(z,0)]^m}{(m+1)^{3/2}} \longrightarrow (9)$$

where m is an integer. The value of q_0 is obtained from the theoretical fit to the open aperture Z-scan experimental data. Using the values of nonlinear absorption coefficient β , the imaginary part of third order susceptibility $\chi^{(3)}$ can be calculated using the equation

$$\text{Im}(\chi^{(3)}) = \frac{\lambda \varepsilon_0 n_0^2 c \beta}{4\pi} \longrightarrow (10)$$

where λ is the excitation wavelength, ε_0 is the permittivity of free space, n_0 is the linear refractive index of the sample and c is the velocity of light. Equation(10) gives the value of $\text{Im}(\chi^{(3)})$ in units of m^2V^{-2} .

Saturable absorption(SA) occurs when a sample is excited at its resonant wavelengths. In this case β is negative due to the depletion of the ground state population. SA is characterized by a parameter called saturation intensity I_s . The

simplest model to explain SA is a two level model in which the steady state can be expressed as

$$\frac{dN}{dt} = \frac{\sigma}{h\nu} I(N_g - N) - \frac{N}{\tau} = 0 \quad \longrightarrow \quad (11)$$

Here N is the concentration of the excited state molecules, N_g is the undepleted ground state concentration, σ is the absorption cross section, $h\nu$ is the photon energy and τ is the excited state life time. The absorption coefficient α is proportional to ground state population i.e;

$$\alpha = \sigma (N_g - N) \quad \longrightarrow \quad (12)$$

In the presence of SA, intensity dependent absorption coefficient $\alpha(I)$ can be written as

$$\alpha(I) = \alpha_0 \frac{1}{1 + \frac{\sigma I}{h\nu}} = \alpha_0 \frac{1}{1 + \frac{I}{I_s}} \quad \longrightarrow \quad (13)$$

where $I_s = h\nu / \sigma \tau$ is the saturation intensity.

The relation connecting nonlinear absorption coefficient β and I_s is given by

$$\beta = \frac{-\alpha_0}{I_s}$$

1.7.5. Closed aperture Z-scan experiment

Closed aperture z-scan method is based on the phenomena of self-refraction and self-phase modulation. In this experiment, the transmittance of the samples are measured through a finite aperture . The transmittance of the medium is taken along the z position in the far field. Two types of transmittance traces are obtained from the closed aperture z-scan method and are as shown in the figure 1.10. A material with negative nonlinear refraction n_2 exhibits a pre-focal peak followed by a post-focal valley[80,89]. In this case the diameter of beam decreases near the aperture resulting in large amount of throughput near the

detector. If the material exhibits a positive nonlinear refraction, a pre-focal valley followed by a post-focal peak is obtained [89].

For a medium having third-order optical nonlinearity, the index of refraction n can be written as

$$n = n_0 + n_2 I$$

where n_0 is the linear index of refraction, n_2 the intensity dependent refractive index and I denotes the irradiance of the laser beam within the sample.

Figure 1.10 shows a typical closed aperture response for (a) negative nonlinear refraction and (b) positive nonlinear refraction.

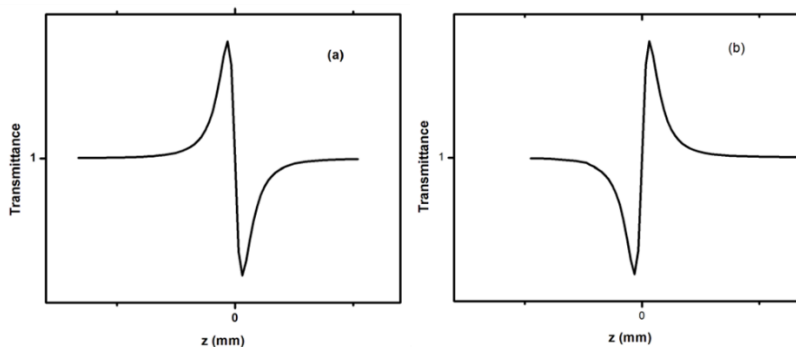


Figure 1.10: (a) Negative nonlinear refraction and (b) Positive nonlinear refraction for closed aperture Z-scan curve

A pre-focal transmittance valley and a post-focal transmittance peak is the Z-scan signature of positive refraction nonlinearity. A pre-focal transmittance peak and a post-focal transmittance valley is the z-scan signature of negative nonlinear refraction. For a positive n_2 , self-focusing occurs. For negative n_2 , self-defocusing occurs. This is the case of nonlinear refraction (symmetric peak and valley) curve in the absence of nonlinear absorption

The nonlinear phase change ($\Delta\phi$), can be obtained by the best theoretical fit of experimental data using the equation

$$T_{(z,\Delta\varphi)} = 1 - \frac{4 \Delta\varphi x}{(x^2+9)(x^2+1)}$$

Where nonlinear phase change, $\Delta\varphi = 2\pi \frac{\Delta n L_{\text{eff}}}{\lambda}$ and $x = z/z_0$, Δn is related to the nonlinear refraction coefficient, n_2 through the relation, $\Delta n = n_2 I$

Using the closed aperture measurement, the real part of third order susceptibility can be calculated.

1.8 Nonlinear Absorption –Mechanism by Two-photon absorption

The simultaneous absorption of two photons from the ground state to a higher energy electronic state is known as two photon absorption (TPA). The simultaneous absorption of these photons were taken from an incident radiation field [90]. The sum of the energies of the two photons gives the energy difference between the lower and upper states of the molecule. It is a nonlinear optical process since the absorption strength depends on the square of the light intensity. TPA is a third-order process which possesses several orders of magnitude weaker than linear absorption. The order of TPA can be rationalized by considering a second order process that creates a polarization with the frequency doubling. A schematic representation of two photon absorption process is as shown in figure 1.11 [78].

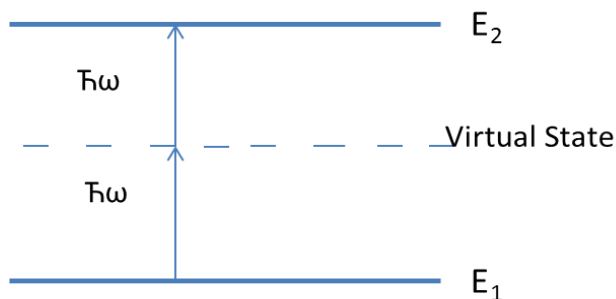


Figure.1.11: TPA Energy level diagram

Where E_1 is the energy level corresponds to the ground state and E_2 is the excited energy level. Two-photon absorption can be nonlinear transmission. Pulsed lasers are most often used because TPA is a third-order nonlinear optical process efficient at very high intensities. Single photon absorption occurs between opposite parity states. On the other hand, TPA occurs between states of same parity [78]. The probability of TPA is proportional to the fourth power of the electric field corresponding to the square of the intensity I and is given by the equation [91-101].

$$-\frac{dI}{dz} = \alpha I + \beta I^2$$

where α is the linear absorption coefficient and β is the two photon absorption coefficient.

and

$$\beta(\omega) = \frac{2\hbar\omega}{I^2} W_T^{(2)}(\omega)$$

where $W_T^{(2)}(\omega)$ is the transition rate for TPA, I is the irradiance, ω is the photon frequency and the thickness of the slice is dz [93].

To study the TPA phenomena, high intensity lasers are required. A frequency-doubled Nd:YAG are used as the excitation sources[92-101].

1.9 Scope of the thesis

Nonlinear crystals have found many applications in different areas of optoelectronics. The vast interest of these crystalline materials portray the importance of crystal growth studies in the nonlinear optics and photonics regime. Nonlinear photonic crystals have always been identified as strategic materials with a global business potential. These factors have lead the

investigators to concentrate on the development of new varieties of crystals with high purity. In this modern scientific world, the theories and technologies are developed hand in hand to grow specific crystals for specific utilities. Making use of the tremendous advantages of the gel method we aim to prepare good quality crystals of Lead Halides and Metal Tartrates. Some of the lead halides and metal tartrates were shown to exhibit higher optical nonlinearity in the presence of external fields and beam irradiations[102]. In the case of lead chloride sample, the beam irradiation and field application have impact on their optical linear and nonlinear aspects. But there is no valuable change in the nonlinear behaviour of lead bromide and lead fluoride crystals by the application of electric and magnetic fields. The beam irradiation does not alter the optical and nonlinear characteristics of metal tartrates. All the studies were carried out on super saturated solution of respective crystals. By employing the nonlinear measurements the role of these nonlinear crystals have been established in photonic applications.

Conclusions

In this chapter a general review on nonlinear crystals is presented. The works on nonlinear crystals by several researchers give a glimpse of knowledge about the utilities of these materials in various fields. The vast areas of nonlinear optics are also discussed. Various nonlinear processes are taking place in different metal compound crystals. The theory and experimentation of X-ray diffraction studies are briefly described. The experimental description of non-radiative decay studies by dual beam mode matched thermal lens technique are mentioned in this chapter. Nonlinear absorption measurements can be done using Z-scan experimental technique. The theory of two photon absorption mechanism is also discussed. In the subsequent chapters, synthesis, optical linear and nonlinear characterizations of Lead Halides and Metal Tartrates have been taken up.

References

- [1] Craxton, R. Stephen, Stephen D. Jacobs, J. Rizzo, and R. O. B. E. R. T. Boni. "Basic properties of KDP related to the frequency conversion of 1 μm laser radiation." *IEEE Journal of Quantum Electronics*, 17, no. 9 (1981): 1782-1786.
- [2] Mori, Yusuke, Ikuo Kuroda, Satoshi Nakajima, Takatomo Sasaki, and Sadao Nakai. "New nonlinear optical crystal: cesium lithium borate." *Applied Physics letters* 67, no. 13 (1995): 1818-1820.
- [3] Hirano, Shin-ichi, Toshinobu Yogo, Kō-ichi Kikuta, and Katsuya Yamagiwa. "Preparation of β -BaB₂O₄ Powders and Thin Films by Sol-Gel Method." *Journal of the American Ceramic Society* 75, no. 9 (1992): 2590-2592
- [4] Bierlein, John D., and Herman Vanherzeele. "Potassium titanyl phosphate: properties and new applications." *JOSA B* 6, no. 4 (1989): 622-633.
- [5] Lin, Shujie, Zhaoyang Sun, Bochang Wu, and Chuangtian Chen. "The nonlinear optical characteristics of a LiB₃O₅ crystal." *Journal of Applied Physics* 67, no. 2 (1990): 634-638.
- [6] Eckardt, R. O. B. E. R. T. C., Hisashi Masuda, Yuan Xuan Fan, and Robert L. Byer. "Absolute and relative nonlinear optical coefficients of KDP, KD*P, BaB₂O₄, LiIO₃, MgO:LiNbO₃, and KTP measured by phase-matched second-harmonic generation." *Quantum Electronics, IEEE Journal of* 26, no. 5 (1990): 922-933.
- [7] Nikogosyan, D. N. "Beta barium borate (BBO)." *Applied Physics A* 52, no. 6 (1991): 359-368.
- [8] Singh, Narsingh Bahadur, W. M. B. Duval, and B. N. Rosenthal. "Characterization of directionally solidified lead chloride." *Journal of Crystal Growth* 89, no. 1 (1988): 80-85.
- [9] Wu, Xu, J. P. Denis, G. Özen, Ph Goldner, and F. Pellé. "The UV, blue and green up-conversion luminescence of PbF₂+ GeO₂: Er₂O₃ pumped with 650 nm." *Applied Physics B* 56, no. 5 (1993): 269-273.
- [10] Zamkov, A. V., I. T. Kokov, and A. T. Anistratov. "The Acousto-Optical Properties and Photoelasticity of PbBr₂ Single Crystals." *Physica Status Solidi (a)* 79, no. 2 (1983): K177-K180.
- [11] Kaladevi, C., and C. K. Mahadevan. "Growth and Characterization On Sodium Lead Bromide Crystals." In *International Journal of Engineering Research and Technology*, 1, no. 8(2012): 1-12.

- [12] Plekhanov, V. "Optical constants of lead halides." *Physica Status Solidi (b)* 57, no. 1 (1973): K55-K59.
- [13] Nakagawa, H., M. Terakami, and K. Yasuda. "Elementary processes of photolysis in lead halide crystals." *Radiation Measurements* 33, no. 5 (2001): 819-822.
- [14] Kink, R., T. Avarmaa, V. Kisand, A. Lohmus, I. Kink, and I. Martinson. "Luminescence of cation excitons in and crystals in a wide excitation VUV region." *Journal of Physics: Condensed Matter* 10, no. 3 (1998): 693-700
- [15] Iwanaga, Masanobu, and Tetsusuke Hayashi. "Exciton-relaxation dynamics in lead halides." *arXiv preprint Cond-Mat/0208320* (2002):1-5
- [16] Nikl, M., and K. Polak. "Luminescence kinetics of PbF₂ single crystals." *Physica Status Solidi (a)* 117, no. 1 (1990): K89-K92.
- [17] Kink, R., A. Lohmus, and M. Selg. "Self-trapping and hot luminescence of excitons in rare gas solids." *Physica Status Solidi (b)* 107, no. 2 (1981): 479-490.
- [18] Ahmed, G., Y. Sharma, and B. L. Ahuja. "Electronic properties of PbCl₂ and PbBr₂ using Compton scattering technique." *Applied Radiation and Isotopes* 67, no. 6 (2009): 1050-1056.
- [19] Eijkelenkamp, A. J. H., and K. Vos. "Reflectance Measurements on Single Crystals of PbFCl, PbFBr, and PbBr₂." *Physica Status Solidi (b)* 76, no. 2 (1976): 769-778.
- [20] Beaumont, J. H., A. J. Bourdillon, and J. Bordas. "Optical properties of PbI₂ and PbF₂." *Journal of Physics C: Solid State Physics* 10, no. 5 (1977): 761-771
- [21] Málková, Zuzana, Karel Nitsch, and Josef Novák. "Determination of oxidic impurities in some lead halides." *Analytica Chimica Acta* 355, no. 2 (1997): 171-174.
- [22] De Gruijter, W. C., and J. Kerssen. "Luminescence of PbCl₂ and PbBr₂ single crystals II. Luminescence and EPR of uv irradiated crystals." *Journal of Solid State Chemistry* 5, no. 3 (1972): 467-476.
- [23] Almeida, Vilson R., Carlos A. Barrios, Roberto R. Panepucci, and Michal Lipson. "All-optical control of light on a silicon chip." *Nature* 431, no. 7012 (2004): 1081-1084.

Chapter 1

- [24] Zentai, G., L. Partain, R. Pavlyuchkova, C. Proano, M. Schieber, K. Shah, P. Bennett, L. Melekhov, and H. Gilboa. "Comparison of mercuric iodide and lead iodide X-ray detectors for X-ray imaging applications." *Nuclear Science, IEEE Transactions on* 53, no. 5 (2006): 2506-2512.
- [25] Fujita, M., M. Itoh, Y. Bokumoto, H. Nakagawa, D. L. Alov, and M. Kitaura. "Optical spectra and electronic structures of lead halides." *Physical Review B* 61, no. 23 (2000): 15731-15737.
- [26] Hermann, J. A. "Nonlinear optical absorption in thick media." *JOSA B* 14, no. 4 (1997): 814-823.
- [27] Giordmaine, J. A., and Robert C. Miller. "Tunable Coherent Parametric Oscillation in LiNb O 3 at Optical Frequencies." *Physical Review Letters* 14, no. 24 (1965): 973-976.
- [28] Harris, S.E.: Tunable optical parametric oscillators, *Proc. IEEE* 57, 2096–2113 (1969)
- [29] Edelstein, D. C., E. S. Wachman, and C. L. Tang. "Broadly tunable high repetition rate femtosecond optical parametric oscillator." *Applied Physics Letters* 54, no. 18 (1989): 1728-1730.
- [30] Bosenberg, W. R., and Dean R. Guyer. "Single-frequency optical parametric oscillator." *Applied Physics Letters* 61, no. 4 (1992): 387-389.
- [31] Gon, H. B. "Ferroelectricity in calcium tartrate single crystals grown by gel technique." *Journal of Crystal Growth* 102, no. 3 (1990): 501-504.
- [32] Arora, S. K., Vipul Patel, Brijesh Amin, and Anjana Kothari. "Dielectric behaviour of strontium tartrate single crystals." *Bulletin of Materials Science* 27, no. 2 (2004): 141-147.
- [33] Kumar, B. Suresh, MH Rahim Kutty, MR Sudarsana Kumar, and K. Rajendra Babu. "Growth and characterization of pure and lithium doped strontium tartrate tetrahydrate crystals by solution-gel technique." *Bulletin of Materials Science* 30, no. 4 (2007): 349-355.
- [34] Desai, C. C., and A. H. Patel. "Synthesis, characterization and properties of ferroelectric rubidium hydrogen tartrate single crystals." *Bulletin of Materials Science* 11, no. 1 (1988): 31-37.
- [35] Torres, Manuel E., Trinidad López, Josefina Stockel, Xavier Solans, Maite García-Vallés, Enrique Rodríguez-Castellón, and Cristina González-Silgo.

- "Structural characterization of doped calcium tartrate tetrahydrate." *Journal of Solid State Chemistry* 163, no. 2 (2002): 491-497.
- [36] Rahimkuty, M. H., K. Rajendra Babu, K. Sreedharan Pillai, MR Sudarsana Kumar, and C. M. K. Nair. "Thermal behaviour of strontium tartrate single crystals grown in gel." *Bulletin of Materials Science* 24, no. 2 (2001): 249-252.
- [37] Freeda, M. Mary, R. Krishna Priya, T. H. Freeda, and S. Mary Delphine. "Crystallization and characterization of mixed crystals of strontium calcium barium tartrate." *Archives of Applied Science Research* 4, no. 1 (2012): 128-136.
- [38] Suryanarayana, K., S. M. Dharmaprakash, and K. Sooryanarayana. "Optical and structural characteristics of strontium doped calcium tartrate crystals." *Bulletin of Materials Science* 21, no. 1 (1998): 87-92.
- [39] Selvarajan, P., B. N. Das, H. B. Gon, and K. V. Rao. "Infrared spectroscopic and thermal studies of calcium tartrate single crystals grown by silica-gel technique." *Journal of Materials Science Letters* 12, no. 15 (1993): 1210-1211.
- [40] Suthar, S. R., and M. J. Joshi. "Growth and characterization of Mn²⁺ doped calcium l-tartrate crystals." *Crystal Research and Technology* 41, no. 7 (2006): 664-670.
- [41] Arora, S. K., Vipul Patel, Bhupendra Chudasama, and Brijesh Amin. "Single crystal growth and characterization of strontium tartrate." *Journal of Crystal Growth* 275, no. 1 (2005): e657-e661.
- [42] Sahaya Shajan, X., and C. Mahadevan. "FT-IR spectroscopic and thermal studies on pure and impurity added calcium tartrate tetrahydrate crystals." *Crystal Research and Technology* 40, no. 6 (2005): 598-602.
- [43] Quasim, I., A. Firdous, B. Want, S. K. Khosa, and P. N. Kotru. "Single crystal growth and characterization of pure and sodium-modified copper tartrate." *Journal of Crystal Growth* 310, no. 24 (2008): 5357-5363.
- [44] Arora, S. K., Vipul Patel, Anjana Kothari, and Brijesh Amin. "Gel growth and preliminary characterization of strontium tartrate trihydrate." *Crystal growth & design* 4, no. 2 (2004): 343-349.
- [45] Firdous, A., I. Quasim, M. M. Ahmad, and P. N. Kotru. "Growth and characterization of strontium tartrate pentahydrate crystals." *Crystal Research and Technology* 43, no. 10 (2008): 1015-1021.

Chapter 1

- [46] Arora, S. K., Vipul Patel, R. G. Patel, Brijesh Amin, and Anjana Kothari. "Electrical characterization of strontium tartrate single crystals." *Journal of Physics and Chemistry of Solids* 65, no. 5 (2004): 965-973.
- [47] Greena, J. Angel Mary, X. Sahaya Shajan, and H. Alex Devadoss. "Electrical conductivity studies on pure and barium added strontium tartrate trihydrate crystals." *Indian Journal of Science and Technology* 3, no. 3 (2010): 250-252.
- [48] Suryanarayana, K., and S. M. Dharmaparakash. "Physico-chemical characterization of calcium strontium tartrate crystals." *Journal of Physics and Chemistry of Solids* 58, no. 10 (1997): 1599-1602.
- [49] Suryanarayana, K., and S. M. Dharmaparakash. "Crystal growth and characterization of barium doped calcium tartrate tetrahydrate crystals." *Materials Letters* 42, no. 1 (2000): 92-96.
- [50] Dharmaparakash, S. M., and K. Suryanarayana. "Physico-chemical characterization of calcium strontium tartrate crystals." *Journal of Physics and Chemistry of Solids* 10, no. 58 (1997): 1599-1602.
- [51] Patel, Ambalal Ranchhodhbhai, and A. Venkateswara Rao. "Crystal growth in gel media." *Bulletin of Materials Science* 4, no. 5 (1982): 527-548.
- [52] Pillai, K. Sreedharan, and M. A. Ittyachen. "Observations on the growth of single crystals of lead molybdate from gels." *Journal of Crystal Growth* 39, no. 2 (1977): 287-290.
- [53] Saban, K. V., T. Jini, and G. Varghese. "Influence of magnetic field on the growth and properties of calcium tartrate crystals." *Journal of Magnetism and Magnetic Materials* 265, no. 3 (2003): 296-304.
- [54] Rahimkutty MH, PhD Thesis of Kerala University, 1988.
- [55] Buckley, Harold Eugene, and A. C. Walker. "Crystal growth." *American Journal of Physics* 19, no. 7 (1951): 430-430.
- [56] Hensch, Heinz K. *Crystal growth in gels*. Courier Corporation, 1970.
- [57] De Yoreo, James J., and Peter G. Vekilov. "Principles of crystal nucleation and growth." *Reviews in Mineralogy and Geochemistry* 54, no. 1 (2003): 57-93.
- [58] Rethinam, F. Jesu, D. Arivu Oli, S. Ramasamy, and P. Ramasamy. "Growth and Characterisation of Pure and Nickel-doped Strontium Tartrate Tetrahydrate Single Crystals." *Crystal Research and Technology* 28, no. 6 (1993): 861-865.

Nonlinear Crystals and Optical Nonlinear Processes

- [59] Joshi, S. J., B. B. Parekh, K. D. Vohra, and M. J. Joshi. "Growth and characterization of gel grown pure and mixed iron-manganese levo-tartrate crystals." *Bulletin of Materials Science* 29, no. 3 (2006): 307-312.
- [60] Günter, P., and H. Arend. "Noncentrosymmetry Observed in $\text{CaC}_4\text{H}_4\text{O}_6 \cdot 4\text{H}_2\text{O}$ Crystals by Nonlinear Optical Measurements." *Physica Status Solidi (b)* 143, no. 2 (1987): 749-754.
- [61] S.O.Pillai, *Solid State Physics*, New age International , 6th Edition, 2005.
- [62] Pavia,Lampman,Kriz, *Introduction to Spectroscopy*,Thomson Brooks/Cole, 3rd Edition, 2001
- [63] Charles Kittel, Paul McEuen, , *Introduction to solid state physics*. 7th edition, Wiley India, 2006.
- [64] Bahaa.E.A.Saleh, Malvin carl Teich, *Fundamentals of Photonics*,John Wiley & Sons.Inc., 1991
- [65] Pankove, Jacques I. *Optical processes in semiconductors*. Courier Corporation, 2012
- [66] Fox, Anthony Mark, and Mark Fox. *Optical properties of solids*. Vol. 2010. New York: Oxford university press, 2001.
- [67]. Almond, Darryl P., and Pravin Patel. *Photothermal science and techniques*. Vol. 10. Springer Science & Business Media, 1996.
- [68] Bialkowski, Stephen. *Photothermal spectroscopy methods for chemical analysis*. Vol. 134. John Wiley & Sons, 1996.
- [69]. Boccara, A. C., Warren Jackson, Nabil M. Amer, and D. Fournier. "Sensitive photothermal deflection technique for measuring absorption in optically thin media." *Optics letters* 5, no. 9 (1980): 377-379.
- [70] Jackson, Warren B., Nabil M. Amer, A. C. Boccara, and D. Fournier. "Photothermal deflection spectroscopy and detection." *Applied optics* 20, no. 8 (1981): 1333-1344.
- [71] A.C.Tam," *Photothermal Investigation of solids and Fluids* "Academic press Inc. Newyork, 1989
- [72] Boyd, Robert W. *Nonlinear optics*. Academic press, 2003.

Chapter 1

- [73] Shen, Yuen-Ron The Principles of Nonlinear Optics. Wiley-Interscience. (2002).
- [74] Agrawal, Govind Nonlinear Fiber Optics (4th edition.). Academic Press. (2006). .
- [75] Paschotta, Rüdiger. Encyclopedia of laser physics and technology. Vol. 1. Berlin: Wiley-vch, 2008.
- [76] Robert W. Boyd ,3rd edition, Parametric versus Nonparametric Processes, Nonlinear Optics pp. 13-15.(2003)
- [77] Armstrong, J. A., N. Bloembergen, J. Ducuing, and P. S. Pershan. "Interactions between light waves in a nonlinear dielectric." Physical Review 127, no. 6 (1962): 1918- 1939.
- [78] B.B.Laud, Lasers and Nonlinear Optics, second edition, Wiley Eastern limited, (1991).
- [79] Boyd, Robert . Nonlinear Optics 3rd edition, Academic Press, (2008)
- [80] Sheik-Bahae, Mansoor, Ali A. Said, T-H. Wei, David J. Hagan, and Eric W. Van Stryland. "Sensitive measurement of optical nonlinearities using a single beam." Quantum Electronics, IEEE Journal of 26, no. 4 (1990): 760-769.
- [81] Olbright, G. R., and N. Peyghambarian. "Interferometric measurement of the nonlinear index of refraction, n_2 , of CdSxSe1- x-doped glasses." Applied Physics Letters 48, no. 18 (1986): 1184-1186.
- [82] Friberg, Stephen R., and Peter W. Smith. "Nonlinear optical glasses for ultrafast optical switches." Quantum Electronics, IEEE Journal of 23, no. 12 (1987): 2089-2094.
- [83] Adair, Robert, L. L. Chase, and Stephen A. Payne. "Nonlinear refractive-index measurements of glasses using three-wave frequency mixing." JOSA B 4, no. 6 (1987): 875-881.
- [84] Owyong, Adelbert. "Ellipse rotation studies in laser host materials." Quantum Electronics, IEEE Journal of 9, no. 11 (1973): 1064-1069.
- [85] Williams, William E., M. J. Soileau, and Eric W. Van Stryland. "Optical switching and n_2 measurements in CS 2." Optics communications 50, no. 4 (1984): 256-260.

- [86] Hermann, J. A., and R. G. McDuff. "Analysis of spatial scanning with thick optically nonlinear media." *JOSA B* 10, no. 11 (1993): 2056-2064.
- [87] Hill, J. R., Gr Parry, and A. Miller. "Non-linear refractive index changes in CdHgTe at 175 K with 10.6 μm radiation." *Optics Communications* 43, no. 2 (1982): 151-156.
- [88] Boggess, T. F., S. C. Moss, I. W. Boyd, and A. L. Smirl. "Picosecond nonlinear-optical limiting in silicon." In *Ultrafast Phenomena IV*,. Springer Berlin Heidelberg, 1984. pp. 202-204.
- [89] Irimpan, Litty, V. P. N. Nampoori, and P. Radhakrishnan. "Spectral and nonlinear optical characteristics of nanocomposites of ZnO–CdS." *Journal of Applied Physics* 103, no. 9 (2008): 094914,1-8.
- [90] Richard L Sutherland; "Handbook of nonlinear optics", CRC press(2003).
- [91] Singh, Stoicheff, and B. P. Stoicheff. "Double-Photon Excitation of Fluorescence in Anthracene Single Crystals." *The Journal of Chemical Physics* 38, no. 8 (1963): 2032-2033.
- [92] Chluba, J., and R. A. Sunyaev. "Induced two-photon decay of the 2s level and the rate of cosmological hydrogen recombination." *Astronomy & Astrophysics* 446, no. 1 (2006): 39-42.
- [93] Spitzer Jr, Lyman, and Jesse L. Greenstein. "Continuous emission from planetary nebulae." *The Astrophysical Journal* 114 (1951): 407.420.
- [94] G Gurzadyan, G. A. "Two-photon emission in planetary nebula IC 2149." *Publications of the Astronomical Society of the Pacific* (1976): 891-895.
- [95] Hayat, Alex, Pavel Ginzburg, and Meir Orenstein. "Observation of two-photon emission from semiconductors." *Nature photonics* 2, no. 4 (2008): 238-241.
- [96] Hayat, Alex, Amir Nevet, Pavel Ginzburg, and Meir Orenstein. "Applications of two-photon processes in semiconductor photonic devices: invited review." *Semiconductor Science and Technology* 26, no. 8 (2011): 083001.1-18
- [97] Kogej, T., D. Beljonne, F. Meyers, J. W. Perry, S. R. Marder, and J. L. Bredas. "Mechanisms for enhancement of two-photon absorption in donor–acceptor conjugated chromophores." *Chemical Physics Letters* 298, no. 1 (1998): 1-6.
- [98] Kamada, Kenji, Koji Ohta, Takashi Kubo, Akihiro Shimizu, Yasushi Morita, Kazuhiro Nakasuji, Ryohei Kishi et al. "Strong Two-Photon Absorption of

Chapter 1

- Singlet Diradical Hydrocarbons." *Angewandte Chemie* 119, no. 19 (2007): 3614-3616.
- [99] Dragonmir, Adrian, John G. McInerney, and David N. Nikogosyan. "Femtosecond measurements of two-photon absorption coefficients at $\lambda = 264$ nm in glasses, crystals, and liquids." *Applied Optics* 41, no. 21 (2002): 4365-4376.
- [100] Nikogosyan, David N., and Dmitrij A. Angelov. "Formation of free radicals in water under high-power laser UV irradiation." *Chemical Physics Letters* 77, no. 1 (1981): 208-210.
- [101] Underwood, J., and C. Wittig. "Two-photon photodissociation of H₂O via the \tilde{B} state." *Chemical physics letters* 386, no. 1 (2004): 190-195.
- [102] G.Lilibai ,PhD Thesis, "Nonlinear optical properties of certain tartrate and halide crystals grown by gel technique in the presence of electric field magnetic field and dopants ", December 2012.(My Research collaborator)

Chapter 2

Spectral and Optical Nonlinear studies on Lead Bromide (PbBr_2) crystals

Abstract

The synthesis and characterization of lead bromide crystals are discussed. The structure of the gel medium for the growth of good quality crystals is also given in this chapter. The optical characteristics of this crystalline material are studied using absorption and photoluminescence mechanisms. The thermal diffusivity measurements are performed using Thermal lens experiment. The optical nonlinearity measurements are done by employing Z-scan experiment without an aperture. The optical limiting studies on these crystalline samples of PbBr_2 in solution phase are also carried out.

2.1 Introduction

Lead bromide (PbBr_2) crystals possess good mechanical properties which make them suitable for acousto-optical devices. Electro-optic and acousto-optic devices are used with lasers as Q-switches, beam deflectors, modulators, and mode-lockers. The electro-optic effect is a change in the index of refraction for certain crystals as a function of applied voltage. The index change is dependent on the direction and polarization of the incident beam. The acousto-optic effect involves an interaction between sound waves and light waves traveling through certain types of crystals [1]. The acousto-optic effect can be used to control the frequency, intensity, and direction of an optical beam. The optical transparency range of PbBr_2 is very large so that it is very useful for wideband acousto-optical tunable filter applications [2-4]. Q.Ren et al reported on Lead bromide (PbBr_2) crystals in $[0\ 0\ 1]$ orientation obtained by the Bridgman growth method[5]. They determined the orientation of the principal refractive axes of the crystals and their principal refractive indices by the least deviation angle at eight selected wavelengths. Using Sellmeier's formula, the optical axial angle and the dispersion of refractive index in the visible spectral range were calculated by them. N.B.Singh et al reported the optical transparency range of PbBr_2 crystals [4]. They performed a comparative study of thermo solutal convection by growing lead bromide single crystals in a transparent Bridgman furnace. T.Henninsen et al described the infrared birefringence interferometer capable of evaluating the bulk quality of crystals[6]. They noted that the birefringence interferometer, like the more familiar Mach—Zehnder interferometer is a sensitive tool for measuring the refractive index homogeneity in bulk materials, but it does not require the optical surface quality and parallelism needed for Mach—Zehnder measurements. It is ideally suited for the preliminary screening of large quantities of material without the need for precision fabrication.

Lead bromide belongs to the orthorhombic symmetry class [2]. PbBr₂ exhibits extraordinary properties, including an anomalously slow longitudinal wave velocity in the [0 1 0] direction, a large birefringence and a high figure of merit about twelve times higher than that of PbMoO₂ [3]. Lead bromide exhibit Schottky disorder, and anion conductivity [7-10]. Lead bromide show complete mutual solid solubility and the solid solutions in the system PbCl₂-PbBr₂ shows the PbCl₂-type orthorhombic symmetry [11-12]. J.F.Verwey worked on the conductivity studies of lead bromide single crystals both undoped and doped with monovalent and trivalent cations and oxygen. Irradiation of pure lead bromide with ultraviolet light gives a characteristic damaging as is made visible by electron and optical microscopy [13]. Point defects in lead bromide are thermally generated according to a Schottky mechanism. It has been known for a long time that the transport number of the bromide ions in lead bromide is unity up to the melting point [14]. The luminescence properties of lead bromide are very interesting [15-18]. Masanobu Iwanaga reported that the excitonic transitions in lead halides are partly explained by the 6s-to-6p transition in lead ions [19-20]. The present chapter discusses the preparation, spectral, thermal, optical, nonlinear and the optical limiting studies carried out on lead bromide crystals.

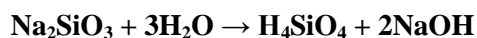
2.2 Synthesis

Lead bromide crystals are prepared by employing gel method. This method has attracted because it can be used for growing a variety of crystals. Gels are formed from the suspension of the solution by the establishment of a three-dimensional system of cross linkages between the molecules of one component. The second component permeates this system as a continuous phase. When the dispersion medium is water, the material should be called hydrogel.

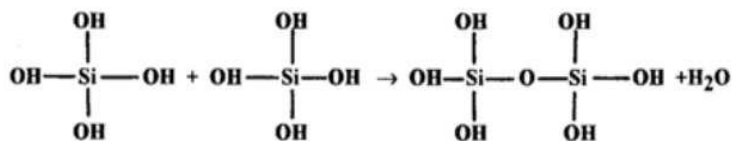
2.2.1 Structure of Hydro Silica gel

Silica hydrogel has been commonly used, due to its far better suitability compared to other organic gels, to grow good quality single crystals[21]. The process of gelling can be brought about in a number of ways, by cooling of a sol, by chemical reaction or by the addition of precipitating agents or incompatible solvents. The time taken for the gelling process varies widely from a few minutes to many days, depending on the nature of the material, its temperature and history.

Gels have minute pores of various sizes. The rate of diffusion of reagents through gels depends, obviously, on the size of the diffusing particles relative to the pore size in the gel and the possible interaction between the solute and the internal gel surface. Silica hydrogel is the most ideal medium for growth experiments. Therefore the study of its structure is imperative. When sodium meta silicate goes into solution, it may be concluded that monosilicic acid is produced, in accordance with the dynamic equilibrium.



Monosilicic acid can polymerize with the liberation of water as follows.



This can happen again and again until a three dimensional network of Si-O links is established, as in silica. The polymerization process continues and water accumulates on the top of the gel surface. This phenomenon is called Synerisis. During this process two types of ions are produced (H_3SiO_4^- and $\text{H}_2\text{SiO}_4^{2-}$). The time required for gelation is very sensitive to the pH. Their relative amounts depend on the hydrogen ion concentration. High pH values favour the formation of $\text{H}_2\text{SiO}_4^{2-}$ ion, which is more reactive. The H_3SiO_4^- ion is

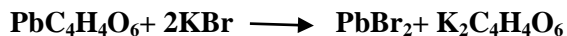
moderately favoured by low pH values and is responsible for the initial formation of a long chain of polymerization products. The cross linkages are formed between these chains and these contribute to the sharp increase in viscosity that gives the indication of the onset of gelation. The stability of the silicon-oxygen bonds makes the above polymerization process largely irreversible. It is also indubitable that it is the basic gel structure that controls the crystal growth characteristics.

In the single diffusion system, the average crystal growth is largest near the top of the gel column, where the concentration gradient is higher than that near the bottom. It is clear that the super saturation of the gel medium self-adjusts to the needs of the growth process. This leads to the formation of crystals with a high degree of perfection. A very prominent role played by the gel is in suppressing nucleation and thereby reducing the competitive nature of the growth. It is this nucleation control that is the key to the success of the gel method.

2.2.2 Preparation of PbBr₂ single crystals

The crystalline PbBr₂ samples for our studies were prepared using gel method introduced by H.K.Henish. For a good quality crystal, a stock solution of sodium meta silicate (SMS) having specific gravity 1.03 was prepared by adding sufficient amount of sodium meta silicate to 500 ml of distilled water. The pH of the solution was adjusted to 6, 7 and 8. The acidic component treated was 1M tartaric acid and kept the solution of SMS and Tartaric acid for gelling. 4N Potassium Bromide solution was poured over the gel in a test tube which was incorporated with a colloidal precipitate of 1N lead tartrate. Growth experiments were conducted for different densities of the gel ranging from 1.02 to 1.06. Even though the growth kinetics were the same, the growth rates, amount and critical size of the PbBr₂ formed were different by varying the molarity, density of gel and pH values. Good crystals were separated from gel using distilled water and dried for characterization.

The chemistry behind the crystal formation is as follows



2.3 Structural Characterization by X-ray Diffraction Studies

X-ray diffractogram is an efficient tool for the determination of the crystallinity of our samples. The sol-gel derived PbBr_2 samples were subjected to X-ray diffraction studies (XPRT-PRO using K-Alpha 1.54060 \AA^0 (XRDMML)). The grown crystal of lead bromide at pH 6 was characterized by X-ray diffraction method. The diffraction patterns were analyzed and the calculated 'd' spacing and peak spacing intensities were compared with those of lead bromide reported in JCPDS files. The occurrence of intense peaks at specific Bragg angle at 2θ indicates the crystallinity of the grown crystal. The X-ray diffraction pattern of PbBr_2 is as shown in figure 2.1. The crystal structure of PbBr_2 is confirmed to be orthorhombic.

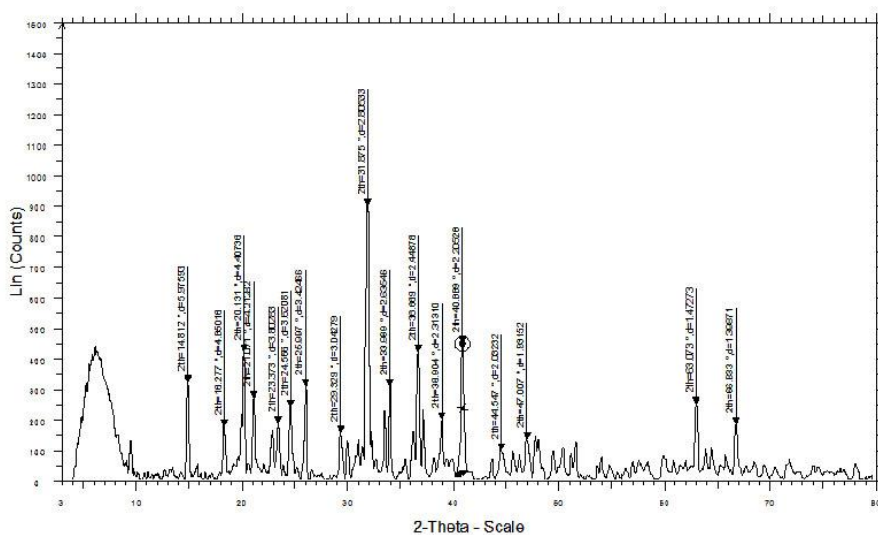


Figure 2.1: XRD of gel derived PbBr_2 crystal

2.4 Optical Characterizations

The optical properties of lead bromide crystals were studied using optical absorption measurements, optical band gap determination and photoluminescence studies. For these studies, the solution samples were employed. The prepared crystal samples were powdered using mortar and pestle, weighed and dissolved in 20 ml of single distilled water to obtain a concentration 0.02 gm/ml. For the dissolution, a magnetic stirrer was used and the solvent evaporation was prevented by using a sealed glass container. Linear absorption of the crystal samples in solution phase was recorded using Jasco V-570 UV/VIS/IR Spectrophotometer.

2.4.1 Linear Absorption studies of PbBr₂ in solution phase

The room temperature absorption spectrum of PbBr₂ of concentration 0.02 gm/ml gives the variation of absorbance against the wavelength in nm scale. Figure 2.2 reveals the linear optical absorption response of lead bromide single crystal in single distilled water.

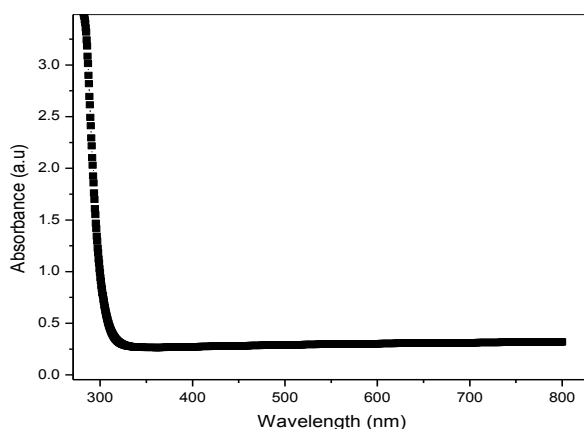


Figure.2.2: Linear absorption spectrum of PbBr₂

The size of the absorbing system and the probability that the electronic transition will take place control the absorptivity. The absorption edge of our

sample is located in the UV region at 270 nm. The band gap at this wavelength corresponds to 4.2 eV. The absorption spectra of PbBr₂ solution indicates the wide transparency of the crystal samples in solution phase in the entire ultraviolet and visible regions. The optical transparency of PbBr₂ is reported and this wide transparency of the material makes them to apply in multiband acousto-optical tunable filters [22]. The peak at this particular wavelength is due to the electronic transition from the valence band to the level occupied by PbBr⁺ cation.

2.4.2 Optical band gap studies

The optical band gap studies on PbBr₂ in solution phase in single distilled water were done using the linear absorption spectra of the respective sample. The linear absorption coefficient α can be determined from absorption spectra, which is related to the band gap E_g as

$$(\alpha h\nu)^2 = k (h\nu - E_g)$$

where $h\nu$ is the incident light energy;

k is a constant

and E_g is the optical band gap of lead bromide.

A graph of $E_g = h\nu$ verses $(\alpha h\nu)^2$ gives the direct band gap of PbBr₂ for a concentration of 0.02 gm/ml. Figure 2.3 shows the direct band gap behaviour of PbBr₂ sample. A graph of $E_g = h\nu$ verses $(\alpha h\nu)^{1/2}$ gives the indirect band gap of PbBr₂ crystal in solution phase. Figure 2.4 shows the indirect band gap response of lead bromide crystal sample.

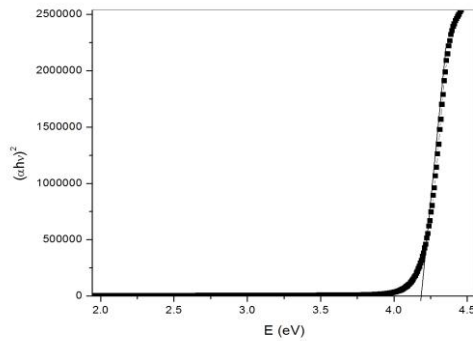


Figure.2.3: Direct band gap plot of PbBr₂ sample

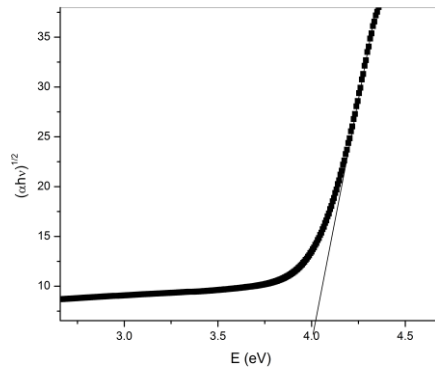


Figure.2.4: Indirect band gap plot of PbBr₂ sample

We obtained the direct optical band gap value for PbBr₂ as 4.2 eV and indirect band gap value is 4 eV. From the above figures, it is evident that the lead bromide crystal has the band gap in connection with the 6s-to-6p gap in lead ions and tend to become highly luminescent coming from the odd transition. In solutions linear optical absorption spectrum leads to optical band gap edge like structure yielding band gap of 4.2 eV as described in the thesis. It should be . The energy corresponding to the absorption in PbBr₂ can be attributed to the

creation of Frenkel excitons localized on the Pb^{2+} ions. The optical band gap of PbBr_2 is arising from the absorption in the band edge due to the creation efficiency of free carriers within the crystal [23].

2.4.3 Fluorescence emission characteristics of PbBr_2 from photoluminescence studies

The emission and excitation studies were carried out by taking the room temperature fluorescence spectra of these PbBr_2 samples using a Cary Eclipse fluorescence spectrophotometer (Varian). Lead bromide crystal samples in single distilled water were subjected to fluorescence excitation in order to measure the emission peaks of the material at different excitation wavelengths. The PbBr_2 sample solution at the above particular concentration was excited at a wavelength of 240 nm and gave four main emission peaks around 422 nm, 441 nm, 492 nm and 527 nm respectively as shown in the figure 2.5(a).

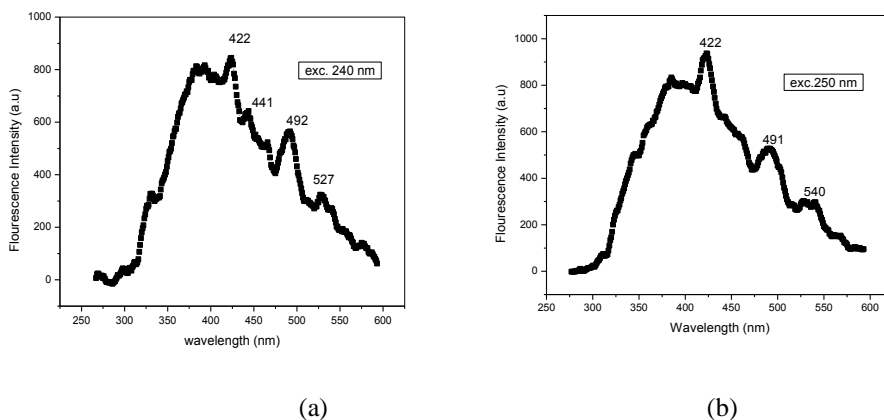


Figure 2.5. Fluorescence emission spectra of PbBr_2 at an excitation wavelength (a) 240 nm (b) 250 nm

From the figure 2.5(b), it is evident that for an excitation of 250 nm wavelength, three strong emission peaks were obtained at 422, 491 and 540 nm respectively. The excitonic transitions in lead bromide crystals are explained by the 6s-to-6p transition in lead ions. Luminescence in PbBr_2 is composed of broad

Gaussian bands with large Stokes shifts and is indicative of strong exciton acoustic–phonon interaction. The exciton relaxation in PbBr₂ results in spontaneous electron–hole separation. Optical and luminescent properties of PbBr₂ and PbCl₂ are similar in the electronic-band structures. Our work on luminescence of PbCl₂ single crystals is already reported [24]. The PbBr₂ solution shows many peaks due to the Stokes shift by the crystal field interactions resulting from the strong interaction between phonon and Pb²⁺ ions. From the fluorescence spectra given in the figure, it is evident that the emission peaks at 491 and 540 nm are assigned to the excitonic emissions. Thus the emission bands obtained for the PbBr₂ are due to the 6s_{6p}-6s² transition of the Pb²⁺ cation strongly influenced by the first Br⁻ coordination sphere. The emission peaks at 422, 492 and 527nm in PbBr₂ can be attributed to the association of Pb²⁺ cation with nearby intrinsic defect due to anion or cation vacancies [25-29].

2.5. Thermal lensing in PbBr₂ crystal

Thermal lens spectroscopy is a highly sensitive technique to measure the thermal properties of crystalline materials like lead bromide [30-33]. The experimental set up of this technique is given in chapter.1.

The thermal diffusivity measurements of lead bromide crystals have not been reported so far. Thermal diffusivity measurements were done by using a mode matched thermal lens experiment. The thermal lens technique is based on the measurement of the temperature rise that is produced in an illuminated sample as a result of non radiative relaxation of the energy absorbed from a laser. Because the technique is based on direct measurement of the absorbed optical energy, its sensitivity is higher than conventional absorption techniques. However, advantages of the thermal lens technique are not only limited to its ultra-sensitivity but also include other unique characteristics including small-volume sample capability and dependency on thermo-optical properties of solvents. Thermal lens experiment to calculate thermal diffusivity were made in water medium. Since the crystal solution was made in water, small amount of

Rhodamine-6G was dissolved in order to get thermal lens data. Presence of dye will not affect the thermal property of the solution. Hence the result we obtained corresponds to that of the crystal solution. Rhodamine-6G solution was prepared by adding 0.01 g of Rhodamine-6G in 10 ml of single distilled water. The solution of 0.5 ml Rhodamine-6G and 2.5 ml of PbBr_2 was taken in a 1 cm cuvette of 5 mm path length for various sets of measurements. The presence of Rhodamine enhanced the absorption of the crystal sample and did not alter the thermal diffusivity values.

2.5.1 Thermal diffusivity measurements

In the dual-beam thermal lens measurement, when the PbBr_2 with Rhodamine-6G sample was excited by a TEM_{00} Gaussian laser beam, a temperature rise was produced by non radiative decay processes following the optical energy absorption. Since the refractive index of the sample was changed with temperature, a refractive index gradient was produced, creating a lens-like optical element, the so called thermal lens. The variation of the intensity at the centre of the probe beam caused by the thermal lens has also been reported [33]. Thermal blooming measurement was done by employing a laser beam of appropriate frequency focused using a long focal length lens.

The decay time t_c and fitting parameter θ were obtained by the theoretical fit of the measured values of the probe beam intensity versus time plot.

The parameter θ is related to the thermal power radiated as heat P_{th} through the relation given as

$$\theta = \frac{P_{th}}{\lambda k} \left(\frac{dn}{dt} \right)$$

where λ is the laser wavelength, k is the thermal conductivity and dn/dt is the refractive index gradient.

From the values of t_c and beam waist radius w at the sample position, the thermal diffusivity D of PbBr₂ sample can be calculated as

$$D = w^2 / 4t_c$$

A typical plot of photo detector output against time is as shown in figure 2.6

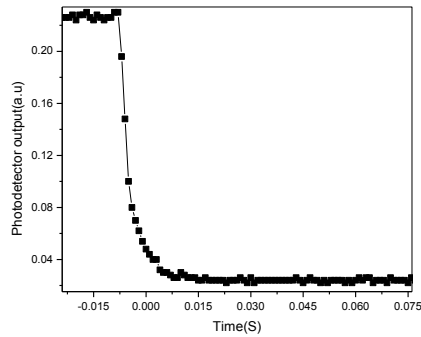


Figure.2.6: A thermal lens signal of Rh-PbBr₂ at a power of 50 mW

The thermal lens(TL) curve of the lead bromide sample is as shown in figure.2.7

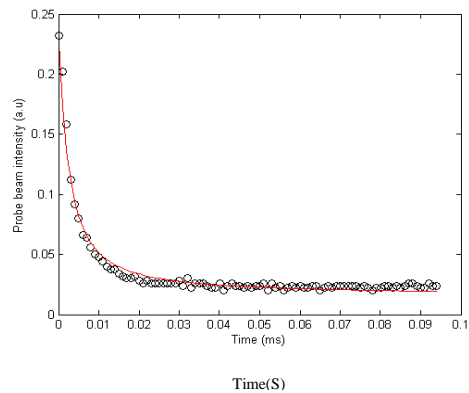


Figure.2.7: Time dependent TL plot of PbBr₂

From the figure.2.7, it is clear that the amplitude of the TL signal reaches a steady state, reflecting an equilibrium in the concentration of the absorbing species. By illuminating the sample solution using laser radiation,

some of the radiation is absorbed by the sample and excited states are formed that lose energy non radiatively generating heat. The dark circles in figure 2.7 represent the experimental data for rhodamine-PbBr₂(Rh-PbBr₂) sample and the solid line corresponds to the theoretical fit to the experimental data. Thus the thermal diffusivity values can be calculated from the fitting parameters. Measured values of thermal diffusivity D , θ , and t_c are given in the table.2.1

Table.2.1.Measured values of D , θ and t_c for Rhodamine-6G incorporated lead bromide solution

Sample in gm/ml	θ	t_c (mS)	D (cm ² /S)
Rh-PbBr ₂	-4.36	27.7	4.57×10^{-3}

For our sample a negative lens is obtained indicating that it expands on heating. Thus a weak TEM Gaussian laser beam which is co-linear with the excitation beam, passing through the thermal lens, will be affected, resulting in a variation in its spot size and hence intensity at the beam centre. By measuring these changes, information on the thermal and optical properties of the sample can be obtained. The reported value of thermal diffusivity of lead bromide-silver bromide system in literature is 1.28×10^{-3} cm²/S. [34] This shows that the thermal diffusivity of PbBr₂ solution by our experiment is four times the value reported in literature. Thus the thermal lensing study on PbBr₂ suggests that it can be used as a coolant due to its high value of thermal diffusion [31].

2.6. Measurement of optical nonlinearity

2.6.1 Open aperture Z-scan experiment on lead bromide crystal

Optical nonlinear characteristics of the PbBr₂ crystals are investigated using open aperture Z-scan technique. The experimental technique involving a single beam and developed by Sheik Bahae et al (1989) is described in Chapter.1. The main peculiarity of this Z-scan technique is its simplicity. The

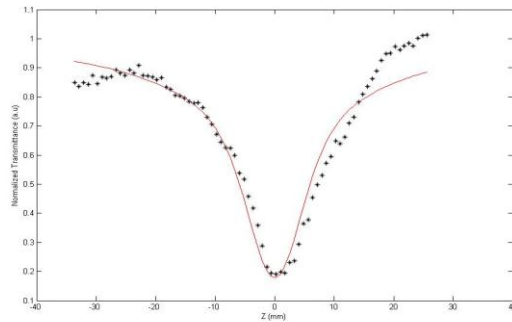
sensitivity of this type of nonlinear measurements is too high .The laser source used in this open aperture experiment is an Nd: YAG laser. The source of irradiation is Q-switched emitting 532 nm pulses with 7ns duration at 10 Hz (Spectra physics Lab-1760) .M.S.Bahae et al has explained the open aperture experimental set up for measuring the optical nonlinearity [35-37]. Lead Bromide crystal in solution phase having a concentration of 0.02 gm/ml is taken in a sample cell. The size of the sample holder is 1mm. It is mounted on a computer controlled translational stage. The sample solution of lead bromide in the cell is moved along the z axis through the focal point of a lens of 0.2m focal length. Rayleigh length z_0 can be calculated using the formula

$$z_0 = \pi w_0^2 / \lambda$$

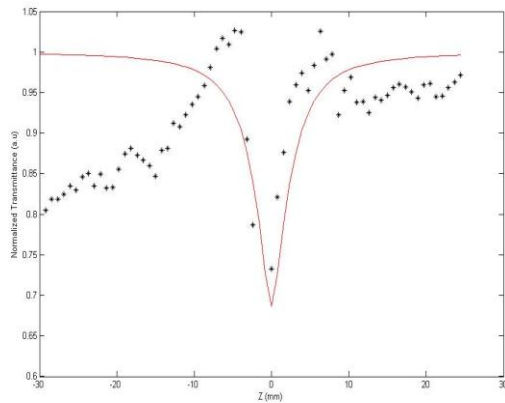
where w_0 is the radius of the beam waist and it is related to the wavelength of the laser source λ and is as given below

$$w_0 = F \lambda / D$$
 where F is the focal length of the lens and D is the beam radius.

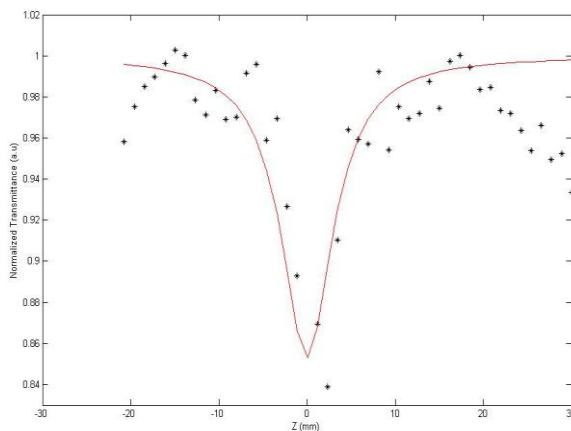
The Rayleigh length is calculated to be 10.6 mm which is much greater than the thickness of the sample cell (1 mm). Thus Raleigh length satisfies the basic criteria of taking Z-scan. By using an energy ratio meter (Rj 7620 Laser Probe Corp) having two identical pyro electric detector heads (Rjp 735), the transmitted beam energy, reference beam energy and their ratios are simultaneously measured. We used CS₂ as the standard for the initial calibration of Z-scan set up.



(a)



(b)



(c)

Figure.2.8:Open aperture Z-scan plot of PbBr₂. at different laser powers, (a)100 MW/cm², (b)150 MW/cm² and (c) 200 MW/cm²

Some scatterings are present in the above Z-scan traces that may be due to the noise by the signal and the movement of the particles as well as a

convective flow in the medium. Open aperture Z-scan studies were carried out by focusing the input beam onto the sample at 532 nm using a Q switched Nd:YAG laser. In order to estimate the limits to which the lead bromide sample would be showing SA or RSA behavior, Z-scan curves were recorded at different fluences in ns regime. Figure.2.8 shows the open aperture Z-scan plot of PbBr₂ solution at a concentration of 0.02 gm/ml. The solid curves are theoretical fit to the open aperture z-scan experimental data. The nonlinear absorption coefficient β can be obtained from this open aperture z-scan data by fitting the normalized transmittance data to the open aperture formula given as [37-39]

$$T(Z, S = 1) = \sum_{m=0}^{\infty} \sum_{m=0}^{\infty} \frac{[-q_o(z)]^m}{[m+1]^{3/2}} |q_o(z)| < 1 \longrightarrow (1)$$

$$\text{where: } q_o(z) = \frac{[I_0 \beta L_{eff}]}{1 + (Z^2 / Z_0^2)} \longrightarrow (2)$$

$Z_0 = k w_0^2 / 2$ is the diffraction length of the beam

$k = 2\pi / \lambda$ is the wave vector,

w_0 = the beam waist radius at the focal point, $L_{eff} = (1 - \exp(-\alpha L)) / \alpha$

is the effective thickness of the sample, I_0 is the laser intensity at the focal plane.

Using the relation (2), the nonlinear absorption coefficient β can be evaluated at different I_0 values. We measured the transmittance of PbBr₂ sample as a function of the sample position z measured with respect to the focal plane. From figure.2.8, it is clear that the nonlinear absorption coefficient is positive due to the transmission minimum at the focal point. For our samples, there is no depletion of ground state population because the transmission curves exhibit reverse saturable absorption (RSA). Using a single Gaussian laser beam, we measured the transmittance of the sample at three different input fluences 100, 150 and 188 MW/cm² as shown in the figure.2.8.

The source wavelength in our experiment is 532nm, which corresponds to two photon absorption (TPA) in the sample. The photon energy is within the range $2h\nu > E_g > h\nu$, where $h\nu = 2.33\text{eV}$ and $E_g = 4\text{ eV}$, the optical band gap of PbBr_2 . Lead Bromide solution suppresses the peak and enhances the valley to show RSA in the transmittance curve. Nonlinear absorption coefficient β for three input fluence values are given in table.2.2

Table.2.2. Measured values of nonlinear absorption coefficient, $\text{Im}(\chi^{(3)})$ and optical limiting threshold for PbBr_2 .

Input laser power density (I_0) (MW/cm ²)	Nonlinear absorption coefficient, β (cm/GW)	Optical limiting threshold (MW/cm ²)	$\text{Im}(\chi^{(3)}) \times 10^{-10}$ (esu)
100	168	76	5.66
150	76	134	2.56
200	26	176	0.88

The nonlinearity in the PbBr_2 crystal sample is found to be of third order, as it fits to a two photon absorption process (TPA). Here the energy for lifting the atom to the excited state was double the energy of exciting photon. The imaginary part of third order susceptibility are determined using the nonlinear absorption values β and is given in table 2.2.

Table 2.2 shows that high nonlinearity is obtained for 100 MW/cm² and comparatively small value for 200 MW/cm². Thus when the incident intensity exceeds the saturation intensity, the nonlinear absorption coefficient of the medium decreases. From these values of β , it is clear that as the input laser intensity I_0 increases, the nonlinear behavior of lead Bromide decreases, which is due to the removal of an appreciable fraction of photo carriers from the ground state. Z-scan curves are normalized plots. In the revised manuscript of the thesis, theoretical aspects of Z-scan are incorporated. Experiment shows minimum

transmission at focal point corresponding to inputs of 100 MW/cm² and 200 MW/cm². In the focused beam data with 200 MW/cm² intensity, Z-scan theory does not expect the minimum transmission corresponding to 100 MW/cm² on either side of data related to 100 MW/cm² input power.

Thus the mechanism of nonlinear absorption in PbBr₂ solution is TPA and a positive nonlinearity is attained. From the literature survey, it is observed that there is not much work regarding the optical nonlinear absorption of PbBr₂. The exciton nonlinearity of lead iodide have been already reported [40]. But the value of nonlinear absorption is taken at a very low laser input intensity. We reported the optical nonlinearity of PbCl₂ for the first time [41-42].

2.7 Optical Limiting in PbBr₂ crystal

The basis of an optical limiting device originates from the reverse saturable absorption behaviour. An optical limiter is a device that obeys the properties like low limiting threshold, large dynamic range, longer excited state life time to accumulate the population, high optical damage threshold, broadband response, fast response time and high linear transmittance [38-43]. This limiting devices can be used for protection of sensors and eyes from energetic light pulses. In lead Bromide sample optical limiting is due to two photon absorption.

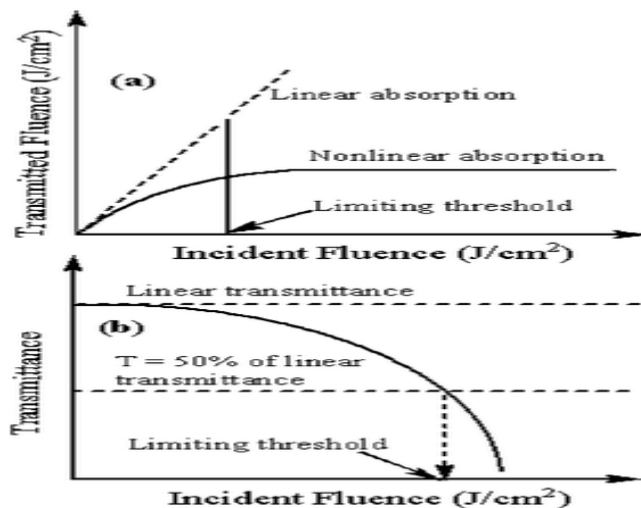


Figure.2.9. The response of an optic limiter

Open aperture Z- scan set up can be used for the optical limiting studies. This is possible because the sample is translated through the focus of the Gaussian beam, the sample experience variation in the incident fluence levels. From the value of fluence at the focus, the fluence values at the at other positions could be calculated by the following equation

$$I(z) = \frac{E}{\pi\omega^2(z)t}$$

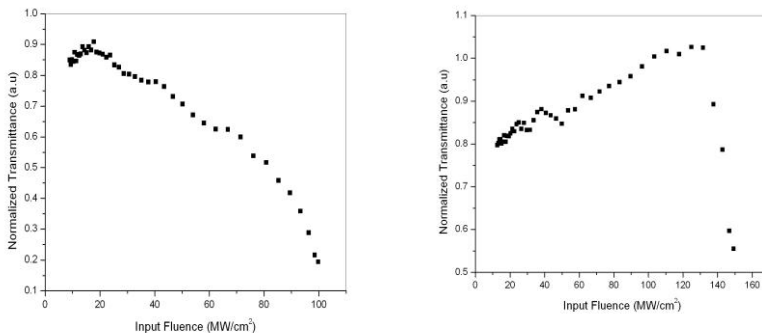
using the standard equations for Gaussian beam waist,

$$\omega^2(z) = \omega_0^2 \left[1 + \frac{z^2}{z_0^2} \right]$$

where the beam waist radius at the focus, $\omega_0 = \frac{f\lambda}{D}$

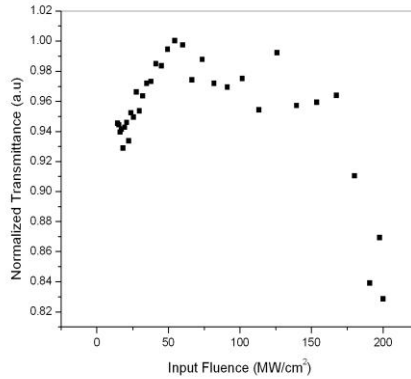
f being the focal length of the lens, D and λ the radius and wavelength of the beam respectively, E is the energy per pulse and t is the pulse width[38].

The open aperture transmittance data at the same concentration of PbBr₂ are taken for plotting the limiting response. Lead Bromide single crystal is a good optical limiter that transmits light at low input intensity .For high input fluences, our material becomes opaque. PbBr₂ should have high transmittance for weak incident light and instantaneous response over a broad spectral range [43].



(a)

(b)



(c)

Figure.2.10: Optical limiting response of PbBr₂ at a laser power density of (a) 100 MW/cm² (b) 150 MW/cm² and (c) 200 MW/cm²

Figure.2.10 shows the optical limiting response of PbBr₂ at three different laser powers 100 MW/cm², 150 MW/cm² and 200 MW/cm² respectively. The limiting threshold is an important factor which decides the efficiency of optical limiter. A better optical limiting material corresponds to a lower optical limiting threshold. The optical limiting property occurs mainly due to absorptive nonlinearity which corresponds to the imaginary part of the third order susceptibility [41]. The optical limiting threshold values at three different laser intensities are shown in table.2.2. The limiting threshold for low input fluence is small and limiting threshold increases with increase in I₀ values. From the values of fluence at the focus, the fluence values at other positions could be calculated using the standard equations for Gaussian beam waist [38].

Conclusions

In this chapter we have discussed the growth of single crystals of lead bromide using solution-gel technique. X-ray diffraction study confirms the orthorhombic crystal structure of PbBr_2 . The spectral studies including absorption, band gap determination and photo luminescence of gel grown lead bromide single crystals were done. The high quality crystals show the absorption peak in the UV region. Optical band gap measurements indicate that lead bromide crystal has the band gap associated with the 6s-to-6p gap in lead ions and tend to become highly luminescent coming from the odd transition. The strong fluorescence emission peaks of PbBr_2 crystals in solution phase reveal their excitonic relaxation mechanisms. Photo luminescence aspects were explained using fluorescence emission characteristics of the PbBr_2 . The thermal diffusivity of the crystalline solution of PbBr_2 along with Rhodamine-6G dye was measured and the negative value of fitting parameter indicates the expansion of PbBr_2 on heating. The thermal diffusivity shows a higher value compared to that of a doped PbBr_2 available in the literature. The transmittance curve obtained from the open aperture Z-scan experiment reveals the reverse saturable absorption for PbBr_2 crystal. The nonlinearity enhances the valley giving a positive value for non linear absorption. The RSA nature of the PbBr_2 sample suggests that it is well suited for optical limiting applications.

References

- [1] Eklund, H., A. Roos, and S. T. Eng. "Rotation of laser beam polarization in acousto-optic devices." *Optical and Quantum Electronics* 7, no. 2 (1975): 73-79.
- [2] Ahmed, G., Y. Sharma, and B. L. Ahuja. "Electronic properties of PbCl_2 and PbBr_2 using Compton scattering technique." *Applied Radiation and Isotopes* 67, no. 6 (2009): 1050-1056.
- [3] Eijkelenkamp, A. J. H., and K. Vos. "Reflectance Measurements on Single Crystals of PbFCl , PbFBr , and PbBr_2 ." *Physica Status Solidi (b)* 76, no. 2 (1976): 769-778.
- [4] Singh, N. B., M. Gottlieb, T. Henningsen, R. H. Hopkins, R. Mazelsky, M. E. Glicksman, S. R. Coriell, G. J. Santoro, and W. M. B. Duval. "Growth and

- characterization of lead bromide crystals." *Journal of Crystal Growth* 123, no. 1 (1992): 221-226.
- [5] Ren, Q., L. Q. Liu, Z. G. Wang, X. S. An, G. H. Zhang, and D. Xu. "Refractive index and absorption of lead bromide crystals." *Materials Research Bulletin* 35, no. 3 (2000): 471-476.
- [6] T. Henningsen, T., and N. B. Singh. "Crystal characterization by use of birefringence interferometry." *Journal of Crystal Growth* 96, no. 1 (1989): 114-118.
- [7] Lumbreras, M., J. Protas, S. Jebbari, G. J. Dirksen, and J. Schoonman. "Crystal growth and characterization of mixed lead halides PbCl₂x Br₂(1-x)." *Solid State Ionics* 16 (1985): 195-199.
- [8] Verwey, J. F., and N. G. Westerink. "Photoconductivity in lead chloride and lead bromide." *Physica* 42, no. 2 (1969): 293-302.
- [9] Schoonman, J. "The ionic conductivity of pure and doped lead bromide single crystals." *Journal of Solid State Chemistry* 4, no. 3 (1972): 466-474.
- [10] Nakagawa, H., M. Terakami, and K. Yasuda. "Elementary processes of photolysis in lead halide crystals." *Radiation Measurements* 33, no. 5 (2001): 819-822.
- [11] Kink, R., T. Avarmaa, V. Kisand, A. Lohmus, I. Kink, and I. Martinson. "Luminescence of cation excitons in and crystals in a wide excitation VUV region." *Journal of Physics: Condensed Matter* 10, no. 3 (1998): 693-700.
- [12] Zamkov, A. V., I. T. Kokov, and A. T. Anistratov. "The Acousto-Optical Properties and Photoelasticity of PbBr₂ Single Crystals." *Physica Status Solidi (a)* 79, no. 2 (1983): K177-K180.
- [13] Verwey, J. F., and J. Schoonman. "Crystal growth, ionic conductivity, and photolysis of pure and impurity-doped lead bromide single crystals." *Physica* 35, no. 3 (1967): 386-394.
- [14] Alov, D. L., and S. I. Rybchenko. "Luminescence of orthorhombic PbF₂." *Journal of Physics: Condensed Matter* 7, no. 7 (1995): 1475.
- [15] Itoh, Minoru, Hideyuki Nakagawa, Mamoru Kitaura, Masami Fujita, and Dmitri L. Alov. "Photoluminescence of orthorhombic and cubic single crystals." *Journal of Physics: Condensed Matter* 11, no. 14 (1999): 3003.
- [16] Kaladevi, C., and C. K. Mahadevan. "Growth and Characterization On Sodium Lead Bromide Crystals." In *International Journal of Engineering Research and Technology*, ESRSA Publications, 1, no. 8 (2012):1-12.

Chapter 2

- [17] Kitaura, M., and H. Nakagawa. "Self-trapped exciton and recombination luminescence in PbCl₂, PbBr₂ and their mixed crystals." *Journal of Luminescence* 72 (1997): 883-884.
- [18] De Gruijter, W. C., and T. Bokx. "Luminescence of PbCl₂ and PbBr₂ single crystals. III. The blue and violet luminescence; Mechanism of energy transport." *Journal of Solid State Chemistry* 6, no. 2 (1973): 271-279.
- [19] Iwanaga, Masanobu, Masayuki Watanabe, and Tetsusuke Hayashi. "Relaxation of excitons into charge-separated pairs in PbBr₂ and PbCl₂ crystals." *International Journal of Modern Physics B* 15, no. 28 (2001): 3677-3680.
- [20] Fujita, M., M. Itoh, Y. Bokumoto, H. Nakagawa, D. L. Alov, and M. Kitaura. "Optical spectra and electronic structures of lead halides." *Physical Review B* 61, no. 23 (2000): 15731-15737.
- [21] G.Lillibai ,PhD Thesis, "Nonlinear optical properties of certain tartrate and halide crystals grown by gel technique in the presence of electric field magnetic field and dopants ", December 2012.(My Research collaborator)
- [22] Ren, Quan, Lan-Ying Ding, Fu-Sheng Chen, Rui-Ping Cheng, and Dong Xu. "The optical properties of lead bromide crystals." *Journal of Materials Science Letters* 16, no. 15 (1997): 1247-1248.
- [23] De Gruijter, W. C. "Luminescence of lead chloride and lead bromide single crystals: I. The excitation and emission spectra." *Journal of Solid State Chemistry* 6, no. 1 (1973): 151-162.
- [24] Rejeena, I., B. Lillibai, B. Nithyaja, PN V. Nampoory, and P. Radhakrishnan. "Optical Studies on Sol-Gel Derived Lead Chloride Crystals." *Journal of Engineering Computers & Applied Sciences* 2, no. 4 (2013): 5-9.
- [25] Nitsch, K., V. Hamplová, M. Nikl, K. Polák, and M. Rodová. "Lead bromide and ternary alkali lead bromide single crystals—growth and emission properties." *Chemical Physics Letters* 258, no. 3 (1996): 518-522.
- [26] De Gruijter, W. C., and J. Kerksen. "EPR and luminescence of uv irradiated PbCl₂ and PbBr₂ crystals." *Solid State Communications* 10, no. 9 (1972): 837-841.
- [27] Eijkelenkamp, A. J. H. "Photoluminescence of PbFCl and PbFBr single crystals." *Solid State Communications* 18, no. 3 (1976): 295-296.
- [28]. De Gruijter, W. C., and J. Kerksen. "Luminescence of PbCl₂ and PbBr₂ single crystals II. Luminescence and EPR of uv irradiated crystals." *Journal of Solid State Chemistry* 5, no. 3 (1972): 467-476.
- [29]. Iwanaga, Masanobu, and Tetsusuke Hayashi. "Exciton-relaxation dynamics in lead halides." *Journal of Luminescence* 102 (2003): 663-668.

- [30] Shen, Jun, Roger D. Lowe, and Richard D. Snook. "A model for cw laser induced mode-mismatched dual-beam thermal lens spectrometry." *Chemical Physics* 165, no. 2 (1992): 385-396.
- [31] Joseph, Santhi Ani, Misha Hari, S. Mathew, Gaurav Sharma, V. M. Hadiya, P. Radhakrishnan, and V. P. N. Nampoore. "Thermal diffusivity of rhodamine 6G incorporated in silver nanofluid measured using mode-matched thermal lens technique." *Optics Communications* 283, no. 2 (2010): 313-317.
- [32] Fuentes, R. Gutiérrez, JA Pescador Rojas, J. L. Jiménez-Pérez, JF Sánchez Ramírez, A. Cruz-Orea, and J. G. Mendoza-Alvarez. "Study of thermal diffusivity of nanofluids with bimetallic nanoparticles with Au (core)/Ag (shell) structure." *Applied Surface Science* 255, no. 3 (2008): 781-783.
- [33] Santhi, A., M. Umadevi, V. Ramakrishnan, P. Radhakrishnan, and V. P. N. Nampoore. "Effect of silver nano particles on the fluorescence quantum yield of Rhodamine 6G determined using dual beam thermal lens method." *Spectrochimica Acta Part A: Molecular and Biomolecular Spectroscopy* 60, no. 5 (2004): 1077-1083.
- [34] Singh, N. B., A. M. Stewart, R. D. Hamacher, R. Mazelsky, W. M. B. Duval, G. J. Santoro, R. De Witt, and S. L. Lehoczky. "Convecto-diffusive growth of lead bromide crystals: a test of theories." *Journal of Crystal Growth* 139, no. 1 (1994): 158-164.
- [35]. Sheik-Bahae, Mansoor, Ali A. Said, T-H. Wei, David J. Hagan, and Eric W. Van Stryland. "Sensitive measurement of optical nonlinearities using a single beam." *Quantum Electronics, IEEE Journal of* 26, no. 4 (1990): 760-769.
- [36] Irimpan, Litty, V. P. N. Nampoore, and P. Radhakrishnan. "Spectral and nonlinear optical characteristics of nanocomposites of ZnO–CdS." *Journal of Applied Physics* 103, no. 9 (2008): 094914,1-8.
- [37] Irimpan, Litty, V. P. N. Nampoore, and P. Radhakrishnan. "Spectral and nonlinear optical characteristics of nanocomposites of ZnO–Ag." *Chemical Physics Letters* 455, no. 4 (2008): 265-269.
- [38] Irimpan, Litty, A. Deepthy, Bindu Krishnan, V. P. N. Nampoore, and P. Radhakrishnan. "Nonlinear optical characteristics of self-assembled films of ZnO." *Applied Physics B* 90, no. 3-4 (2008): 547-556.
- [39] Tintu, R., V. P. N. Nampoore, P. Radhakrishnan, and Sheenu Thomas. "Nonlinear optical studies on nanocolloidal Ga–Sb–Ge–Se chalcogenide glass." *Journal of Applied Physics* 108, no. 7 (2010): 073525.
- [40] Ishihara, Teruya, and Takenari Goto. "Excitonic optical nonlinearity in PbI 2." *Journal of Luminescence* 38, no. 1 (1987): 252-254.

Chapter 2

- [41] Rejeena, I., B. Lillibai, Roseleena Toms, VP N. Nampoori, and P. Radhakrishnan. "Non-Linear Optical Studies On Sol-Gel Derived Lead Chloride Crystals Using Z-Scan Technique." *Journal of Engineering Computers & Applied Sciences* 3, no. 4 (2014): 46-50.
- [42] Rejeena, I., M. H. Rahimkutty, V. P. N. Nampoori, and P. Radhakrishnan. "Effect of nonlinear absorption on electric field applied lead chloride by Z-scan technique." In *Light and its interactions with matter*, AIP Publishing 1620, no. 1(2014): pp. 422-425.
- [43] Aneeshkumar, B., Pramod Gopinath, C. P. G. Vallabhan, V. P. N. Nampoori, P. Radhakrishnan, and Jayan Thomas. "Optical-limiting response of rare-earth metallo-phthalocyanine-doped copolymer matrix." *JOSA B* 20, no. 7 (2003): 1486-1490.

Chapter 3

Spectral and Optical Nonlinear studies on Lead Chloride (PbCl_2) crystals

Abstract

The properties and applications of lead chloride crystals are discussed. The preparation of five different types of PbCl_2 and some of their linear and nonlinear behavior are illustrated in this chapter. The fluorescence emission spectra of lead chloride crystal samples at different excitation wavelengths reveal that all the PbCl_2 samples are highly luminescent in nature. The non radiative decay mechanism of these materials are investigated using thermal lens experimental technique. The nonlinear absorption of PbCl_2 is determined by employing the Z-scan technique. All the five PbCl_2 samples including UV and IR irradiated and the electro-magnetic field applied exhibit positive nonlinear absorption and the corresponding responses have been studied.

3.1 Introduction

Lead chloride is a well-known photosensitive material possessing ionic crystalline nature belonging to orthorhombic system [1]. PbCl_2 is the model material from heavy element halogenide group since it satisfies high birefringence, low attenuation coefficient and wide transparency range [2]. The purification studies on lead chloride by directional freezing method were reported [3]. They showed the simple and inexpensive procedure for the purification of lead chloride single crystals by analyzing the impurities. Zuzana Ma lkova determined the oxidic impurities in PbCl_2 crystals measuring the oxygen concentrations by means of physical methods like Auger electron spectroscopy, radiation methods and high temperature extraction with carbon [4]. These methods mainly give information on the exact oxygen concentration in the surface layers, but they require a good sample surface, and they are not suitable for easily evaporating compounds.

K. J. De vries and J. H. Van santen measured the ionic conductivity of the lead chloride crystals [5-6]. J. F. Verwey investigated the photolysis on PbCl_2 [7]. The electron spin resonance measurements were performed on lead chloride doped with europium by Q. H. F. Vrethen and J. Volger, and gadolinium ion localization in lead chloride were also studied. [8-9]. For all these investigations, single crystals of good quality had to be prepared. Many of the researchers reported the luminescence property of PbCl_2 [10]. These materials are important for their luminescent properties. Two types of luminescence are observed in PbCl_2 , the excitonic luminescence and the recombinational luminescence. Under excitation in the fundamental absorption region, PbCl_2 crystals exhibit two types of intrinsic luminescence [11]. W.C.De Gruijter had done emission studies on PbCl_2 [12]. The top of the valence band is composed of Pb^{2+} -6s with considerable admixing of chlorine-np, while the bottom of the conduction band is made up of Pb^{2+} -6p [13].

PbCl₂ is classified as a normal class I crystal and its transmission range is wide [14]. PbCl₂ finds importance in experimental field due to their large band gap and exhibiting interesting features from the stand point of electron-lattice interaction [15-24]. Lead halide based materials can be used as laser hosts with low phonon energies. The Pb²⁺ in the PbCl₂ crystal is known to be emissive in aqueous solution [25-28]. PbCl₂ is marked as an insulator with a moderate band gap. They belong to the space symmetry group D_{2h}¹⁶ with layers perpendicular to the [010] direction. The lead chloride crystal is characterized by an excitonic fundamental edge, which are formed by electronic states of lead ion. The acousto optic figure of merit of PbCl₂ crystals is high and their transmission range is wide. The band gap of PbCl₂ is also large[29]. A large set of 15 optical functions contains the most complete information on the optical properties and electronic structure of PbCl₂ [30-31]. V.V.Sobolev et al reported the electronic structure and anisotropic optical properties of PbCl₂ crystals. PbCl₂ is an ionic crystal with orthorhombic structure with four molecules in the unit cell [32]. A.Kaldor and G.A.Somrjai reported the photodecomposition in PbCl₂ [33]. Photonic materials with optical limiting properties find applications in devices for protecting eyes and sensors from intense optical radiations. A non linear optical crystal like PbCl₂ can be employed for applications depending on their band gap and nonlinearities. PbCl₂ exists in nature in crystalline form as large needles. This chapter presents the optical and nonlinear optical studies on lead chloride crystals.

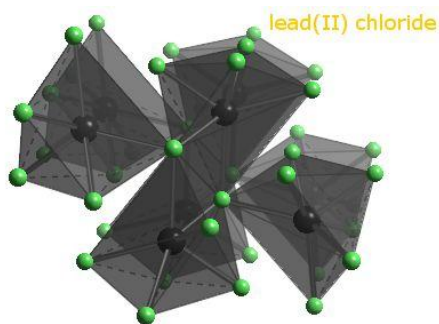


Figure.3.1.Crystal structure of PbCl₂

Table 3.1 Properties of PbCl₂ from literature

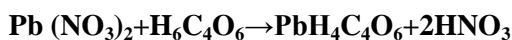
Properties	
Molecular formula	PbCl ₂
Molar mass	278.10 g/mol
Appearance	white odourless solid
Density	5.85 g/cm ³
Melting point	501 °C
Boiling point	950 °C
Solubility in water	10.8 g/L (20 °C)[1]
Solubility product, K _{sp}	5.89×10 ⁻⁵ (20 °C)

3.2 Synthesis

PbCl₂ crystal samples for our experimental measurements were prepared by the relevant gel method [34]. The peculiarity of this preparation technique is explained in the former chapters 1 and 2. The first and the most important stage of the sample crystal preparation is the production of gel. Using a stock solution of sodium meta silicate (SMS) a good quality gel can be prepared. 25 ml. of SMS solution of specific gravity 1.03, for which the pH was adjusted to be 6.5, 7.0, 7.5, 8.0 and 8.5 by titration with 1M tartaric acid was allowed to gel in five various boiling test tubes without any disturbances. Growth experiments were conducted for different densities of the gel ranging from 1.02 to 1.06. It was found that for the same concentration of HCl, tartaric acid and lead nitrate solution, the rate of growth of the needles was conspicuously larger and the needles were larger for lesser densities of the gel. This is due to the increased rate of diffusion of HCl in the gel and increased mobility of the molecules of the crystals at lower densities of the gel. PbCl₂ crystals were obtained by the reactions of lead nitrate, tartaric acid and HCl (99.9% Sigma-Aldrich). Two

different PbCl₂ crystal samples were obtained by irradiating the test tube containing gel and top solution with ultra violet (UV lamp (insect Killer)) and Infrared radiations (HL4311 (PHILIPS) 230V~50Hz~150W). The other two samples were prepared by subjecting to an electric field of 20 V using parallel plate arrangement and subjecting the test tube containing top solution and gel to a magnetic field using two bar magnets kept on either side of the experimental test tube and perpendicular to its length. Thus five PbCl₂ samples were obtained for our studies viz pure, UV and IR irradiated, samples subjected to electric and magnetic fields

The crystal formation of lead chloride can be obtained using the following chemical reaction equations



3.3 X-ray Diffraction studies

We used the X –ray diffraction technique for structural analysis of the sol-gel grown lead chloride crystals by five different methods [34]. It is the widely used technique for the confirmation of the crystalline nature of most of the solids. This diffraction method can be used to measure the average spacing between layers or rows of atoms of the lead chloride crystals. The sol-gel derived PbCl₂ samples are subjected to X-ray diffraction studies employing XPERT-PRO using K-Alpha 1.54060 Å⁰ (XRDML). The X-ray diffraction pattern of PbCl₂ is as shown in figure 3.2. The orientations of the grown crystals are directly determined from the X-ray diffractogram. The crystal structure of PbCl₂ is confirmed to be orthorhombic dipyramidal with each Pb having a coordination under 9. From the plot of angle 2θ verses intensity, the sharp peaks depict the crystallinity of PbCl₂ crystals [35].

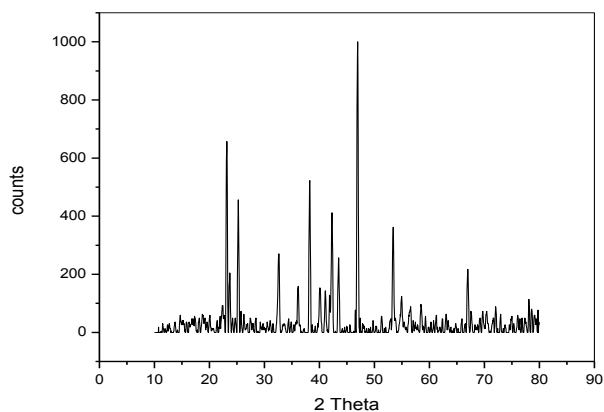


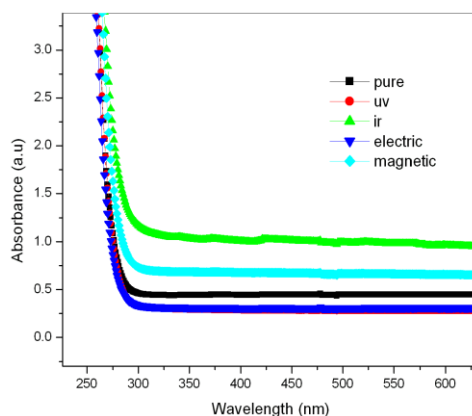
Figure3.2. XRD of gel derived PbCl_2 crystal

3.4 Spectral studies on Lead chloride crystals

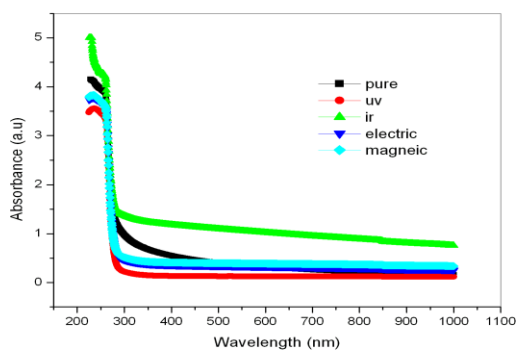
In the present section, we discuss the spectral aspects of the five lead chloride crystal samples prepared by solution gel method. We took the solution of the pure, ultraviolet radiated, infrared radiated, electric field applied and magnetic field applied PbCl_2 crystal samples for absorption and photoluminescence measurements. In order to obtain the solution samples at two different concentrations, the prepared crystals of PbCl_2 were powdered using mortar and pestle, weighed about 0.15g and dissolved in 15 ml of single distilled water (SDW) to obtain a concentration $c_1=0.01$ gm/ml. Another concentration $c_2=0.02$ gm/ml was obtained by dissolving 0.32gm in 15ml of SDW. For the dissolution, a magnetic stirrer was used and the solvent evaporation was prevented by using a sealed glass container.

3.4.1 Optical absorption studies

Optical absorption of the lead chloride crystal samples in solution phase was recorded using Jasco V-570 UV/VIS/IR Spectrophotometer. The wavelength range of this spectrometer ranges from 190 nm to 2500 nm[36]. The resolution within the ultra violet(UV)/Visible region is about 0.1 nm and the resolution corresponding to near infrared (NIR) region is 0.5nm. Optical absorption spectra of $PbCl_2$ samples at two different concentrations c1 and c2 are shown in the figure 3.3.



(a)



(b)

Figure .3.3. Room temperature absorption spectra of five $PbCl_2$ crystal samples at concentrations (a) c1 and (b) c2

The absorption peak of PbCl_2 at the two concentrations c_1 and c_2 are located in the UV region around 266 nm. The optical absorption edge at this value corresponds to an energy of 4.6 eV. The peak at this particular wavelength is due to the electronic transition from the valence band to the level occupied by PbCl^+ cation [37]. There is no appreciable change in absorption peak at the other concentration. The linear absorption coefficient α can be determined from the absorption spectra of PbCl_2 at the concentrations c_1 and c_2 . Table 3.2 shows the values of linear absorption coefficient α for the five gel grown PbCl_2 samples in solution phase at a concentration of c_1 . There is no appreciable change in these values at concentration c_2 .

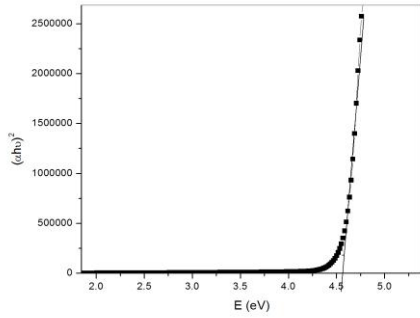
Table.3.2. Measured values of linear absorption coefficient α for the five different PbCl_2 crystals

Sample	α (cm^{-1})
Pure PbCl_2	0.45
UV irradiated PbCl_2	0.28
IR irradiated PbCl_2	0.98
Electric field applied PbCl_2	0.31
Magnetic field applied PbCl_2	0.67

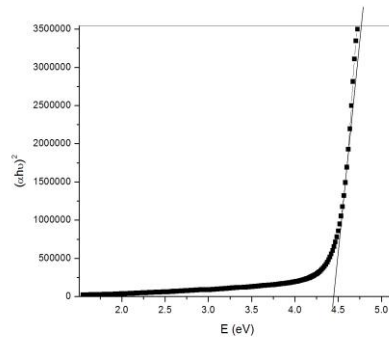
3.4.2 Band gap determination from Linear Absorption Spectra

The linear absorption spectra of the lead chloride crystals (figure.3.3) plotted above can be used for optical band gap studies on PbCl_2 in solution phase in single distilled water. The linear absorption coefficient α is related to the band gap as $(\alpha h\nu)^2 = k (h\nu - E_g)$, where $h\nu$ is the incident light energy, k is a constant and E_g is the optical band gap of lead chloride as described in chapter.2. The direct band gap of these five different samples of PbCl_2 at two

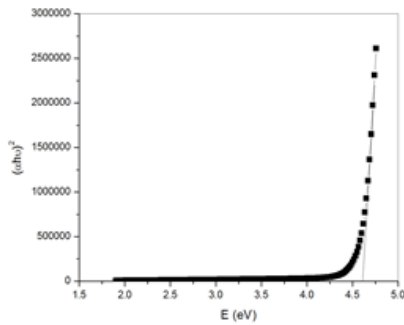
concentrations c_1 and c_2 were determined by plotting a graph between $h\nu$ along the X- axis and $(\alpha h\nu)^2$ along the Y- axis.



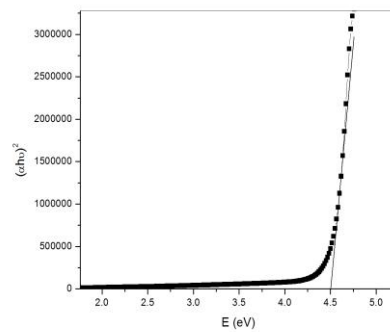
(a)



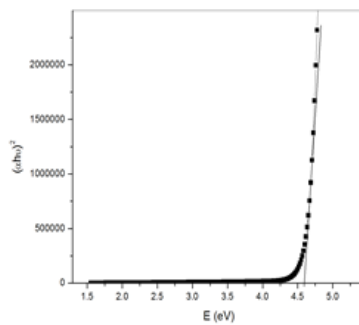
(b)



(c)



(d)



(e)

Figure.3.4. Optical band gap plot of (a) pure (b) UV (c) IR (d) electricfield and (e) magneticfield applied PbCl₂samples at c_1 .

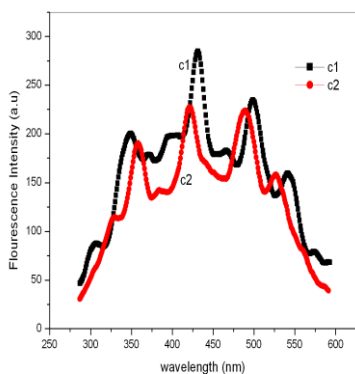
Figure.3.4 shows the band gap diagrams of the five PbCl_2 samples. From the figure, it is evident that the optical band gap of PbCl_2 for concentration c1 is varying from 4.54 eV (pure) to 4.67 eV (magnetic). For UV irradiated and electric field applied PbCl_2 samples, E_g is 4.53 eV and 4.57 eV respectively. When concentration is c2, E_g varies between 4.61 and 4.46 eV. The values of direct band gap for c1 and c2 are listed in the table3.3. Several types of chloride ion vacancies can exist in the lead chloride lattice which are electron traps in the energy range 4.2-4.4 eV above the valence band [32,37]. The chloride ions at the largest distance are surrounded by four lead ions whereas the closest chloride ions are surrounded by five lead ions [38]. It is suggested that the 4.6 eV absorption is due to an exciton absorption, but on the other hand it might also be ascribed to a characteristic $6s^2-6s6p$ transition inside the lead ion. The optical band gap values are given in table3.3. These results of our work on the optical band gap of PbCl_2 are published [39].

Table 3.3. Measured values of optical band gap of PbCl_2 at two concentrations c1 and c2

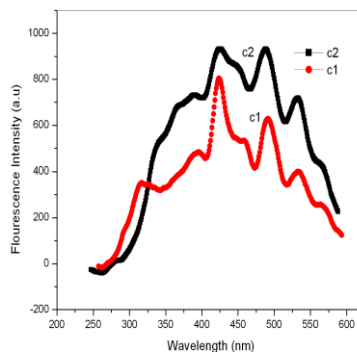
Sample	Optical direct band gap E_g (eV) at concentrations	
	C1	C2
PbCl_2 pure	4.54	4.61
PbCl_2 UV	4.53	4.54
PbCl_2 IR	4.62	4.40
PbCl_2 electric	4.57	4.55
PbCl_2 magnetic	4.67	4.46

3.4.3. Fluorescence Studies

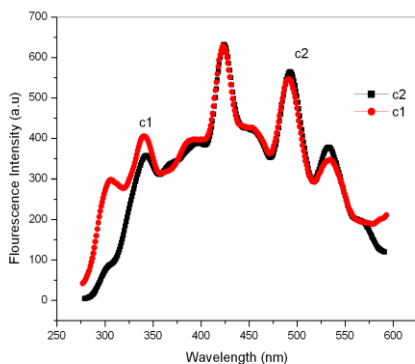
Fluorescence spectra of $PbCl_2$ were taken at two different concentrations c_1 and c_2 for photoluminescence studies. The emission and excitation studies were carried out by taking the room temperature fluorescence spectra of these $PbCl_2$ samples using a Cary Eclipse fluorescence spectrophotometer (Varian). Figure 3.5 represents the fluorescence emission spectra of five $PbCl_2$ samples in SDW. $PbCl_2$ sample solutions at concentrations c_1 and c_2 excited at a wavelength of 270 nm gives three strong emissions at around 421 nm, 491 nm and 533 nm respectively. The excitonic transitions in lead chloride are partly explained by the 6s-6p transition in lead ions which gives the emission bands at three of the above transitions. Fluorescence in $PbCl_2$ is composed of broad Gaussian band with large Stokes shift and it is indicative of strong exciton-acoustic phonon interaction [40]. The electric dipole transition from the 6p to 6s states also produces luminescence in $PbCl_2$. The exciton can relax into pairs of a self trapped electron (STEL) and a self trapped hole (STH) when both electrons and holes strongly interact with acoustic phonons. A repulsive correlation is ascribable to the origin of electron-hole separation. The repulsive correlation through acoustic phonons with the formation of cooper pairs mediated by these acoustic phonons cause the spontaneous breaking of exciton [41].



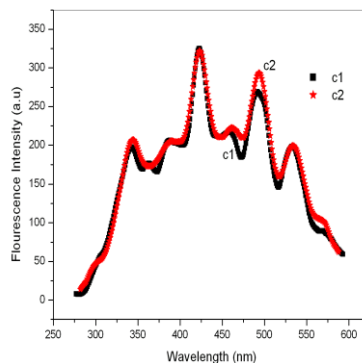
(a)



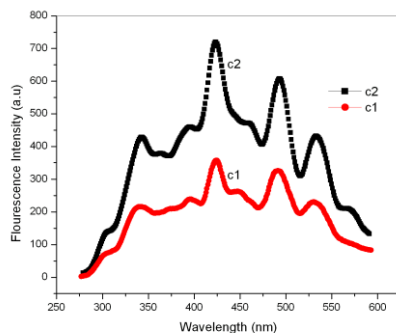
(b)



(c)



(d)



(e)

Figure 3.5. Fluorescence emission spectra of PbCl_2 at an excitation wavelength 270 nm for (a) pure (b) UV (c) IR (d) electric field and (e) magnetic field applied samples

As concentration is increased, phonon vibration will induce more non radiative de excitations[41]. Our PbCl_2 solutions show many peaks due to the stokes shift by the crystal field resulting from the strong interaction between phonon and Pb^{2+} ions. From the fluorescence spectra given in the figure, it is evident that the emission peaks at 491 and 533 nm are assigned to the excitonic emissions. The IR irradiated and electric field applied samples have almost same emission peak at 423, 492 and 533 nm for the two concentrations c1 and c2. The shifting of emission peaks for pure PbCl_2 sample is due to the band edge emission which

are attributed to the quasi free recombination at the absorption band edge. Thus the spontaneous exciton dissociation has been revealed by the fluorescence emission in sol- gel derived PbCl₂ samples in solution phase. Our work on the emission characteristics of PbCl₂ are published [39].

The values of emission peaks at an excitation wavelength of 270 nm are shown in table 3.4.

Table 3.4. Measured values of emission peaks for PbCl₂ at concentrations c1 and c2(gm/ml)

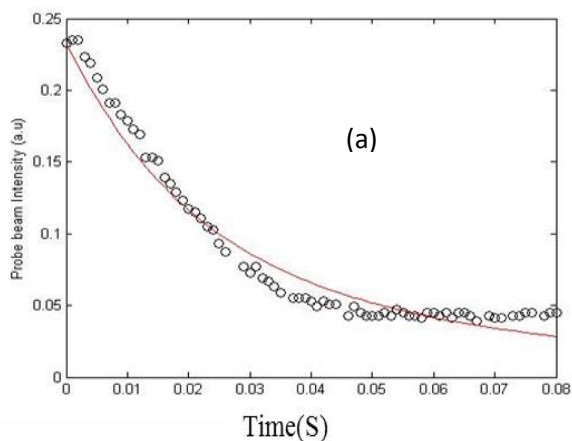
PbCl ₂ sample	Emission peak corresponding to two different concentrations (nm)	
	C1 (gm/ml)	C2 (gm/ml)
pure	348	357
	431	422
	498	490
	540	525
UV	-	-
	422	423
	491	487
	534	532
IR	339	342
	423	423
	492	492
	533	533
Electric	342	342
	421	421
	493	492
	533	533
Magnetic	338	342
	424	423
	490	493
	531	533

3.5 Thermal diffusivity studies on PbCl₂

The lensing effect of lead chloride sample crystals was studied using a mode matched thermal lens technique. A solution of 0.3 ml Rhodamine-6G dye and 3 ml of PbCl₂ sample was taken in a 1 cm cuvette for experimentation. The experiment was carried out at a concentration of c1. Rhodamine 6G was mixed with the PbCl₂ crystal samples to enhance the absorption of the crystal. The Rhodamine incorporated lead chloride sample was excited by a 532 nm diode pumped solid state laser with a maximum power of 150 mW. The probe laser was a He-Ne laser having a power of 2mW. The two beams were focused into the PbCl₂ sample cell such that the beam area at the sample plane was the same for both pump and probe resulting in a mode matched TL configuration as given in Chapter.1. When the crystal sample was irradiated by the source laser, the temperature was increased. The increase of temperature varies the refractive index of the material. Thus our PbCl₂ itself acts as a thermal lens.

The experimental data values were plotted using a program which gave the values of decay time t_c and fitting parameter θ . From the values of t_c and beam waist radius w at the PbCl₂ position, the thermal diffusivity D can be calculated as

$$D = w^2 / 4t_c$$



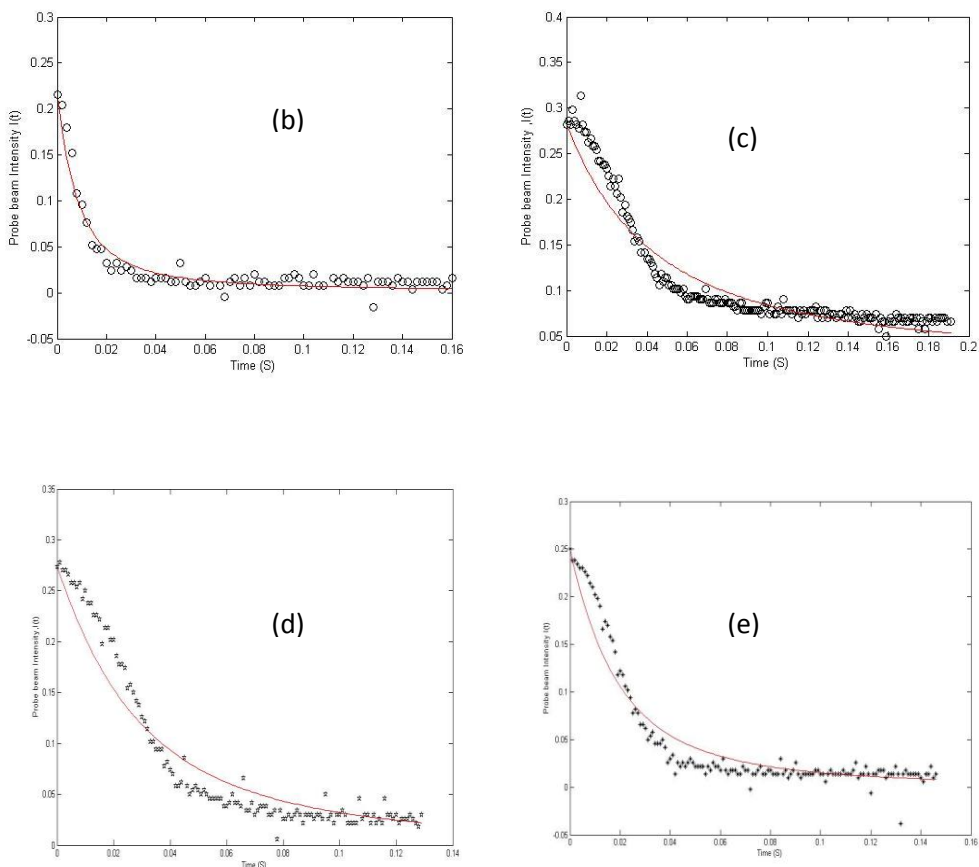


Figure.3.6: TL plot of $PbCl_2$ (a) pure (b) UV (c) IR (d) electric field and (e) magnetic field applied samples

The solid line in the figure 3.6 corresponds to the theoretical fit to the experimental data represented by the dark circles. During the thermal lens experiment there is a chance of internal conversion in the lead chloride crystal solution with Rhodamine -6G dye. This interaction within the crystal makes it to act as a lens- like optical element by the non radiative decay mechanism. The non radiative emission by the interaction within the $PbCl_2$ sample results in the formation of heat. We obtained a negative lens since the solution of lead chloride expands on heating.

Table.3.5.Measured values of D, θ , and t_c for Rhodamine incorporated lead chloride solution

Sample	t_c (mS)	θ	D (cm ² /S) x 10 ⁻³
PbCl ₂ pure	25.24	-463.95	5.01
PbCl ₂ UV	22.29	-660.81	5.50
PbCl ₂ IR	48.48	-444.73	2.64
PbCl ₂ electric	49.25	-744.61	2.57
PbCl ₂ magnetic	32.05	-748.20	3.95

The above table depicts the values of decay constant t_c , fitting parameter and the thermal diffusivity D of the gel grown PbCl₂ crystal samples incorporated with Rhodamine-6G. The visual inspection of the thermal lens plots shows variations in the time response of the thermal lens signal. Quantities like t_c and θ were obtained directly from the fitting made. The table tells us that the infrared irradiated PbCl₂ have the low decay time corresponding to a thermal diffusion of the order of 2.64x10⁻³ cm²/sec. The high value of thermal diffusion for PbCl₂ IR makes it suitable for coolant applications. The thermal diffusivity of the electric field applied sample shows a low value for D corresponding to a decay rate of 0.049 seconds. The low value of thermal diffusivity suggests that the effect of electric field on PbCl₂ enhances the decay time to a great extent and have found applications in the field of thermal insulators [42]. The obtained values of thermal diffusivity of PbCl₂ sample solutions are found to be high compared to the values available in the literature [43].

3.6 Nonlinear optical Studies on PbCl₂

Open aperture Z-scan experiment was used for the measurement of optical nonlinear characteristics of lead chloride crystals prepared by five different methods. The theory and experimental set up of this technique are explained in chapters 1 and 2. This highly sensitive method plays an important role in the determination of nonlinear absorption coefficients of our lead chloride

crystal samples in solution phase. In the open aperture set up, no aperture is needed. Here we translated the five crystals along the focus of the lens using a computer controlled translational stage. While experimenting on these crystal samples, the traces of transmittance are noted. The shape of the transmittance plot decides the sign of nonlinear absorption coefficient. The symmetric curves thus obtained are used for the calculations of nonlinearity in the crystal samples.

We measured the transmittance of PbCl₂ at laser energies 40 and 50 μJ corresponding to the power densities 100 MW/cm² and 125 MW/cm² respectively. The data obtained experimentally were plotted using a theoretical fit. The fitting of open aperture data gives rise to the values of q. The mathematical relation connecting the q and the sample positions z is written as

$$q = q_0(z)(1+Z^2/Z_0^2).....(1)$$

From this value of q, the value of nonlinear absorption coefficient β can be calculated using the relation

$$\beta = q/(I_0 L_{eff}).....(2)$$

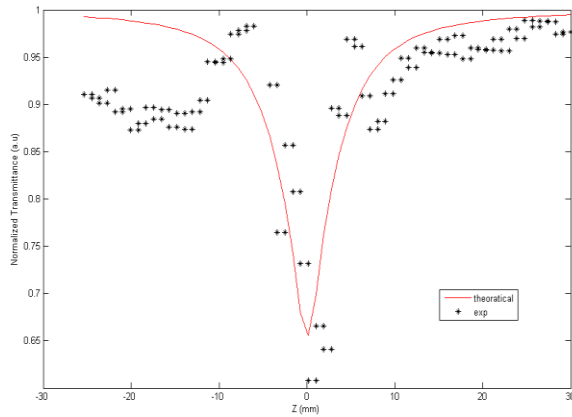


Figure.3.7(a): Open aperture Z-scan plot of pure PbCl₂ at a laser power 100 MW/cm²

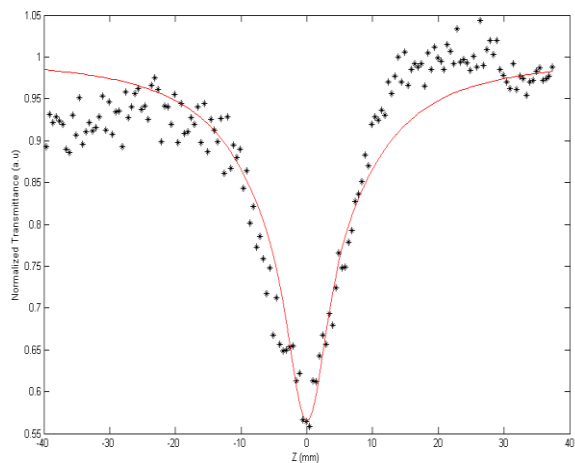


Figure.3.7(b): Open aperture Z-scan plot of UV irradiated PbCl₂ at a laser power 100 MW/cm²

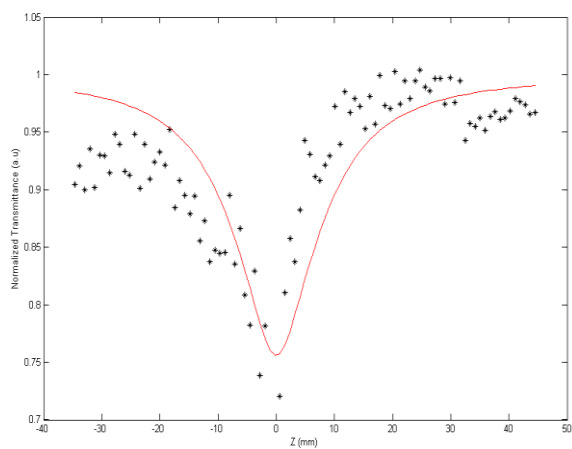


Figure.3.7(c): Open aperture Z-scan plot of IR irradiated PbCl₂ at a laser power 100 MW/cm²

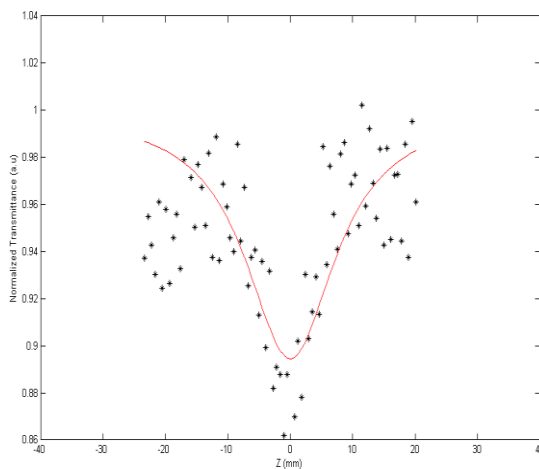


Figure.3.7(d): Open aperture Z-scan plot of electric field applied PbCl₂ at a laser power 100 MW/ cm²

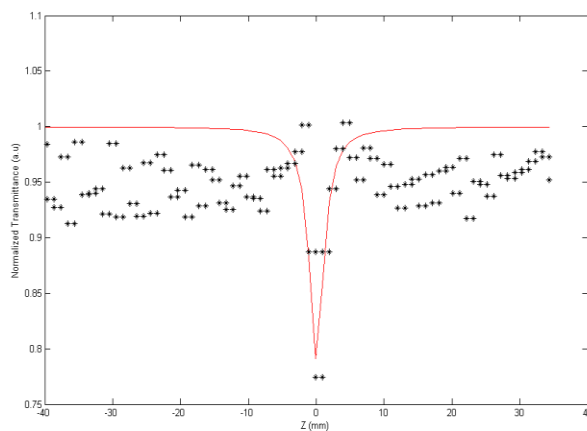


Figure.3.7(e): Open aperture Z-scan plot of magnetic field applied PbCl₂ at a laser power 100 MW/cm²

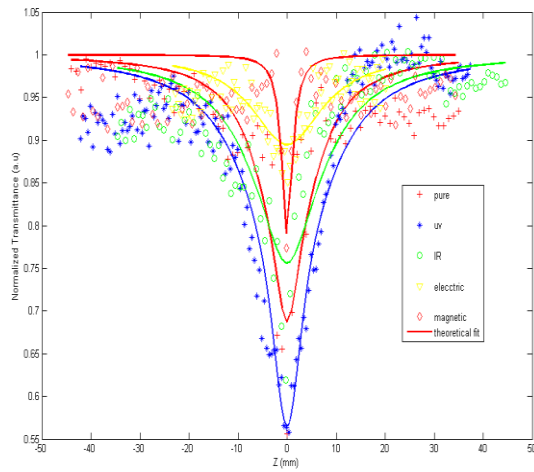


Figure 3.8. Combined Z-scan trace of PbCl_2 at $I_0 = 100 \text{ MW/cm}^2$

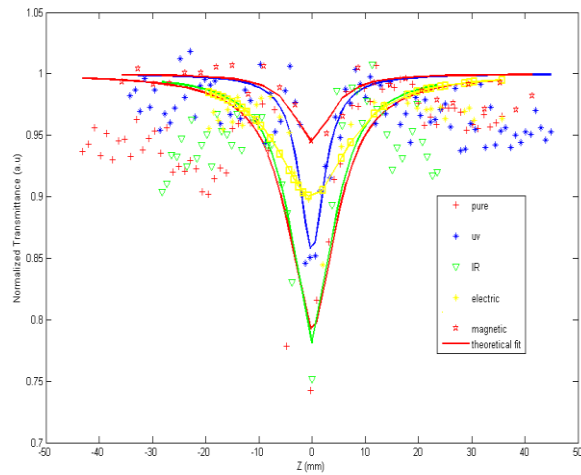


Figure 3.9. Combined Z-scan trace of PbCl_2 at $I_0 = 125 \text{ MW/cm}^2$

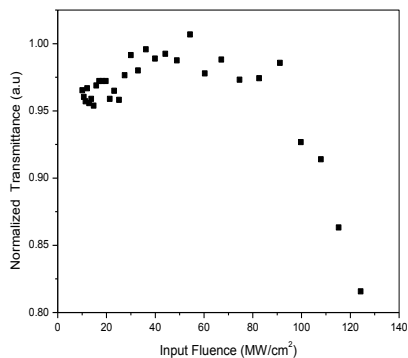
The above figures represent the open aperture Z-scan of PbCl₂ crystals at different input laser powers. The scattered data present in some of the above Z-scan traces can be due to the signal noise, the movement of the particles as well as a convective flow in the medium. The figures clearly establish the reverse saturable absorption of these crystalline materials. The transmittance of PbCl₂ shows a valley nature instead of a peak which is the real face of reverse saturable absorber. The RSA behaviour of PbCl₂ indicate that the ground states of these crystal samples are not depleted. Since the excitation laser has a wavelength of 532 nm, we can suggest that nonlinearity is coming from two photon absorption. The theory and mechanism of two photon absorption is described in chapter.1. Table 3.6 gives the measured values of nonlinear absorption coefficient at two input laser power densities. The third order susceptibility (imaginary part) [Im ($\chi^{(3)}$)] values are also given. Our work on the nonlinear optical and limiting studies on gel derived samples of PbCl₂ are published [44-45].

Table 3.6. Measured values of nonlinear absorption coefficient and optical limiting threshold for PbCl₂ samples

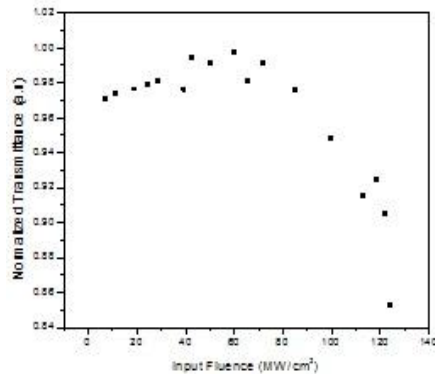
Sample	β (cmGW ⁻¹)		Optical limiting threshold (MWcm ⁻²)		Im ($\chi^{(3)}$) x10 ⁻¹⁰ (esu)	
	I ₀ (100 MWcm ⁻²)	I ₀ (125 MWcm ⁻²)			I ₀ (100 MWcm ⁻²)	I ₀ (125 MWcm ⁻²)
PbCl ₂ pure	122	65	68	83	3.89	2.08
PbCl ₂ UV	135	42	43	85	4.31	1.34
PbCl ₂ IR	98	70	72	84	3.12	2.24
PbCl ₂ electric	36	27	76	85	1.14	0.87
PbCl ₂ magnetic	83	14	82	95	2.65	0.44

3.7 Optical limiting Studies on PbCl₂

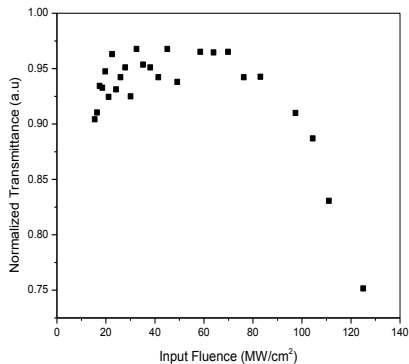
Materials that exhibit RSA are currently of interest for use in optical limiting devices for protection of sensors and eyes from energetic light pulses. The maximum criteria identified for a material to act as an effective optical limiter are low limiting threshold, large dynamic range, longer excited state life time to accumulate the population, high optical damage threshold, broadband response, fast response time and high linear transmittance [46-47]. In lead chloride samples optical limiting is due to TPA. The optical limiting studies were also carried out at a concentration of c1 .Lead chloride is a good optical limiter that transmits light at low input intensity while it becomes opaque at high input fluences. PbCl₂ should have high transmittance for weak incident light and instantaneous response over a broad spectral range [48].



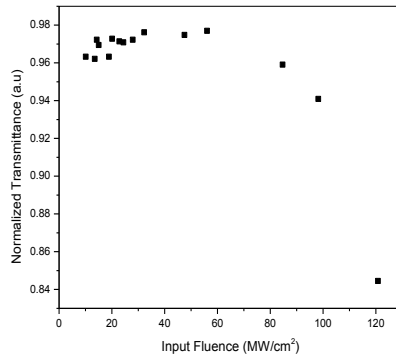
(a)



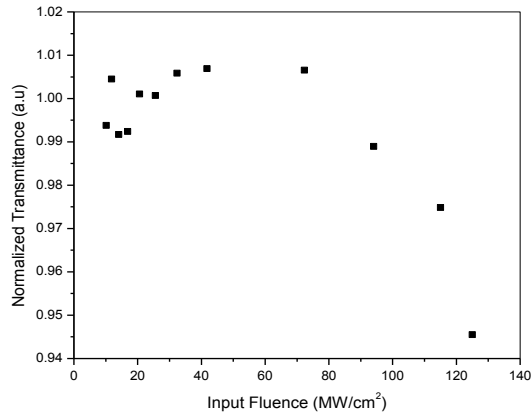
(b)



(c)



(d)



(e)

Figure 3.10 optical limiting response of $PbCl_2$ (a) pure ,(b) UV irradiated, (c) IR irradiated, (d) electric field and (e) magnetic field applied samples

Figure 3.10 shows the optical limiting response of $PbCl_2$. The limiting threshold is an important factor which decides the efficiency of optical limiter. It is obvious that lower the optical limiting threshold, better the optical limiting material. The optical limiting property occurs mainly due to absorptive nonlinearity which corresponds to the imaginary part of the third order susceptibility [49]. The optical limiting threshold values at two different laser intensities are shown in table.3.6. From the table, it is observed that there is a small limiting threshold for low input fluence and limiting threshold increases with increase in I_0 values. From the values of fluence at the focus, the fluence values at other positions could be calculated using the standard equations for Gaussian beam waist[50].

Conclusions

High quality lead chloride crystals were prepared by sol-gel technique. The linear absorption spectra gives the optical band gap details of these crystals. The absorption peak of PbCl_2 in the UV region is due to the electronic transition from the valence band to the level occupied by PbCl^+ cation. The optical band gap values were found to range from 4.4 eV to 4.67 eV. The fluorescence emission of these crystals shows that PbCl_2 crystals have the band gap associated with the 6s to 6p gap in lead ions. The high luminescence nature of lead chloride makes them suitable for applications in photography, acousto-optical devices and radiation detectors. The thermal lensing studies on PbCl_2 suggest that the IR irradiated samples can be used in coolants owing to their high value of thermal diffusion. Optical nonlinearity in five different PbCl_2 samples were investigated using Z-scan technique. Observed nonlinearity is third order and the nonlinear curves exhibit valleys demonstrating reverse saturable absorption indicating a positive nonlinear absorption. RSA nature of the samples makes them suitable for optical limiting applications. The optical limiting threshold of these samples were also evaluated. The nonlinear studies on these crystal solutions gives a clear picture that these materials are highly nonlinear due to their high values of nonlinear absorption coefficients. Thus these PbCl_2 crystals prepared by sol-gel technique are well suited for applications in optoelectronics and nonlinear optical devices.

References

- [1] Nakagawa, H., Y. Doi, and T. Nakamura. "Absorption and luminescence in PbCl₂: Tl⁺ crystals." *Journal of Luminescence* 87 (2000): 1130-1132.
- [2] Nisha Santha Kumari, P., and S. Kalainathan. "Characterization of lead (II) chloride single crystals grown in silica gel." *Crystal Research and Technology* 43, no. 4 (2008): 413-416.
- [3] Singh, Narsingh Bahadur, W. M. B. Duval, and B. N. Rosenthal. "Characterization of directionally solidified lead chloride." *Journal of Crystal Growth* 89, no. 1 (1988): 80-85.
- [4] Málková, Zuzana, Karel Nitsch, and Josef Novák. "Determination of oxidic impurities in some lead halides." *Analytica Chimica Acta* 355, no. 2 (1997): 171-174.
- [5] K. J. De Vries, Thesis, University of Utrecht, The Netherlands, 1967.
- [6] De Vries, K. J., and J. H. Van Santen. "Note on the Koch and Wagner effect in lead chloride single crystals." *Physica* 29, no. 5 (1963): 482-484.
- [7] Verwey, J. F. "Time and intensity dependence of the photolysis of lead halides." *Journal of Physics and Chemistry of Solids* 31, no. 1 (1970): 163-168.
- [8] Vrehen, Q. H. F., and J. Volger. "Paramagnetic resonance of divalent europium in lead chloride." *Physica* 31, no. 6 (1965): 845-865.
- [9] Vazhenin, V. A., A. P. Potapov, A. N. Ivachev, M. Yu Artyomov, and V. B. Guseva. "Gadolinium ion localization in RbPb₂Cl₅ crystals." *Physics of the Solid State* 54, no. 6 (2012): 1249-1253.
- [10] Kitaura, M., and H. Nakagawa. "Self-trapped exciton and recombination luminescence in PbCl₂, PbBr₂ and their mixed crystals." *Journal of Luminescence* 72 (1997): 883-884.
- [11] Wanaga, Masanobu, Masayuki Watanabe, and Tetsusuke Hayashi. "Relaxation of excitons into charge-separated pairs in PbBr₂ and PbCl₂ crystals." *International Journal of Modern Physics B* 15, no. 28n30 (2001): 3677-3680.
- [12] De Gruijter, W. C., and T. Bokx. "Luminescence of PbCl₂ and PbBr₂ single crystals. III. The blue and violet luminescence; Mechanism of energy transport." *Journal of Solid State Chemistry* 6, no. 2 (1973): 271-279.
- [13] Fujita, M., M. Itoh, Y. Bokumoto, H. Nakagawa, D. L. Alov, and M. Kitaura. "Optical spectra and electronic structures of lead halides." *Physical Review B* 61, no. 23 (2000): 15731

Chapter 3

- [14] Kitaura, Mamoru, and Hideyuki Nakagawa. "Origin of the luminescence bands in PbCl₂ crystals induced by UV light at low temperatures." *Journal of the Physical Society of Japan* 70, no. 8 (2001): 2462-2467.
- [15] Plekhanov, V. "Optical constants of lead halides." *Physica Status Solidi (b)* 57, no. 1 (1973): K55-K59.
- [16] Iwanaga, Masanobu, Masanobu Shirai, Koichiro Tanaka, and Tetsusuke Hayashi. "Self-trapped states and related luminescence in PbCl₂ crystals." *Physical Review B* 66, no. 6 (2002): 064304.
- [17] De Gruijter, Wouter Cornelis. "Luminescence of lead chloride and lead bromide single crystals." *Physics Letters A* 34, no. 5 (1971): 251-252.
- [18] De Gruijter, W. C., and J. Kerssen. "EPR and luminescence of uv irradiated PbCl₂ and PbBr₂ crystals." *Solid State Communications* 10, no. 9 (1972): 837-841.
- [19] Itoh, Minoru, Hideyuki Nakagawa, Mamoru Kitaura, Masami Fujita, and Dmitri L. Alov. "Photoluminescence of orthorhombic and cubic single crystals." *Journal of Physics: Condensed Matter* 11, no. 14 (1999): 3003
- [20] Kink, R., T. Avarmaa, V. Kisand, A. Lohmus, I. Kink, and I. Martinson. "Luminescence of cation excitons in and crystals in a wide excitation VUV region." *Journal of Physics: Condensed Matter* 10, no. 3 (1998): 693-700
- [21] Voloshinovskii, A., S. Myagkota, A. Gloskovskii, and S. Zazubovich. "Luminescence of CsPbCl₃ microcrystals in CsCl: Pb and PbCl₂: Cs crystals under synchrotron excitation." *Physics of the Solid State* 43, no. 10 (2001): 1885-1891.
- [22] Sun, H., L. Zhang, L. Wen, M. Liao, J. Zhang, L. Hu, S. Dai, and Z. Jiang. "Effect of PbCl₂ addition on structure, OH⁻ content, and upconversion luminescence in Yb³⁺/Er³⁺-codoped germanate glasses." *Applied Physics B* 80, no. 7 (2005): 881-888.
- [23] Kitaura, Mamoru, Minoru Itoh, Hideyuki Nakagawa, and Masami Fujita. "Multiplication processes of electronic excitations in PbCl₂ crystals excited by vacuum ultraviolet radiation." *Journal of the Physical Society of Japan* 72, no. 3 (2003): 730-734.
- [24] Cruz-Zaragoza, E., R. Meléndrez, V. Chernov, M. Barboza-Flores, and T. M. Pitors. "Thermoluminescence properties of KCl_{1-x}KBr_x: Pb²⁺ mixed crystals." *Radiation protection dosimetry* 100, no. 1-4 (2002): 455-457.
- [25] Cheng, Z. Y., B. X. Gao, M. L. Pang, S. Y. Wang, Y. C. Han, and J. Lin. "Preparation and characterization of a novel layered perovskite-type organic/inorganic hybrid material containing silica networks." *Chemistry of materials* 15, no. 25 (2003): 4705-4708.

- [26] Pascual, J. L., J. M. Cabrera, and F. Agulló-López. "Absorption spectra of NaCl: Pb 2+ at the A-band region." *Solid State Communications* 19, no. 9 (1976): 917-920.
- [27] Kalužný, J., D. Ležala, J. Pedlíková, M. Kubliha, V. Labaš, J. Zavadil, and E. Mariani. "Electrical, dielectric and optical properties of TeO₂-PbCl₂-PbF₂ glass systems." *Journal of Optoelectronics and Advanced Materials* 7, no. 5 (2005): 2309-2315.
- [28] Okpala, U. V., F. I. Ezema, and R. U. Osuji. "A study of the optical properties of un-doped and potash doped lead chloride crystal in silica gel." *Advances in Applied Science Research*, 3,no.1(2012,):103-109.
- [29] Amitin, L. N., A. T. Anistratov, and A. I. Kuznetsov. "Comparison of the Electronic Structure of CsPbCl₃, PbCl₂, and CsCaCl₃ on the Basis of Optical Spectroscopy Data." *Physica Status Solidi (b)* 101, no. 1 (1980): K65-K68.
- [30] Plekhanov, V. G. "Investigation of the reflectance spectra of PbCl₂ and PbBr₂ single crystals with orthorhombic structure." *Physica Status Solidi (b)* 68, no. 1 (1975): K35-K38.
- [31] Dexter, David L. "A theory of sensitized luminescence in solids." *The Journal of Chemical Physics* 21, no. 5 (1953): 836-850.
- [32] Sobolev, V. V., A. I. Kalugin, I. V. Vostrikov, and V. Val Sobolev. "Electronic structure and optical properties of lead chloride." *Journal of Surface Investigation. X-ray, Synchrotron and Neutron Techniques* 3, no. 1 (2009): 48-57.
- [33] Kaldor, A., and G. A. Somorjai. "Photodecomposition of lead chloride." *The Journal of Physical Chemistry* 70, no. 11 (1966): 3538-3544.
- [34] G.Lillibai ,PhD Thesis, December 2012.
- [35] Uche, Don Okpala V. "Synthesis and characterization of local impurities doped lead chloride (PbCl₂) crystal in silica gel." *Advances in Applied Science Research*, 2013, 4(1):477-487.
- [36] Hardware Manual. *Jasco 570*, Jasco Corporation, Tokyo, Japan.
- [37] K.J.Devries, Doctoral Dissertation, University of Utrecht (1965)
- [38] De Vries, K. J., and J. H. Van Santen. "Ultraviolet absorptions of non-stoichiometric lead chloride PbCl₂." *Physica* 30, no. 11 (1964): 2051-2058.
- [39] Rejeena, I., B. Lillibai, B. Nithyaja, PN V. Nampoori, and P. Radhakrishnan. "Optical Studies on Sol-Gel Derived Lead Chloride Crystals." *Journal of Engineering Computers & Applied Sciences* 2, no. 4 (2013): 5-9.
- [40] Liidja, G., and VI Plekhanov. "Low-temperature X-ray and photoluminescence of lead halide crystals." *Journal of Luminescence* 6, no. 2 (1973): 71-76.

Chapter 3

- [41] Iwanaga, Masanobu, Masayuki Watanabe, and Tetsusuke Hayashi. "Relaxation of excitons into charge-separated pairs in pbbr 2 and pbcl 2 crystals." *International Journal of Modern Physics B* 15, no. 28n30 (2001): 3677-3680.
- [42] Parker, W. J., R. J. Jenkins, C. P. Butler, and G. L. Abbott. "Flash method of determining thermal diffusivity, heat capacity, and thermal conductivity." *Journal of Applied Physics* 32, no. 9 (1961): 1679-1684.
- [43] King, J., *Material Handbook for Hybrid Microelectronics*, Artec House, Norwood, Mass., 1988
- [44] Rejeena, I., B. Lillibai, Roseleena Toms, V.P.N. Nampoore, and P. Radhakrishnan. "Non-Linear Optical Studies On Sol-Gel Derived Lead Chloride Crystals Using Z-Scan Technique." *Journal of Engineering Computers & Applied Sciences* 3, no. 4 (2014): 46-50.
- [45] Rejeena, I., M. H. Rahimkutty, V. P. N. Nampoore, and P. Radhakrishnan. "Effect of nonlinear absorption on electric field applied lead chloride by Z-scan technique." In *Light and its Interactions with Matter*, AIP Publishing, 1620, no. 1(2014), pp. 422-425.
- [46] Sheik-Bahae, Mansoor, Ali A. Said, T-H. Wei, David J. Hagan, and Eric W. Van Stryland. "Sensitive measurement of optical nonlinearities using a single beam." *Quantum Electronics, IEEE Journal of* 26, no. 4 (1990): 760-76937.
- [47] Kiran, P. Prem, NKM Naga Srinivas, D. Raghunath Reddy, Bhaskar G. Maiya, Aditya Dharmadhikari, Arvinder S. Sandhu, G. Ravindra Kumar, and D. Narayana Rao. "Heavy atom effect on nonlinear absorption and optical limiting characteristics of 5, 10, 15, 20-(tetraolyl) porphyrinato phosphorus (V) dichloride." *Optics Communications* 202, no. 4 (2002): 347-352.
- [48] Aneeshkumar, B., Pramod Gopinath, C. P. G. Vallabhan, V. P. N. Nampoore, P. Radhakrishnan, and Jayan Thomas. "Optical-limiting response of rare-earth metallo-phthalocyanine-doped copolymer matrix." *JOSA B* 20, no. 7 (2003): 1486-1490.
- [49] Irimpan, Litty, A. Deepthy, Bindu Krishnan, V. P. N. Nampoore, and P. Radhakrishnan. "Nonlinear optical characteristics of self-assembled films of ZnO." *Applied Physics B* 90, no. 3-4 (2008): 547-556.
- [50] Tintu, R., V. P. N. Nampoore, P. Radhakrishnan, and Sheenu Thomas. "Nonlinear optical studies on nanocolloidal Ga-Sb-Ge-Se chalcogenide glass." *Journal of Applied Physics* 108, no. 7 (2010): 073525-1-5.

Chapter 4

Linear and Nonlinear Optical studies on Lead Fluoride (PbF₂) Crystals

Abstract

This chapter gives extensive details regarding the spectral and optical nonlinear characteristics of gel grown lead fluoride crystals of pure, UV irradiated and IR irradiated samples. The photoluminescence and decay mechanisms are also explained in this chapter. The nonlinear optical characterisation of these materials are performed using Bahae's method at different laser intensities. The nature and sign of nonlinear absorption coefficient is also found out.

4.1 Introduction

The heavy metal halide crystals like lead fluoride have found many applications in the field of optoelectronics owing to their significant optical properties. From the literature survey, it is clear that many researchers worked on lead halides because of their wide applications.[1–21]. R. W. G. Wyckoff worked on the structural modifications of lead halides. Out of the three lead halide crystals, lead fluoride crystallizes in an orthorhombic structure [22]. Major works on lead fluorides were done by M.Fujitha et al [1]. They give a clear picture of the optical and electronic characteristics of PbF_2 . R.Kink and M..Kituara studied the multiplication of electronic excitations in lead halides using a light source of synchrotron radiation [8, 11]. The crystallization of lead fluoride includes two phases namely the α -lead fluoride and the β -lead fluoride. The α - PbF_2 corresponds to an orthorhombic structure like lead chloride or lead bromide and the β - PbF_2 exhibits a cubic structure like calcium fluoride. PbF_2 is widely used in scintillation devices which is reported by D.L.Alov et al[2]. The layer properties of lead fluoride are also seen in literature[19]. The layered nature of lead fluoride produced two dimensional excitons and give low crystal symmetry. A.D.Brothers and J.T.Pajor studied the temperature and hydrostatic pressure effects on the exciton spectra of lead fluoride[23].

There is only a few studies on the nonlinear aspects of lead fluoride .Our aim is to find out the optical nonlinear responses of the lead fluoride crystals prepared by gel method. The nature of nonlinearity in the crystals of lead fluoride are determined using the open aperture Z-scan experiment. This chapter also explains the limiting response of the crystal samples in solution phase.

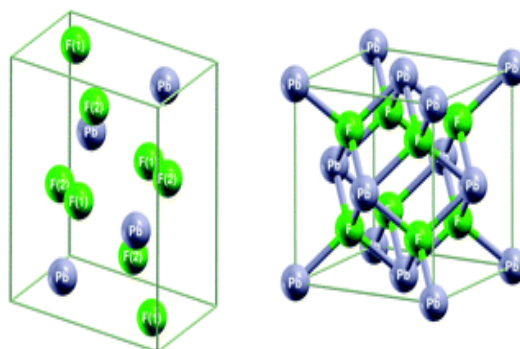


Figure.4.1. Crystal structure of orthorhombic α - PbF_2

Table.4.1. Properties of lead fluoride from literature

Molecular formula	PbF_2
Molar mass	245.20 g/mol
Appearance	white powder
Odor	odourless
Density	8.445 g/cm ³ (orthorhombic) 7.750 g/cm ³ (cubic)
Melting point	824°C
Boiling point	1293°C
Solubility product, K_{sp}	2.05×10^{-8} (20 °C)
Solubility	soluble in nitric acid; insoluble in acetone and ammonia

4.2 Lead Fluoride sample preparation

The synthesis of lead fluoride goes through the following steps

4.2.1 Preparation of hydro silica gel

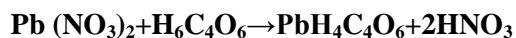
Hydro silica gel is prepared for growing single crystals of lead fluoride. It can be prepared from an aqueous solution of sodium meta silicate powder by changing the pH of the solution. An acid component added to the solution helps to vary the pH level. Here tartaric acid is employed. After adjusting the pH, the solution is transferred to crystallization vessels for polymerization. The size and shape of the vessels depend on the mode of experiment and the specific requirement. The mechanical properties of a fully developed gel varies widely with the density of the sodium meta silicate solution. Greater the gel density, smaller the pore size which in turn decreases the diffusion rate of ions through it.

4.2.2 Lead Fluoride crystals from gel

To the hydro silica gel, 4N Potassium Fluoride solution was poured over the gel in a test tube which was incorporated with a colloidal precipitate of 1N lead tartrate.

The reactions of lead nitrate, tartaric acid and potassium fluoride (99.9% Sigma-Aldrich) gives the lead fluoride crystal.

The chemistry behind the crystal formation is as follows



4.2.3 Ultra Violet irradiated PbF₂

The test tube containing the gel and top solution of potassium fluoride and lead nitrate is irradiated with ultra violet radiations using a UV lamp (insect Killer)

for two weeks. The PbF₂ crystals obtained by this method is notated as PbF₂ UV.

4.2.4 Infrared Irradiated PbF₂

Using the infrared radiations (HL4311 (PHILIPS) 230V~50Hz~150W) another PbF₂ sample is prepared and is represented as PbF₂ IR.

Thus we prepared three types of lead fluoride crystals via PbF₂ pure, PbF₂ UV and PbF₂ IR for our studies in this chapter.

4.3 Structural studies

Lead fluoride crystals prepared from the gel method were subjected to X-ray diffraction for structural determination and crystallinity confirmation. Figure 4.2 illustrates the X-ray diffraction pattern of PbF₂ crystal. The distinct peaks with sufficient intensities tell us that the gel derived lead fluoride is a crystal belonging to the orthorhombic group.

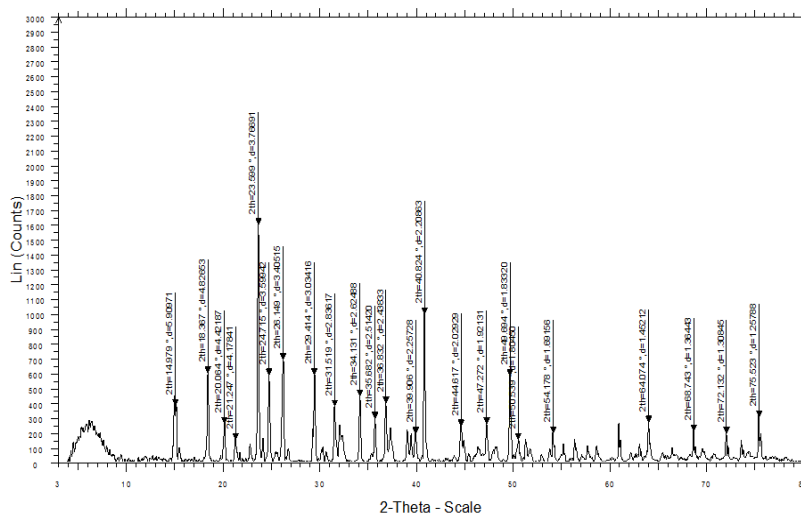


Figure.4.2. Powder X-ray diffraction pattern of PbF₂ crystal

4.4 Linear optical Measurements

4.4.1 Absorption

In order to study the variation of transmittance in the lead fluoride samples, a linear absorption spectra was taken at room temperature. The crystalline samples of PbF_2 were powdered and dissolved in single distilled water to prepare a sample solution of 0.02 gm/ml concentration. The preparation of the solution sample and the theory of absorption spectroscopy were discussed in chapter 2. The sample solution of PbF_2 was taken in a cuvette of 1cm thickness and the absorbance of the solution was recorded using a spectrophotometer. Figure.4.3 shows the linear uv/visible absorption spectra of PbF_2 samples.

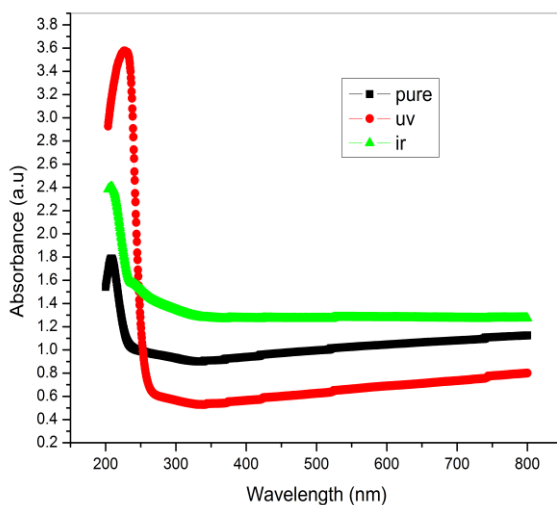


Figure 4.3. UV/VIS absorption spectra of pure, UV irradiated and IR irradiated PbF_2 crystals

The size of the absorbing system and the probability that the electronic transition will take place control the absorptivity. The values of absorption coefficient α of the three PbF_2 crystals can be determined from the linear

absorption measurements. The absorption edge for pure PbF₂ is located in the ultra violet region corresponding to a wavelength of 250 nm. The peak wavelength of absorption for UV and IR irradiated samples are 265nm and 255 nm respectively. The peak obtained at this particular wavelength suggested that these lead fluoride crystals in solution phase are suited for nonlinear measurements using a laser of 532 nm wavelength. The absorption edges are corresponding to the electronic transition to the heavy metal cation. The absorption of ultra violet radiations result from the excitation of electrons from ground to excited states. The values of linear absorption coefficient α and the wavelength corresponding to the absorption peak (λ_{Peak}) for the three different lead fluoride samples are given in table.4.2

Table.4.2. Measured values of α and λ_{Peak} for the three different PbF₂ crystals

Sample crystal	λ_{Peak} (nm)	α (cm ⁻¹)
Pure PbF ₂	250	1.0194
UV irradiated PbF ₂	265	0.6561
IR irradiated PbF ₂	255	1.2765

4.4.2 Optical band gap of PbF₂ crystals

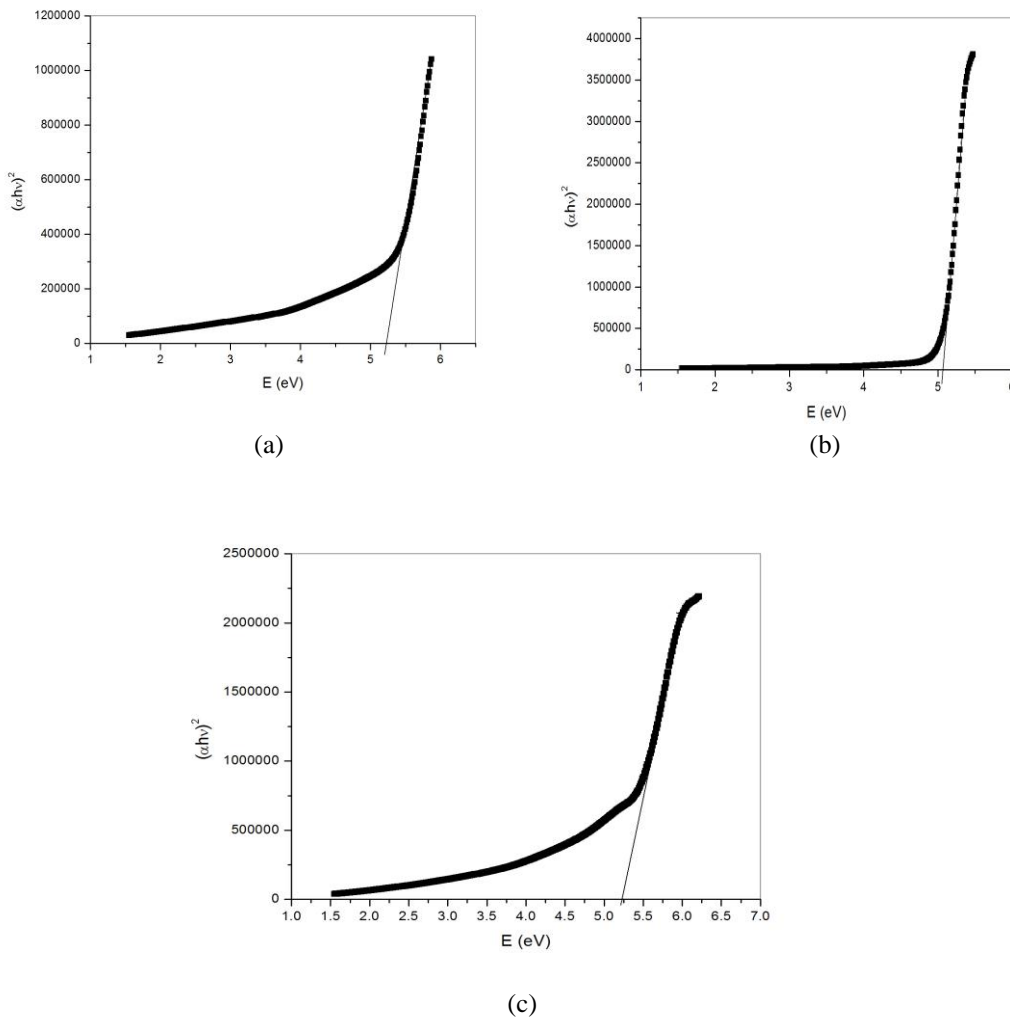


Figure.4.4. Optical band gap plot of (a) pure (b) UV irradiated and (c) IR irradiated PbF₂ samples.

Figure.4.4 shows the optical band gap plots of the three PbF₂ samples. The band gap of lead fluoride samples were determined by using the UV –VIS spectra. The extrapolation of the curves to the X-axis gives the values of direct

band gap for pure, UV irradiated and IR irradiated PbF₂ crystals in solution phase. The band gap values obtained are 5.22 eV for pure PbF₂, 5.05 eV for UV irradiated PbF₂ and 5.15 eV for IR irradiated PbF₂. The direct band gap of PbF₂ is comparable with that reported in literature [24]. The band gap values are attributed to the transition from 6s to 6p states in lead ions as in the case of PbCl₂ and PbBr₂.

4.4.3 Fluorescence Emission Studies

The emission characteristics of the gel derived lead fluoride crystals were carried out by taking the fluorescence spectra at different excitation wavelengths. The specification of the fluorimeter used for these luminescence studies on PbF₂ crystals were already described in chapter 2. The following figures (Figure.4.5) illustrate the photoluminescence spectra in the lead fluoride samples.

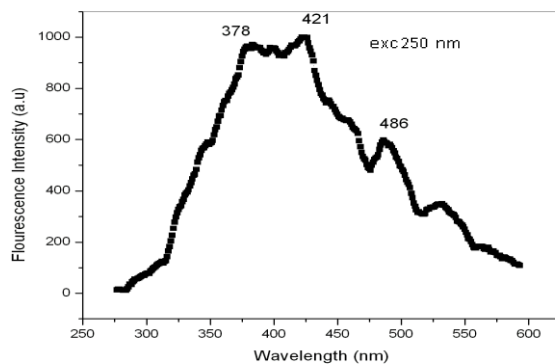


Figure.4.5.(a) Emission spectra of pure PbF₂ at an excitation wavelength of 250 nm.

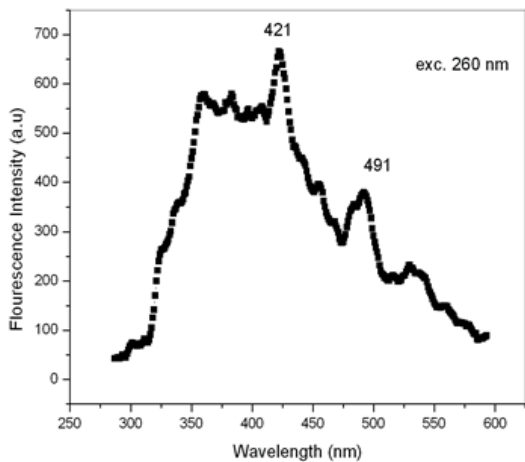


Figure.4.5(b) Emission spectra of pure PbF_2 at an excitation wavelength of 260 nm.

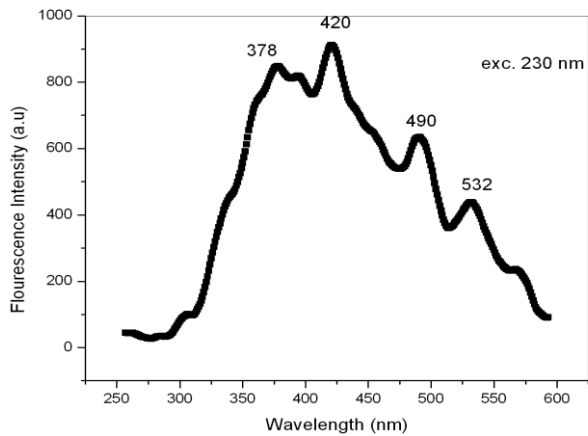


Figure.4.5(c) Emission spectra of ultra violet (UV) irradiated PbF_2 at an excitation wavelength of 230 nm.

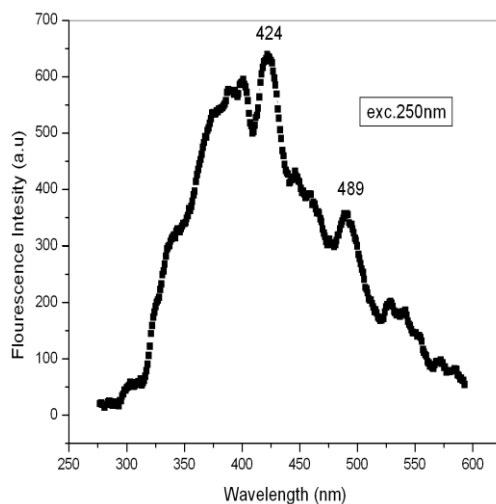


Figure.4.5(d) Emission spectra of ultra violet (UV) irradiated PbF_2 at an excitation wavelength of 250 nm.

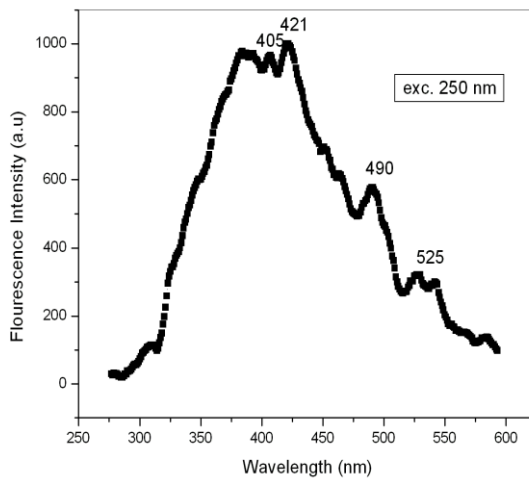


Figure.4.5(e) Emission spectra of infrared (IR) irradiated PbF_2 at an excitation wavelength of 250 nm.

From the fluorescence emission spectra of pure PbF_2 sample (figure 4.5(a)), we have obtained three emission peaks at wave lengths 378 nm, 421 nm and 486 nm respectively for an excitation of 230 nm. If the excitation wavelength is increased to a value of 260 nm, two strong emissions are obtained for pure PbF_2 at 421nm and 491 nm respectively(figure.4.5(b)). For UV irradiated PbF_2 ,four strong emissions at 378 nm, 420 nm, 490 nm and 532 nm are located by an excitation of 230 nm. When the wavelength of excitation becomes 250 nm, only two peaks are obtained at 424 nm and 489 nm respectively. The IR PbF_2 shows three powerful emissions at 421, 490 and 525 nm at an excitation of 250 nm as shown in figure.4.5(e).

The emission mechanism in these lead fluoride in solution phase can be explained on the basis of radiative transitions in the crystals[20]. The shape of the fluorescence spectra of these materials are affected by the distribution of electrons and holes within their bands. The photoluminescence in these samples are due to the broad Gaussian bands having large values of Stokes shift. These shifts in the crystalline PbF_2 indicate a strong exciton-phonon interaction within the crystal [25-26]. Thus the fluorescence of lead fluoride is composed of excitonic luminescence. The mechanism of luminescence in PbF_2 can be explained on the basis of the self-trapped exciton model suggested. Alov, D. L, and S. I. Rybchenko [2].

4.5. Thermal Diffusivity Measurements in PbF_2 crystal.

A mode matched dual beam thermal lens experimental technique was employed to study the heat expansion and thereby the thermal diffusivity of the lead fluoride crystal samples. Rhodamine 6G dye was added to the crystal solutions for enhancing the absorption of PbF_2 . The experimental procedure is discussed in the former chapters 2 and 3. A thermal lens curve is obtained by plotting the probe beam intensity against the time in milliseconds. Figure 4.6 represents the thermal lens plot of Rhodamine incorporated PbF_2 samples. The

transient change in the refractive index by thermal fluctuations prompt the lead fluoride crystal samples to behave like a lens called thermal lens.

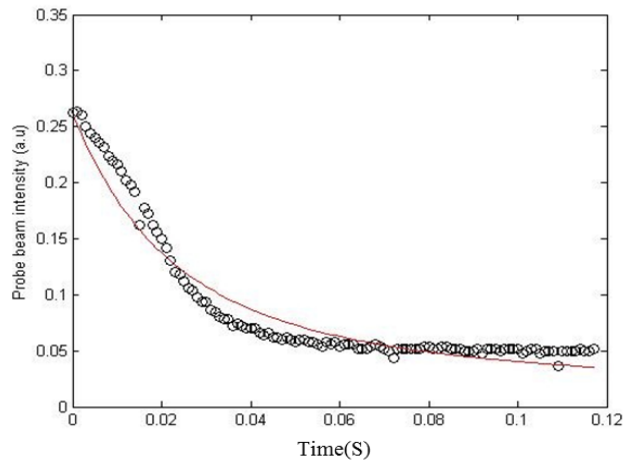


Figure.4.6.(a) Thermal lens plot of pure Rh-PbF₂

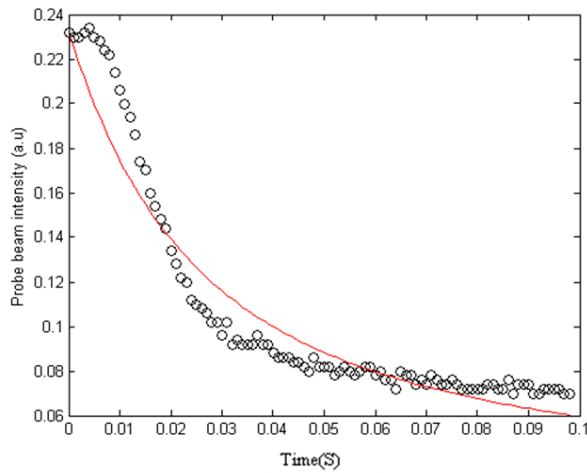


Figure.4.6.(b) Thermal lens plot of ultra violet irradiated Rh-PbF₂

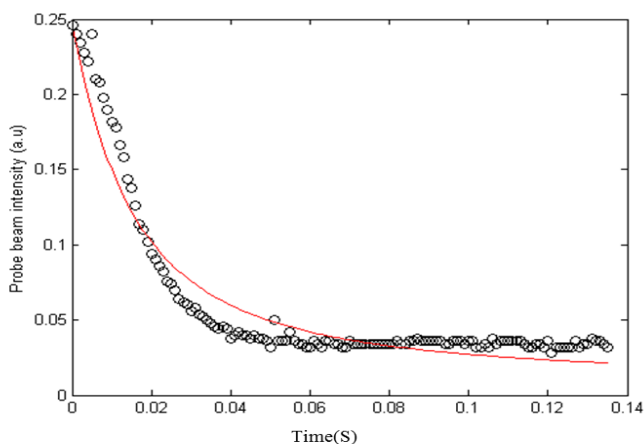


Figure.4.6.(c) Thermal lens plot of infrared irradiated Rh-PbF₂

Table.4.3 Measured values of D, θ_c , and t_c for Rhodamine-6G incorporated lead Fluoride solution

Sample	t_c (mS)	θ_c	D (cm ² /S) x 10 ⁻³
PbF ₂ Pure	40.39	-707.18	3.30
PbF ₂ UV	20.21	-3033.27	6.08
PbF ₂ IR	20.27	-447.31	4.75

The thermal lens plots of the pure, UV irradiated and IR irradiated lead fluoride incorporated with Rhodamine indicate the lensing behavior of these crystals. Thermal diffusion D of these materials were calculated using the values of decay time and the fitting parameter which is obtained from the theoretical fit to the experimental data. Diffusivity of UV irradiated PbF₂ is high compared to that of pure and IR irradiated ones. The high value of thermal diffusivity of PbF₂ indicates that they are well suited for coolant applications .

4.6. Nonlinear optical Studies on PbF₂ crystals using Z-scan Experiment

The optical nonlinearity in the lead fluoride samples was measured using open aperture Z-scan experimental set up. The detailed theory and experimental descriptions were explained in chapter.2. We plot the transmittance values of PbF₂ against the position z along the focal point of a lens. The following figures (figure.4.7, 4.8 and 4.9) show the normalized transmittance of these PbF₂ crystals in solution phase at three input laser powers 100 MW/cm², 150 MW/cm² and 200 MW/cm².

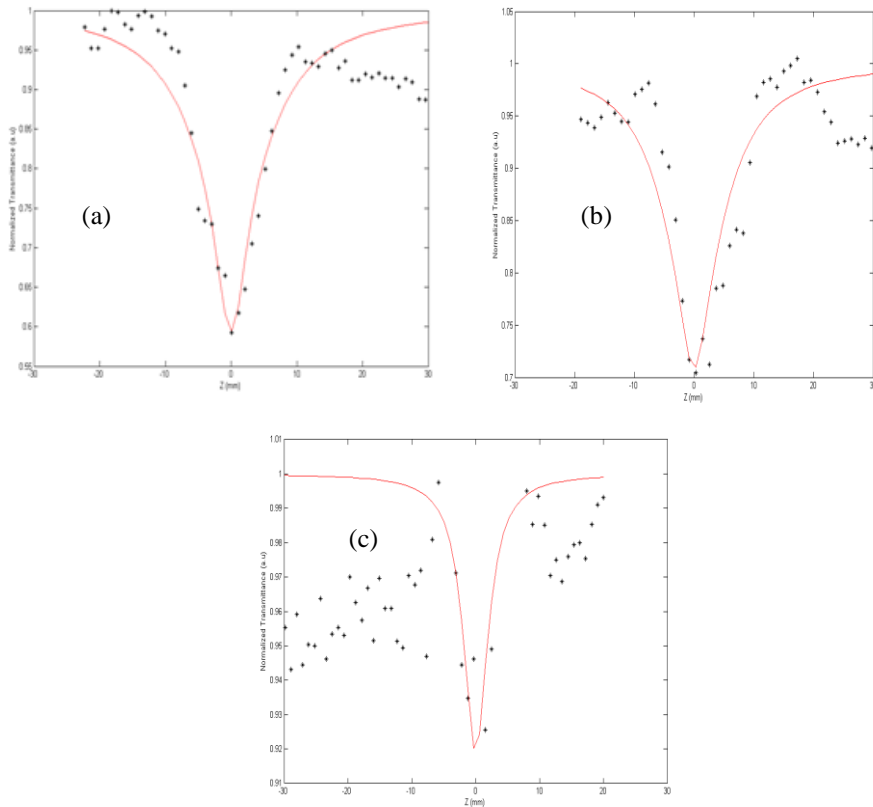


Figure.4.7. :Open aperture Z-scan plot of pure PbF₂. at different laser powers, (a)100 MW/cm², (b)150 MW/cm² and (c) 200 MW/cm²

Chapter 4

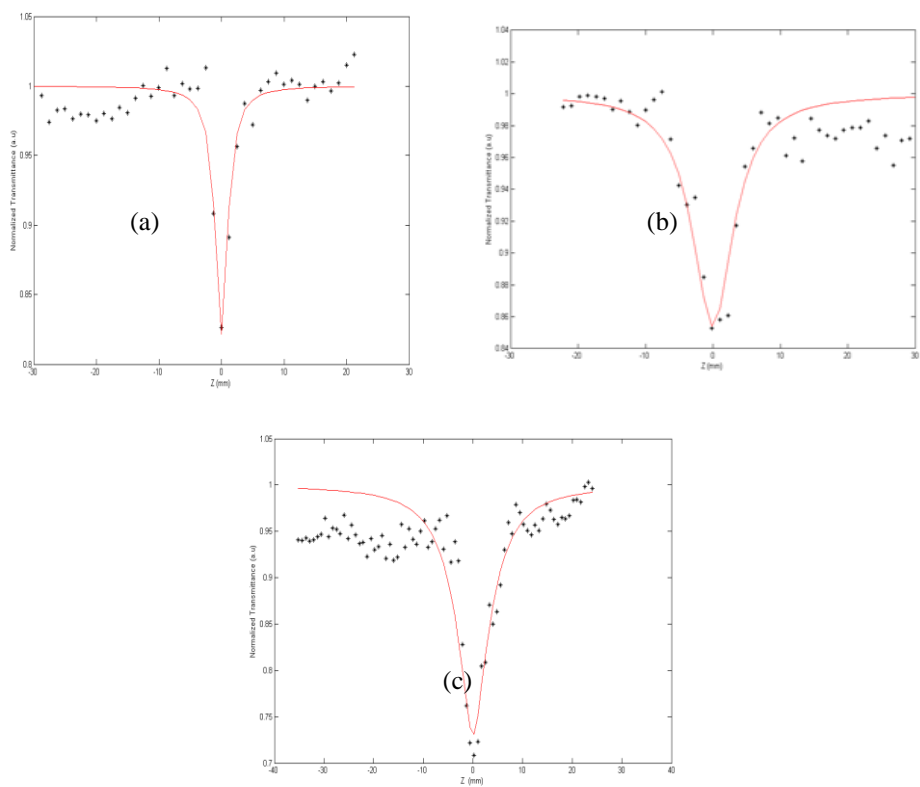
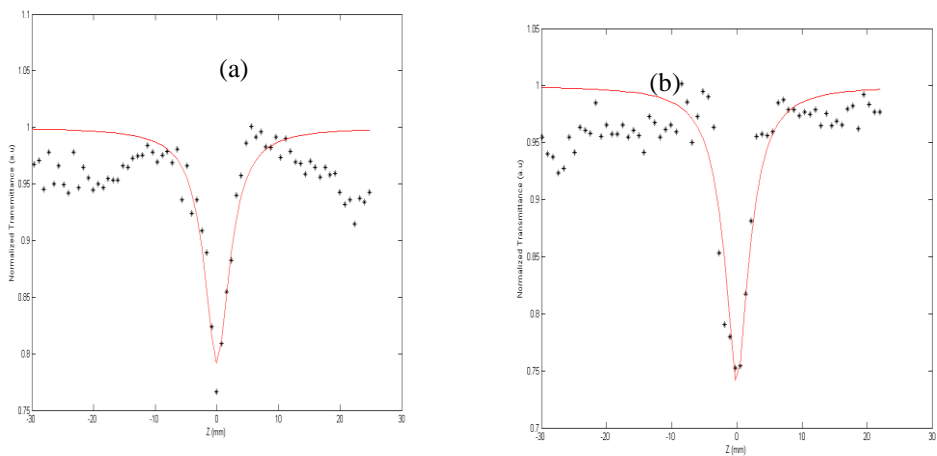


Figure 4.8. : Open aperture Z-scan plot of UV irradiated PbF_2 at laser powers, (a) 100 MW/cm^2 , (b) 150 MW/cm^2 and (c) 200 MW/cm^2



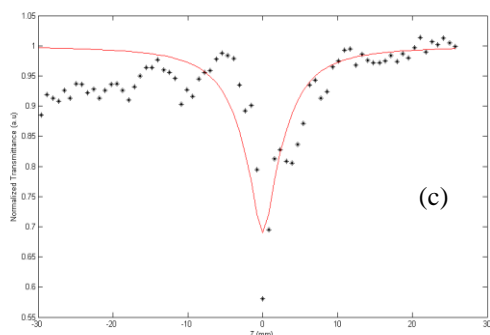


Figure.4.9. :Open aperture Z-scan plot of IR irradiated PbF₂ at laser powers, (a)100 MW/cm², (b)150 MW/cm² and (c) 200 MW/cm²

The scattered traces are due to the signal noise and the convective movement of the particles in the medium. This highly sensitive method of scanning the crystal samples is an effective tool for studying the nonlinear absorption of the respective samples of PbF₂. The absorptive nonlinearity in these materials are due to the modification of optical properties of the PbF₂ by the irradiation of a 532 nm Q switched laser. The transmittance of PbF₂ decreases with the input laser intensity towards the focus and then increases to give a symmetric shape to the nonlinear Z-scan curves showing a valley in the nonlinearity. The valley type transmittance are due to the reverse saturable absorption of lead fluoride crystals in solution phase. The nonlinear absorption coefficient β is calculated from the values of q that determines the depth of the open aperture curves of PbF₂. Knowing the effective thickness of the PbF₂ sample, absorptive nonlinearity can be calculated using the equation(2) given in chapter3. Table 4.4 gives the values of nonlinear absorption coefficient at three input laser power densities 100, 150 and 200 MW/cm². From the values of β , the imaginary part of third order susceptibility $\{ \text{Im}(\chi^3) \}$ is calculated and the values are tabulated .

Table.4.4. Measured values of nonlinear absorption coefficient and imaginary part of third order susceptibility for PbF₂.

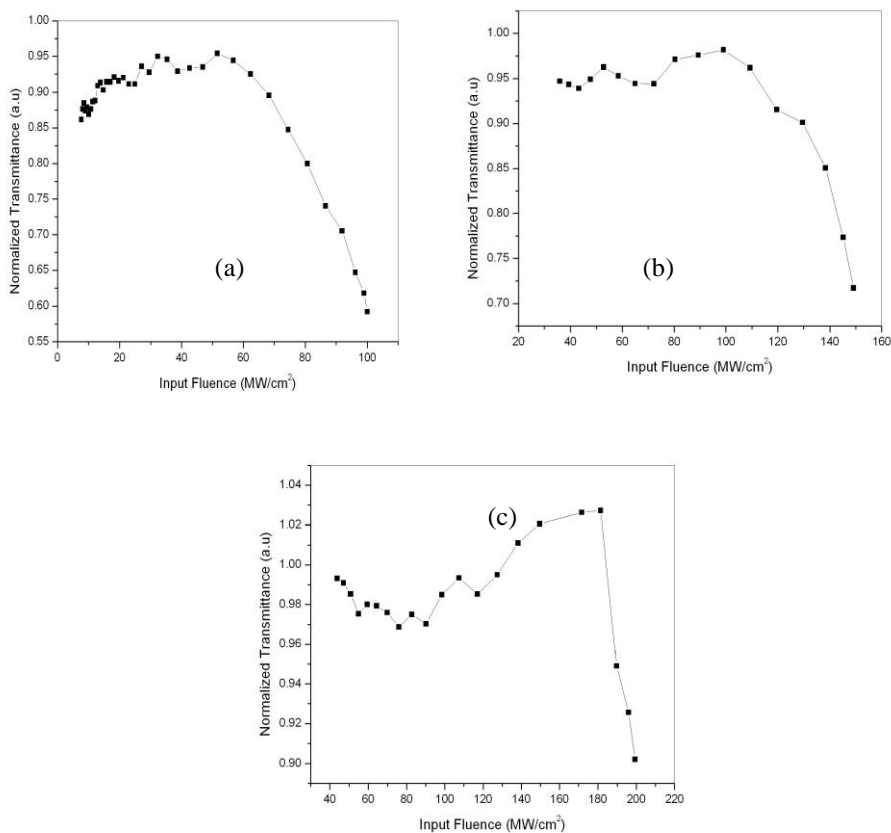
Sample	β (cmGW ⁻¹)			$\text{Im}(\chi^{(3)})$ (esu) $\times 10^{-10}$		
	I_0 (100 MWcm ⁻²)	I_0 (150 MWcm ⁻²)	I_0 (200 MWcm ⁻²)	I_0 (100 MWcm ⁻²)	I_0 (150 MWcm ⁻²)	I_0 (200 MWcm ⁻²)
PbF ₂ Pure	136	75	13	3.99	2.20	0.38
PbF ₂ uv	68	36	52	1.99	1.05	1.52
PbF ₂ IR	84	70	59	2.47	2.05	1.73

For the pure PbF₂ sample, the nonlinear absorption varies from 136 cm/GW to 13 cm/GW as the power varies from 40 μ J to 80 μ J. The ultra violet irradiated sample shows an absorptive nonlinearity of 68 cm/GW at an input fluence of 100 MW/cm². The nonlinear absorption of infrared irradiated samples ranges from 84 to 59 cm/GW. From the table, it is clear that the β values are large for 100 MW/cm² laser power and small for 200 MW/cm². This is due to the production of the states with higher absorption cross sections compared to that of the ground state[27]. The laser light used has a wavelength of 532 nm which indicates that the reverse saturable absorption in PbF₂ is due to the absorption of two photons. Thus we can conclude that the mechanism behind the nonlinearity in sol-gel derived lead fluoride crystal samples is TPA. The nonlinearity of lead halide based glasses have been reported [28] But the reported values of nonlinear absorption is smaller compared to that of our lead samples. This clearly indicates that our crystals of lead halides prepared by gel method are very much suited for nonlinear applications.

4.7 PbF₂ as an optical limiter

Open aperture experiment on the gel grown lead fluoride crystal samples shows that they have a third order nonlinearity associated with two photon absorption.

The reverse saturable absorption nature of these fluoride samples gives them the optical limiting response to a great extent[29-30]. The theory and applications of an optical limiter are discussed in chapter 2. The limiting characteristics of the PbF_2 sample solutions were taken at three input fluences 100 MW/cm^2 , 150 MW/cm^2 and 200 MW/cm^2 respectively. Figure 4.10 depicts the optical limiting of pure PbF_2 at these laser powers. The limiting behaviour of ultraviolet and infrared irradiated PbF_2 samples are shown in figures 4.11 and 4.12. The threshold limits are also evaluated and is given in table 4.5.



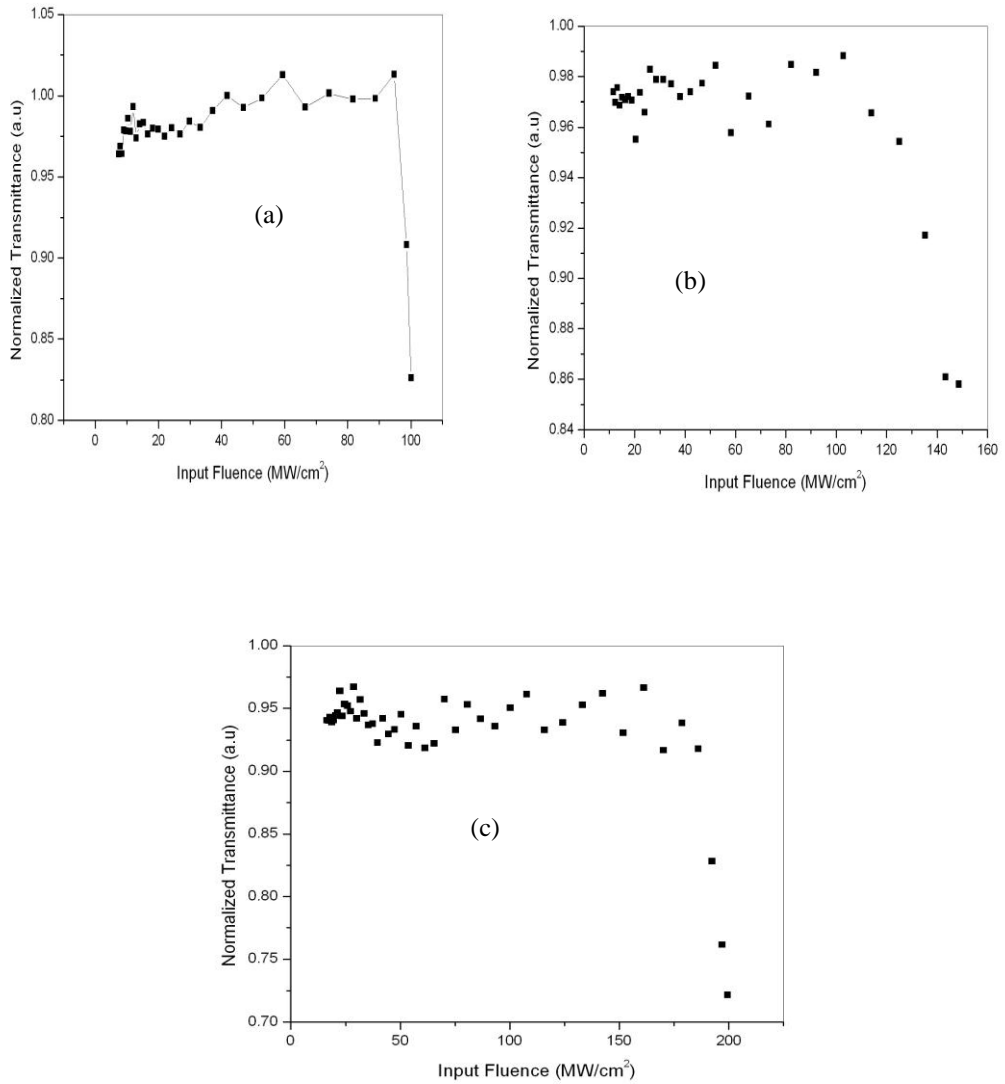


Figure.4.11: Optical limiting response of UV irradiated PbFr_2 at a laser power density of (a) $100 \text{ MW}/\text{cm}^2$ (b) $150 \text{ MW}/\text{cm}^2$ and (c) $200 \text{ MW}/\text{cm}^2$

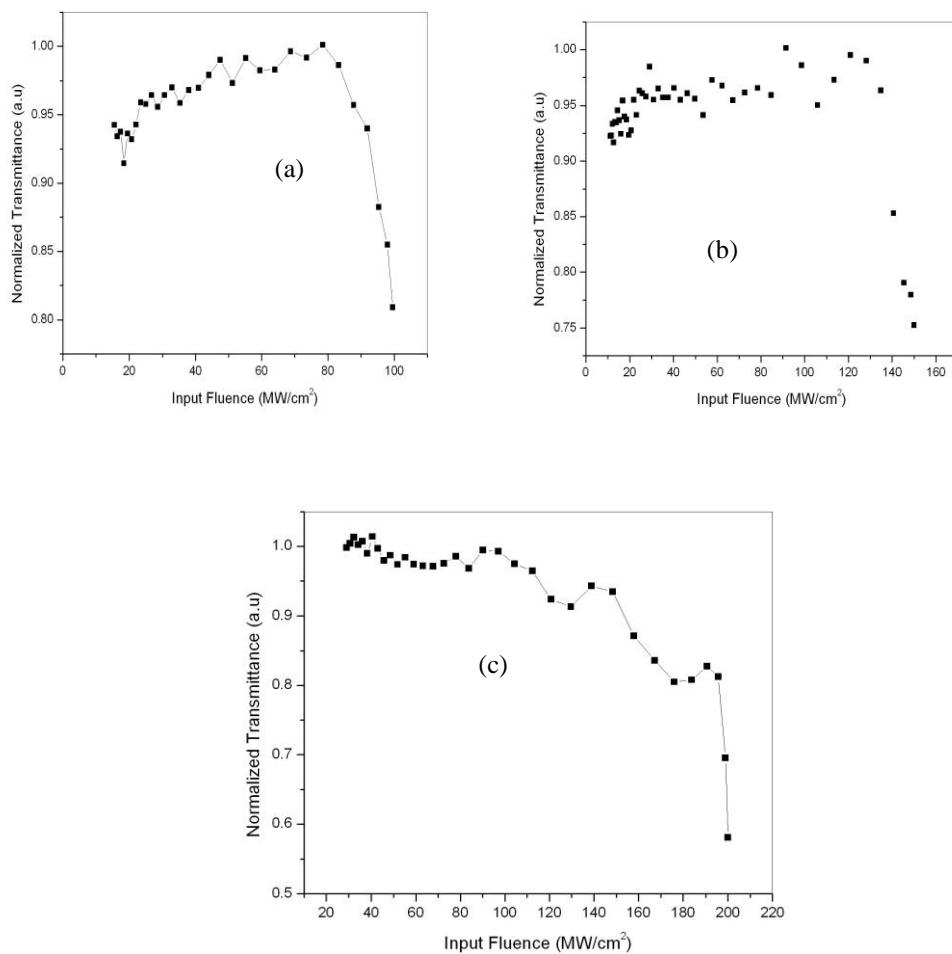


Figure.4.12: Optical limiting response of IR irradiated PbF_2 at a laser power density of (a) 100 MW/cm^2 (b) 150 MW/cm^2 and (c) 200 MW/cm^2

Table.4.5. Measured values optical limiting threshold for PbF₂ sample solutions

Sample	Optical limiting threshold (MWcm ⁻²)		
	I ₀ (100 MWcm ⁻²)	I ₀ (150 MWcm ⁻²)	I ₀ (200 MWcm ⁻²)
PbF ₂ Pure	68	108	181
PbF ₂ UV	89	115	185
PbF ₂ IR	82	125	174

Conclusions

Three types of lead fluoride crystals were prepared by solution–gel method. PbF₂ sample solution exhibits a UV absorption peak and the direct band gap varies from 5.05 eV to 5.22 eV. The photoluminescence in lead fluoride is due to the excitonic relaxations within the crystal. The heat diffusion mechanism is studied using TL technique. The high values of thermal diffusion of PbF₂ suggest that these materials have found applications in heat sinks. The nonlinear absorption of these materials by highly sensitive open aperture Z- scan experiment reveals that the normalized transmittance of PbF₂ shows a reverse saturable absorption at the three input laser power densities employed for the studies. A positive non linearity due to two photon absorption is obtained and the corresponding values are measured. The third order non linearity by RSA in PbF₂ crystal samples make them suitable for optical limiting applications. The limiting threshold of these samples are also determined.

References

- [1] Fujita, M., M. Itoh, Y. Bokumoto, H. Nakagawa, D. L. Alov, and M. Kitaura. "Optical spectra and electronic structures of lead halides." *Physical Review B* 61, no. 23 (2000): 15731-15737.
- [2] Alov, D. L., and S. I. Rybchenko. "Luminescence of orthorhombic PbF₂." *Journal of Physics: Condensed Matter* 7, no. 7 (1995): 1475.
- [3] Zamkov, A. V., I. T. Kokov, and A. T. Anistratov. "The Acousto-Optical Properties and Photoelasticity of PbBr₂ Single Crystals." *Physica Status Solidi (a)* 79, no. 2 (1983): K177-K180.
- [4] Ren, Q., L. Q. Liu, Z. G. Wang, X. S. An, G. H. Zhang, and D. Xu. "Refractive index and absorption of lead bromide crystals." *Materials Research Bulletin* 35, no. 3 (2000): 471-476.
- [5] Plekhanov, V. "Optical constants of lead halides." *Physica Status Solidi (b)* 57, no. 1 (1973): K55-K59.
- [6] Nistor, S. V., E. Goovaerts, and D. Schoemaker. "Direct observation of electron self-trapping in PbCl₂ crystals." *Physical Review B* 48, no. 13 (1993): 9575.
- [7] Eijkelenkamp, A. J. H., and K. Vos. "Reflectance Measurements on Single Crystals of PbFCl, PbFBr, and PbBr₂." *Physica Status Solidi (b)* 76, no. 2 (1976): 769-778.
- [8] Kitaura, M., and H. Nakagawa. "Self-trapped exciton and recombination luminescence in PbCl₂, PbBr₂ and their mixed crystals." *Journal of Luminescence* 72 (1997): 883-884.
- [9] Itoh, Minoru, Hideyuki Nakagawa, Mamoru Kitaura, Masami Fujita, and Dmitri L. Alov. "Photoluminescence of orthorhombic and cubic single crystals." *Journal of Physics: Condensed Matter* 11, no. 14 (1999): 3003
- [10] Kink, R., T. Avarmaa, V. Kisand, A. Lohmus, I. Kink, and I. Martinson. "Luminescence of cation excitons in and crystals in a wide excitation VUV region." *Journal of Physics: Condensed Matter* 10, no. 3 (1998): 693-700
- [11] Kink, R., A. Lohmus, and M. Selg. "Self-trapping and hot luminescence of excitons in rare gas solids." *Physica Status Solidi (b)* 107, no. 2 (1981): 479-490.

Chapter 4

- [12] J. Kanbe, Jun-ichiro, Hideo Takezoe, and Ryumyo Onaka. "Reflection spectra of PbCl₂ in the exciton region." *Journal of the Physical Society of Japan* 41, no. 3 (1976): 942-949.
- [13] J. Kanbe, Ph.D. thesis, Kyoiku University, 1977.
- [14] Chen, Jianming, Dingzhong Shen, Guohao Ren, Rihua Mao, and Zhiwen Yin. "A high-density inorganic scintillator: lead fluoride chloride." *Journal of Physics D: Applied Physics* 37, no. 6 (2004): 938-941.
- [15] Findley, Paul R., Zenglie Wu, and W. C. Walker. "Temperature dependence of the electronic band gap and exciton states of superionic Pb F 2." *Physical Review B* 28, no. 8 (1983): 4761.
- [16] Nakagawa, H., M. Terakami, and K. Yasuda. "Elementary processes of photolysis in lead halide crystals." *Radiation measurements* 33, no. 5 (2001): 819-822.
- [17] Achenbach, P., S. Baunack, K. Grimm, T. Hammel, D. Von Harrach, A. Lopes Ginja, F. E. Maas, E. Schilling, and H. Ströher. "Measurements and simulations of Cherenkov light in lead fluoride crystals." *Nuclear Instruments and Methods in Physics Research Section A: Accelerators, Spectrometers, Detectors and Associated Equipment* 465, no. 2 (2001): 318-328.
- [18] Woody, C. L., J. A. Kierstead, P. W. Levy, S. Stoll, A. B. Weingarten, D. F. Anderson, E. J. Ramberg et al. "A study on the use of lead fluoride for electromagnetic calorimetry." *Nuclear Science, IEEE Transactions on* 40, no. 4 (1993): 546-551.
- [19] Ren, Guohao, Dingzhong Shen, Shaohua Wang, and Zhiwen Yin. "Structural defects and characteristics of lead fluoride (PbF₂) crystals grown by non-vacuum Bridgman method." *Journal of crystal growth* 243, no. 3 (2002): 539-545.
- [20] Popov, P. A., A. V. Matovnikov, N. V. Moiseev, I. I. Buchinskaya, D. N. Karimov, N. I. Sorokin, E. A. Sulyanova, B. P. Sobolev, and M. A. Krutov. "Thermophysical characteristics of Pb_{0.679}Cd_{0.321}F₂ solid-solution crystals." *Crystallography Reports* 60, no. 1 (2015): 111-115.
- [21] Anderson, D. F., J. A. Kierstead, Paul Lecoq, S. Stoll, and C. L. Woody. "A search for scintillation in doped and orthorhombic lead fluoride." *Nuclear Instruments and Methods in Physics Research Section A: Accelerators, Spectrometers, Detectors and Associated Equipment* 342, no. 2 (1994): 473-476.
- [22] R. W. G. Wyckoff, *Crystal Structures*, 2nd edition, Wiley, New York, Vol. 1. 1963.

- [23] Brothers, A. D., and J. T. Pajor. "Temperature and hydrostatic pressure effects on the exciton spectra of some lead and cadmium halides." *Physical Review B* 14, no. 10 (1976): 4570-4577.
- [24] Findley, Paul R., Zenglie Wu, and W. C. Walker. "Temperature dependence of the electronic band gap and exciton states of superionic PbF₂." *Physical Review B* 28, no. 8 (1983): 4761.
- [25] Fox, Anthony Mark, and Mark Fox. *Optical properties of solids*. Vol. 2010. New York: Oxford university press, 2001.
- [26] Masanobu Iwanagaa,* , Tetsusuke Hayashib , "Exciton-relaxation dynamics in lead halides" *Journal of Luminescence* 102–103 (2003) 663–668.
- [27] Tintu, R., V. P. N. Nampoore, P. Radhakrishnan, and Sheenu Thomas. "Nonlinear optical studies on nanocolloidal Ga–Sb–Ge–Se chalcogenide glass." *Journal of Applied Physics* 108, no. 7 (2010): 073525-1-5.
- [28] de Araujo, Renato E., Cid B. de Araújo, Gäel Poirier, Marcel Poulain, and Younes Messaddeq. "Nonlinear optical absorption of antimony and lead oxyhalide glasses." *Applied physics letters* 81, no. 25 (2002): 4694-4696.
- [29] Sheik-Bahae, Mansoor, Ali A. Said, T-H. Wei, David J. Hagan, and Eric W. Van Stryland. "Sensitive measurement of optical nonlinearities using a single beam." *Quantum Electronics, IEEE Journal of* 26, no. 4 (1990): 760-76937.
- [30] Irimpan, Litty, V. P. N. Nampoore, and P. Radhakrishnan. "Spectral and nonlinear optical characteristics of nanocomposites of ZnO–CdS." *Journal of Applied Physics* 103, no. 9 (2008): 094914,1-8.

Chapter 5

Spectral and Nonlinear Optical studies on Calcium Tartrate (CaTT) crystals

Abstract

In the present chapter, the investigations on the optical linear and nonlinear responses of three different types of Calcium Tartrate single crystals (CaTT) viz pure, electric field and magnetic field applied samples are described. The sample crystals are prepared by sol-gel technique using a stock solution of sodium meta silicate. Absorption and emission studies performed on these crystals are explained. The mechanism of non radiative decay is also discussed. Absorptive nonlinear characteristics of the samples are studied by employing highly sensitive Z scan experimental technique using a Q- switched Gaussian laser beam. Optical limiting and switching characteristics of these samples are also taken up.

5.1 Introduction

The large interest in Calcium Tartrate (CaTT) nonlinear optical crystalline materials has been motivated by their potential use in the fabrication of all-optical photonic devices [1]. Transparent crystalline materials can exhibit different kinds of optical nonlinearities which are associated with a nonlinear polarization. Calcium Tartrate single crystals are famous for their ferroelectric, spectral and nonlinear optical characteristics. So these crystals have found many applications in the field of optoelectronics [2-9]. Medrano *et al* reported the ferroelectric behaviour of CaTT crystals [2]. CaTT crystals belong to the orthorhombic system with space group $P2_12_12_1$ having four molecules in the elementary unit cell [3,10]. Manuel E. Torres *et al* reported the structural characterization of CaTT crystals [11]. They prepared the crystals of Calcium Tartrate doped with barium, cobalt, nickel, zinc, manganese, strontium and cadmium. They found that the doped crystals exhibit a very high dielectric permittivity than the pure crystals.

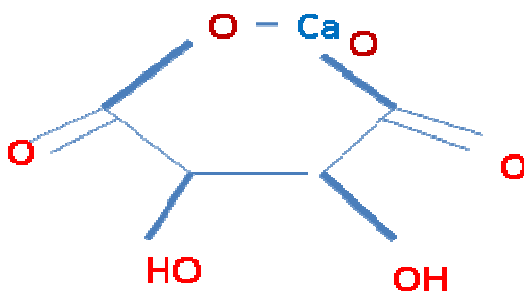


Figure.5.1 Structure of Calcium Tartrate crystal

FTIR and thermal properties of crystalline CaTT have been reported by X. Sahaya Shajan [12]. Influence of magnetic field on the growth and properties of Calcium Tartrate crystals were studied in detail by K.V. Saban and T. Jini [13]. Saban *et al* reported that the properties of materials can be improved by the application of magnetic field while designing. Fields are shown to influence the

size, nucleation rate, thermal stability, quality and lattice spacing of crystals [14-16]. Fujiwara et al. reported on magnetically oriented crystallization of organic diamagnetic materials [17-18]. K.Suryanarayana et al worked on the optical and structural characteristics of strontium doped Calcium Tartrate crystals[19]. They found that the strontium doped Calcium Tartrate crystals are optically transparent in nature. They studied the optical characteristics and effect of doping on the structural role of tartrate ion in the presence of two divalent metallic elements. The CaTT crystal exhibits optical nonlinearity approximately 0.1 times that of quartz. The optical linear and nonlinear responses of gel grown Calcium Tartrate crystals have been discussed in this chapter, Table 5.1 shows the properties of Calcium Tartrate crystals including its appearance, density, melting point and solubility.

Table 5.1 properties of Calcium Tartrate from literature

Molecular formula	$\text{CaC}_4\text{H}_4\text{O}_6$
Molar mass	190.16484 g/mol (anhydrous) 260.21 g/mol (tetra hydrate)
Appearance	hygroscopic white powder or colorless crystals
Density	1.817 g/cm ³
Melting point	160 °C
Solubility	0.037 g/100 ml (0 °C)

5.2. Preparation of sample crystal

The method of preparation is solution-gel technique which is described in the earlier chapters [20]. The first step of the synthesis of Calcium Tartrate is the preparation of hydro silica gel which acts as a medium for crystal growth. The specific gravity of the gel and pH of the solution determine the quality of the

crystals prepared. A stock solution of sodium meta silicate(SMS) was used for preparing good quality single crystals of CaTT. To the solution of sodium meta silicate having specific gravity 1.05, 1M tartaric acid was added and the pH was adjusted to be 4, 5, 6, 7 and 8 .This solution of SMS and tartaric acid was allowed to gel without any disturbances. Solution was kept for 24 to 36 hours to form a firm gel. The single diffusion method was employed to grow CaTT crystals in the gel medium. pH plays an important role in the growth of gel. Here we used 1M calcium nitrate solution as the top solution which is supernated over the gel. After 20 days, CaTT crystals were separated from the gel. Thus duration of two week was taken for the crystallization. The steps involved in the production of Calcium Tartrate crystals are shown in the figure 5.2. Only small crystals were produced by nucleation at lower pH values. Large sized crystals were produced for the studies conducted with pH7&8.

5.2.1. Preparation of Electric field applied Calcium Tartrate crystal- CaTT-ELE

Application of a potential difference of 10V to the test tube containing the gel (formed from SMS and Tartaric acid) and the top solution gives an electric field applied sample. The electric field is subjected to the solution in such a way that the applied field is perpendicular to the direction of diffusion of ions i.e; perpendicular to the length of the experimental test tube The crystal produced in this way is notated as CaTT-ELE.

5.2.2. Preparation of Magnetic field applied Calcium Tartrate crystal- CaTT-MAG

A magnetic field of 0.1 Tesla is applied across the test tube containing the gel and top solution of 1M calcium nitrate. The crystal thus obtained by the effect of magnetic field is represented as CaTT- MAG.

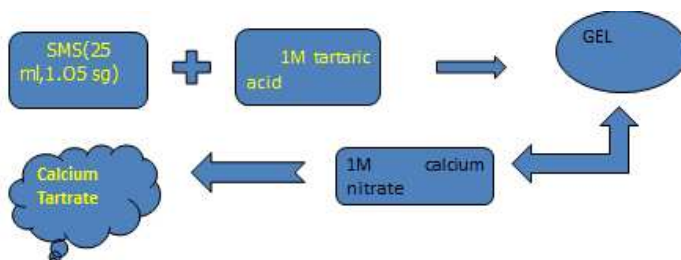


Figure.5.2. Schematic of crystal preparation of CaTT

The growth experiment was repeated for different densities of SMS and the pH values. The pH of the solution was varied by adding sufficient amount of SMS to the 1M tartaric acid. Thus three types of CaTT crystal samples were obtained for our studies viz pure, electric field applied and sample subjected to magnetic field.

5.3. Structural study using XRD

The crystal samples of Calcium Tartrate were separated from the gel using a filter paper and washed them[20]. Then the crystals were subjected to X-ray diffraction studies (XPERT-PRO using K-Alpha 1.54060Å⁰ (XRDML)) for structure determination. The crystalline nature was confirmed by the powder XRD. The variation in the intensity of diffracted ray only changes the optical property of CaTT. For our CaTT crystals, sharp peaks were obtained due to large crystallite size and high relaxation time. The XRD data of lattice parameters was compared with JCPDS values for identification of crystal structure. From this comparison, we confirmed that the crystal structure of Calcium Tartrate is orthorhombic. Figure 5.3 illustrates the XRD pattern of gel grown CaTT.

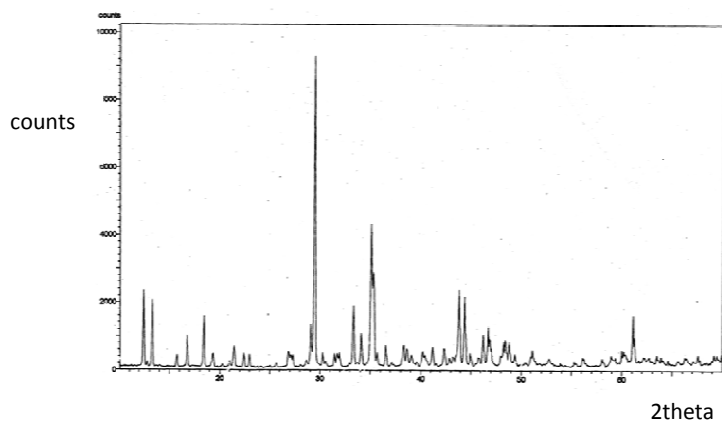


Figure 5.3. XRD of CaTT crystal

5.4 Linear Optical Characteristics

For the optical studies, the sample solutions of Calcium Tartrate were employed. The sample crystals were powdered using mortar and pestle. The powdered crystals were weighed about 0.344 gm and dissolved in 15 ml of single distilled water to prepare a solution of concentration 0.02 gm/ml. A magnetic stirrer was used for the dissolution process and the solvent evaporation was prevented by using a sealed glass container.

5.4.1 Absorption Studies

Calcium Tartrate single crystals have found applications in the field of optoelectronics. So the awareness of optical transmission range and the absorption edge of CaTT are essential. Efficient crystals exhibiting optical nonlinearity should have the cutoff wavelength in the range of 200 nm to 400 nm. In order to study the optical absorption mechanism of gel grown Calcium Tartrate crystals in solution phase, a room temperature linear UV-visible absorption spectra is taken using a JASCO UV/VIS spectrophotometer. The details of the device including the wavelength range and specifications are given in chapter.2. Figure.5.4 shows the absorption spectra of Calcium Tartrate

Spectral and Nonlinear optical studies on Calcium Tartrate (CaTT) crystals

crystals in solution phase. The spectral response of CaTT single crystal in solution phase gives the variation of absorbance against wavelength in nm scale.

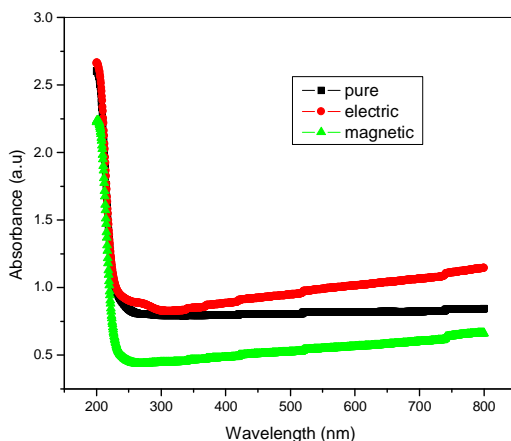


Figure.5.4 UV/VIS absorption spectra of CaTT crystal

The combined linear absorption of the Calcium Tartrate crystal in single distilled water is given in the above figure. From figure 5.4, it is obvious that all the three types of Calcium Tartrate samples exhibit a wide transmission in the entire visible and IR region. The absorption peak of Calcium Tartrate crystals in solution phase at the concentration 0.02 gm/ml is located in the ultraviolet region around 250 nm. The absorption peak at this wavelength is attributed to an excitonic peak[21]. In order to quantify the absorption of light through the CaTT crystals, it is necessary to evaluate the absorption coefficient α . The linear absorption coefficient α for the pure sample at 532 nm is 0.82 cm^{-1} while that for the electric and magnetic field applied samples are 0.98 cm^{-1} and 0.54 cm^{-1} respectively. The values of cut-off wavelength and the absorption coefficients of the three CaTT crystal samples are given in the following table.

Table.5.2. Measured values of α and λ_{Peak} for the three different CaTT crystals

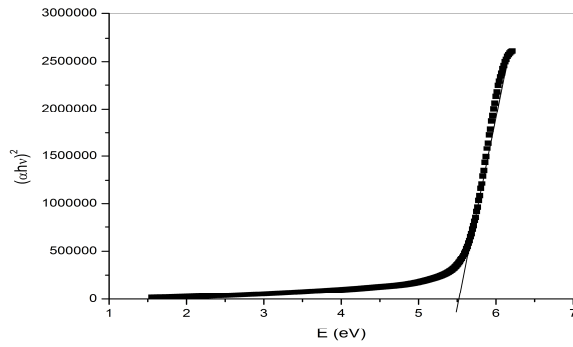
Sample crystal	λ_{Peak} (nm)	α (cm^{-1})
Pure CaTT	251	0.82
CaTT-ELE	257	0.98
CaTT-MAG	245	0.54

From the table, it is clear that the presence of electric field enhances the absorption of Calcium Tartrate while the magnetic field lowers the edge of linear absorption and the value of α shows a decrease. In these crystals the absorption edge at 250 nm is occurring by the optical transitions across the fundamental band gap of the Calcium Tartrate .

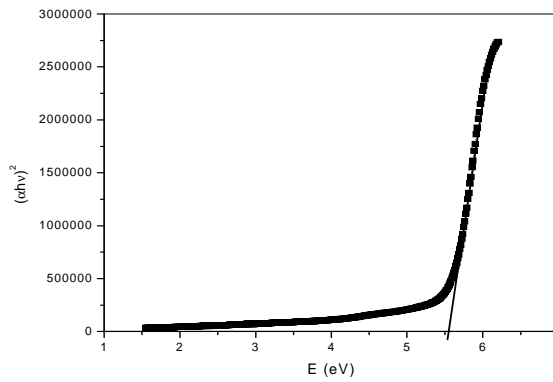
5.4.2 Optical Band gap of CaTT

Using the data of linear absorption, the band gap of the sample crystals can be calculated. This is done by plotting a graph between $(\alpha h\nu)^2$ along the Y-axis and $E=h\nu$ along the X axis. The curve thus obtained is extrapolated to $\alpha=0$ axis to obtain the optical band gap of CaTT crystal. The optical band gap plots of the Calcium Tartrate crystals in solution phase are shown in figure.5.5. The band gap corresponding to this particular wavelength of absorption is due to the electronic transition. The absorption spectrum of this crystal shows that Calcium Tartrate is suitable for nonlinear optical studies. The band gap values of the three types of sample crystals of CaTT are given in table.5.3. The magnetic field applied CaTT exhibits a high band gap of 5.58 eV. This high value may be due to the lessening of nucleation rate caused by the increase in the free energy of formation of crystal nuclei in the presence of magnetic field [13].

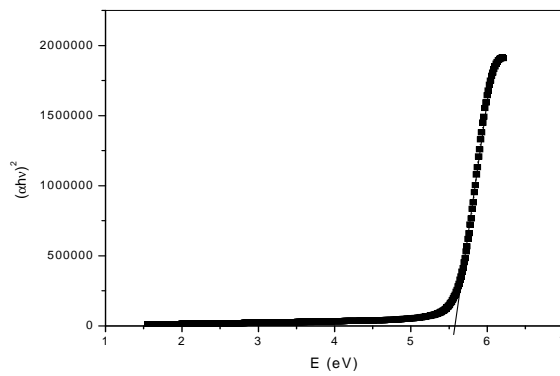
Spectral and Nonlinear optical studies on Calcium Tartrate (CaTT) crystals



(a)



(b)



(c)

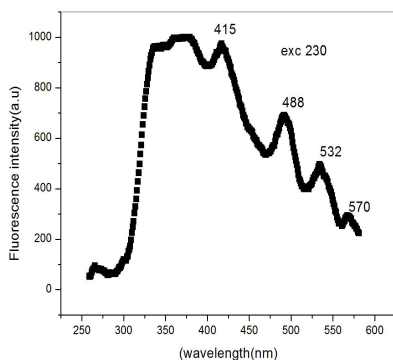
Figure 5.5. Optical band gap plot of (a) pure (b) electric field applied and (c) magnetic field applied CaTT samples.

Table 5.3. Measured values of optical band gap of CaTT

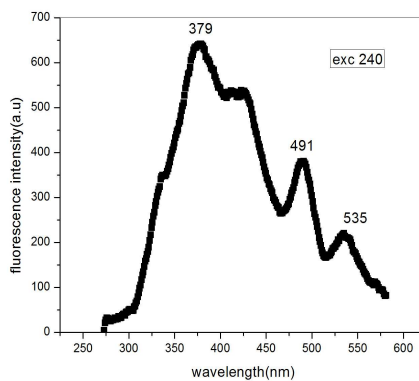
Sample	Optical Band gap (eV)
CaTT pure	5.52
CaTT electric	5.51
CaTT magnetic	5.58

5.4.3. Fluorescence Emission studies on CaTT

The room temperature fluorescence spectra reveal the emission characteristics of Calcium Tartrate crystals. The sample solution of Calcium Tartrate crystals was taken in a cuvette of 1 cm thickness and fluorescence was recorded using a fluorimeter. The luminescence of CaTT is investigated from the emission characteristics at different excitation wavelengths. The figures 5.6 to 5.11 illustrate the fluorescence emission of gel derived Calcium Tartrate. The excitation wavelengths used are 230 nm, 240 nm, 250 nm, 260 nm and 280 nm. For these excitation wavelengths, the fluorescence spectra of CaTT sample solutions are plotted as shown below.



(a)



(b)

Spectral and Nonlinear optical studies on Calcium Tartrate (CaTT) crystals

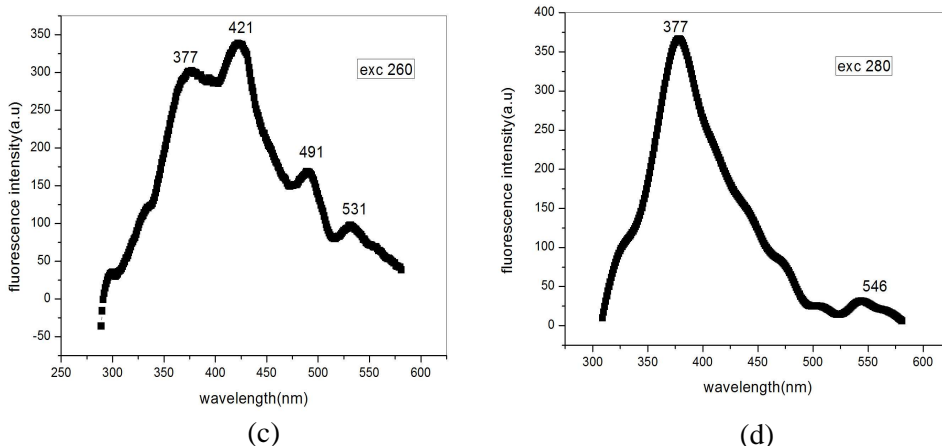


Figure.5.6 Emission spectra of pure CaTT at an excitation wavelength of (a) 230 nm (b) 240nm (c)260 nm and (d) 280 nm

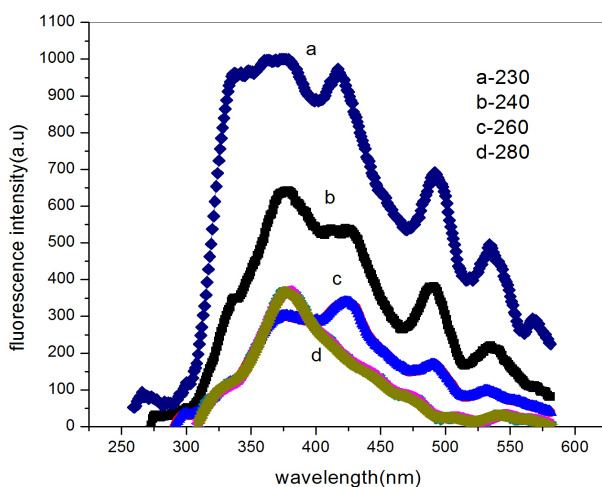


Figure.5.7 Combined fluorescence emission spectra of pure CaTT crystal

From the fluorescence spectra of CaTT crystals, it is inferred that the CaTT exhibits a sharp response of photoluminescence both in pure form and in the electric-magnetic field applied cases. When the solution of pure CaTT sample is excited using a wavelength of 230 nm, four emission peaks are

obtained at 415 nm, 488 nm, 532 nm and 570 nm. As the excitation wavelength is increased to a value of 240 nm, three strong emissions are obtained as shown in the figure 5.6(b). The peak values are 379 nm, 491 and 535 nm. For an excitation of 260 nm, four emissions are located around 377nm, 421 nm, 491 and 531 nm. The excitation of 280 nm gives a sharp peak at 377 nm and a short peak at 546 nm as given in figure 5.6(d). The dependence of fluorescence emission on the different excitations of CaTT pure crystals are illustrated in figure 5.7.

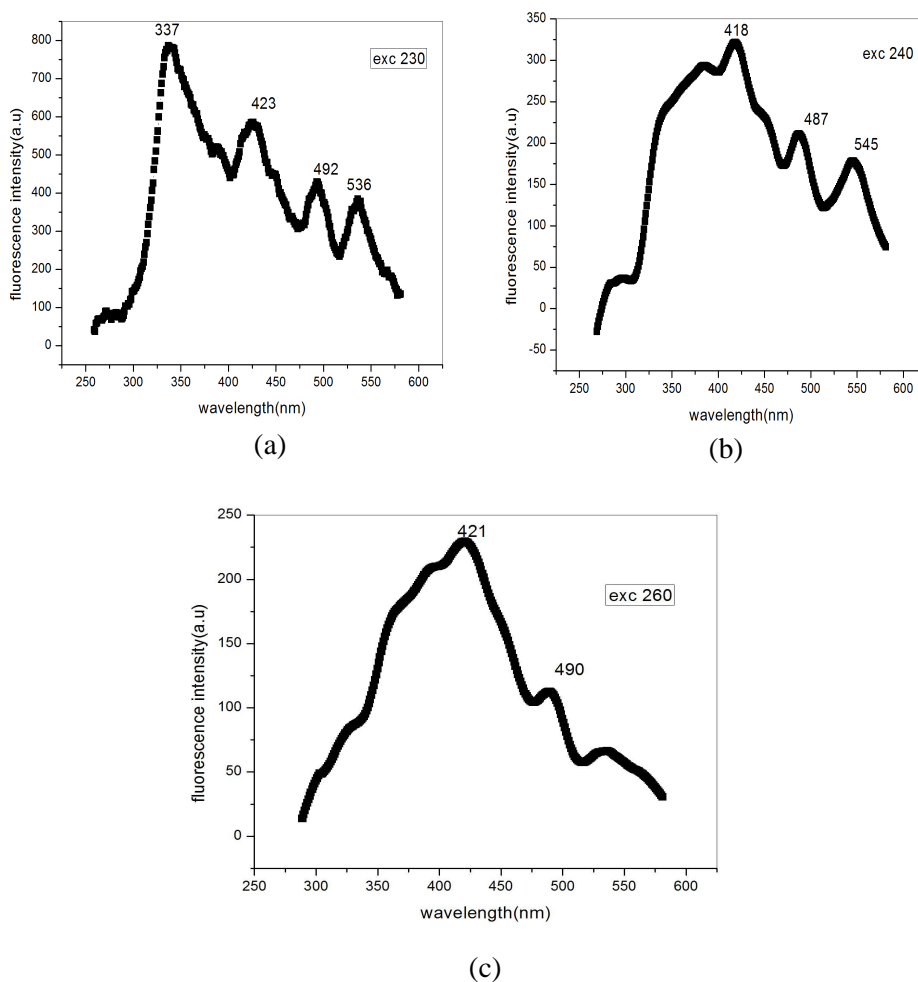


Figure.5.8 Fluorescence emission from electric field applied CaTT (CaTT-ELE) at an excitation wavelength of (a) 230 nm, (b) 240 nm and (c) 260 nm

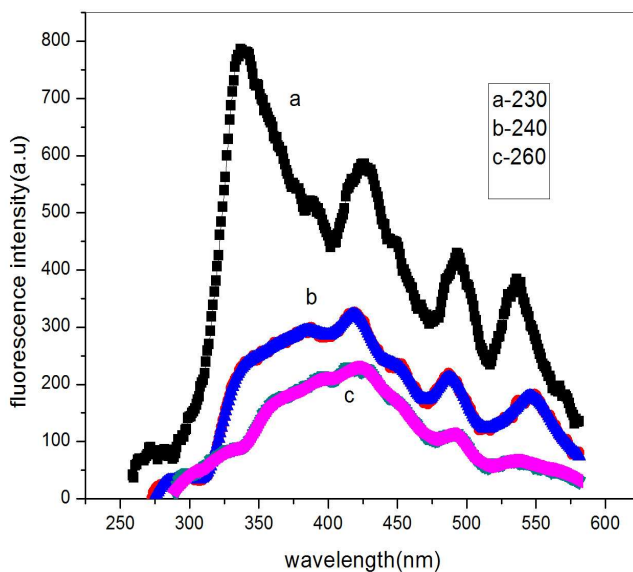
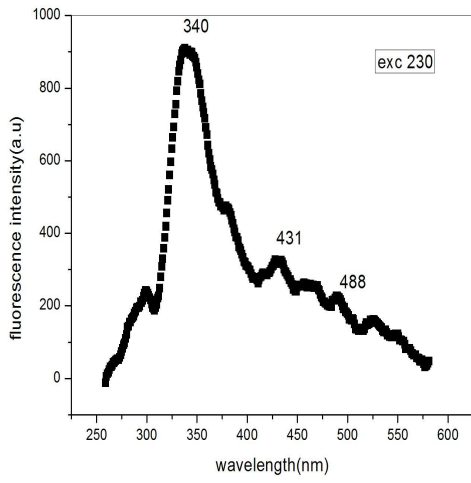


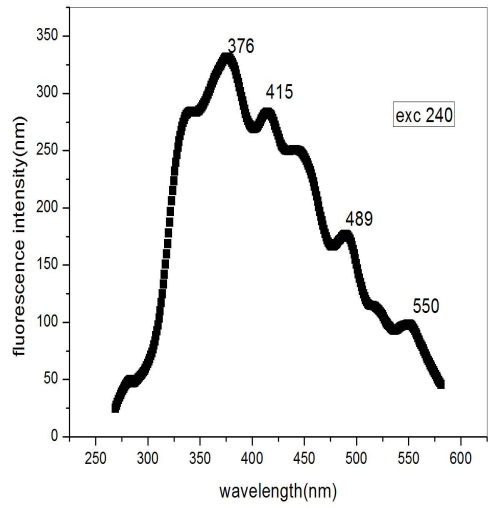
Figure.5.9 Combined fluorescence Emission spectra of CaTT-ELE

In the case of electric field applied sample, an excitation of 230 nm produces four emissions at 337 nm, 423nm, 492 nm and 536 nm as shown in figure 5.8(a). If the excitation wavelength is 240 nm, three emissions are observed around 418nm, 487 nm and 545 nm. For an excitation of 260 nm, two intense emissions at 421nm and 490 nm are obtained. Figure 5.9 depicts the combined photoluminescence emission spectra obtained at different excitation wavelengths for the CaTT-ELE crystals.

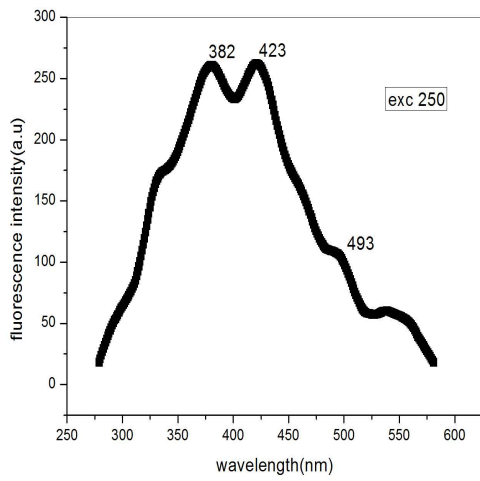
Chapter 5



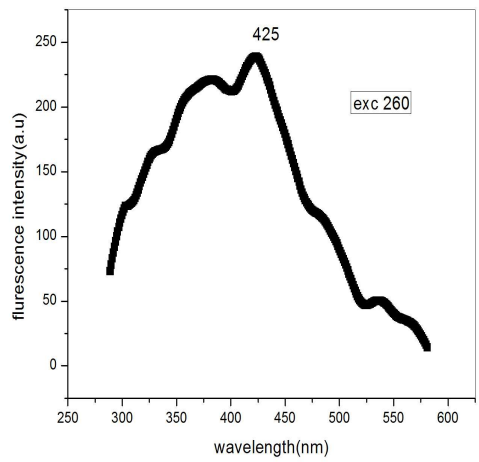
(a)



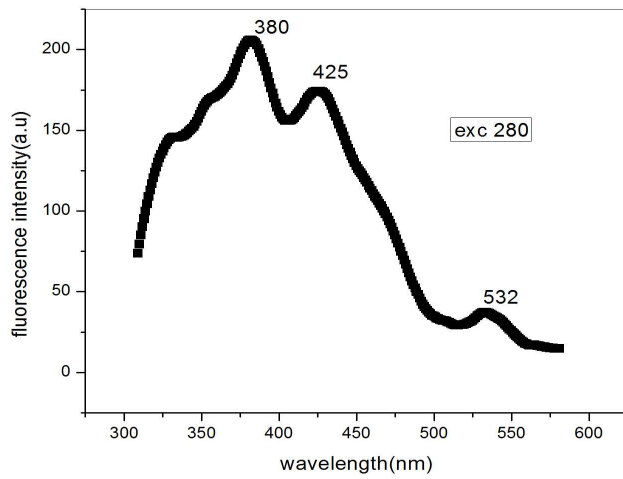
(b)



(c)



(d)



(e)

Figure.5.10 Emission spectra of CaTT-MAG at an excitation wavelength of (a) 230 nm (b) 240 (c) 250 nm (d) 260 nm and (e) 280 nm

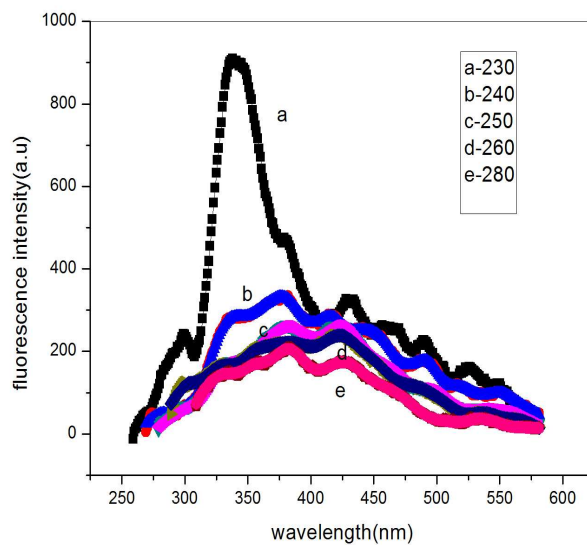


Figure.5.11 Combined fluorescence Emission spectra of CaTT-MAG

The samples subjected to magnetic field give three strong emission peaks at 340 nm, 431nm and 488 nm for an excitation wavelength of 230nm as given in figure5.10 (a). The excitation of 240 nm produces emissions at 376 nm, 489 and 550 nm respectively. For an excitation of 250nm, the fluorescence emission takes place at 382 nm, 423 nm and 493 nm. The excitation of CaTT- MAG at a wavelength of 260 nm produces a sharp emission peak at 425 nm as shown in the figure 5.10(d). As the excitation wavelength is increased to a value of 280 nm, the emission peaks are obtained at 380 nm, 425 nm and 532nm as given in the figure 5.10(e). The intense peaks of emission indicate that the luminescence of Calcium Tartrate is composed of excitonic luminescence by the strong coupling of electron-phonon within the crystal. Here, the efficiency of luminescence is tied up with the dynamics of the de-excitation mechanisms in the atoms of CaTT.

5.4.4 Luminescence Mechanism in CaTT

A large number of normal modes of vibration are possessed by CaTT which can be obtained from the FTIR spectrum of the compound [20] and the spectrum is given in figure 5.12. The table 5.4 gives the FTIR band assignments of CaTT.

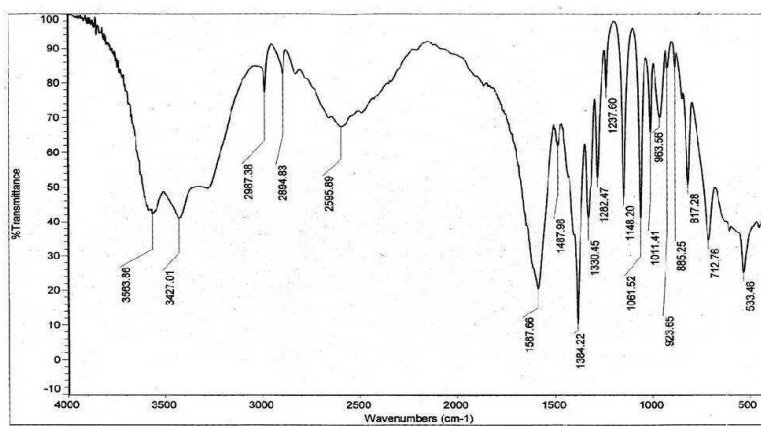


Figure.5.12 FTIR spectra of CaTT [20]

Table 5.4. FTIR band assignments of CaTT [20]

Peak positions pureCaTT cm-1	Assignments
3563.5b,L 3427b,L	Symmetric stretch, H ₂ O CH- antisymmetric & CH -stretch
2987,s,h 2844,s,h 2595 b,h	CH ₃ antisymmetric CH ₃ symmetric stretch CH stretch on CHO
1587 s,VL	Bending of H ₂ O
1487s,h	Anti-symmetric deformation CH ₃
1384,s,VL 1330,s,L	CH rock, in-plane bend on CHO CH symmetric deformation C=C
1282,s,h 1237,s,h	CH antisymmetric deformation C=C
1148s,L	CH ₃ in plane rock
1061s,L 1011s,L	C-CHO stretch
963s,h 923s,h	C-CH ₃ stretch Inversion of two hydrogen through the centre of the C=C bond
885s,h 817s,h	CH wag, out-of-plane bend on CHO
712s,h	CH symmetric deformation on C=C bond CH wagg on CHO
533s,VL	CH ₃ -C=C, bend .

S-sharp, b-broad, h-high intensity, VL-very low intensity, L-low intensity

The values of wave numbers ν_1 to ν_{13} were taken from the FTIR spectrum of CaTT [20] and the assigned values are given in table 5.5

Table 5.5. Values of ν taken from FTIR spectra of CaTT

$\nu(\text{cm}^{-1})$	The values taken from FTIR spectra of CaTT (cm^{-1})
ν_1	533
ν_2	712
ν_3	1062
ν_4	1148
ν_5	1282
ν_6	1330
ν_7	1384
ν_8	1588
ν_9	2596
ν_{10}	2895
ν_{11}	2987
ν_{12}	3427
ν_{13}	3584

Table.5.6. Details of fluorescence bands and assignments of CaTT

Emission wavelength(nm)	Observed Wave number ($\bar{\nu}_{\text{ob}}$) (cm^{-1})	Assignments	Calculated Wave number ($\bar{\nu}_{\text{ca}}$) (cm^{-1})	Difference ($\bar{\nu}_{\text{ob}} - \bar{\nu}_{\text{ca}}$) (cm^{-1})
570	17544	T_e	-	-
532	18797	$T_e + \nu_5$	18826	29
488	20491	$T_e + \nu_{11}$	20531	40
415	24096	$T_e + \nu_2 + 2\nu_{10}$	24046	50
375	26667	$T_e + \nu_5 + 3\nu_9$	26662	5
350	28571	$T_e + \nu_2 + 3\nu_{12}$	28537	34
325	30769	$T_e + 2\nu_5 + 3\nu_{13}$	30860	91

Here T_e represents the difference in electronic levels T_e' and T_e'' where T_e' is the excited electronic level and T_e'' is the ground electronic level. From the table, it is clear that the peaks in the fluorescence emission of CaTT corresponds to various combinations and overtones of the molecules in the excited electronic levels. The details of band assignments are also given in table.5.6. The various transitions and the corresponding fluorescence emission bands of CaTT are illustrated in figure.5.13.

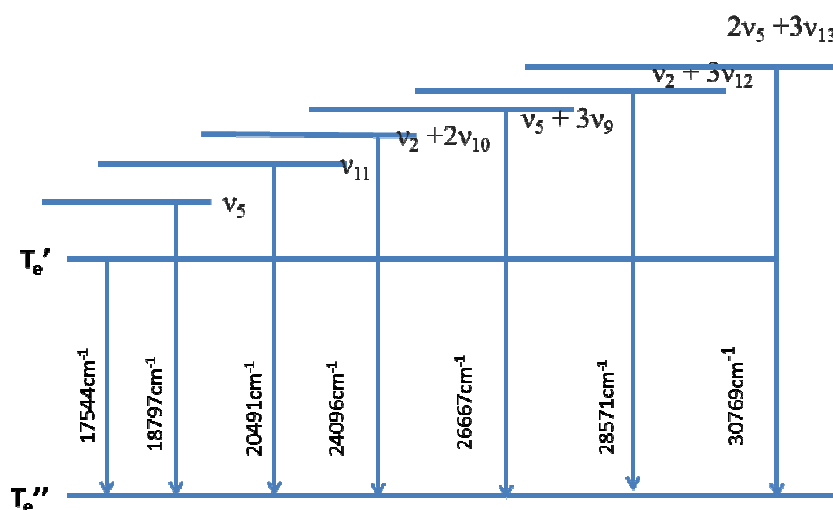


Figure 5.13. Schematic of the energy levels involved in the fluorescence spectra of CaTT based on combinations and overtones of various modes

5.4.5. Non radiative decay mechanism in CaTT

The decay mechanism of Calcium Tartrate crystals are studied using thermal lens experiment. The theory and experimental method are described in the earlier chapters. In this method the lensing behaviour of Calcium Tartrate is investigated using a dual beam mode matched set up. For the experimentation, a compound solution of 3 ml CaTT and 0.5 ml dye was taken in a sample cuvette. The cuvette containing Rh-CaTT solution was illuminated by a laser

Chapter 5

beam. The absorption edge of CaTT was only in the UV range. In order to enhance the absorption, the Rhodamine 6G dye was incorporated to the solution of CaTT. During the laser irradiation on the sample, radiation was absorbed by the sample which subsequently de-excited radiatively and non-radiatively. Non-radiative relaxations lead to a thermal refractive index gradient which resulted in a thermal blooming. This blooming is due to the self-defocussing [22]. Figure 5.14 illustrates the lensing characteristics of CaTT in solution phase.

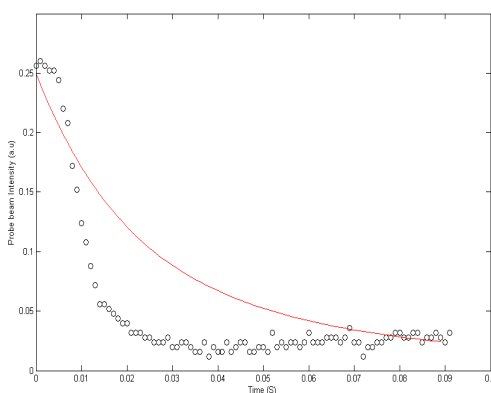


Figure.5.14(a) Thermal lens plot of Rh-CaTT- pure

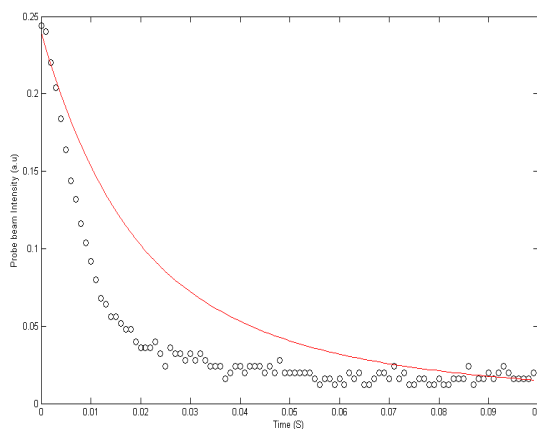


Figure.5.14(b) Thermal lens plot of Rh-CaTT- ELE

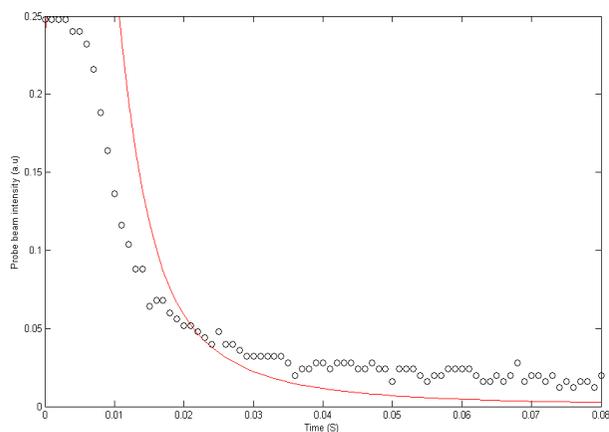


Figure.5.14(c) Thermal lens plot of Rh-CaTT- MAG

Table.5.7.Measured values of D, θ_c , and t_c for Rhodamine incorporated CaTT solution

Sample	t_c (mS)	θ_c	D (cm ² /S) x 10 ⁻³
CaTT pure	35.59	-608.81	3.56
CaTT electric	31.38	-606.60	4.03
CaTT magnetic	26.44	-609.26	4.78

The experimental data is to be fitted using a program and the values of decay time t_c and fitting parameter θ_c . Using the values of t_c and θ_c , the thermal diffusivity D of CaTT can be calculated using the relation

$$D=w^2/4t_c$$

where w is the beam waist radius of the beam.

Thermal diffusion is minimum for the pure sample and have a high value for the field applied crystals. It indicates that the effect of electric and magnetic fields decrease the decay time thereby increasing the diffusivity. The gel grown crystals of Calcium Tartrate solution exhibit lens like nature and all these crystals of CaTT expand on heating which is given by the negative values of fitting parameter.

5.5. Nonlinear optical studies on CaTT

Highly sensitive single beam Z-scan experiment based on spatial beam distortion was used for the optical nonlinear studies on Calcium Tartrate crystals[23]. A Q-switched Nd:YAG laser was used as the source of excitation. The CaTT sample solutions were taken in a 1 mm thick cell and moved along the Z-axis through the focal point of a lens of focal length 20 cm. The experimental set up was as explained in detail [24-25]. The radius of the beam waist w_0 was calculated as $42.6\mu\text{m}$ and Rayleigh length $z_0=\pi w_0^2/\lambda$ is estimated to be 10.7 mm which is much greater than the thickness of the sample cell (1 mm).

Absorptive nonlinearity in our crystal samples were measured using open aperture Z-scan experiment. A single Gaussian laser beam in tight focus geometry was used in this method. Here, we measured the transmittance of the CaTT samples with respect to the position z along the focus without an aperture. Figure 5.15 represents the open aperture Z- scan plot of pure CaTT crystals.

Open aperture Z-scan studies were carried out by focusing the input beam on to the sample at 532 nm. In order to estimate the limits to which the CaTT would be showing the transmittance, Z-scan curves were recorded at different fluences in the ns regime. The transmittance of the samples was measured at different input fluences such as 50 MW/cm^2 , 87 MW/cm^2 , 125 MW/cm^2 and 251 MW/cm^2 and are as shown in the following figures.

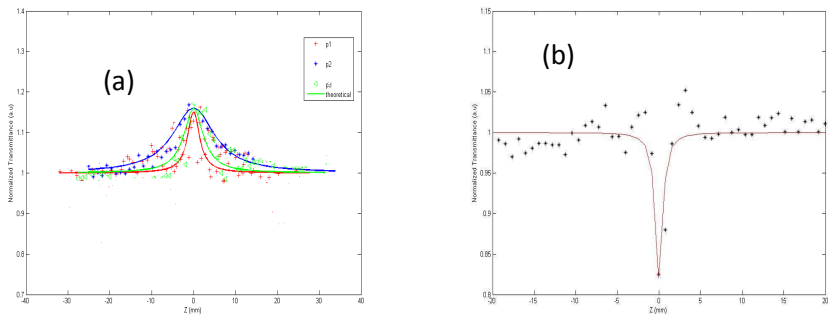


Figure.5.15: Z- scan plot of pure CaTT (a) at various laser power densities ($P_1=50$ MW/cm², $P_2=87$ MW/cm² and $P_3=251$ MW/cm²) and (b): 125 MW/cm²

From figure 5.15(a) it is clear that the nonlinear absorption coefficient β is negative due to the transmission maximum at the focal point. This shows saturable absorption(SA) behavior of pure CaTT samples at laser power densities 87 and 251 mW/cm². As a saturable absorber, it exhibits reduced absorption coefficient at higher input intensities. The Z-scan data shows that the increase in the laser intensity induces bleaching in the ground state absorption, which results in a transmittance increase giving rise to SA process. Thus pure CaTT at input power densities 87 MW/cm² and 251 MW/cm² are well suited for passive Q-switching or mode locking of lasers.

Figure 5.15(b) reveals a reverse saturable absorption (RSA) nature for pure CaTT in single distilled water. At a laser input power of 125 MW/cm², pure CaTT acts as a reverse saturable absorber. At this particular input fluence value, we obtained a valley in the transmittance curve for pure CaTT.

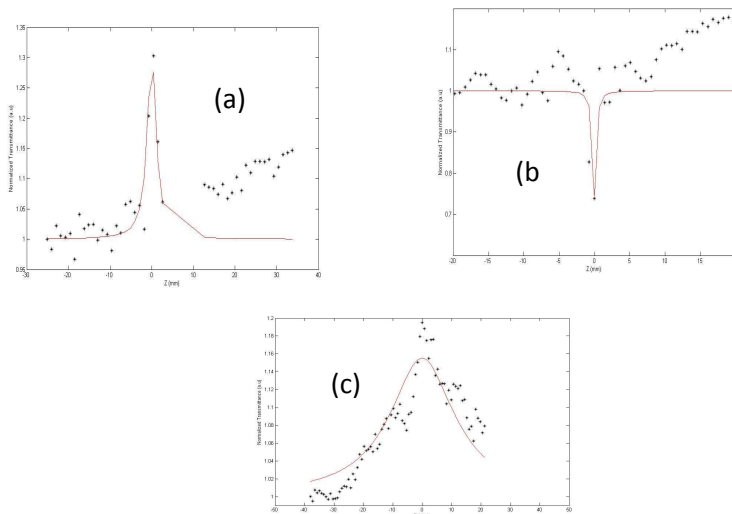


Figure.5.16: Open aperture Z-scan plot of CaTT-ELE at I_0 =(a)87 MW/cm²,(b)125MW/cm² and (c) 251 MW/cm²

Figure 5.16 depicts the optical nonlinear response of CaTT-ELE sample solutions at three different laser power densities. From figures 5.16(a) and (c), it is clear that CaTT-ELE is a saturable absorber at laser power densities 87 MW/cm² and 251 MW/cm² just as in the case of the pure CaTT sample. The RSA nature of CaTT-ELE at 125MW/cm² is indicated by figure 5.16(b).

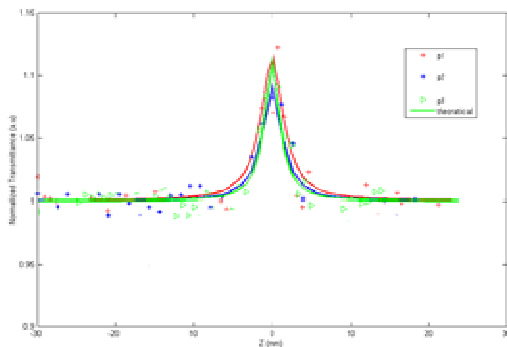


Figure.5.17: combined Z scan plot of CaTT-MAG at three laser power densities $P_1=87$ MW/cm², $P_2=125$ MW/cm² and $P_3=251$ MW/cm²

Spectral and Nonlinear optical studies on Calcium Tartrate (CaTT) crystals

Figure 5.17 represents the nonlinear response of CaTT-MAG sample at three different laser power densities. It is a saturable absorber at all these power densities. Since the wavelength used in our experiment is 532nm, the RSA behaviour shown by some of the CaTT samples at 125 MW/cm² corresponds to two photon absorption (TPA)[26-27]. Nonlinear absorption coefficient β of the sample evaluated for three input fluence values are given in table.5.8. The saturation intensity I_s values for the saturable absorbed CaTT samples are also given in the table.

The relation connecting nonlinear absorption coefficient β and I_s is given as

$$\beta = \frac{-\alpha_0}{I_s}$$

where α_0 is the linear absorption coefficient of CaTT.

From the table.5.8, it is clear that pure -CaTT shows SA nature at input laser power densities (I_0) 87 and 251 MWcm⁻² indicating the negative β values. For I_0 at 125 MWcm⁻², RSA is obtained for pure and electric field applied CaTT samples. The RSA of the respective samples are due to the decrease in transmittance at the focus giving a valley. The sign of β is positive for the samples giving a valley. The magnetic field applied CaTT sample solutions exhibit SA only due to the depletion of ground state ions.

Table 5.8 shows that the high nonlinearity exhibited at 125 MW/cm² gets reduced at 251 MW/cm². Thus the nonlinear study on CaTT indicate that CaTT pure and CaTT-ELE samples exhibit SA at laser intensities 87 MW/cm² and 251 MW/cm² and RSA at 125 MW/cm². The RSA is due to the induced absorption and SA is caused by the bleaching effect[28]. The nonlinearity in CaTT-MAG samples are due to SA only. From the switching characteristics of CaTT from SA to RSA, it is evident that these crystals are well suited for applications in optical pulse compression, optical switching and laser pulse narrowing [29].

Table 5.8. Measured values of nonlinear absorption coefficient, saturation intensity and optical limiting threshold for CaTT

Sample	β (cmGW ⁻¹)			I_s (GWcm ⁻²)			Optical limiting threshold (MWcm ⁻²)
	$I_0(87$ MWcm ⁻²)	$I_0(125$ MWcm ⁻²)	$I_0(251$ MWcm ⁻²)	$I_0(87$ MWcm ⁻²)	$I_0(125$ MWcm ⁻²)	$I_0(251$ MWcm ⁻²)	
CaTT pure	-42.9	57	-15	0.019	–	0.055	103
CaTT - ELE	-68	83	-14	0.014	–	0.069	116
CaTT-MAG	-33	-19	-11	0.016	0.028	0.049	–

The imaginary part of third order susceptibility { $\text{Im}(\chi^{(3)})$ } of the gel grown CaTT crystals are evaluated from the values of nonlinear absorption obtained from the open aperture data and is given in the table 5.9.

Table 5.9. Measured value of $\text{Im}(\chi^{(3)})$ of CaTT at three different input fluences

Sample	$\text{Im}(\chi^{(3)})$ (esu) $\times 10^{-10}$		
	I_0 (87 MWcm ⁻²)	I_0 (125 MW/cm ²)	I_0 (251 MWcm ⁻²)
CaTT pure	-1.22	1.62	-0.43
CaTT-ELE	-1.93	2.36	-0.39
CaTT-MAG	-0.94	-0.54	-0.33

5.6. Optical limiting Studies on CaTT.

At a laser power of 125 MW/cm^2 , Calcium Tartrate crystals exhibit positive nonlinear absorption giving RSA. The RSA nature of CaTT makes it suitable for optical limiting applications. Here CaTT is an effective optical limiter having low limiting threshold, large dynamic range, and longer excited state life time to accumulate the population. Figure 5.18 shows the optical limiting response of CaTT single crystals. The efficiency of an optical limiter is decided by its limiting threshold. It is obvious that lower the optical limiting threshold, better the optical limiting material. The limiting threshold values of the CaTT sample solutions are given in the table 5.8 The optical limiting property in CaTT occurs mainly due to absorptive nonlinearity which corresponds to the imaginary part of the third order susceptibility [25].

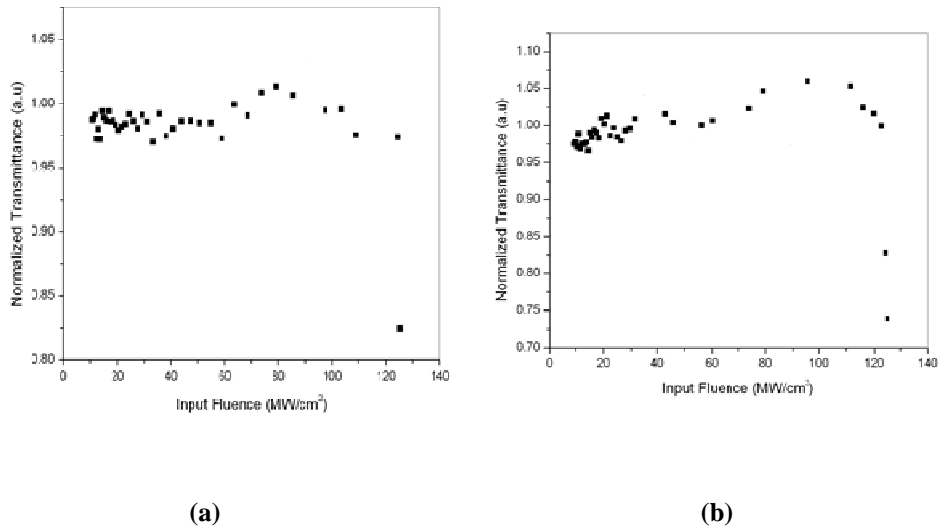


Figure 5.18. Optical limiting response of (a) CaTT-pure and (b) CaTT-ELE

Conclusions

Three categories of Calcium Tartrate single crystals were prepared by sol-gel technique and characterized using XRD, spectral and optical nonlinear studies. Optical band gap of these crystalline materials are determined using linear optical measurements. The optical band gap studies suggest that the application of magnetic field during the preparation of the sample crystal increases the band gap of CaTT. The range of band gap values reveals the application of CaTT in band gap tuning. The emission aspects of CaTT in solution phase are investigated using different excitations at room temperature. The fluorescence emission at different excitation wavelengths exhibit intense peaks indicating their luminescence properties. The decay mechanism in CaTT are studied using thermal lens technique and the diffusivity values are evaluated. Nonlinear investigations have been done using highly sensitive Z-scan experiment with a Gaussian laser beam. The transmittance curves of CaTT at three different fluences show saturable and reverse saturable absorption characteristics and their corresponding nonlinear absorption coefficients are evaluated. The Z-scan data for SA gives the values of saturation intensity and their relation with input powers are also investigated. It has also been established that these crystal samples in solution phase are well suited for optical limiting and passive switching applications.

References

- [1] Craxton, R. Stephen, Stephen D. Jacobs, J. Rizzo, and R. O. B. E. R. T. Boni. "Basic properties of KDP related to the frequency conversion of 1 μm laser radiation." *Quantum Electronics, IEEE Journal of* 17, no. 9 (1981): 1782-1786.
- [2] Medrano, C., P. Günter, and H. Arend. "Noncentrosymmetry observed in CaC_2O_6 crystals by nonlinear optical measurements." *Ferroelectrics* 94, no. 1 (1989): 111-116.
- [3] Ambady, G. K. "The crystal and molecular structures of strontium tartrate trihydrate and Calcium Tartrate tetrahydrate." *Acta Crystallographica Section B: Structural Crystallography and Crystal Chemistry* 24, no. 11 (1968): 1548-1557.
- [4] Sawant, D. K., H. M. Patil, D. S. Bhavsar, J. H. Patil, and K. D. Girase. "Structural and Optical Properties of Calcium Cadmium Tartrate." *Archives of Physics Research* 2, no. 2 (2011): 67-73.
- [5] Quasim, I., A. Firdous, B. Want, S. K. Khosa, and P. N. Kotru. "Single crystal growth and characterization of pure and sodium-modified copper tartrate." *Journal of Crystal Growth* 310, no. 24 (2008): 5357-5363.
- [6] Suthar, S. R., and M. J. Joshi. "Growth and characterization of Mn^{2+} doped calcium l-tartrate crystals." *Crystal Research and Technology* 41, no. 7 (2006): 664-670.
- [7] Suryanarayana, K., and S. M. Dharmaprakash. "Crystal growth and characterization of barium doped Calcium Tartrate tetrahydrate crystals." *Materials Letters* 42, no. 1 (2000): 92-96.
- [8] Suryanarayana, K., and S. M. Dharmaprakash. "Physico-chemical characterization of calcium strontium tartrate crystals." *Journal of Physics and Chemistry of Solids* 58, no. 10 (1997): 1599-1602.
- [9] Mooseker, Mark S., Theresa A. Graves, Kristi A. Wharton, Nancy Falco, and Christine L. Howe. "Regulation of microvillus structure: calcium-dependent solation and cross-linking of actin filaments in the microvilli of intestinal epithelial cells." *The Journal of cell biology* 87, no. 3 (1980): 809-822.
- [10] Torres, M. E., J. Peraza, A. C. Yanes, T. Lopez, J. Stockel, D. Marrero-Lopez, Xavier Solans, Eduardo Bocanegra, and C. Gonzalez Silgo. "Electrical conductivity of doped and undoped Calcium Tartrate." *Journal of Physics and Chemistry of Solids* 63, no. 4 (2002): 695-698.

- [11] Torres, Manuel E., Trinidad López, Josefina Stockel, Xavier Solans, Maite García-Vallés, Enrique Rodríguez-Castellón, and Cristina González-Silgo. "Structural characterization of doped Calcium Tartrate tetrahydrate." *Journal of Solid State Chemistry* 163, no. 2 (2002): 491-497.
- [12] Sahaya Shajan, X., and C. Mahadevan. "FT-IR spectroscopic and thermal studies on pure and impurity added Calcium Tartrate tetrahydrate crystals." *Crystal Research and Technology* 40, no. 6 (2005): 598-602.
- [13] Saban, K. V., T. Jini, and G. Varghese. "Influence of magnetic field on the growth and properties of Calcium Tartrate crystals." *Journal of magnetism and magnetic materials* 265, no. 3 (2003): 296-304.
- [14] Selvarajan, P., B. N. Das, H. B. Gon, and K. V. Rao. "Infrared spectroscopic and thermal studies of Calcium Tartrate single crystals grown by silica-gel technique." *Journal of Materials Science Letters* 12, no. 15 (1993): 1210-121.
- [15] Dharmaprasanna, S. M., and K. Suryanarayana. "Physico-chemical characterization of calcium strontium tartrate crystals." *Journal of Physics and Chemistry of Solids* 10, no. 58 (1997): 1599-1602.
- [16] Gon, H. B. "Ferroelectricity in Calcium Tartrate single crystals grown by gel technique." *Journal of Crystal Growth* 102, no. 3 (1990): 501-504.
- [17] Fujiwara, M., R. Tokunaga, and Y. Tanimoto. "Crystal growth of potassium nitrate in a magnetic field of 80 kOe." *The Journal of Physical Chemistry B* 102, no. 31 (1998): 5996-5998.
- [18] Fujiwara, M., T. Chidiwa, R. Tokunaga, and Y. Tanimoto. "Crystal Growth of trans-Azobenzene in a Magnetic Field of 80 kOe." *The Journal of Physical Chemistry B* 102, no. 18 (1998): 3417-3419.
- [19] Suryanarayana, K., S. M. Dharmaprasanna, and K. Sooryanarayana. "Optical and structural characteristics of strontium doped Calcium Tartrate crystals." *Bulletin of Materials Science* 21, no. 1 (1998): 87-92.
- [20] G.Lillibai ,PhD Thesis, December 2012.
- [21] Sonawane, S. S., and R. R. Ahire. "Optical, structural and elemental analysis of Calcium Tartrate crystals grown by gel method." *Archives of Physics Research* 5, no. 5 (2014): 31-36.
- [22] Joseph, Santhi Ani, Misha Hari, S. Mathew, Gaurav Sharma, V. M. Hadiya, P. Radhakrishnan, and V. P. N. Nampoori. "Thermal diffusivity of Rhodamine 6G incorporated in silver nanofluid measured using mode-matched thermal lens technique." *Optics Communications* 283, no. 2 (2010): 313-317.

Spectral and Nonlinear optical studies on Calcium Tartrate (CaTT) crystals

- [23] Sheik-Bahae, Mansoor, Ali A. Said, T-H. Wei, David J. Hagan, and Eric W. Van Stryland. "Sensitive measurement of optical nonlinearities using a single beam." *Quantum Electronics, IEEE Journal of* 26, no. 4 (1990): 760-769.
- [24] Irimpan, Litty, V. P. N. Nampoory, and P. Radhakrishnan. "Spectral and nonlinear optical characteristics of nanocomposites of ZnO–CdS." *Journal of Applied Physics* 103, no. 9 (2008): 094914,1-8.
- [25] Irimpan, Litty, V. P. N. Nampoory, and P. Radhakrishnan. "Spectral and nonlinear optical characteristics of nanocomposites of ZnO–Ag." *Chemical physics letters* 455, no. 4 (2008): 265-269.
- [26] Irimpan, Litty, A. Deepthy, Bindu Krishnan, V. P. N. Nampoory, and P. Radhakrishnan. "Nonlinear optical characteristics of self-assembled films of ZnO." *Applied Physics B* 90, no. 3-4 (2008): 547-556.
- [27] Tintu, R., V. P. N. Nampoory, P. Radhakrishnan, and Sheenu Thomas. "Nonlinear optical studies on nanocolloidal Ga–Sb–Ge–Se chalcogenide glass." *Journal of Applied Physics* 108, no. 7 (2010): 073525
- [28] Litty Mathew Irimpan ,Phd Thesis, June 2008.
- [29] Band, Yehuda B., D. J. Harter, and Raanan Bavli. "Optical pulse compressor composed of saturable and reverse saturable absorbers." *Chemical Physics Letters* 126, no. 3 (1986): 280-284.

Chapter 6

Linear and Nonlinear Optical studies on Strontium Tartrate (SrTT) crystals

Abstract

This chapter explains the studies on Strontium Tartrate crystals (SrTT) of three different types namely SrTT-pure, SrTT-ELE and SrTT-MAG. The optical characterization of these crystals in ethanol was investigated by performing absorption and fluorescence spectral measurements. Thermal diffusivity of these samples was also determined using thermal lens experiment. The nonlinear optical studies on these crystal solutions were performed by employing open aperture z-scan experimental technique with a Q-switched laser. The limiting studies were also done and the threshold values were evaluated

6.1 Introduction

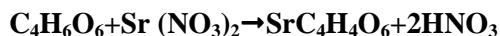
Strontium Tartrate (SrTT) is a material with device applications since it possesses ferroelectric behaviour [1-3]. M.H.Rahimkuty *et al* studied the thermal behaviour of gel grown Strontium Tartrate crystals using thermo gravimetric and differential thermal analyses [3].SrTT have found applications in the field of nonlinear optics based on their harmonic generation. They can also be used as crystal oscillators and devices central to laser emissions. Selva Sekarapandian reported that Strontium Tartrate is a strategic material with a global business potential [4]. H.Brehath[5], N,Nagatani[6] and H.B.Gon [7] reported that the divalent tartrates are ferroelectric and piezoelectric compounds and these materials exhibit nonlinear optical and spectral characteristics. From the work of M.E.Torres, we can conclude that the tartrates are used in transducers and several linear and mechanical devices [8-9]. There are many studies reported employing Strontium Tartrate due to their attractive properties [10-13]. B.Sureshkumar *et al* reported the growth and characterization of pure and lithium doped Strontium Tartrate tetra hydrate crystals by solution–gel technique [14]. In recent years great attention has been devoted to the studies of nonlinear crystals like Strontium Tartrate due to their wide range of applications [15-20]. The dielectric behaviour of Strontium Tartrate single crystals was studied by S.K.Arora *et al*. They gave a clear picture of various polarization mechanisms such as atomic polarization of lattice, orientational polarization of dipoles and space charge polarization in the grown crystals using the results of the measurements of dielectric constant and dielectric loss as functions of frequency and temperature [1]. Strontium Tartrate belongs to the space group $P2_12_12_1$ containing four molecules per unit cell with dimensions $a = 0.948$, $b = 1.096$ and $c = 0.946$ nm [21-23]. As the solubility of tartrate compounds in water is very poor and they decompose before melting, single crystals of tartrate compounds cannot be grown by either slow evaporation or melt techniques. Here arises the significance of gel method. Henisch *et al* reported the growth of single

Linear and Nonlinear optical studies on Strontium Tartrate (SrTT) crystals

crystals of Calcium Tartrate[24-25]. In the present chapter, the linear absorption, photoluminescence, thermal lensing and nonlinear optical characteristics of Strontium Tartrate crystals prepared by solution-gel technique are discussed.

6.2. Preparation of SrTT crystals

Gel method was employed for preparing the crystal samples for our studies as described in the earlier chapters [26]. Initially, a stock solution of sodium meta silicate of specific gravity 1.03 was prepared for gel formation. To the solution of sodium meta silicate, a 1 molar tartaric acid was mixed and the pH of the solution was varied. The solution was kept undisturbed for two days to form firm gel. To the gel, a 1 molar strontium nitrate solution was gently poured through the sides of the test tube without disturbing the gel surface. The chemistry behind the crystal formation is given below.



Two different SrTT samples were obtained by applying an electric field of 10V perpendicular to the length of the experimental test tube and by providing a magnetic field of 0.1 Tesla across the test tube. The fields were applied on the test tube containing the top solution and gel. The crystals formed by the effect of electric field are termed as SrTT-ELE. The magnetic field applied crystals of SrTT are named as SrTT-MAG. The reaction between the strontium nitrate and tartaric acid were studied for different gel density and molarity of the top solution. Thus three types of SrTT crystal samples were obtained for our studies viz pure, electric field applied and sample subjected to magnetic field.

6.3. Structural study using XRD

The crystallinity of the gel grown SrTT is confirmed by taking the powder X-ray diffractogram. Figure 6.1 gives the XRD pattern of SrTT crystal. From the figure, it is evident that the prepared material is crystalline in nature because of the presence of sharp intense peaks in the diffractogram. The

6.4.1 Linear Absorption Studies

Linear absorption of the crystal samples in solution phase was recorded using Jasco V-570 UV/VIS/IR Spectrophotometer . By taking the room temperature absorption spectra, the optical transparency of the SrTT sample solutions were determined. It is very necessary to take the absorption measurements to find the region where the crystalline samples in solution phase exhibit the transparency. The crystal samples in ehanol solution were taken in the sample cuvette and ethanol alone was used as reference. Figure.6.2 picturises the absorption behaviour of three different SrTT samples viz SrTT- pure, electric field applied (SrTT-ELE) and magnetic field applied (SrTT-MAG) crystal samples in solution phase.

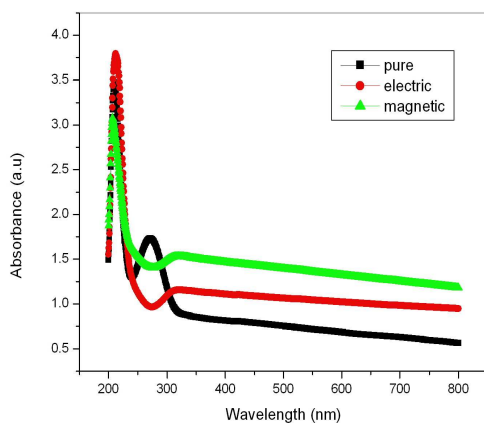


Figure.6.2 UV/VIS absorption spectra of SrTT solution

The combined absorption spectra of SrTT is as shown in figure 6.2. These plots of absorption tell us that SrTT solution has an absorption edge at the ultraviolet region. The cut off wavelength around 265 nm is close to the UV region. SrTT exhibits a peak transparency around 265 nm which is obvious from the above figures. This wide transparency of SrTT makes them suitable for nonlinear studies especially for harmonic generation. The absorption spectra of

SrTT indicates that the sample solutions exhibit wide optical transmission ranging from 200 nm -800 nm. The absorption spectra was used to measure the coefficient of linear absorption α which is essential for the determination of optical nonlinearity in the respective crystals. The following table 6.1 gives the values of peak absorption wavelength (λ_{Peak}) and α for three types of SrTT.

Table.6.1. Measured values of α and λ_{Peak} for the three different SrTT crystals

Sample crystal	λ_{Peak} (nm)	α (cm^{-1})
Pure SrTT	268	0.73
SrTT -ELE	272	1.05
SrTT -MAG	277	1.37

The magnetic field applied crystals have high value of linear absorption compared to the pure and electric field applied samples. Thus the linear absorption studies on SrTT ensured that the gel grown crystals in aqueous state is well suited for nonlinear measurements .

6.4.2 Optical Band gap studies

The optical band gap of SrTT solution samples were studied using the absorption spectra. The values of $h\nu$ were plotted against $(\alpha h\nu)^2$, where, α is linear absorption coefficient which is obtained from the optical linear absorption measurements. α is related to the band gap E_g as $(\alpha h\nu)^2 = k(h\nu - E_g)$, where $h\nu$ is the incident light energy, k is a constant and E_g is the optical band gap of the SrTT sample. Figure 6.3 indicates the band gap plot of Strontium Tartrate. The peak at this particular wavelength is due to the electronic transition .The direct band gap values of SrTT varies from 5.3 to 5.4 eV. The range of band gap suggests that SrTT can be suited for band gap tuning applications. The band gap values of SrTT were tabulated for the pure , electric field applied and magnetic field applied cases as given in the table 6.2.

Linear and Nonlinear optical studies on Strontium Tartrate (SrTT) crystals

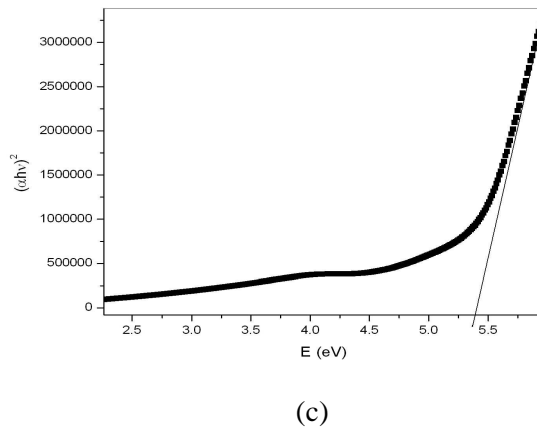
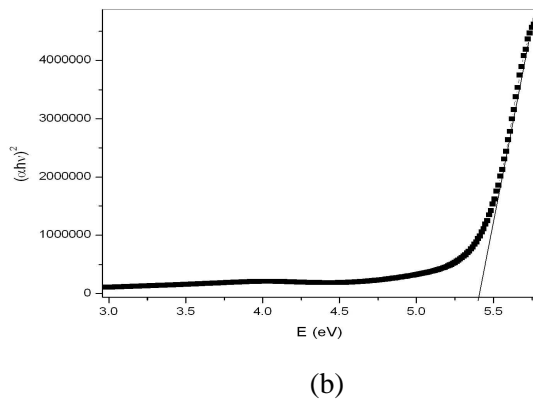
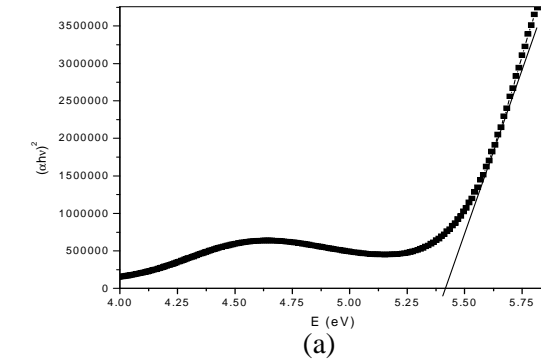


Figure 6.3. Optical band gap plot of (a) pure (b) electric field applied and (c) magnetic field applied SrTT samples.

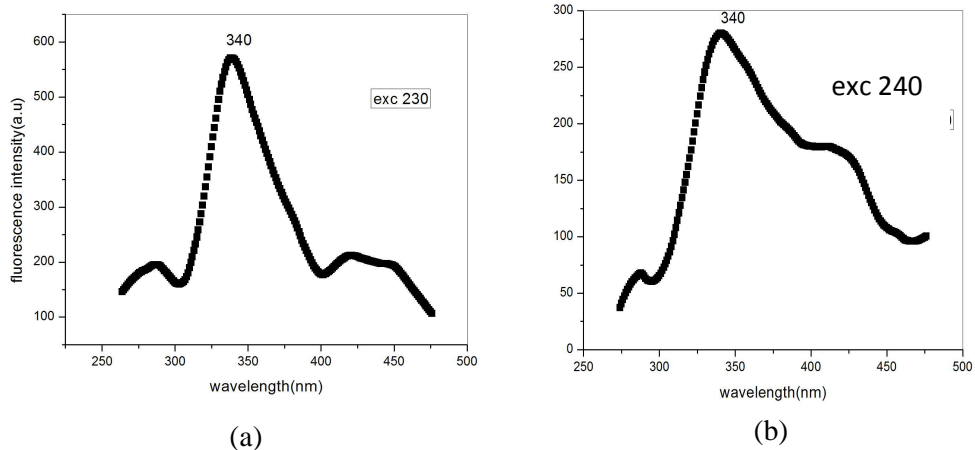
Table 6.2 Measured values of optical band gap of SrTT

Sample	Optical Band gap (eV)
SrTT pure	5.40
SrTT- ELE	5.40
SrTT- MAG	5.37

The direct band gap values of SrTT indicate that the material possess a wide band gap. From the wide band gap of SrTT, it is suggested that the allowed transitions prevails in the region of higher photon energy[2].

6.4.3 Fluorescence spectral studies

The emission characteristics of SrTT sample crystals were studied using the fluorescence spectroscopy. In order to take the fluorescence, the sample crystals were dissolved in ethanol as a solvent and then the aqueous solution of the samples were placed in a Cary Eclipse fluorescence spectrophotometer (Varian-2000). The sample solutions of SrTT were excited using different wavelengths and the corresponding emissions were plotted. The following figures illustrate the photoluminescence of SrTT crystals in solution phase.



Linear and Nonlinear optical studies on Strontium Tartrate (SrTT) crystals

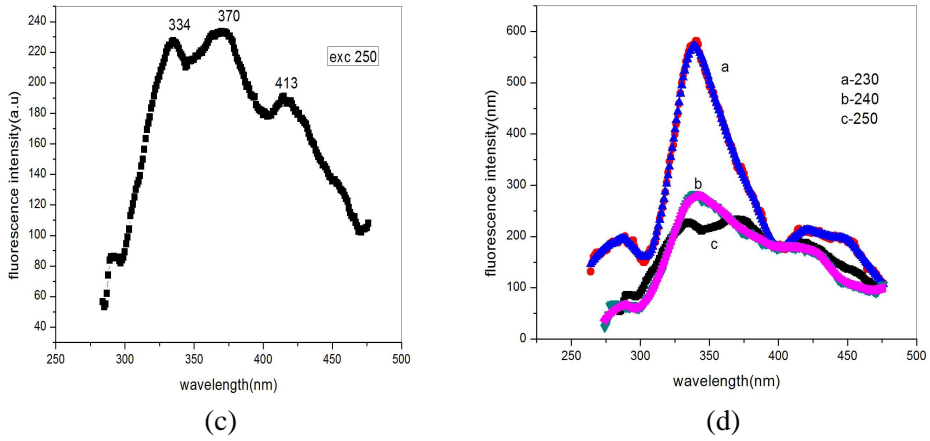
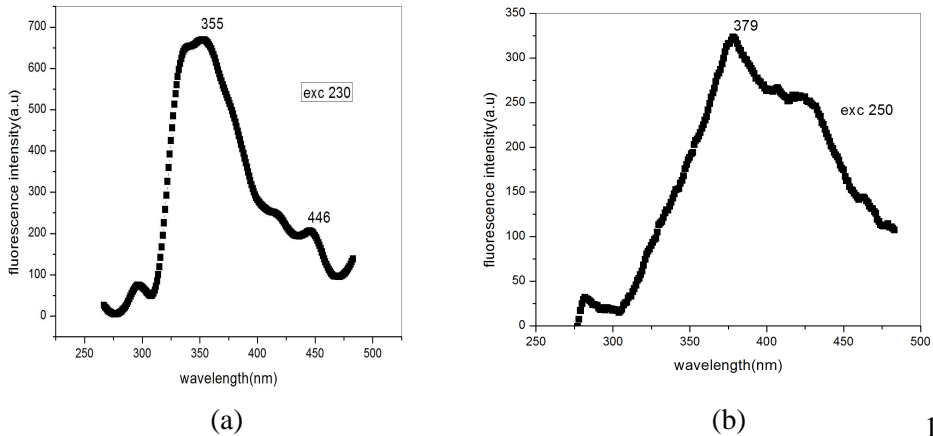


Figure.6.4 Emission spectra of pure SrTT at an excitation wavelength of (a) 230 nm (b) 240nm (c)250 nm and (d) Combined fluorescence emission spectra of pure SrTT

SrTT pure crystal sample solutions were excited at three wavelengths 230 nm, 240 nm and 250 nm as shown in figure 6.4. For an excitation of 230 nm, the emission of pure samples were located at 340 nm which is indicated by figure 6.4(a). The excitation of 240 nm gives an emission around 340 nm as given in figure 6.4(b). If the excitation becomes 250 nm, three strong emissions around 334nm, 370 nm and 413 nm were obtained. All these emissions belong to the violet-blue range as shown in the figure 6.4(c). Figure(d) represents the combined emission spectra of pure crystal samples of SrTT.



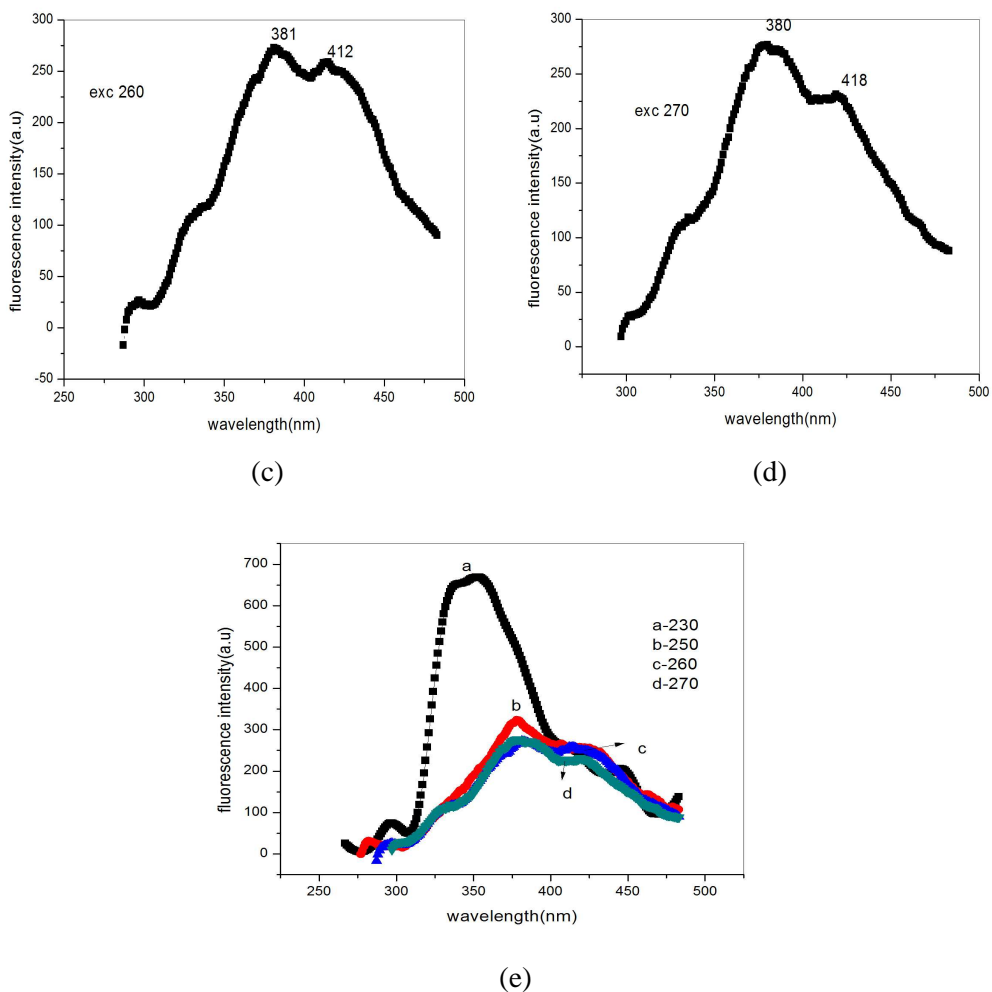


Figure.6.5 Fluorescence emission from electric field applied SrTT (SrTT-ELE) at an excitation wavelength of (a) 230 nm, (b) 250 nm, (c) 260 nm, (d) 270 nm and (e) combined spectra

The crystals prepared by the application of electric field were excited at four different wavelengths 230 nm, 250 nm, 260 nm and 270 nm as shown in figure 6.5. The excitation of 230 nm gave a violet and blue emission. For an excitation of 250 nm, a strong violet emission at 379 nm was obtained. The excitations by 260 and 270 nm produce almost same emissions as given in figure 6.5(c) and (d).

Linear and Nonlinear optical studies on Strontium Tartrate (SrTT) crystals

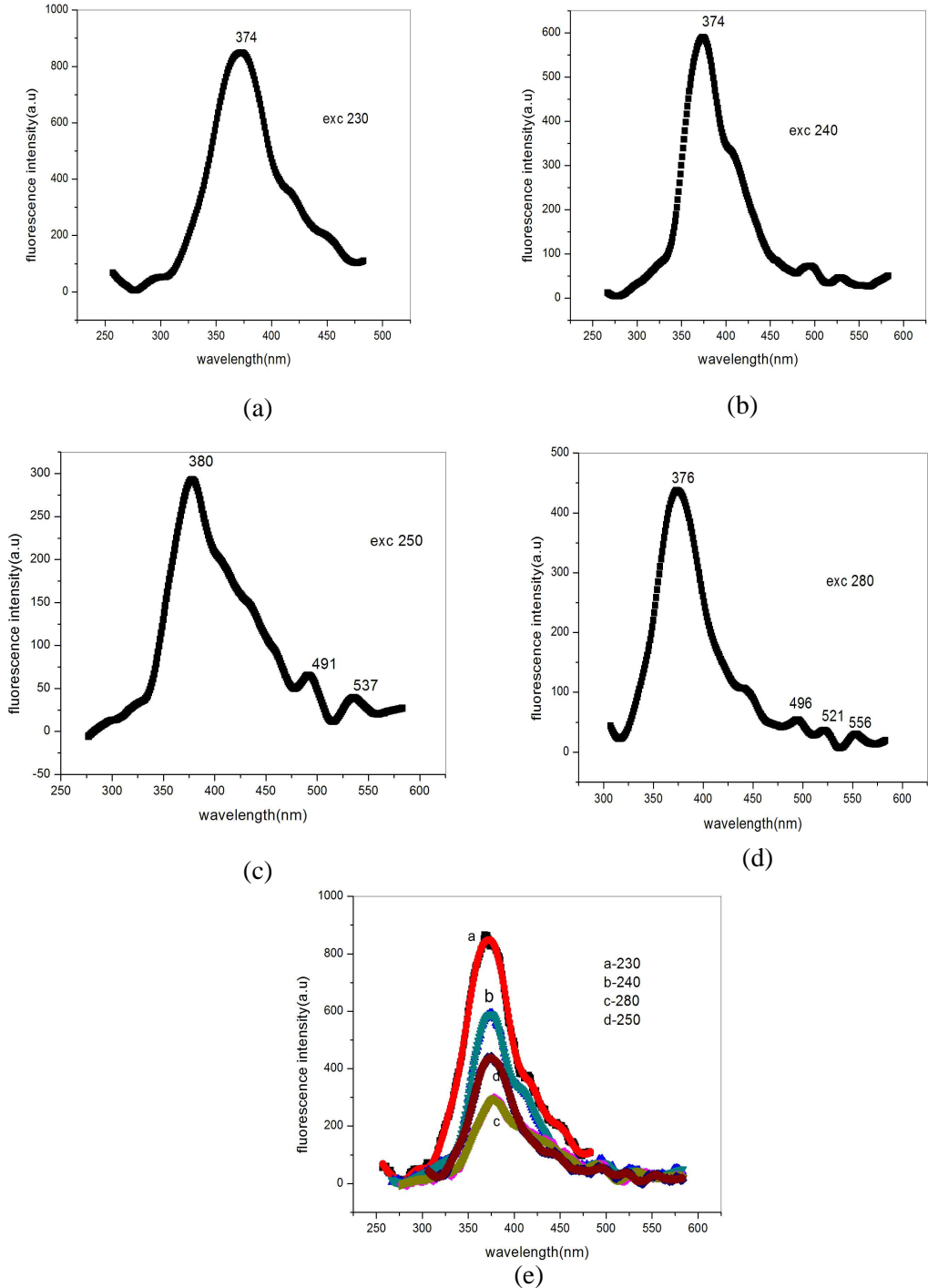


Figure.6.6 Emission spectra of SrTT-MAG at an excitation wavelength of (a) 230 nm (b) 240 (c) 250 nm (d) 280 nm and (e) combined emission spectra

The effect of magnetic field on the fluorescence emission of SrTT was studied using the figure 6.6. The intensity of the emission is decreased as the excitation wavelength is increased. This was depicted in figure (e). The excitation of 280 nm gave four emissions at 376-violet, 496 nm- blue, 521 nm-green and a 556 nm-yellow as shown in figure 6.6(d).

6.4.4 Mechanism of photoluminescence in SrTT

The FTIR spectrum of SrTT showed the presence of various vibration modes[26]. Figure 6.7 represents the FTIR spectra of SrTT sample which was taken from reference[26].

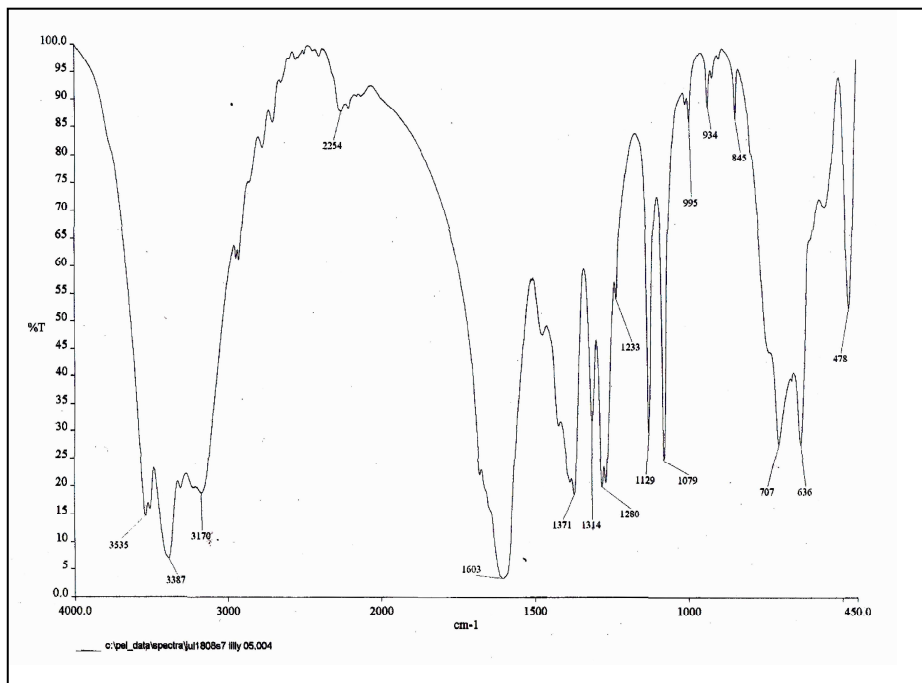


Figure 6.7 FTIR spectrum of SrTT[26]

Linear and Nonlinear optical studies on Strontium Tartrate (SrTT) crystals

The mechanism of luminescence in SrTT samples can be explained using the electronic transitions and the assignments given to the electronic levels. For determining the mechanism, the emission peaks obtained from the emission spectra of SrTT were taken into account. The observed wave numbers (ν_{ob}) were obtained from the corresponding peak values of emission. The electronic levels T_e' and T_e'' were taken as explained in chapter 5. The assignments and the difference in wave numbers are given in the table 6.4. The values of wave numbers ν_1 to ν_{12} were taken from the FTIR spectrum of SrTT [26]. The assigned values of ν are given in table 6.3

Table 6.3. Values of ν taken from FTIR spectra of SrTT

$\nu(\text{cm}^{-1})$	The values taken from FTIR spectra of SrTT(cm^{-1})
ν_1	514
ν_2	707
ν_3	1079
ν_4	1129
ν_5	1280
ν_6	1314
ν_7	1371
ν_8	1603
ν_9	2254
ν_{10}	3170
ν_{11}	3387
ν_{12}	3535

Table.6.4. Details of fluorescence bands and assignments of SrTT

Emission wavelength(nm)	Observed wave number ($\bar{\nu}_{ob}$) (cm^{-1})	Assignments	Calculated Wave number ($\bar{\nu}_{ca}$) (cm^{-1})	Difference ($\bar{\nu}_{ob} - \bar{\nu}_{ca}$) (cm^{-1})
556	17985	T_e	-	-
521	19194	$T_e + \nu_5$	19265	71
496	20161	$T_e + \nu_9$	20239	78
427	23419	$T_e + 2\nu_4 + \nu_{10}$	23413	6
376	26596	$T_e + \nu_8 + 2\nu_{12}$	26658	62
334	29940	$T_e + \nu_2 + \nu_3 + 3\nu_{11}$	29932	8

Like the CaTT samples, the fluorescence in SrTT are composed of various combinations and overtones of the molecules in the excited electronic levels. The various transitions and corresponding fluorescence emission bands of SrTT are shown in figure.6.8 The small difference in observed and calculated wave numbers of SrTT suggest that this model strongly agrees with the fluorescence observed in SrTT.

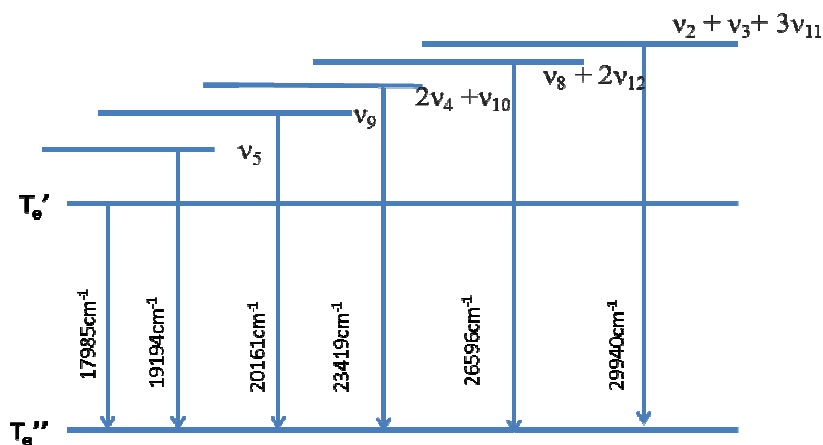
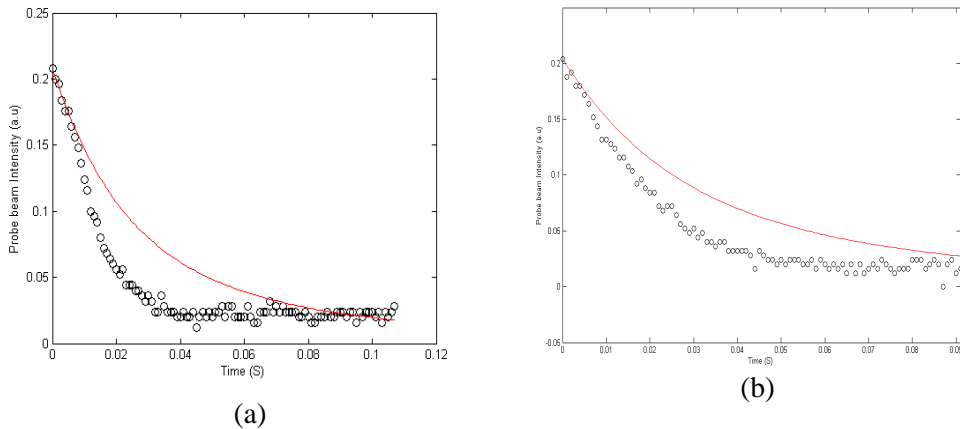


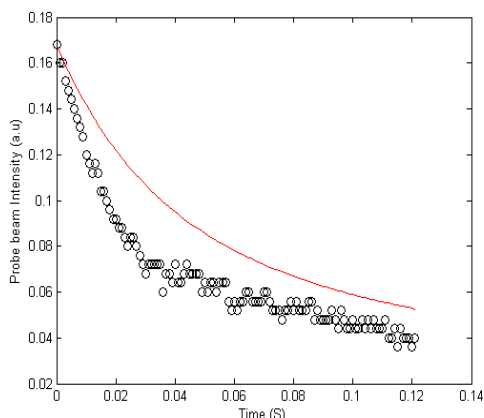
Figure 6.8. Schematic of the energy levels involved in the fluorescence spectra of SrTT based on combinations and overtones of various modes

6.4.5. Thermal diffusivity Measurements

The thermal diffusivity of SrTT sample solutions were studied using the dual beam mode-matched thermal lens experiment. This is a highly sensitive method which can be used to find the non radiative decay mechanism of the gel grown SrTT crystal samples in solution phase. The experimental procedure and the details of the lasers used for experimentation were explained in earlier chapters. In order to avoid aberrations, attenuators were used for adjusting the power at the crystal sample. To enhance the absorption of SrTT crystal in ethanol solution, Rhodamine-6G(Rh-6G) dye was incorporated. A solution of 0.5 ml Rhodamine-6G and 3 ml of SrTT sample solution was taken in a 1 cm cuvette of 5 mm path length for various sets of measurements. The addition of Rh-6G doesnot alter the thermal diffusivity of SrTT sample[27].

Figure.6.9 shows the thermal lensing plots of SrTT crystals with Rhodamine6G dye.





(c)

**Figure.6.9 Thermal lens plot of (a) Rh-SrTT- pure
(b) Rh-SrTT-ELE and (c) Rh-SrTT- MAG**

Following the optical energy absorption and subsequent non radiative decay process, a temperature rise was produced . A lens like optical element was obtained as a result of the change in refractive index with temperature of the SrTT crystal sample. From the TL plot, the decay time t_c and fitting parameter θ were obtained using a theoretical fit of the measured values. From the values of t_c and the beam waist radius w at the sample position, the thermal diffusivity D of SrTT samples can be calculated as

$$D = w^2 / 4t_c$$

The solid line in the figure corresponds to the theoretical fit to the experimental data represented by the circles. The SrTT sample absorbed the radiations and excited states were formed. They loose energy non radiatively generating heat. The thermal diffusivity values of SrTT-Rh-6G can be calculated from the fitting parameters. Measured values of thermal diffusivity D , θ and t_c are given in the table. 6.5

Table.6.5.Measured values of D, θ ,and t_c for Rhodamine-6G incorporated SrTT solution

Sample in gm/ml	t_c (mS)	θ_c	D (cm ² /S) x 10 ⁻³
Rh-SrTT pure	34.25	-602	3.69
Rh-SrT electric	40.29	-603	3.14
Rh-SrT magnetic	71.41	-295	1.77

From the values of θ ,it is evident that SrTT crystals exhibit a negative lens.Thus the Rh-6G added SrTT sample solution expand on heating explaining the presence of negative θ values. These results reveal that a weak TEM Gaussian laser beam passing through the thermal lens, will be affected, resulting in a variation in its spot size and hence intensity at the beam centre.The thermal diffusivity of SrTT is not available in literature. However a comparison of the thermal diffusivity value with that of Strontium Niobate reveals that SrTT has a higher value [28].

6.5 Optical Nonlinear Studies on SrTT

The optical nonlinearity of the SrTT sample solutions were studied using the Open aperture Z-scan experiment[29]. The theory and experimental set up of this highly sensitive method was described in chapter 1. Here the three samples of SrTT were irradiated with a laser having wavelength of 532 nm. The samples were moved along the focal regions of a lens of focal length 20 cm. The laser energies(E_0) used were 30 μ J, 65 μ J, 80 μ J and 100 μ J. The laser power densities (I_0) corresponding to these energies were 75 MW/cm², 163 MW/cm², 200 MW/cm² and 251 MW/cm² respectively. We measured the transmittance of

SrTT at these laser power densities. The following figures illustrate the nonlinear response of three different types of SrTT sample solutions.

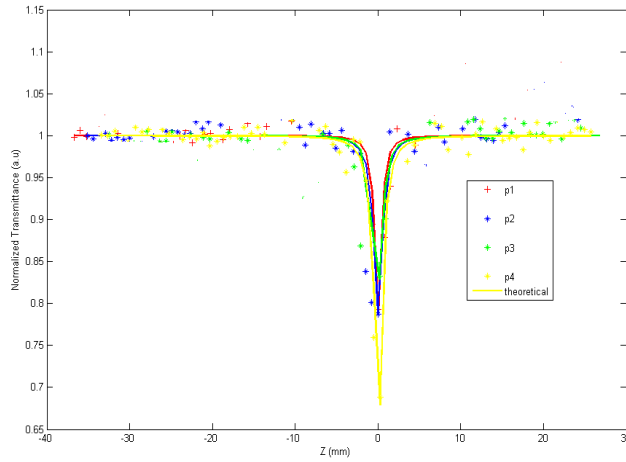


Figure.6.10 (a): Combined Z-scan plot of SrTT- pure at four laser power densities ($P_1=75 \text{ MW/cm}^2$, $P_2=163 \text{ MW/cm}^2$, $P_3= 200 \text{ MW/cm}^2$ and $P_4=251 \text{ MW/cm}^2$)

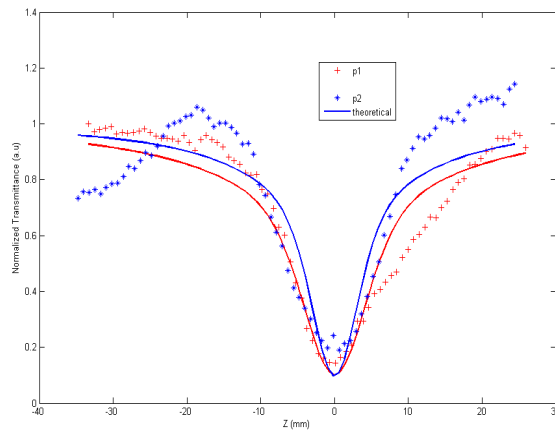


Figure.6.10(b): Open aperture Z-scan plot of SrTT-ELE at two laser power densities ($P_1=163 \text{ MW/cm}^2$ and $P_2=251 \text{ MW/cm}^2$)

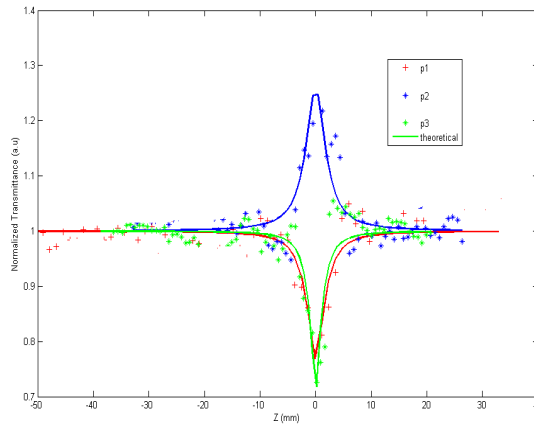


Figure.6.10(c): Combined Z-scan plot of SrTT-MAG at three laser powers densities ($P_1=75 \text{ MW/cm}^2$, $P_2=163 \text{ MW/cm}^2$ and $P_3=251 \text{ MW/cm}^2$)

From the open aperture Z-scan plot of pure SrTT sample given in figure 6.10 (a), it is clear that the transmittance of the sample solution shows a decrease with increase in input laser intensity. The decreasing transmittance reaches a minimum value at the focus. This is the peculiarity of reverse saturable absorption(RSA). Thus the sample solutions of pure SrTT exhibit RSA in its transmittance. The nonlinear absorption of these pure samples were determined using the open aperture transmittance data that is theoretically fitted. The solid lines in the plots of Z-scan represent the theoretical value. The values of nonlinear absorption coefficient β were evaluated using the equation(2) given in chapter 2. The electric field applied samples also showed the RSA nature giving a valley in their transmittance curves as shown in figure 6.10(b). The magnetic field applied SrTT showed RSA at $I_0 = 75$ and 251 MW/cm^2 . But SrTT-MAG gives a saturable absorption (SA) behaviour at $I_0 = 163 \text{ MW/cm}^2$. At this laser intensity, the transmittance of SrTT increases and gives a maximum value at the focal point. This is due to the depletion of ground states as that of CaTT sample. The SA is indicated by a peak response in the Z-scan trace of SrTT. From the

values of β , the imaginary part of third order susceptibility were calculated. The values of nonlinear absorption coefficient β and $\text{Im}(\chi^{(3)})$ of SrTT samples were given in table 6.6.

Table 6.6. Measured values of nonlinear absorption coefficient and imaginary part of third order susceptibility [$\text{Im}(\chi^{(3)})$] of SrTT

Sample	β (cmGW ⁻¹)				$\text{Im}(\chi^{(3)})$ (esu) $\times 10^{-10}$			
	I_0 (75 MW/cm ²)	I_0 (163 MW/cm ²)	I_0 (200 MW/cm ²)	I_0 (251 MW/cm ²)	I_0 (75 MW/cm ²)	I_0 (163 MW/cm ²)	I_0 (200 MW/cm ²)	I_0 (251 MW/cm ²)
SrTT pure	113	51	36	60	3.25	1.46	1.03	1.72
SrTT- ELE	-	110	-	72	-	3.17	-	2.07
SrTT- MAG	127	-34	-	46	3.65	-0.98	-	1.32

The blank spaces in the table correspond to the cases where the experimental data did not fit with the theoretical ones. β is positive for pure and electric field applied SrTT samples and negative for magnetic field applied SrTT at 163 MW/cm². The nonlinearity in SrTT samples are due to two photon absorption mechanism[30-31]. The switching response of SrTT can be used in applications such as optical pulse compression and laser pulse narrowing.

6.6. Optical limiting Studies on SrTT

Open aperture Z-scan study on SrTT reveals that they are reverse saturable absorbers at certain input laser power densities. The RSA nature of the samples confirm that they were well suited for optical limiting studies. The limiting threshold of these SrTT samples were determined from the optical limiting curves plotted using the normalized transmittance data from the open aperture Z-scan measurement. Figure 6.11 illustrates the limiting response of SrTT sample solutions.

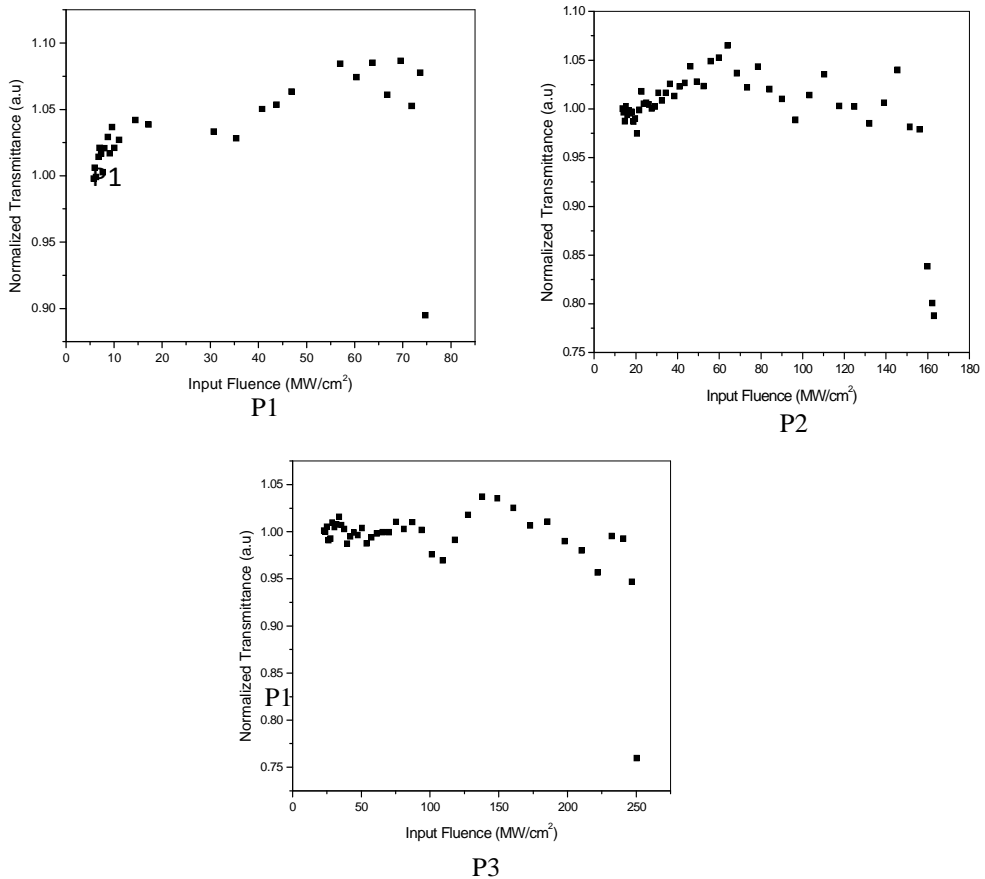
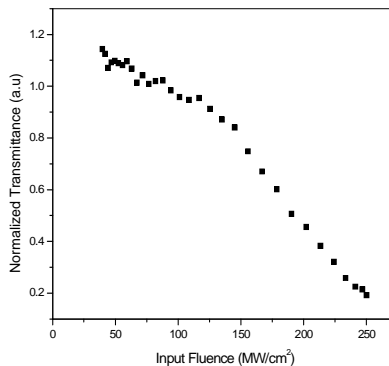
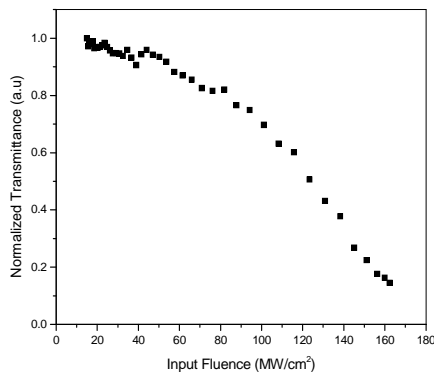
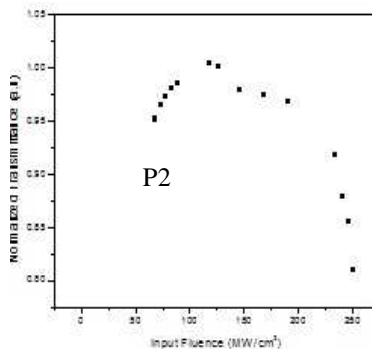
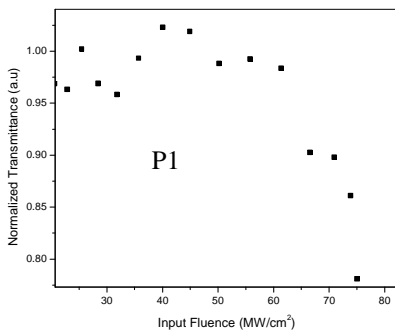


Figure 6.11(a). Optical limiting response of SrTT-pure at three laser power densities ($P_1=75 \text{ MW/cm}^2$, $P_2=200 \text{ MW/cm}^2$ and $P_3=251 \text{ MW/cm}^2$)



P1
Figure 6.11(b). Optical limiting response of SrTT-ELE at two laser powers ($P_1=163 \text{ MW/cm}^2$ and $P_2=251 \text{ MW/cm}^2$)



P2
Figure 6.11(c). Optical limiting response of SrTT-MAG at two laser power densities $P_1=75 \text{ MW/cm}^2$ and $P_2=251 \text{ MW/cm}^2$

The important parameter of an optical limiter is its limiting threshold. The values of limiting threshold for the SrTT samples which show RSA were evaluated and given in table.6.7

Table.6.7 .Observed values of limiting threshold for SrTT

Sample	Optical limiting threshold (MWcm ⁻²)			
	I ₀ (75 MW/c m ²)	I ₀ (163 MW/c m ²)	I ₀ (200 MW/ cm ²)	I ₀ (251 MW /cm ²)
SrTT pure	67	151	178	200
SrTT- ELE	-	108	-	202
SrTT- MAG	61	-	-	212

The blank spaces in the table correspond to the cases where the experimental data did not fit with the theoretical ones.

Conclusions

Strontium Tartrate crystals prepared by solution-gel method belongs to the orthorombic system which was confirmed using XRD analysis. Linear absorption spectra of three different SrTT crystals were taken at room temperature. Absorption peaks were located in UV region giving a wide transparency range to these crystal samples. Optical band gap of the samples varies from 5.37 eV to 5.4 eV suggest their applications in the field of band gap tuning. The fluorescence in SrTT are composed of various combinations and overtones of the molecules in the excited electronic levels. Thermal diffusivity of the pure , electric and magnetic fields applied SrTT samples were calculated from the TL plots. The negative value of fitting parameter indicates that Strontium Tartrate solution exhibits a negative lens. Nonlinear optical

measurements done by single beam Z-scan technique on SrTT exhibits SA and RSA behaviour in their transmittance traces which can be exploited for optical limiting and switching applications.

References

- [1] Arora, S. K., Vipul Patel, Brijesh Amin, and Anjana Kothari. "Dielectric behaviour of Strontium Tartrate single crystals." *Bulletin of Materials Science* 27, no. 2 (2004): 141-147.
- [2] Arora, S. K., Vipul Patel, Bhupendra Chudasama, and Brijesh Amin. "Single crystal growth and characterization of Strontium Tartrate." *Journal of Crystal Growth* 275, no. 1 (2005): e657-e661.
- [3] Rahimkuty, M. H., K. Rajendra Babu, K. Sreedharan Pillai, MR Sudarsana Kumar, and C. M. K. Nair. "Thermal behaviour of Strontium Tartrate single crystals grown in gel." *Bulletin of Materials Science* 24, no. 2 (2001): 249-252.
- [4] Selvasekarapandian, S., K. Vivekanandan, and P. Kolandaivel. "Vibrational studies of gel grown ferroelectric RbHC₄H₄O₆ and SrC₄H₄O₆ 4H₂O crystals." *Crystal Research and Technology* 34, no. 7 (1999): 873-880.
- [5] Brehat, F., and B. Wyncke. "Calculation of double-refraction walk-off angle along the phase-matching directions in non-linear biaxial crystals." *Journal of Physics B: Atomic, Molecular and Optical Physics* 22, no. 11 (1989): 1891-1898.
- [6] Nakatani, Noriyuki. "Point group determination of calcium tartrate by etch figure." *Japanese Journal of Applied Physics* 30, no. 11B (1991): L1961.
- [7] Gon, H. B. "Ferroelectricity in calcium tartrate single crystals grown by gel technique." *Journal of Crystal Growth* 102, no. 3 (1990): 501-504.
- [8] Torres, M. E., J. Peraza, A. C. Yanes, T. Lopez, J. Stockel, D. Marrero-Lopez, Xavier Solans, Eduardo Bocanegra, and C. Gonzalez Silgo. "Electrical conductivity of doped and undoped calcium tartrate." *Journal of Physics and Chemistry of Solids* 63, no. 4 (2002): 695-698.
- [9] Torres, Manuel E., Trinidad López, Josefina Stockel, Xavier Solans, Maite García-Vallés, Enrique Rodríguez-Castellón, and Cristina González-Silgo. "Structural characterization of doped calcium tartrate tetrahydrate." *Journal of Solid State Chemistry* 163, no. 2 (2002): 491-497.
- [10] Henisch, Heinz K. *Crystals in gels and Liesegang rings*. Cambridge University Press, 2005.

Linear and Nonlinear optical studies on Strontium Tartrate (SrTT) crystals

- [11] Arora, S. K., Vipul Patel, R. G. Patel, Brijesh Amin, and Anjana Kothari. "Electrical characterization of Strontium Tartrate single crystals." *Journal of Physics and Chemistry of Solids* 65, no. 5 (2004): 965-973.
- [12] Patel, Ambalal Ranchhodhbhai, and S. K. Arora. "Growth of Strontium Tartrate tetrahydrate single crystals in silica gels." *Journal of Materials Science* 11, no. 5 (1976): 843-846.
- [13] Murphy, J. C., and J. Bohandy. "Electron Spin Resonance of Cu²⁺ in Strontium Tartrate." *The Journal of Chemical Physics* 46, no. 3 (1967): 1215-1216.
- [14] Kumar, B. Suresh, MH Rahim Kutty, MR Sudarsana Kumar, and K. Rajendra Babu. "Growth and characterization of pure and lithium doped Strontium Tartrate tetrahydrate crystals by solution-gel technique." *Bulletin of Materials Science* 30, no. 4 (2007): 349-355.
- [15] Greena, J. Angel Mary, X. Sahaya Shajan, and H. Alex Devadoss. "Electrical conductivity studies on pure and barium added Strontium Tartrate trihydrate crystals." *Indian Journal of Science and Technology* 3, no. 3 (2010): 250-252.
- [16] Anderson, Joseph Chapman. "Dielectrics." (1964).
- [17] Arora, S. K., Vipul Patel, Anjana Kothari, and Brijesh Amin. "Gel growth and preliminary characterization of Strontium Tartrate trihydrate." *Crystal Growth & Design* 4, no. 2 (2004): 343-349.
- [18] Suryanarayana, K., S. M. Dharmaprakash, and K. Sooryanarayana. "Optical and structural characteristics of strontium doped calcium tartrate crystals." *Bulletin of Materials Science* 21, no. 1 (1998): 87-92.
- [19] Firdous, A., I. Quasim, M. M. Ahmad, and P. N. Kotru. "Dielectric and thermal studies on gel grown Strontium Tartrate pentahydrate crystals." *Bulletin of Materials Science* 33, no. 4 (2010): 377-382.
- [20] Freeda, M. Mary, R. Krishna Priya, T. H. Freeda, and S. Mary Delphine. "Crystallization and characterization of mixed crystals of strontium calcium barium tartrate." *Archives of Applied Science Research* 4, no. 1 (2012): 128-136.
- [21] Bohandy, Joseph, and John C. Murphy. "Electron Spin Resonance Study of Transition Elements in Strontium Tartrate and Calcium Tartrate." *The Journal of Chemical Physics* 52, no. 6 (1970): 3301-3302.
- [22] Sawant, D. K., and K. S. Bhavsar. "Photo-luminescence and band gap energy of Ca-Sr tartrate." *Archives of Physics Research* 3, no. 1 (2012): 29-35.
- [23] Vijayakumari, T., C. M. Padma, C. K. Mahadevan, Mr S. Balamurugan, V. Kanmani, S. Radhika, M. K. Abd-ELhamed et al. "Effect of Co doping on the structural and physical properties of SrC₄H₄O₆. 3H₂O and SrC₄H₄O₆. 4H₂O

- crystals." *International Journal of Modern Engineering Research* 4, no. 12 (2014): 69-72.
- [24] Henisch, Heinz K. *Crystal growth in gels*. Courier Corporation, 1970.
- [25] Henisch, Heinz K. *Crystals in gels and Liesegang rings*. Cambridge University Press, 2005.
- [26] G.Lillibai, PhD Thesis, December 2012.
- [27] Joseph, Santhi Ani, Misha Hari, S. Mathew, Gaurav Sharma, V. M. Hadiya, P. Radhakrishnan, and V. P. N. Nampoory. "Thermal diffusivity of Rhodamine 6G incorporated in silver nanofluid measured using mode-matched thermal lens technique." *Optics Communications* 283, no. 2 (2010): 313-317.
- [28] Sparks, Taylor D., Paul A. Fuierer, and David R. Clarke. "Anisotropic Thermal Diffusivity and Conductivity of La-Doped Strontium Niobate Sr₂Nb₂O₇." *Journal of the American Ceramic Society* 93, no. 4 (2010): 1136-114.
- [29] Sheik-Bahae, Mansoor, Ali A. Said, T-H. Wei, David J. Hagan, and Eric W. Van Stryland. "Sensitive measurement of optical nonlinearities using a single beam." *Quantum Electronics, IEEE Journal of* 26, no. 4 (1990): 760-769.
- [30] Irimpan, Litty, V. P. N. Nampoory, and P. Radhakrishnan. "Spectral and nonlinear optical characteristics of nanocomposites of ZnO–CdS." *Journal of Applied Physics* 103, no. 9 (2008): 094914, 1-8.
- [31] Irimpan, Litty, V. P. N. Nampoory, and P. Radhakrishnan. "Spectral and nonlinear optical characteristics of nanocomposites of ZnO–Ag." *Chemical physics letters* 455, no. 4 (2008): 265-269.

Chapter 7

Linear and Nonlinear Optical studies on Cadmium Tartrate (CdTT) crystals

Abstract

The studies on two different types of Cadmium Tartrate viz CdTT pure and CdTT-MAG crystals have been discussed in this chapter. The optical transparency and the band gap characteristics of the crystals in ethanol solutions were studied using UV Visible absorption spectroscopy at room temperature. The photoluminescence in CdTT samples in solution phase were investigated. The mechanism of emission bands in pure and magnetic field applied CdTT crystals in aqueous state have been discussed in this chapter. The non radiative relaxation of gel grown crystals of CdTT incorporated with Rhodamine 6G dye was studied by employing the thermal lens technique. The optical nonlinearity of these samples were measured using Bahae's method.

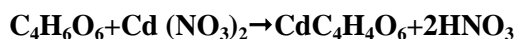
7.1 Introduction

The crystalline materials of Cadmium Tartrate (CdTT) have found many applications in optoelectronics owing to their optical and piezoelectric characteristics[1-4]. S.K Arora et al worked on the crystals of Cadmium Tartrate penta hydrate [1]. They studied the slow and controlled reaction between Cd^{2+} ions and tartrate $(\text{C}_4\text{H}_4\text{O}_6)^{2-}$ ions in hydro silica gel and the optical characterization of this crystal was reported. The electrical conductivity of CdTT was also studied and reported [5]. Harshkant Jethva reported on the thermal study of Cadmium Levo-Tartrate crystals[6]. Harshkant characterized the CdTT by thermo gravimetric analysis and the thermodynamic parameters were evaluated for the different stage of decomposition. Many works have been done on CdTT crystals to calculate the kinetic parameters of solid state reaction including mass [7-11]. H.O. Jethva reported the results of FTIR spectroscopic studies on Cadmium Levo Tartrate crystals [12]. Jethva found the presence of O-H, C-H, C-O and C=O functional groups with metal-oxygen vibrations in the FTIR spectrum of CdTT. Cadmium Tartrate Oxalate single crystals were prepared and studied by D.Arumugam et al employing the sol gel technique [13]. Many researchers in crystal growth field adapted the gel technique for the preparation of crystals owing to the major advantages of this method[14-19]. The gel method can be used for growing single crystals which decompose below the melting point [20-23]. The growth and characterization of Barium doped Cadmium Tartrate were studied by N.S.Patil et al[24]. The studies on mixed crystals of Calcium-Cadmium Tartrate were reported in literature [25]. D. K. Sawant et al concluded that the crystals of Calcium Cadmium Tartrate exhibit transparent and diamond like morphology. Many researchers worked on the mixed crystals by solution gel method[26-27]. The thermal studies on Barium doped Cadmium Tartrate crystals were carried out and reported[28]. Strontium doped Cadmium Tartrate Oxalate single crystals were studied by D.Arumugam et al[29]. S.S. Sonawane and R.R. Ahire prepared single crystals of CdTT and

characterized them[30]. In this chapter, the linear and nonlinear optical studies of pure and magnetic field applied Cadmium Tartrate (CdTT) crystals are presented.

7.2 CdTT sample Synthesis

The good quality crystals of CdTT were prepared by the relevant solution-gel method. The various steps involved in this gel technique and the advantage of this particular method for growing crystals have been discussed in chapter 1 [31] .The medium in which the CdTT crystals were grown was hydro silica gel prepared from an aqueous solution of sodium meta silicate(SMS) which is acidified with tartaric acid. To the set gel, cadmium nitrate solution of 1 M concentration was supernated without disturbing the medium. The specific gravity of the gel was varied from 1.02 to 1.04. The pH of the solution of SMS and tartaric acid was changed by adding sufficient amount of SMS and the values of pH were varied between 5 and 7. The crystals of CdTT were obtained after 10 days. Another sample crystal of CdTT was prepared by applying a magnetic field. In this process two bar magnets were tightly fixed across the test tube containing the gel and top solution of cadmium nitrate. Thus two different types of CdTT crystals were prepared by gel method. The former crystal is named as CdTT-pure and the latter one is CdTT-MAG. The steps involved in the crystal preparation of CdTT is illustrated in figure 7.1. The chemistry involved in the crystal formation is



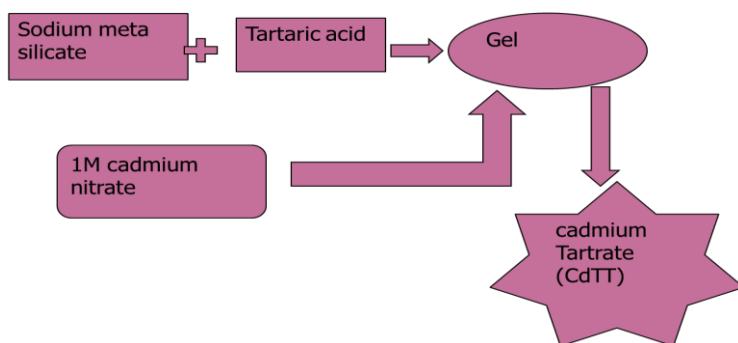


Figure 7.1 Schematic of crystal preparation of CdTT

7.3 Structural Characteristics

In order to find the crystalline nature of the prepared sample, the X ray diffractogram of the material was taken [31]. Figure 7.2 represents the XRD of CdTT crystal. The presence of intense peaks in the diffractogram confirmed the crystalline nature of Cadmium Tartrate by gel method. The values of d spacing and hkl plane values were compared with those of JCPDS file of CdTT. The structure of CdTT is then identified as monoclinic [31].

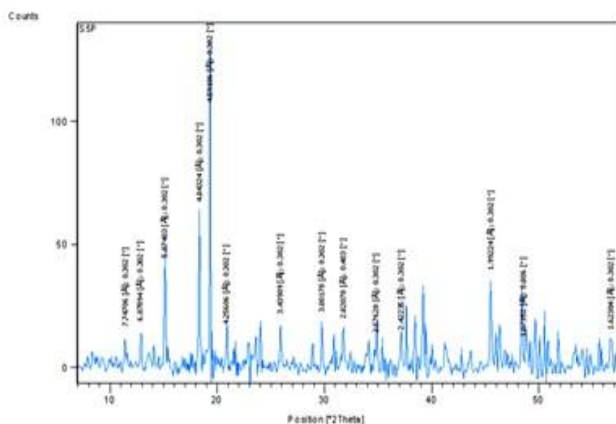


Figure 7.2. XRD of CdTT crystal

7.4. Linear Optical Characterizations

The solution samples of CdTT crystals were used for the optical and nonlinear studies. The sample solutions of CdTT were prepared by dissolving the powdered crystals in ethanol solvent. The concentration of the CdTT solution taken was 0.02 gm/ml.

7.4.1 Absorption Measurements

In order to determine the optical transparency of the grown crystals of Cadmium Tartrate, the room temperature linear absorption spectra was taken. The UV-Visible spectra of the pure and magnetic field applied CdTT samples were taken in the wavelength range 200nm to 800 nm and are shown in the following figure 7.3.

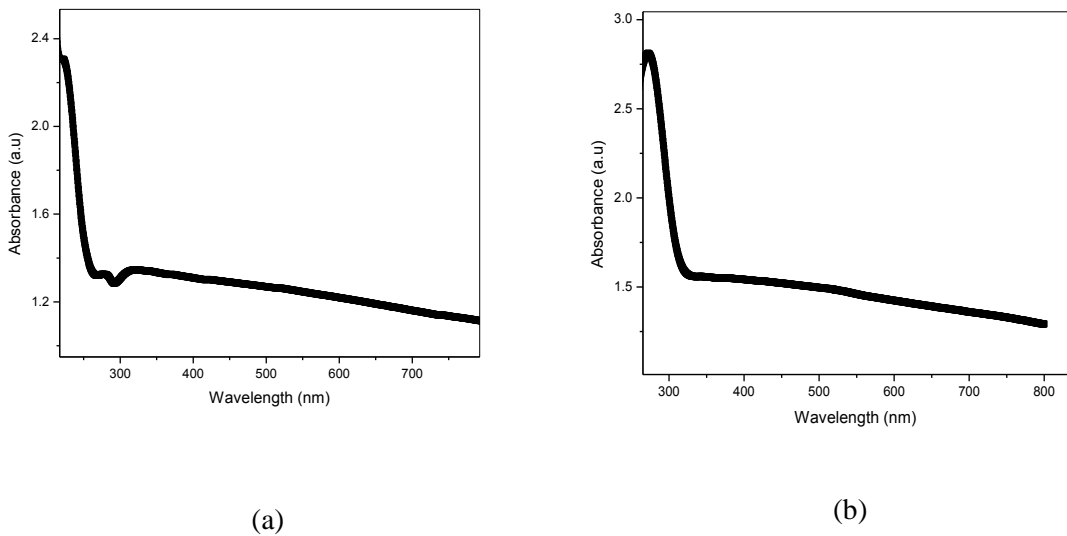
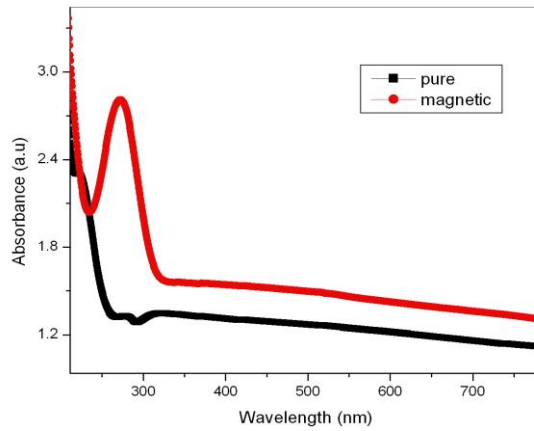


Figure.7.3. Linear absorption spectra of (a) CdTT –pure and (b) CdTT-MAG



(c)

Figure.7.3. (c) combined Linear absorption spectra

Figure 7.3(a) represents the linear absorption of pure sample. It shows that CdTT pure sample has a wide transparency in the entire visible region. The absorption peak corresponding to the pure sample is lying in the ultra violet region which is clearly indicated in figure 7.3(a). The linear absorption of magnetic field applied CdTT is given in figure 7.3(b). The absorption edge is located in the UV region corresponding to a peak wavelength of 277 nm. The transparency of magnetic field applied CdTT is as wide as that of the pure sample. Figure 7.3(c) shows that the effect of magnetic field has red-shifted the absorption edge of CdTT crystal samples. The values of linear absorption coefficient α for the pure and magnetic field applied CdTT samples were determined using the spectra. The absorption coefficient is smaller for the pure sample having a value 1.26 cm^{-1} . The peak wavelength of absorption and corresponding α values for both the pure and magnetic field applied CdTT are given in the table 7.1. The wide transparency of the sample crystals make them suitable for nonlinear optical applications.

**Table.7.1. Measured values of α and λ_{peak}
for the two different CdTT samples**

Sample crystal	λ_{peak} (nm)	α (cm^{-1})
CdTT- Pure	260	1.26
CdTT-MAG	277	1.48

7.4.2. Optical Band gap of CdTT

CdTT sample solutions exhibit a UV absorption in the linear measurements. The determination of band gap of the crystalline CdTT material in solution phase is a means for finding the semiconductor or dielectric nature. The direct band gap of the CdTT solutions were measured from the graph of $(\alpha h\nu)^2$ versus E_g , where E_g is the optical band gap of CdTT in ethanol. Figure 7.4(a) represents the direct band gap plot of pure CdTT sample. The optical band gap of magnetic field applied CdTT was determined from the figure 7.4(b). The pure sample exhibits a direct band gap of 4.61 eV. The direct band gap value for CdTT-MAG is 3.9 eV. The band gap value of CdTT sample solution got decreased by the application of magnetic field. The high value of band gap in the pure sample may be attributed to the confinement of exciton in pure CdTT crystal. The band gap values evaluated in both cases are given in table 7.2. The optical band gap energy in the CdTT was associated with the excitation of an electron from the valence band to the conduction band by the absorption of a photon.

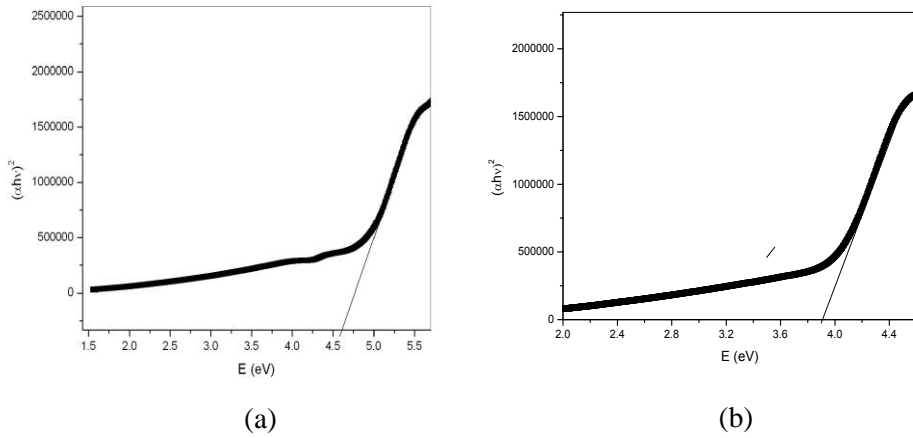


Figure 7.4 Optical direct band gap plot of (a) pure and (b) magnetic field applied CdTT samples.

Table 7.2 Measured values of optical band gap of CdTT

Sample	Direct Band gap (eV)	Indirect Band gap (eV)
CdTT -pure	4.61	4.25
CdTT- MAG	3.90	3.50

CdTT samples also exhibit indirect band gap [1]. Figure 7.5 represents the indirect band gap response of CdTT solutions. The indirect band gap of CdTT sample solutions were measured by plotting a graph between E_g along the X- axis and $(\alpha hv)^{1/2}$ along the Y- axis. The values of indirect band gap were 4.25 eV for the pure sample and 3.5 eV for the CdTT sample subjected to the magnetic field. The indirect band gap arises from the presence of a broad spectrum of phonons. But only few phonons with required momentum contributed to the inter band transition giving the band gap energy to the CdTT [1].

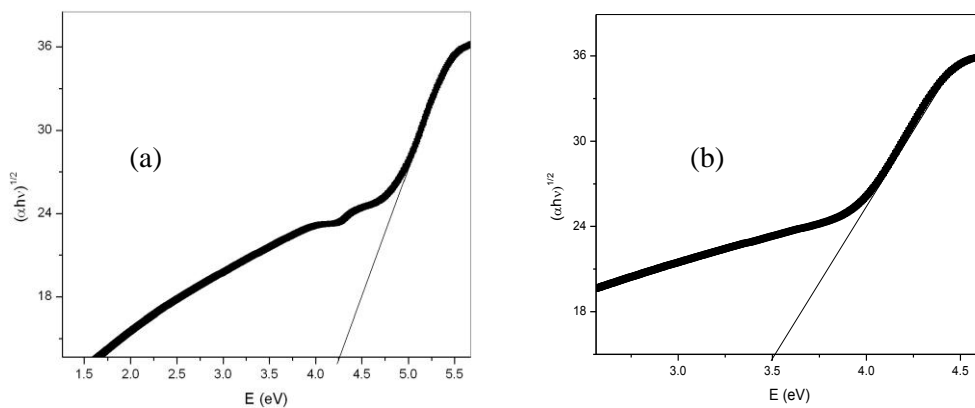
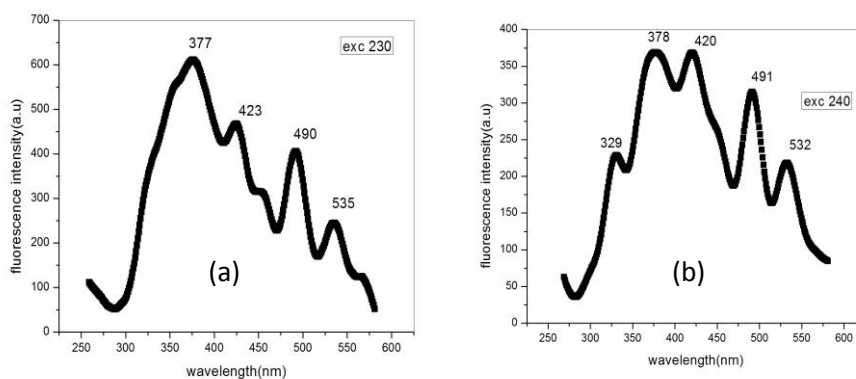


Figure 7.5 Optical Indirect band gap plot of (a) pure and (b) magnetic field applied CdTT samples.

7.4.3 Photoluminescence studies

The emission characteristics of CdTT samples were studied using fluorescence spectroscopy. The emission spectra of both the pure and magnetic field applied CdTT samples in ethanol were taken for different excitation wavelengths. The luminescence of CdTT in solution phase were examined through these studies. The following figures 7.6 and 7.7 illustrate the photoluminescence aspects of CdTT sample solutions.



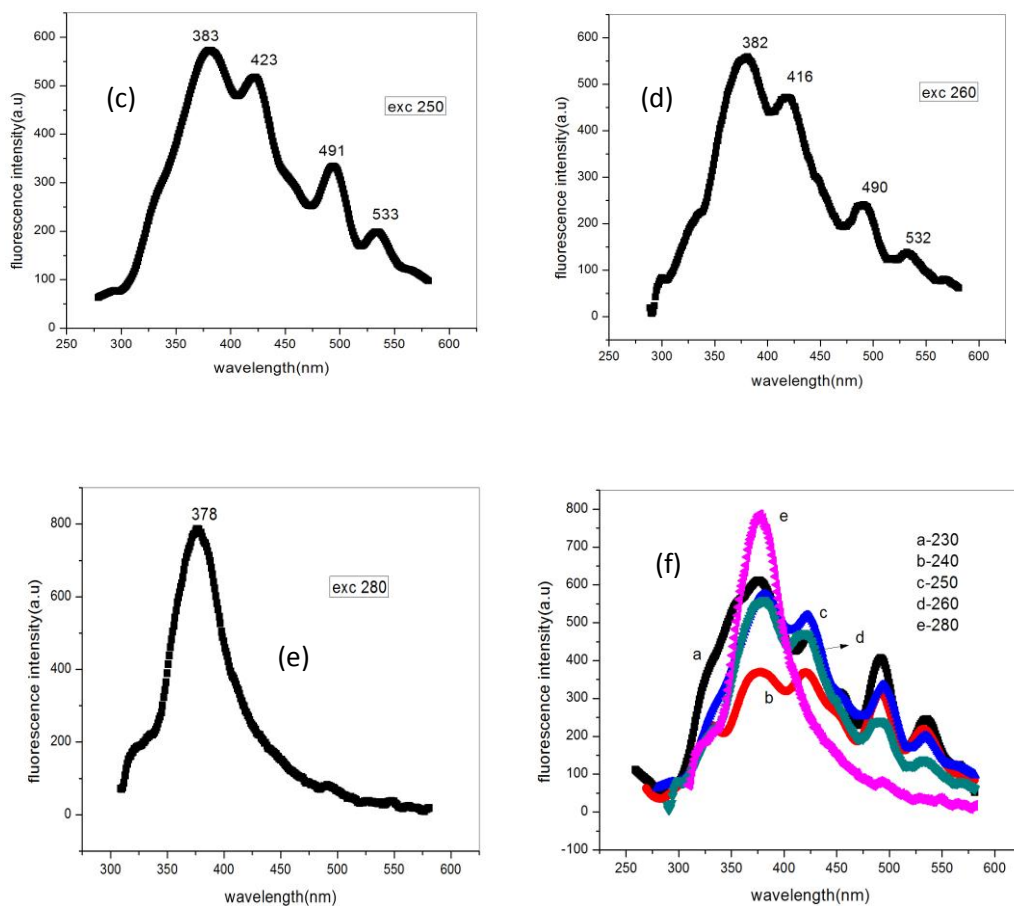


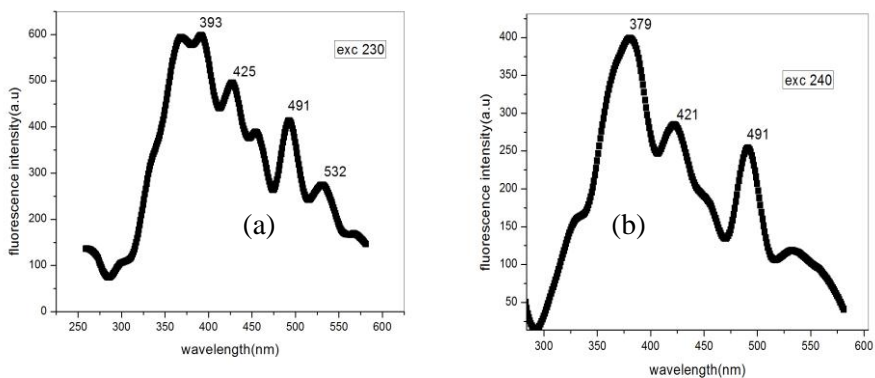
Figure 7.6 Emission spectra of pure CdTT at an excitation wavelength of (a) 230 nm (b) 240nm (c)250 nm and (d) 260 nm(e) 280 nm and(f) combined emission spectra

The wavelengths used for exciting the solution samples of pure CdTT were 230, 240, 250, 260 and 280 nm. The excitations of 230 nm, 250 nm and 260 nm gave four strong emissions. Figure 7.6(b) indicates that five emissions were obtained at an excitation of 240 nm. Only one intense peak was given by CdTT pure sample with an excitation wavelength of 280 nm as shown in the figure 7.6(e). The obtained peaks of emission at different excitations are given in the table 7.3.

Table 7.3 The emission peaks of CdTT pure sample at five different excitations

Excitation wavelength(λ_{exc}) [nm]	Emission wavelengths (λ_{em}) [nm]
230	377, 423,490,535
240	329,378,420,491,532
250	383,423,491,533
260	382,416,490,532
280	378

The fluorescence emission studies of magnetic field applied CdTT were carried out at six different excitations. The excitation of 230nm, 250nm 260nm and 270 nm produce four strong emissions. Three intense peaks were obtained at an excitation of 240nm and one sharp emission at 280 nm as in the case of CdTT pure sample. Figure 7.7 shows the emission spectra of CdTT-MAG sample.



l studies

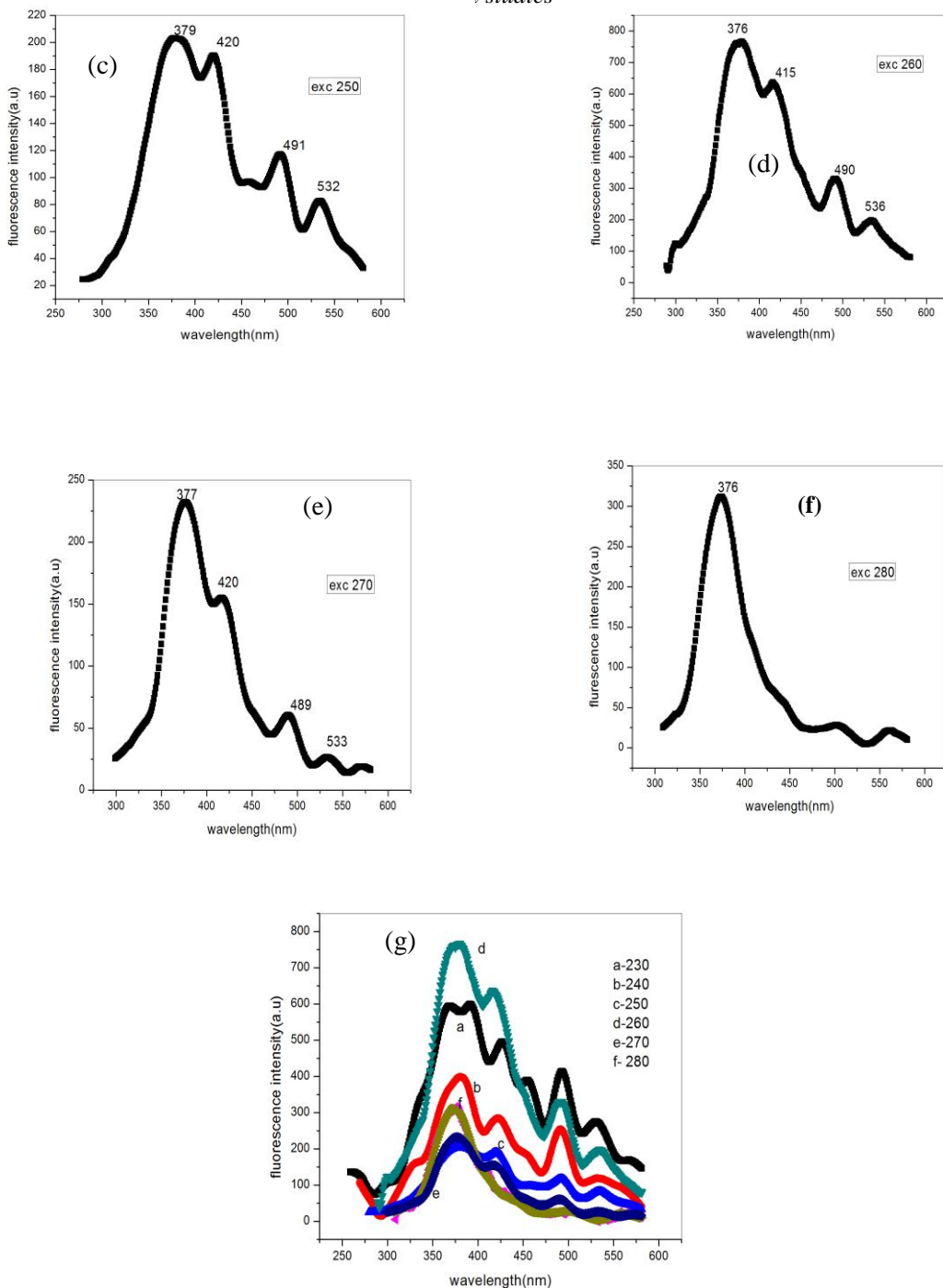


Figure.7.7 Emission spectra of CdTT-MAG at an excitation wavelength of (a) 230 nm (b) 240 (c) 250 nm (d) 260 nm , (e) 270 nm (f) 280 nm and (g) combined emission spectra

The emission peaks of CdTT-MAG sample at different excitation wavelengths are given in the table 7.4.

Table 7.4 The emission peaks of CdTT -MAG sample at six different excitations

Excitation wavelength(λ_{exc}) [nm]	Emission wavelengths (λ_{em}) [nm]
230	393, 425, 491,532
240	379, 421, 491
250	379, 420, 491, 532
260	376, 415, 490, 536
270	377, 420, 489, 533
280	376

7.4.4 Mechanism of photoluminescence in CdTT

The mechanism of fluorescence emission in CdTT samples can be explained using the following model. The values of ν were taken from the FTIR spectra of CdTT crystal [31] and given in table 7.5. Figure 7.8 represents the FTIR spectrum of CdTT crystal[31]. The table 7.6 explains the luminescence of CdTT sample solutions. The term T_e represents the difference in two electronic levels as described in chapter 5. The assignments were given on the basis of fluorescence emission peaks obtained for CdTT. The fluorescence in CdTT arise from the combinations and overtones of the excited electronic levels. The various transitions and corresponding fluorescence emission bands of CdTT are shown in figure.7.9.

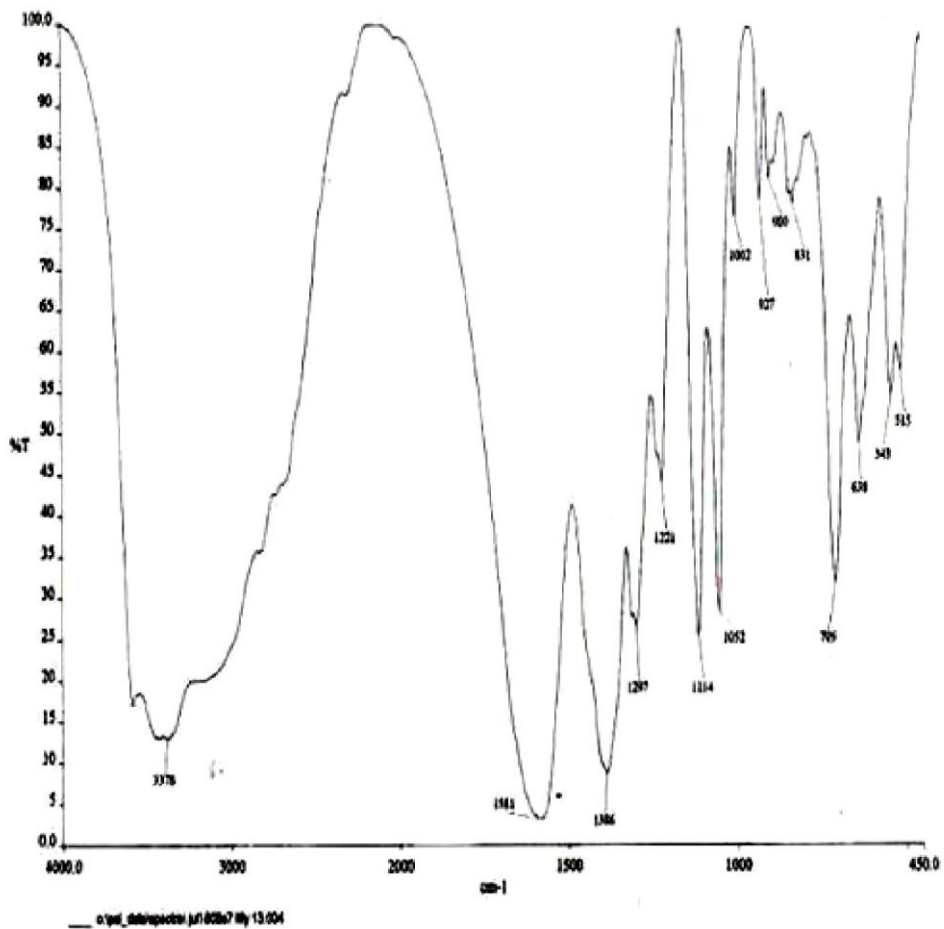


Figure 7.8 FTIR spectrum of CdTT[31]

Table 7.5. Values of ν taken from FTIR spectra of CdTT

$\nu(\text{cm}^{-1})$	The values taken from FTIR spectra of SrTT(cm^{-1})
ν_1	751
ν_2	927
ν_3	1052
ν_4	1141
ν_5	1221
ν_6	1287
ν_7	1346
ν_8	1641
ν_9	3570

Table.7.6 Details of fluorescence bands and assignments of CdTT

Emission wavelength(nm)	Observed Wave number ($\bar{\nu}_{\text{ob}}$) (cm^{-1})	Assignments	Calculated Wave number ($\bar{\nu}_{\text{ca}}$) (cm^{-1})	Difference ($\bar{\nu}_{\text{ob}} - \bar{\nu}_{\text{ca}}$) (cm^{-1})
575	17391	T_e	-	-
532	18797	$T_e + \nu_7$	18737	60
490	20408	$T_e + \nu_7 + \nu_8$	20378	30
450	22222	$T_e + \nu_6 + \nu_9$	22248	26
416	24038	$T_e + \nu_2 + 2\nu_5 + 2\nu_8$	24042	4
382	26178	$T_e + \nu_8 + 2\nu_9$	26172	6
340	29412	$T_e + \nu_7 + 3\nu_9$	29447	35

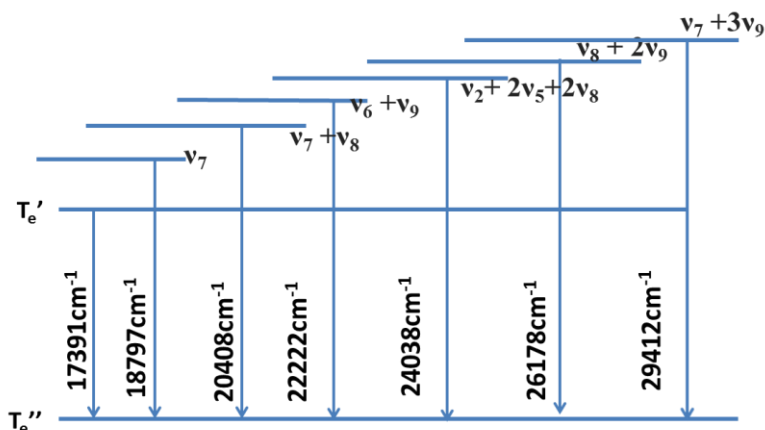


Figure 7.9. Schematic of the energy levels involved in the fluorescence spectra of CdTT based on combinations and overtones of various modes

7.4.5 Non radiative decay mechanism in CdTT

The heat transfer mechanism of CdTT sample solutions were investigated using dual beam mode matched thermal lens technique. The method of experimentation and the theory of TL technique are explained in detail in previous chapters. For the determination of the mechanism of non radiative decay in CdTT samples, a trace of Rhodamine-6G dye was incorporated. The purpose of addition of dye to the sample solutions of CdTT is to enhance the absorption. The presence of dye did not alter the thermal diffusivity of the CdTT samples. Figure 7.10(a) shows a typical thermal lens plot of pure CdTT(Rh-CdTT pure) sample. The solid line in the plot represents the theoretical fit to the experimental data which is represented by dark circles. The diffusivity values were measured using the fitting parameters t_c and θ_c as described in chapter 6. Figure 7.10(b) represents the TL plot for magnetic field applied CdTT – Rhodamine 6G sample.

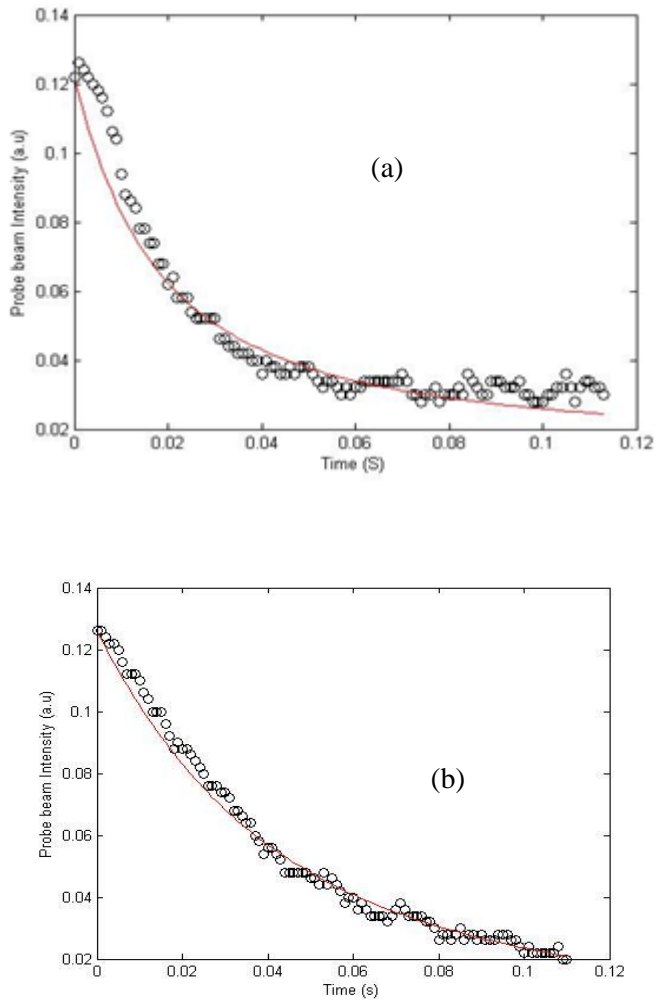


Figure.7.10 Thermal lens plot of (a) Rh-CdTT- pure and (b) Rh-CdTT- MAG

The values of thermal diffusivity of CdTT pure and magnetic field applied samples are given in the table 7.7. For the pure CdTT sample the coefficient of thermal diffusion D is $8.64 \times 10^{-3} \text{ cm}^2/\text{S}$ which is very high due to the low value of t_c . The value of D of CdTT is comparable with that of

Aluminum. Hence CdTT can be employed in heat sink applications [32]. The very small value of t_c indicates the slow decay of pure CdTT sample. The D value of magnetic field applied sample is $7.92 \times 10^{-3} \text{ cm}^2/\text{S}$. This indicates that the effect of magnetic field enhance the decay rate of CdTT to a great extent. This facilitates the tuning of thermal diffusivity values by applying the magnetic field to CdTT sample.

Table.7.7.Measured values of D, θ_c , and t_c for Rhodamine-6G incorporated

Sample in gm/ml	t_c (mS)	θ_c	D (cm^2/S) $\times 10^{-3}$
CdTT Pure	15.00	-329.00	8.64
CdTT magnetic	15.98	-171.25	7.92

CdTT solution

The mechanism of heat transfer in CdTT can be explained using the non radiative relaxation process take place within the crystal. The non radiative decay occurs due to the loss of energy by the negative gradient of refractive index of the sample[33]. There are few reports on the thermal diffusivity values of CdTT available in the literature for comparison [34].

7.5. Nonlinear optical studies on CdTT

The nonlinear measurements of CdTT sample solutions were done by employing open aperture Z- scan experiment. The samples of CdTT in solution

phase were taken in 1 mm thick cuvette for experimentation. The experimental procedure of Z-scan technique is explained in the previous chapters. The Q-switched laser having power densities 75 MW/cm², 163 MW/cm² and 251 MW/cm²

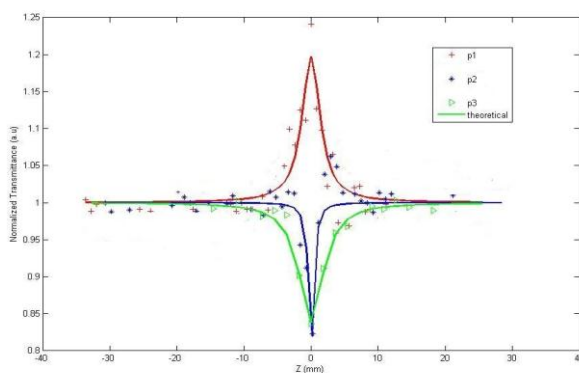
were

CdTT

The

were

along



used for the nonlinear studies on samples. solution samples moved the focal

plane of a lens using a computer controlled translation stage. The transmittance of the samples were detected using two pyro electric detectors. The experimental data of the sample were theoretically fit using a computer program. Figure 7.11(a) illustrates the nonlinear response of the pure sample of CdTT at three different laser power densities.

Figure.7.11 (a): Combined z scan plot of pure CdTT at three laser powers ($P_1=75 \text{ MW/cm}^2$, $P_2=163 \text{ MW/cm}^2$ and $P_3=251 \text{ MW/cm}^2$)

The open aperture Z-scan plots of pure CdTT at various laser power densities show valley and peak responses in normalized transmittance. For a laser power density of 75 MW/cm^2 the transmittance reaches maximum at the focus thereby giving a peak. This response can be attributed to the saturable absorption of CdTT. For 163 MW/cm^2 and 251 MW/cm^2 laser power densities, the transmittance goes on decreasing and gives a valley nature. This decrease in transmittance is due to the reverse saturable absorption (RSA) of CdTT. Figure 7.11(b) gives the open aperture Z-scan trace of magnetic field applied CdTT at two laser power densities 75 MW/cm^2 and 251 MW/cm^2 . From this figure, it is evident that the crystals of CdTT-MAG exhibit RSA nature at these two laser intensities.

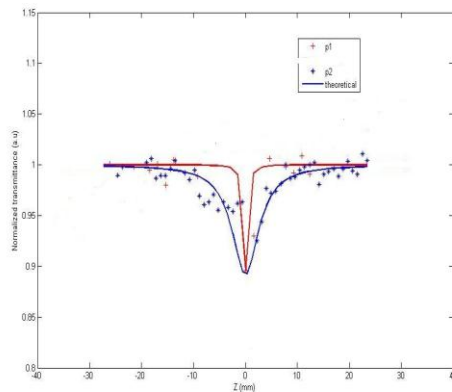


Figure.7.11(b): Combined Z-scan plot of CdTT-MAG at two laser powers 75 MW/cm^2 and 251 MW/cm^2

The nonlinear absorption coefficients of both of the CdTT sample solutions were calculated using the values of q obtained from the theoretical fit. The β values of pure and magnetic field applied CdTT were evaluated. From the β values, the imaginary part of third order susceptibility were also calculated

using the equation(10) given in chapter 1.The table 7.8 gives the values of β and $\text{Im}(\chi^{(3)})$ of CdTT samples.

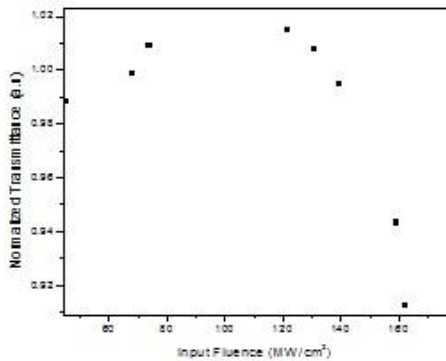
Table 7.8. Measured values of nonlinear absorption coefficient and imaginary part of third order susceptibility [$\text{Im}(\chi^{(3)})$] of CdTT

The blank spaces in the table correspond to the cases where the experimental data did not fit with the theoretical ones. The negative value of β for the CdTT pure sample at $I_0=75 \text{ MW/cm}^2$ indicates the presence of SA. At this laser power density the pure sample exhibits reduced absorption coefficient as in the case of CaTT crystal. As the laser intensity was increased, the CdTT samples show induced absorption thereby giving RSA [35]. The SA of CdTT is indicated by the depletion of ground state population. The mechanism of nonlinear absorption in CdTT samples can be explained through two photon absorption(TPA) since the laser wavelength used is 532 nm. This TPA in CdTT samples explained on the basis of an irradiance dependent process [36].

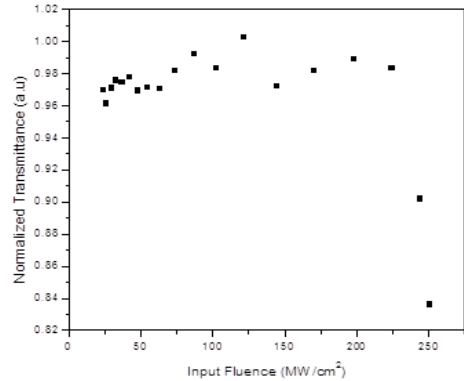
Sample	$\beta \text{ (cmGW}^{-1}\text{)}$			$\text{Im}(\chi^{(3)}) \text{ (esu) } \times 10^{-10}$		
	$I_0 \text{ (75 MW/c m}^2\text{)}$	$I_0 \text{ (163 MW/c m}^2\text{)}$	$I_0 \text{ (251 MW/c m}^2\text{)}$	$I_0 \text{ (75 MW/c m}^2\text{)}$	$I_0 \text{ (163 MW/c m}^2\text{)}$	$I_0 \text{ (251 MW/c m}^2\text{)}$
CdTT Pure	-60	52	25	-1.83	1.58	0.76
CdTT -MAG	51	-	16	1.55	-	0.49

7.6. Optical limiting Studies on CdTT.

The optical limiting response of the CdTT sample solutions were investigated using the nonlinear transmission traces given by the open aperture experiment. Figures 7.12(a) and 7.12(b) show the limiting response of pure and magnetic field applied CdTT samples.

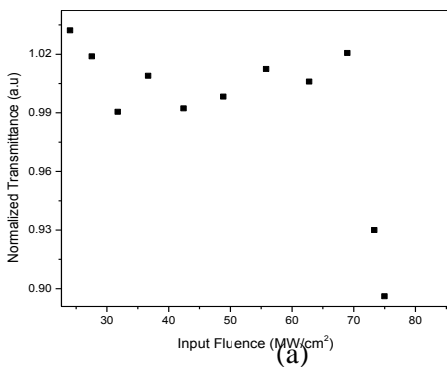


(a)

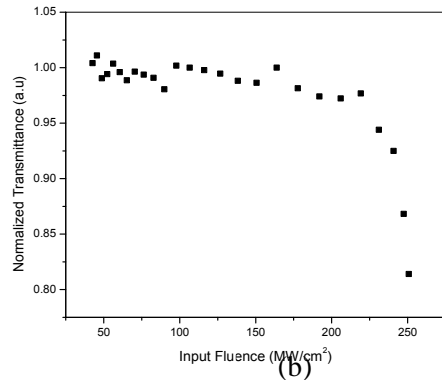


(b)

Figure 7.12(a). Optical limiting response of CdTT-pure at (a) 163 MW/cm² and (b) 251 MW/cm²



(a)



(b)

Figure 7.12(b). Optical limiting response of CdTT-MAG at (a) 75 MW/cm² and (b) 251 MW/cm²

The important factor that decides the performance of an optical limiter is its limiting threshold. The limiting threshold values of CdTT were determined from the plots of transmittance verses fluence as shown in the above figures

7.12. The threshold values of limiting for the CdTT sample solutions are given in table 7.9. The optical limiting property in CdTT arises from the absorptive nonlinearity which corresponds to the imaginary part of the third order susceptibility.

Table.7.9 .Observed values of limiting threshold for CdTT

Sample	Optical limiting threshold (MWcm ⁻²)		
	I ₀ (75 MW/c m ²)	I ₀ (163 MW/c m ²)	I ₀ (251 MW/c m ²)
CdTT pure	-	139	220
CdTT MAG	62	-	219

Conclusions

Two types of Cadmium Tartrate crystals were prepared by solution gel technique. The XRD study on these CdTT confirms the crystallinity and monoclinic structure. The absorption edge of pure and magnetic field applied samples in ethanol solution is located in the ultraviolet region. The wide transparency of these crystals in solution phase is detected using the linear absorption measurements. The magnetic field applied sample exhibits low band gap compared to the pure CdTT. The emission mechanism in CdTT sample solutions is studied and explained on the basis of transitions from electronic excitation levels. The fluorescence in CdTT is composed of combinations and

overtones. The non radiative relaxation from CdTT are investigated using TL technique. The coefficient of thermal diffusion was found to show a wide variation by the application of magnetic field. This sensitively enables us to tailor the thermal properties of the sample by applying a magnetic field. The nonlinear optical studies carried out by open aperture Z-scan experiment reveals the presence of RSA and SA at different laser power densities. The RSA nature of the CdTT makes them suitable for optical limiting applications. The limiting response of pure and CdTT-MAG samples were studied. These studies confirm the utility of CdTT in limiting and switching applications.

References

- [1] Arora, S. K., A. J. Kothari, R. G. Patel, K. M. Chauhan, and B. N. Chudasama. "Optical absorption in gel grown Cadmium Tartrate single crystals." In *Journal of Physics: Conference Series*, IOP Publishing, 28, no. 1(2006):48-52
- [2] Rethinam, F. Jesu, D. Arivuoli, S. Ramasamy, and P. Ramasamy. "Growth and characterization of pure and cadmium doped strontium tartrate tetrahydrate single crystals." *Materials Research Bulletin* 29, no. 3 (1994): 309-316.
- [3] Nakatani, Noriyuki. "Point group determination of calcium tartrate by etch figure." *Japanese Journal of Applied Physics* 30, no. 11B (1991): L1961.
- [4] Selvarajan, P., B. N. Das, H. B. Gon, and K. V. Rao. "Infrared spectroscopic and thermal studies of calcium tartrate single crystals grown by silica-gel technique." *Journal of Materials Science Letters* 12, no. 15 (1993): 1210-1211.
- [5] Arora, S. K., A. Kothari, B. Amin, and B. Chudasama. "Synthesis and characterization of Cadmium Tartrate single crystals." *Crystal Research and Technology* 42, no. 6 (2007): 589-594.
- [6] Harshkant Jethva., "Thermal Study of Cadmium Levo-Tartrate Crystals" *International Journal of Innovative Research in Science, Engineering and Technology* 3, no. 11(2014):17345- 17350.
- [7] Joseph, S., and Joshi, M. J., "Kinetic study of dehydration in the gel grown iron tartrate dihydrate crystals", *Indian J. Phys.* 71A (1997): 183-189.

- [8] Dabhi, R. M., and M. J. Joshi. "Thermal studies of gel-grown Cadmium Tartrate crystals." In *Indian journal of physics A and Proceedings of the Indian Association for the Cultivation of science A*, 77, no. 5(2003): 481-485.
- [9] Coats, A. W., and J. P. Redfern. "Kinetic parameters from thermogravimetric data." *Nature* 201 (1964): 68-69.
- [10] Horowitz, Hugh H., and Gershon Metzger. "A New Analysis of Thermogravimetric Traces." *Analytical Chemistry* 35, no. 10 (1963): 1464-1468.
- [11] Kotru, P. N., K. K. Raina, and M. L. Koul. "Characterization and thermal behaviour of gel grown mixed rare-earth (Didymium) tartrate crystals." *Journal of Materials Science* 21, no. 11 (1986): 3933-3940.
- [12] Jethva, H. O. "FTIR Spectroscopic and XRD analysis of gel-grown, cadmium levo-tartrate crystals." *International Journal of Applied Research IJAR* 1, no. 4 (2015): 1-3.
- [13] Arumugam, D., and A. Krishnan. "Growth and Study Of Cadmium Tartrate Oxalate Single Crystals by Sol Gel Technique." *Transactions* 1, no. 1 (2013): 1835 – 1843.
- [14] Henisch, Heinz K. *Crystals in gels and Liesegang rings*. Cambridge University Press, 2005.
- [15] H.K.Henisch, *Crystal Growth in Gells*, Pennsylvania State University Press, UniversityPark, Pennsylvania, 1970.
- [16] Desai, C. C., and A. H. Patel. "Synthesis, characterization and properties of ferroelectric rubidium hydrogen tartrate single crystals." *Bulletin of Materials Science* 11, no. 1 (1988): 31-37.
- [17] Suthar, S. R., and M. J. Joshi. "Growth and characterization of Mn²⁺ doped calcium l-tartrate crystals." *Crystal Research and Technology* 41, no. 7 (2006): 664-670.
- [18] Bachhav, S. K., N. S. Patil, M. S. Kale, and D. S. Bhavsar. "Crystal growth and characterization of strontium doped barium tartrate crystals by silica gel method." *Advances in Applied Science Research*, 5,no.6(2014) :66-71.
- [19] De Yoreo, James J., and Peter G. Vekilov. "Principles of crystal nucleation and growth." *Reviews in Mineralogy and Geochemistry* 54, no. 1 (2003): 57-93.

- [20] Patel, Ambalal Ranchhodhbhai, and A. Venkateswara Rao. "Crystal growth in gel media." *Bulletin of Materials Science* 4, no. 5 (1982): 527-548.
- [21] Patel, Ambalal Ranchhodhbhai, and A. Venkateswara Rao. "Growth of single crystals of KClO₄ in silica gels." *Journal of Crystal Growth* 38, no. 3 (1977): 288-292.
- [22] Oaki, Yuya, and Hiroaki Imai. "Experimental demonstration for the morphological evolution of crystals grown in gel media." *Crystal growth & Design* 3, no. 5 (2003): 711-716.
- [23] Shedam, M. R., and A. Venkateswara Rao. "Growth of single crystals of cadmium oxalate in silica gels." *Crystal Research and Technology* 28, no. 1 (1993): K5-K7.
- [24] Patil, N. S., S. K. Bachhav, and D. S. Bhavsar. "Growth and characterization of barium doped Cadmium Tartrate crystal by solution gel method." *Archives of Physics Research* 5, no. 1 (2014): 25-30.
- [25] Sawant, D. K., and D. S. Bhavsar. "Study of Gel Grown Mixed Calcium-Cadmium Tartrate crystals." *Der Chemica Sinica* 2, no. 4 (2011): 211-218.
- [26] Suri, Shivani, K. K. Bamzai, and Vishal Singh. "Growth and thermal kinetics of pure and cadmium doped barium phosphate single crystal." *Journal of Thermal Analysis and Calorimetry* 105, no. 1 (2011): 229-238.
- [27] Joshi, S. J., B. B. Parekh, K. D. Vohra, and M. J. Joshi. "Growth and characterization of gel grown pure and mixed iron-manganese levo-tartrate crystals." *Bulletin of Materials Science* 29, no. 3 (2006): 307-312.
- [28] Patil, N. S., Bachhav, S. K., Kale, M. S., & Bhavsar, D. S. "Structural and thermal studies of barium doped Cadmium Tartrate crystals grown by gel method" *Advances in Applied Science Research*, 5 no. 6(2014):139-143.
- [29] Arumugam, D., and A. Krishnan. "Optical and Thermal Studies on Strontium Doped Cadmium Tartrate Oxalate Single Crystals by Sol Gel Technique." *International Journal of ChemTech Research* 7, no.1(2014): 302-309.
- [30] S.S. Sonawane and R.R. Ahire" Single Crystal of Cadmium Tartrate grown by gel technique and its characterization" *International Journal of Science, Environment and Technology* 3, no .6(2014): 2250 – 2257.
- [31] G.Lillibai ,PhD Thesis, December 2012.

- [32] Hofer, Peter, and Erhard Kaschnitz. "Thermal diffusivity of the aluminium alloy Al-10Si-Mn-Mg (Silafont 36) in the solid and liquid states." *High Temperatures--High Pressures* no.40 (2011): 3-4.
- [33] Joseph, Santhi Ani, Misha Hari, S. Mathew, Gaurav Sharma, V. M. Hadiya, P. Radhakrishnan, and V. P. N. Nampoori. "Thermal diffusivity of Rhodamine 6G incorporated in silver nanofluid measured using mode-matched thermal lens technique." *Optics Communications* 283, no. 2 (2010): 313-317.
- [34] Pilla, Viviane, Egberto Munin, and Marcos RR Gesualdi. "Measurement of the thermo-optic coefficient in liquids by laser-induced conical diffraction and thermal lens techniques." *Journal of Optics A: Pure and Applied Optics* 11, no. 10 (2009): 105201.1-7.
- [35] Irimpan, Litty, A. Deepthy, Bindu Krishnan, V. P. N. Nampoori, and P. Radhakrishnan. "Nonlinear optical characteristics of self-assembled films of ZnO." *Applied Physics B* 90, no. 3-4 (2008): 547-556.
- [36] Wei, T. H., D. J. Hagan, M. J. Sence, E. W. Van Stryland, J. W. Perry, and D. R. Coulter. "Direct measurements of nonlinear absorption and refraction in solutions of phthalocyanines." *Applied Physics B* 54, no. 1 (1992): 46-51.

Chapter 8

General Conclusions and Future Suggestions.

Abstract

This chapter presents the conclusions of the entire work done in this thesis. A summary of future prospects are also mentioned here.

8.1. General Conclusions

Nonlinear crystals use the nonlinear effects to produce harmonic generation or other related processes. The crystals exhibiting optical nonlinearity have found applications in various fields. Some of the applications of nonlinear optical crystals include second harmonic generation, up conversions, down conversions, optical parametric oscillators, electro optic devices, optical switches etc. The optical nonlinearities exhibited by transparent crystalline materials are associated with a nonlinear polarization. Nonlinear metal compound crystals show a number of unique features including wide transparency region, broad phase-matching range, large nonlinear coefficient and high damage threshold. The present chapter concludes the results of various studies carried out on certain metallic halides and tartrate crystals .

a. Synthesis

Seventeen different crystals including nine lead halides and eight metal tartrates were prepared by employing the solution gel technique. The crystals of lead halides viz Lead Bromide(PbBr_2), Lead Chloride(PbCl_2) and Lead Fluoride(PbF_2) were synthesized. The tartrate family includes Calcium Tartrate(CaTT), Strontium Tartrate(SrTT) and Cadmium Tartrate(CdTT) . The medium of growth mechanism was hydro silica gel prepared from sodium meta silicate.

b. Structural Study by XRD

The crystalline nature and structure determination were done using X ray diffraction studies. The powder XRD pattern of the gel derived materials confirm the crystallinity. The structure of the crystals of PbBr_2 and PbF_2 is orthorhombic and that of PbCl_2 is orthorhombic bi pyramidal. The CaTT and SrTT crystals belong to the orthorhombic family while the CdTT crystal is monoclinic in structure.

c. Linear Optical Studies

Optical properties of the halide and tartrate crystals in solution phase were studied using linear absorption and fluorescence spectroscopic studies. The thermal diffusivity measurements were performed using dual beam mode-matched thermal lens experiment .

- The absorption edges of all the 17 crystals were lying in the ultra violet region. The absorption spectra reveal that greater the number of molecules capable of absorbing light of a given wavelength, the greater the extent of light absorption. The size of the absorbing system and the probability that the electronic transition will take place control the absorptivity. The linear absorption coefficients of the samples were measured at 532 nm.
- Optical band gap of the lead halide and metal tartrate crystals in solution phase were measured using the room temperature UV-VIS absorption spectra of respective samples. The direct band gap values of lead halides vary from 4.2 eV to 5.2 eV. Lead Bromide solution exhibits minimum band gap energy and pure lead fluoride sample shows maximum band gap in the halide family.
- The tartrate crystals of Calcium and Strontium are found to have large band gap compared to Cadmium. The direct band gap of CaTT crystals are high and the values range from 5.52 eV to 5.58 eV. The magnetic field applied CaTT exhibits the highest band gap .SrTT have band gap of the order of 5.4 eV. The CdTT crystals produced direct and indirect band gap due to the presence of a broad spectrum of phonons. The direct band gap of CdTT ranges from 3.90eV to 4.61 eV and indirect band gap values are from 3.5 eV to 4.25 eV.

- The photoluminescence studies were conducted using the emission spectra of the lead halides and metal tartrate samples at room temperature. The fluorescence emissions of the sample solutions at different excitation wavelengths were taken. The excitonic transitions in lead halide crystals are explained by the 6s-to-6p transition in lead ions. Luminescence is composed of broad Gaussian bands with large Stokes shifts and is indicative of strong exciton acoustic-phonon interaction. The exciton relaxation in lead halide crystals in solution phase results in spontaneous electron-hole separation. A repulsive correlation is ascribable to the origin of electron-hole separation. The emission spectra of lead halides show many peaks due to the Stokes shift by the crystal field interactions resulting from the strong interaction between phonon and Pb^{2+} ions.
- A large number of normal modes of vibration are possessed by Tartrate crystals. The fluorescence emission spectra of tartrate crystals of Calcium, Strontium and Cadmium showed a number of peaks. The emission peaks correspond to various combinations and overtones of the molecules in the excited electronic levels. The model used to explain the luminescence mechanism is well suited for CdTT crystals owing to the minimum difference in the observed and calculated bands.

The non radiative decay mechanism of the halide and tartrate crystals incorporated with Rhodamine-6G dye were investigated. The rhodamine -6G dye was added to the sample solutions for enhancing the absorption. The thermal diffusivity values were calculated using the fitting parameters. The non radiative relaxation of energy in these crystals were due to the formation of a refractive index gradient that created lens-like optical element. Out of the 17 crystals, the pure CdTT crystals exhibit high value of thermal diffusion and the magnetic field applied SrTT shows a minimum in the thermal diffusion value. The heat transfer mechanism of these crystalline materials in solution phase reveal that all

these samples expand on heating. The high thermal diffusivity value of CdTT pure sample facilitates the tuning of thermal diffusivity by applying a magnetic field during the fabrication of the pure crystal.

d. Nonlinear Optical Studies

The optical nonlinearity of these crystal samples were studied using open aperture Z-scan experiment. These studies were carried out by focusing the input beam onto the sample at 532 nm using a Q switched Nd: YAG laser.

- All the lead halide crystals show positive nonlinearity and possess very good nonlinear absorption. The positive nonlinearity is indicated by the transmission minimum at the focal point. The samples of PbCl_2 , PbBr_2 and PbF_2 exhibit reverse saturable absorption (RSA) giving a transmittance valley. The RSA in lead halides reveals that there is no depletion of ground state population. The decrease in nonlinear absorption in PbBr_2 and PbCl_2 at higher laser intensities suggests that there is a removal of an appreciable fraction of photo carriers from the ground state of these crystals. The nonlinear absorption coefficient is maximum for PbBr_2 solution and minimum for electric field applied PbCl_2 .
- The tartrate family shows positive and negative nonlinearity. The negative value of nonlinear absorption coefficient is due to the presence of saturable absorption (SA) in the respective crystals of Calcium, Strontium and Cadmium. The transmittance of these samples exhibiting SA shows a maximum at the focal point. The transmittance trace shows a peak response in the case of tartrate crystals having SA nature. The pure and electric field applied SrTT crystals in solution phase show RSA only while the magnetic field applied sample shows SA and RSA behaviour. The mechanism of nonlinear absorption in halides and tartrate crystals can be explained

on the basis of two photon absorption. It is to be noted that no previous reports are available in the literature with regard to nonlinear absorption measurements of metal tartrate crystals of our study.

- The crystals of lead halides were well suited for optical limiting applications since they exhibit RSA. The limiting threshold is minimum for the ultra violet irradiated PbCl_2 sample. Among the tartrate crystals, magnetic field applied SrTT has minimum limiting threshold. Thus the optical limiting studies suggest that the materials having low limiting threshold are good candidates for optical limiting applications.
- The crystals of CaTT, SrTT and CdTT have found applications in optical switching and limiting devices since they exhibit SA and RSA.

8.2 Future Suggestions

Some of the future prospects are suggested here based on the studies carried out on lead halides and metal tartrates crystals.

- Preparation of Nano crystals of lead halides and their nonlinear studies for Optoelectronic applications.
- Fabrication of lead halide based glasses and their optical characterizations as these glasses are found to have applications in the field of nonlinear optics.
- Fluorescence studies of metal tartrates using lasers. The fluorescence emission from metal tartrate crystals especially the tartrates of Calcium, Strontium and Cadmium can be extended to excitations using lasers.

General Conclusions and future suggestions

- Spectral characterizations of doped crystals for optical applications.
- Preparation of lead based quantum dots owing to their applications in various fields of photonics.
- Nonlinear refractive studies of lead chloride using closed aperture technique in order to find out the coefficients of nonlinear refraction and thereby the value of third order susceptibility.
- Fluorescence quantum yield measurements of Calcium and Strontium tartrates in different solvents for their applications in wavelength shifters.
- Preparation of thin films of lead halides and their nonlinear characterization for photonic applications.
- Preparation and characterization of mixed crystals of halides and comparison with their single crystals.
- Fabrication and studies on lead halide optical fibers. Since the lead halide based optical fibers have found applications in remote spectroscopy.

APPENDIX

Published Articles



Optical Studies on Sol-Gel Derived Lead Chloride Crystals

I.Rejeena, International School of Photonics, Cochin University of Science and Technology, Cochin Kerala, India and M.S.M.College, Kayamkulam, Kerala, India

B.Lillibai, International School of Photonics, Cochin University of Science and Technology, Cochin Kerala, India,

B.Nithyaja, International School of Photonics, Cochin University of Science and Technology, Cochin Kerala, India

V.P.N.Nampoori, International School of Photonics, Cochin University of Science and Technology, Cochin Kerala, India

P.Radhakrishnan, International School of Photonics, Cochin University of Science and Technology, Cochin Kerala, India

ABSTRACT

Optical characterization of lead chloride crystals prepared by sol-gel method is reported. The relevant sol-gel technique is used for the preparation of PbCl₂ samples with five different types. In this paper, we report the absorption and fluorescence behaviour of pure, UV & IR irradiated and electric & magnetic field applied lead chloride crystal samples in solution phase at two different concentrations. Optical bandgap and emission studies of these crystals are also done.

KEYWORDS: Lead chloride, absorption, fluorescence, gel method, spectroscopy

Introduction

Fluorescence spectroscopy is of overwhelming importance in the field of photo physics. Lead chloride is a well known photosensitive material possessing ionic crystalline nature belonging to orthorhombic system [1]. PbCl₂ is the model material from heavy element halogenide group since it satisfies high birefringence, low attenuation coefficient and wide transparency range [2]. Many of the researchers reported the luminescence property of PbCl₂ [3]. Under excitation in the fundamental absorption region, PbCl₂ crystals exhibit two types of intrinsic luminescence [4]. W.C.DE Gruijter had done emission studies on PbCl₂ [5]. The top of the valence band is composed of Pb²⁺-6s with considerable admixing of chlorine-p, while the bottom of the conduction band is made up of Pb²⁺-6p [6]. PbCl₂ is classified as a normal class I crystal and its transmission range is wide [7-8]. PbCl₂ finds importance in experimental field due to their large band gap and exhibiting interesting features from the stand point of electron-lattice interaction [9-18]. Lead halide based materials can be used as laser hosts with low phonon energies. The Pb²⁺ in the PbCl₂ crystal is known to be emissive in aqueous solution [19-22]. In the present study, we report for the first time the absorption and fluorescence emission properties of PbCl₂ crystal samples prepared by sol-gel technique through five different methods. PbCl₂ is marked as an insulator with a moderate bandgap. They belong to the space symmetry group D_{2h}¹⁶

with layers perpendicular to the [010] direction. The lead chloride crystal is characterized by an excitonic fundamental edge, which are formed by electronic states of lead ion. Our experiments on the growth of lead chloride confirm the utility of this method for growing large needles and single crystals. In the visible region the length of the needle is small compared to the growth of lead chloride crystals under the influence of ultraviolet and infrared radiations.

Experimental Technique

In our spectroscopic studies the PbCl₂ crystal samples used were prepared by using a stock solution of sodium meta silicate (SMS). A quantity of 25 ml. of SMS solution of specific gravity 1.03, whose pH was adjusted to be 6.5, 7.0, 7.5, 8.0 and 8.5 by titration with 1M tartaric acid, and was allowed to gel in five various boiling test tubes without any disturbances. Growth experiments were conducted for different densities of the gel ranging from 1.02 to 1.06. It was found that for the same concentration of HCl, tartaric acid and lead nitrate solution, the rate of growth of the needles is conspicuously larger and the needles are larger for lesser densities of the gel. This is due to the increased rate of diffusion of HCl in the gel and increased mobility of the molecules of the crystals at lower densities of the gel. PbCl₂ crystals were obtained by the reactions of lead nitrate, tartaric acid and HCl (99.9% Sigma-Aldrich). Two

different $PbCl_2$ crystal samples were obtained by irradiating pure $PbCl_2$ crystals with ultra violet (UV lamp (insect Killer)) and Infrared radiations (HL4311 (PHILIPS) 230V~50Hz~150w). The other two samples were prepared by subjecting the crystal to an electric field of 20 V using parallel plate arrangement and subjecting the crystal to a magnetic field using two bar magnets kept on either side of the experimental test tube perpendicular to the length of the test-tube. Thus five $PbCl_2$ samples were obtained for our studies viz pure, UV and IR irradiated, samples subjected to electric and magnetic fields. The sol-gel derived $PbCl_2$ samples were subjected to X-ray diffraction studies (XPRT-PRO using K-Alpha 1.54060 Å⁰ (XRDL)). The crystal structure of $PbCl_2$ is confirmed to be orthorhombic dipyramidal with each Pb having a coordination under 9. Observations under petrological microscope reveal that $PbCl_2$ crystals grown under all the five conditions show inclined extinction. The prepared crystal samples were powdered using mortar and pestle, weighed about 0.15g and dissolved in 15 ml of single distilled water (SDW) to obtain a concentration $c_1=0.01$ gm/ml. Another concentration $c_2=0.02$ gm/ml was obtained by dissolving 0.32gm in 20 ml of SDW. For the dissolution, a magnetic stirrer was used and the solvent evaporation was prevented by using a sealed glass container. Linear absorption of the crystal samples in solution phase was recorded using Jasco V-570 UV/VIS/IR Spectrophotometer. Optical band gap of these samples were obtained from linear absorption measurements. The emission and excitation studies were carried out by taking the room temperature fluorescence spectra of these $PbCl_2$ samples using a Cary Eclipse fluorescence spectrophotometer (Varian).

Result And Discussion

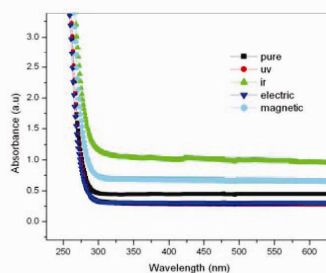
Observations under petrological microscope reveal that $PbCl_2$ crystals grown under all the four conditions show inclined extinction. The dendrites grown under the four conditions show variations from one another. Those grown under infrared radiation are radiating type while those in visible light are fibrolitic. Large massive dendritic growth was observed under ultra violet radiation. The tendency for radiating along the axis of the crystal was found when grown in all the conditions. A study of external morphology shows that the crystals grown in the presence of radiation are needle shaped good quality acicular aggregates with shining edges. Each individual in the aggregate is highly brittle, tubular needles. The habit of lead chloride crystals that is least affected morphologically by external factors can be

described as elongated along the c axis with (100), (010) as main forms and (110), (120) and (210) as smaller faces, while at the top (011) is the dominant form. From the external observations of four sets of lead chloride dihydrate crystals, it is clear that there is no change in the external morphology by naked eye.

1. Absorption Studies

Optical absorption spectra of $PbCl_2$ samples at two different concentrations c_1 and c_2 are shown in the figure 1.

(a)



(b)

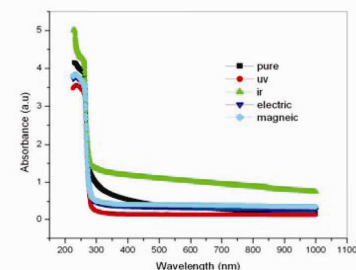


Figure 1. Room temperature absorption spectra of $PbCl_2$ at concentrations (a) c_1 and (b) c_2 . The absorption peak of $PbCl_2$ at the two concentrations c_1 and c_2 are located in the uv region at 266 nm corresponds to 4.6 eV. The peak at this particular wavelength is due to the electronic transition from the valence band to the $PbCl_2^+$ cation [23-24]. There is no valuable change in absorption peak for varying concentration. The above linear absorption spectra can be used for optical band gap studies on $PbCl_2$ in solution phase in single distilled water. The linear absorption coefficient α can be determined from absorption spectra, which is related to the band gap E_g as $(\alpha h\nu)^2 = k (h\nu - E_g)$, where $h\nu$ is the incident light energy, k is a constant



and E_g is the optical band gap of lead chloride. A graph of $E_g = hv$ versus $(ahv)^{-2}$ gives the direct band gap of $PbCl_2$ for five different samples at two concentrations c1 and c2. The optical band gap of $PbCl_2$ for concentration c1 is varying from 4.54 eV (pure) to 4.67 eV (magnetic). For uv irradiated and electric field applied $PbCl_2$ samples, E_g is 4.54 eV and 4.55 eV respectively. When concentration is at c2, E_g varies between 4.6 and 4.46 eV. The values of direct band gap at c1 and c2 are listed in the table1. Several types of chloride ion vacancies can exist in the lead chloride lattice which are electron traps in the energy range 4.2-4.4 eV above the valence band [24].

chloride ions are surrounded by five lead ions [25]. It was suggested that the 4.6 eV absorption to be an exciton absorption, but on the other hand it might also be ascribed to a characteristic $6s^2-6s6p$ transition inside the lead ion.

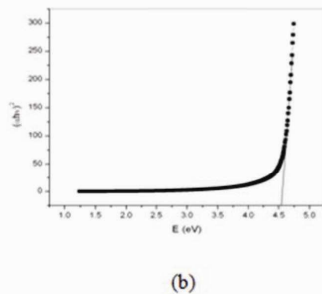
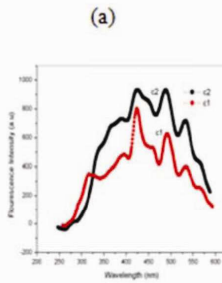
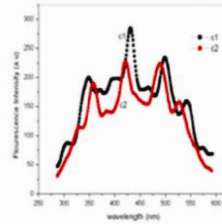
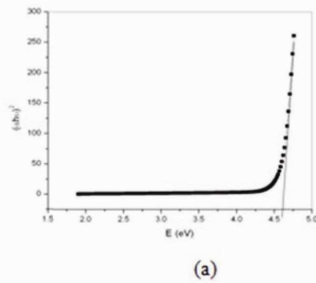
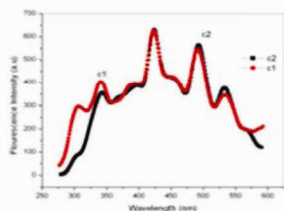
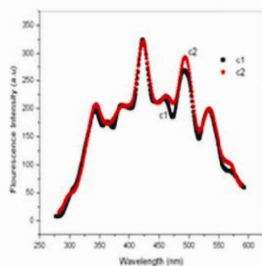


Figure 2. Optical band gap plot of Pure $PbCl_2$ sample at concentrations (a) c1 and (b) c2

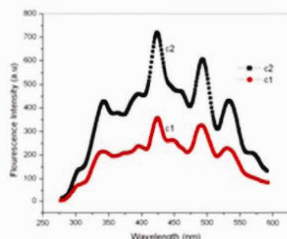
Figure 2 shows the direct band gap behaviour of $PbCl_2$ samples at two different concentrations c1 and c2. The chloride ions at the largest distance are surrounded by four lead ions where as the closest



(c)



(d)



(e)

2. Fluorescence Studies

Fluorescence spectra of $PbCl_2$ are taken at two different concentrations c_1 and c_2 for photoluminescence studies. Figure 3 represents the fluorescence emission spectra of five $PbCl_2$ samples in SDW. $PbCl_2$ sample solutions at concentrations c_1 and c_2 are excited at a wavelength of 270 nm gives three strong emissions at around 421 nm, 491 nm and 533 nm respectively.

Figure 3. Fluorescence emission spectra of $PbCl_2$ at a wavelength 270 nm for (a) pure (b) UV (c) IR (d) electricfield and (e) magneticfield applied samples.

Table 1. Measured values of optical band gap and emission peaks for $PbCl_2$ at concentrations c_1 and c_2 (gm/ml)

PbCl ₂ sample	Optical direct band gap at concentrations		Emission peak at	
	C1 (eV)	C2 (eV)	C1 (nm)	C2 (nm)
pure	4.54	4.61	348	357
			431	422
			498	490
			540	525
UV	4.53	4.54	-	-
			422	423
			491	487
			534	532
IR	4.62	4.40	339	342
			423	423
			492	492
			533	533
Electric	4.57	4.55	342	342
			421	421
			493	492
			533	533
Magnetic	4.67	4.46	338	342
			424	423
			490	493
			531	533

The excitonic transitions in lead chloride are partly explained by the 6s-6p transition in lead ions which gives the emission bands at three of the above transitions. Fluorescence in $PbCl_2$ is composed of broad gaussian band with large stokes shift and it is indicative of strong exciton-acoustic phonon interaction [26]. The electric dipole transition from the 6p to 6s states also produces luminescence in $PbCl_2$. The excitons can relax into pairs of a self trapped electron (STEL) and a self trapped hole (STH) when both electrons and holes strongly interact with acoustic phonons. A repulsive correlation is ascribable to the origin of electron-hole separation. The repulsive correlation through acoustic phonons with the formation of cooper pairs mediated by these acoustic phonons cause the spontaneous breaking of excitons [27].

As concentration is increased, phonon vibration will induce more non radiative de excitations. Our $PbCl_2$ solutions show many peaks due to the stokes shift by the crystal field interactions resulting from

the strong interaction between phonon and Pb^{2+} ions. From the fluorescence spectra given in the figure, it is evident that the emission peaks at 491 and 533 nm are assigned to the excitonic emissions. For pure $PbCl_2$ sample, the emission peak at 431 nm at concentration c2 is red shifted. The IR irradiated and electric field applied samples have almost same emission peak at 423, 492 and 533 nm for the two concentrations c1 and c2. The shifting of emission peaks at pure $PbCl_2$ sample is due to the band edge emission which are attributed to the quasi free recombination at the absorption band edge. Thus the spontaneous exciton dissociation has been revealed by the fluorescence emission in sol-gel derived $PbCl_2$ samples in solution phase.

Conclusions

High quality lead chloride crystals were prepared by sol-gel technique. The obtained $PbCl_2$ crystal samples of five different types in solution phase were subjected to spectrophotometric studies. The linear absorption spectra give the optical band gap details of these crystals. Photo luminescence studies on these lead chloride samples were done by fluorescence spectroscopy. The fluorescence emission of these crystals shows that $PbCl_2$ crystals have the band gap in connection with the 6s to 6p gap in lead ions and tend to become highly luminescent coming from the odd transition. Thus the high luminescence nature of lead chloride makes them suitable for applications in photography, acoustical-optical devices and radiation detectors.

Acknowledgements

The authors acknowledge KSCSTE and Moulana Azad National Fellowship schemes for financial support.

References

[1] H.Nakagawa, Y.Do, T.Nakamura, "Absorption and luminescence in $PbCl_2$: Tl^+ crystals". *J. Lumin.* 87-89 (2000) 1130-1132
[2] P.Nishanthakumari, S.Kalainathan, *Cryst. Res.Technol.* 43 (2008) 4
[3] M.Kituara, H.Nakagawa, *J. Lumin.* 72-74 (1997) 883

[4] M.Kituara, H.Nakagawa, *J. Electron Spectrosc. Relat. Phenom.* 79 (1996) 171
[5] W.C.DE.Grujter, *J. Solid State Chem.* 6 (1973) 151
[6] M. Fujita et al, *J. Phys. Soc.Japan* 60 (1991) 4393
[7] F.E.A.Melo, K.W.Garret, J. Mendes Filho, J.E.Moreira, *Solid State Commn.*, 29-33 (1979) 31
[8] O.Keefe.M, *Comm. Sol.State Phys.* 7 (1977) 163
[9] Plekhanov.V *Phys.StatusSolidi B* 57 (1973) K55
[10] Nistor.S.V, Goovaerts.E and Schoemaker.D 1993 *Phys.Rev.B* 48 9575
[11] Kitaura M, Nakagawa.H 1996 *J.Electron Spectrosc.Relat.Phenom.* 79 171
[12] Kitaura.M and Nakagawa.H 1997 *J.Lumin.* 72-74 883
[13] Itoh.M, Nakagawa.H, Kitaura. M, Fujita.M and Alov.D.L 1999 *J.Phys.:Condens.Matter* 11 3003
[14] Kink.R, Avarmaa.T, Kisand.V. Lohmus.A, Kink.I and Martinson.I 1998 *J.Phys.:Condens.Matter* 10 693
[15] Kanbe.J, Takezoe.H.and Onaka.R 1976 *J.Phys.Soc.Jpn.* 41 942
[16] Eijkelenkamp A.J.H.and V A.J os.K J.. 1976 *Phys.Status Solidi B* 76 769
[17] Beaumont.J.H.,Bourdillon .A.J and Bordas.J 1977 *J.Phys.C* 10 761
[18] Fujita.M, Nakagawa.H, Fukui.K, Matsumoto.H, Miyanaga.T and Watanabe.M 1991 *J.Phys.Soc.Jpn.* 60 4393
[19] Hans Niikol, Alexander Becht, Arnd Vogler, *Inorg. Chem.* 3277-3279 (1992) 31
[20] P. Pringshem, H.Vogels, *Physica* 225 (1940) 7
[21] C.W.Sill, H.E. Peterson, *Anal. Chem.* 1266 (1949) 21
[22] R. Narayanaswamy, P.J. Mayne, G.F. Kirkbright, *J. Inorg. Nucl. Chem.* 129 (1978) 40
[23] K.I Best, *Z. Physik*, 163 (1961) 309
[24] K.J.Devries, Doctoral Dissertation, University of Utrecht (1965)
[25] K.J.Devries, J.H.Vansanten, *Physica* 2051-2058 (1964) 30
[26] G.Liidja, V.I.Plekhanov, *J. Lumin.* 6 (1973) 71
[27] Masanobu Iwanga, Tetsusuke Hayashi, *J. Lumin.* 102-103 (2003) 663-668



Effect of nonlinear absorption on electric field applied lead chloride by Z-scan technique

I. Rejeena, Lillibai, M. H. Rahimkutti, V. P. N. Nampoori, and P. Radhakrishnan

Citation: AIP Conference Proceedings **1620**, 422 (2014); doi: 10.1063/1.4898275

View online: <http://dx.doi.org/10.1063/1.4898275>

View Table of Contents: <http://scitation.aip.org/content/aip/proceeding/aipcp/1620?ver=pdfcov>

Published by the AIP Publishing

Articles you may be interested in

Nonlinear scattering studies of carbon black suspensions using photoacoustic Z-scan technique
Appl. Phys. Lett. **103**, 151104 (2013); 10.1063/1.4824448

Study of nonlinear refraction of organic dye by Z-scan technique using He–Ne laser
AIP Conf. Proc. **1512**, 470 (2013); 10.1063/1.4791115

Z-scan study of nonlinear absorption in reduced LiNbO₃ crystals
J. Appl. Phys. **111**, 103504 (2012); 10.1063/1.4716470

Nonlinear optical properties of lanthanum-modified lead zirconate titanate investigated by the femtosecond Z-scan technique
Appl. Phys. Lett. **99**, 241101 (2011); 10.1063/1.3668099

Optical Nonlinearity in Lead Iodide Di Hydrate grown with UV and IR radiations using Zscan Technique
AIP Conf. Proc. **1391**, 691 (2011); 10.1063/1.3643651

Effect of Nonlinear absorption on Electric field applied Lead chloride by Z-scan Technique

I.Rejeena^{1,2},Lillibai¹,M.H.Rahimkutty²,V.P.N.Nampoori¹,P.Radhakrishnan¹

¹International School of Photonics, Cochin University of Science and Technology, Cochin Kerala, India,

²M.S.M.College, Kayamkulam, Kerala, India

¹Corresponding author: rejeenanauful@gmail.com

Abstract. The preparation, spectral response and optical nonlinearity of gel grown lead chloride single crystals subjected to electric field of 20V using parallel plate arrangements have been investigated. Optical band gap of the samples were determined using linear absorption spectra. Open aperture z-scan was employed for the determination of nonlinear absorption coefficient of PbCl₂ solution. The normalized transmittance curve exhibits a valley shows reverse saturable absorption. The non linear absorption at different input fluences were recorded using a single Gaussian laser beam in tight focus geometry. The RSA nature of the sample makes it suitable for optical limiting applications

I. INTRODUCTION

PbCl₂ has drawn attention of many workers because they exhibit interesting features from the stand point of the electron-lattice interaction. These materials are important for their luminescent properties. Two types of luminescence are observed in PbCl₂, the excitonic luminescence and the recombinational luminescence. The acousto optic figure of merit of PbCl₂ crystals is high and their transmission range is wide. The band gap of PbCl₂ is also large. A large set of 15 optical functions contains the most complete information on the optical properties and electronic structure of PbCl₂. V.V.Sobolev et al reported the electronic structure and anisotropic optical properties of PbCl₂ crystals. PbCl₂ is an ionic crystal with orthorhombic structure with four molecules in the unit cell. A.Kaldor and G.A.Somrjai reported the photodecomposition in PbCl₂. Lead halide based materials have recently emerged as laser hosts with low phonon energies. In this paper we report for the first time, to the best of our knowledge, the linear and non linear optical behavior of PbCl₂ samples in solution phase and their optical limiting properties using open aperture z-scan technique.

II. EXPERIMENTAL

PbCl₂ crystals were prepared by sol-gel technique using sodium meta silicate as stock solution. Lead nitrate, tartaric acid and HCl (99.9% Sigma –Aldrich) were used for the preparation process. Experiments were setup for various concentrations of HCl. It was found that for the same density of the gel and at the same concentration of tartaric acid and lead nitrate solution, the rate of growth of the needles is higher and the needles are longer for higher concentration of HCl. The samples were prepared by subjecting the crystal to an electric field of 20 V using parallel plate arrangements. Linear absorption of the samples was recorded using Jasco V-570 UV/VIS/IR Spectrophotometer. Optical band gap of these samples were obtained from linear absorption measurements. High sensitive single beam z-scan experiment based on spatial beam distortion was used for optical non linear studies. A Q-switched Nd:YAG laser (Spectra physics Lab-1760, 532 nm, 7ns, 10 Hz) was used as the source. The radius of the beam waist w_0 was calculated as 42.6 μ m and Rayleigh length $z_0 = \pi w_0^2 / \lambda$ is estimated to be 10.7 mm which is much greater than the thickness of the sample cell (1 mm). Thus Rayleigh length satisfies the basic criteria of taking z-scan. By using an energy ratiometer (Rj 7620 Laser Probe Corp) having two identical pyro electric detector heads (Rj 735), the transmitted beam energy, reference beam energy and their ratios were simultaneously measured

Light and Its Interactions with Matter

AIP Conf. Proc. 1620, 422-425 (2014); doi: 10.1063/1.4898275
© 2014 AIP Publishing LLC 978-0-7354-1257-6/\$30.00

III. RESULT AND DISCUSSION

The linear stability of steady-state needle crystals in dendritic growth was studied in the presence of anisotropies in both surface tension and interfacial kinetics. The needle crystals were linearly unstable for certain ranges of values of the surface tension and kinetic coefficients. This instability results in complex tip-splitting and side-branching events that lead to morphological transitions. Needle crystals have been observed to be faceted at low velocities of growth. This can be explained by the theory of diffusion-limited growth with the addition of a supplementary condition fixing the shape of the facet depending on the average temperature on it.

Linear absorption spectrum of electric field applied lead chloride sample is as shown in figure.1(A). The absorption edge of PbCl₂ is located at uv region. The direct band gap of the samples was estimated from the graph of $h\nu$ versus $(\alpha h\nu)^2$ where α is linear absorption coefficient and that is related to the band gap E_g as $(\alpha h\nu)^2 = k(h\nu - E_g)$, where $h\nu$ is the incident light energy, k is a constant and E_g is the optical band gap of lead chloride. Figure 1(B) represents the band gap plot of PbCl₂.

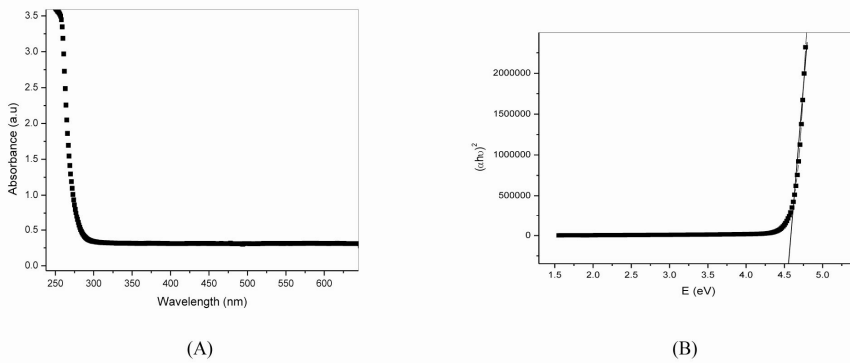


FIGURE1. (A) Linear absorption spectrum and (B) Direct band gap plot of electric field applied PbCl₂.

Figure.2 shows the open aperture z-scan plot of electric field applied PbCl₂. The solid curves are theoretical fit to the open aperture z-scan experimental data. The nonlinear absorption coefficient β can be obtained from this open aperture z-scan data by fitting the normalized transmittance data to the open aperture formula given as

$$T(Z, S = 1) = \sum_{m=0}^{\infty} \sum_{m=0}^{\infty} \frac{[-q_0(z)]^m}{[m+1]^{3/2}} |q_0(z)| < 1 \quad \dots\dots\dots(1)$$

Where:
$$q_0(z) = \frac{[I_0 \beta L_{eff}]}{1 + (Z^2 / Z_0^2)} \quad \dots\dots\dots(2)$$

$Z_0 = k w_0^2 / 2$ is the diffraction length of the beam

$k = 2\pi/\lambda$ is the wave factor, w_0 = the beam waist radius at the focal point, $L_{eff} = (1 - \exp(-\alpha L)) / \alpha$ is the effective thickness of the sample, I_0 is the laser intensity at the focal plane.

For our samples, there is no depletion of ground state population because the transmission curves exhibit RSA. Using a single Gaussian laser beam, we measured the transmittance of the samples at two different input fluences (100 and 125 MW/cm²) as shown in fig.2

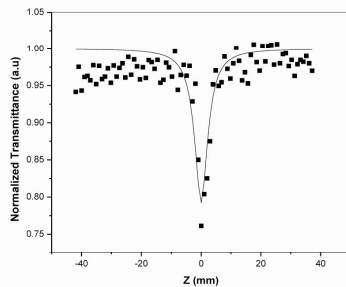


FIGURE 2. Open aperture z-scan plot of PbCl₂ at laser power 100 MW/cm²

The wavelength used in our experiment is 532 m, which corresponds to two photon absorption (TPA). The photon energy is within the range $2h\nu > E_g > h\nu$, where $h\nu = 2.33\text{eV}$ and E_g is the optical band gap of PbCl₂ varying from 4.4 eV to 4.6 eV.. Lead chloride solutions suppress the peak and enhances valley to show RSA in the transmittance curve. Nonlinear absorption coefficient β for two input fluence values are given in table.1

TABLE.1. Measured values of nonlinear absorption coefficient and optical limiting threshold for electric field applied and pure PbCl₂ samples.

Input laser power density (I_0) (MW/cm ²)	Non linear absorption coefficient, β (cm/GW)	Optical limiting threshold (MW/cm ²)
100	36(electric), 122(pure)	76 68
125	27(electric), 65(pure)	85 83

From these values of β , it is clear that as the input laser intensity I_0 increases, the nonlinear behavior of lead chloride decreases, which is due to removal of an appreciable fraction of photo carriers from the ground state.

Figure.3 shows the optical limiting response of PbCl₂. The limiting threshold is an important factor which decides the efficiency of optical limiter.

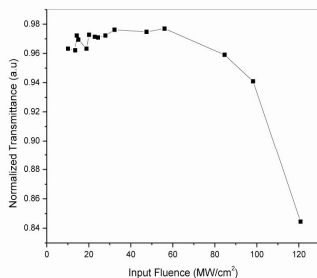


FIGURE.3 optical limiting response of PbCl₂

IV. CONCLUSION

Highly luminescent Lead Chloride crystals were prepared and characterized. Spectrophotometric studies were carried out to evaluate the band gap. Optical nonlinearity in PbCl₂ samples were investigated using z-scan technique. Observed nonlinearity is third order and two photon absorption coefficients were tabulated. The non linear curves exhibit valleys to show reverse saturable absorption indicating positive non linear absorption. RSA nature of the samples makes them suitable for optical limiting applications and the optical limiting threshold of these samples were evaluated. The non linear studies on these crystal solutions gave a clear picture that these materials are highly non linear due to their high values of non linear absorption coefficients. Thus these PbCl₂ crystals prepared by sol-gel technique are well suited for applications in optoelectronic and non linear optical devices.

ACKNOWLEDGMENTS

I.Rejeena thanks UGC for financial support through Moulana Azad National Fellowship. KSCSTE is also acknowledged for financial assistance.

REFERENCES

1. M.S Bahae., A.A Said., and E.W Van Stryland. Opt. Lett. 14, 955(1989).
2. L.Irimpan., B.Krishnan., A.Deepthy., V.P.N.Nampoori. and P.Radhakrishnan. J.Appl. Phys. 103 033105 (2008).
3. L.Irimpan., V.P.N.Nampoori. and P.Radhakrishnan. J. Appl. Phys. 103, 094914 (2008).
4. Litty Irimpan, V.P.N.Nampoori. and .P.Radhakrishnan ,Chem. Phys. Lett. 455 ,265-269(2008).
5. R.Tintu., V.P.N.Nampoori., P.Radhakrishnan. and Sheenu Thomas J. Appl. Phys. 108, 073525 (2010).
6. R.Tintu., V.P.N.Nampoori, P.Radhakrishnan. and Sheenu Thomas, J.Phys.D.Appl.Phys. 44, 025101(2011).
7. F.M.Quereshi., S.J.Martin., X.Long., D.O.C.Bradley., Chem. Phys. 23,7 87 (1998).

Non-Linear Optical Studies on Sol-Gel Derived Lead Chloride Crystals Using Z-Scan Technique

I Rejeena¹, International School of Photonics, Cochin University of Science and Technology, Cochin, Kerala, India
Roseleena Toms, International School of Photonics, Cochin University of Science and Technology, Cochin, Kerala, India
VPN Nampoory, International School of Photonics, Cochin University of Science and Technology, Cochin, Kerala, India
P Radhakrishnan, International School of Photonics, Cochin University of Science and Technology, Cochin, Kerala, India
B Lillibai, S.N.College, Varkala, Thiruvananthapuram, Kerala, India

Abstract

In this paper we report the preparation, optical characterization and non linear optical behavior of pure lead chloride crystals. Lead chloride samples subjected to UV and IR irradiation and electric and magnetic fields have also been investigated. Optical nonlinearity in these lead chloride samples were determined using single beam and high sensitive Z-scan technique. Non linear optical studies of these materials in single distilled water show reverse saturable absorption which makes them suitable for optical limiting applications.

Keywords: Sol gel method; UV irradiation; linear absorption; optical band gap; nonlinear absorption; optical limiting.

Introduction

Lead Chloride is known as a model material for the group of heavy element halogenides since it possesses high birefringence, low attenuation coefficient, wide transparency range and good mechanical properties [1]. PbCl₂ has drawn attention of many workers because they exhibit interesting features from the stand point of the electron-lattice interaction [2-15]. These materials are important for their luminescent properties. Two types of luminescence are observed in PbCl₂, the excitonic luminescence and the recombinational luminescence [7]. The acoustic figure of merit of PbCl₂ crystals is high and their transmission range is wide. The band gap of PbCl₂ is also large.[16]. A large set of 15 optical functions contains the most complete information on the optical properties and electronic structure of PbCl₂ [17-18]. V.V.Sobolev et al reported the electronic structure and anisotropic optical properties of PbCl₂ crystals. PbCl₂ is an ionic crystal with orthorhombic structure with four molecules in the unit cell [19]. A.Kaldor and G.A.Somrjai reported the photodecomposition in PbCl₂ [20]. Photonic materials with optical limiting properties find applications in devices for protecting eyes and sensors from intense optical radiations. A nonlinear optical crystal like PbCl₂ can be employed for applications depending on their band gap and nonlinearities. PbCl₂ exists in nature in crystalline form as large needles. Deviated from the normal way of crystal growth in gels in which two nutrient solutions were allowed to interact in the gel medium, in the method reported here, a two stage reaction is made use of. In the first stage one of the reactants is incorporated in the gel as a colloidal precipitate and the other nutrient is allowed to diffuse into the gel and to produce the crystal in the second stage. Experiments on the growth of Lead chloride confirm the utility of this method for growing large needle-like and single crystals. In the visible region, the length of the needle like crystals is small compared to the growth of lead chloride

crystals under the influence of ultraviolet and infrared radiations. Lead halide based materials have recently emerged as laser hosts with low phonon energies. In this paper we report for the first time, to the best of our knowledge, the linear and nonlinear optical behavior of PbCl₂ samples in solution phase and their optical limiting properties using open aperture z-scan technique.

Experimental Technique

PbCl₂ crystals were prepared by sol-gel technique using sodium meta silicate as stock solution. Lead nitrate, tartaric acid and HCl (99.9% Sigma –Aldrich) were used for the preparation. Samples were prepared for various concentrations of HCl. It was found that for the same density of the gel and at the same concentration of tartaric acid and lead nitrate solution, the rate of growth of the needle-like crystals is higher and is longer for higher concentration of HCl. However, for high concentration of HCl the needle-like crystals are thin and are in large number. The effect is a result of the increase in nucleation due to the high rate of reaction. A compromise between the density of the gel and the concentration of the acid it is possible to establish, in the gel, a conducive environment for the needles and single crystals of lead chloride to be grown in silica gel of specific gravity 1.03 using 2NHCl. Two different PbCl₂ crystal samples were obtained by irradiating pure PbCl₂ crystals with ultraviolet (UV lamp (insect Killer)) and Infrared radiations (HL4311 (PHILIPS) 230V~50Hz~150w). The other two samples were prepared by subjecting the crystal to an electric field of 20 V using parallel plate arrangement and subjecting the crystal to a magnetic field using two bar magnets kept on either side of the experimental test tube perpendicular to the length of the test-tube. Thus five PbCl₂ samples were obtained for our studies viz pure, UV and IR irradiated, samples subjected to electric

and magnetic fields. The sol-gel derived PbCl₂ samples were subjected to X-ray diffraction studies (XPRT-PRO using K-Alpha 1.54060 Å⁰ (XRDM)). The crystal structure of PbCl₂ is confirmed to be orthorhombic dipyramidal with each Pb having coordination under 9. Observations under petrological microscope reveal that PbCl₂ crystals grown under all the five conditions show inclined extinction. A study of external morphology shows the crystals grown in the presence of radiations are needle shaped good quality acicular aggregates with shining edges.

PbCl₂ crystal samples in solution phase were used for linear and nonlinear optical studies. For these studies the crystals were grinded by mortar and pestle and the powder form was dissolved in 20 ml of single distilled water to prepare a solution of 2.8x10⁻³M concentration. A magnetic stirrer was used for the dissolution process and the solvent evaporation was prevented by using a sealed glass container. Linear absorption of the samples was recorded using Jasco V-570 UV/VIS/IR Spectrophotometer. Optical band gap of these samples were obtained from linear absorption measurements. High sensitive single beam z-scan experiment based on spatial beam distortion was used for optical nonlinear studies [21]. A Q-switched Nd:YAG laser (Spectra physics Lab-1760, 532 nm, 7ns, 10 Hz) was used as the source. The PbCl₂ sample solutions were taken in a 1 mm thick cell and moved along the z-axis through the focal point of a lens of focal length 20 cm. The experimental set up was explained in detail in refer [22-23]. The radius of the beam waist w₀ was calculated as 42.6µm and Rayleigh length z₀=πw₀²/λ is estimated to be 10.7 mm which is much greater than the thickness of the sample cell (1 mm). Thus Raleigh length satisfies the basic criteria of taking z-scan. By using an energy ratiometer (Rj 7620 Laser Probe Corp) having two identical pyro electric detector heads (Rjp 735), the transmitted beam energy, reference beam energy and their ratios were simultaneously measured. We used CS₂ as the standard for the initial calibration of z-scan set up.

Result and Discussion

The linear stability of steady-state needle shaped crystals in dendritic growth was studied in the presence of anisotropies in both surface tension and interfacial kinetics. The needle shaped crystals were linearly unstable for certain range of values of the surface tension and kinetic coefficients. This instability results in complex tip-splitting and side-branching events that lead to morphological transitions. Needle crystals have been observed to be faceted at low velocities of growth. This can be explained by the theory of diffusion-limited growth with the addition of a supplementary condition fixing the shape of the facet depending on the average temperature on it. Linear absorption spectrum of lead chloride

samples is as shown in figure1. The absorption edge of PbCl₂ is located in the uv region. The band gap of the samples was estimated from the graph of hv verses (αhv)² where α is linear absorption coefficient which is related to the band gap E_g as (αhv)²=k (hv - E_g), where hv is the incident light energy, k is a constant and E_g is the optical band gap of lead chloride. Figure 2 represents the band gap plot of PbCl₂.

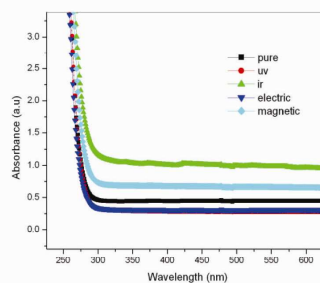


Figure 1. Linear absorption spectra of PbCl₂.

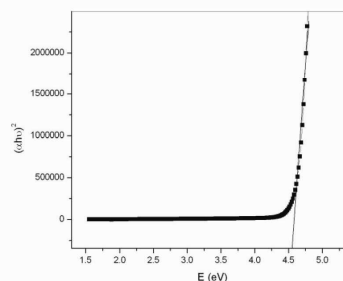


Figure 2 Direct band gap plot of PbCl₂

Figure 3 shows the open aperture z-scan plot of PbCl₂ samples. The solid curves are theoretical fit to the open aperture z-scan experimental data. The nonlinear absorption coefficient β can be obtained from this open aperture z-scan data by fitting the normalized transmittance data to the open aperture formula given as [21]

$$T(Z, S = 1) = \sum_{m=0}^{\infty} \sum_{m=0}^{\infty} \frac{[-q_o(z)]^m}{[m+1]^{3/2}} |q_o(z)| < 1$$

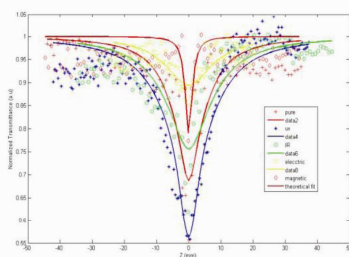
$$q_0(z) = \frac{[I_0 \beta L_{eff}]}{1 + (Z^2 / Z_0^2)}$$

where:

$Z_0 = k w_0^2 / 2$ is the diffraction length of the beam

$k = 2\pi/\lambda$ is the wave vector, $w_0 =$ the beam waist radius at the focal point, $L_{eff} = (1 - \exp(-\alpha L)) / \alpha$ is the effective thickness of the sample, I_0 is the laser intensity at the focal plane.

(a)



(b)

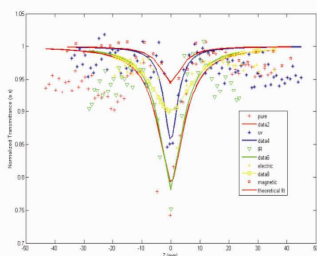


Figure 3. Open aperture z-scan plot of PbCl₂ at different laser powers, (a).100 MW/cm² and (b). 125 MW/cm²

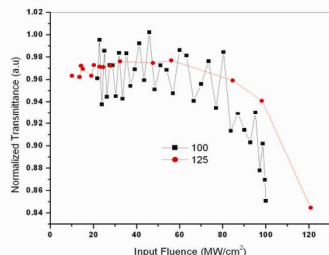
Table 1. Measured values of nonlinear absorption coefficient and optical limiting threshold for PbCl₂ samples

Sample	E _g (eV)	l ₀ ¹⁾	β (cmGW ⁻¹)		Optical limiting threshold (MWcm ⁻²)
			I ₀ (100 MWcm ⁻²)	I ₀ (125 MWcm ⁻²)	
PbCl ₂ pure	4.6	122	65	68	83
PbCl ₂ UV	4.5	135	42	43	85
PbCl ₂ IR	4.4	98	70	72	84
PbCl ₂ electric	4.6	36	27	76	85
PbCl ₂ magnetic	4.5	83	14	82	95

Open aperture z-scan studies were carried out by focusing the input beam on to the sample at 532 nm using a Q switched Nd: YAG laser. In order to estimate the limits to which the molecules would be showing RSA behavior, z-scan curves were recorded at different fluences in the ns regime. The symmetrical traces indicate that no other processes such as scattering or damage occur. We measured the transmittance of PbCl₂ samples as a function of the sample position z measured with respect to the focal plane. Using a single Gaussian laser beam, we measured the transmittance of the samples at two different input fluences (100 and 125 MW/cm²) as shown in figure 3. From figure 3 it is clear that the nonlinear absorption coefficient is positive due to the transmission minimum at the focal point. For our samples, there is no depletion of ground state population because the transmission curves exhibit RSA.

The wavelength used in our experiment is 532 nm, which corresponds to two photon absorption (TPA). The photon energy is within the range $2h\nu > E_g > h\nu$, where $h\nu = 2.33\text{eV}$ and E_g is the optical band gap of PbCl₂ varying from 4.4 eV to 4.6 eV as shown in Table 1. Lead chloride solutions suppress the peak and enhances valley to show RSA in the transmittance curve. Nonlinear absorption coefficient β for two input fluence values are given in table.1

The obtained nonlinearity is found to be of third order, as it fits to a TPA process. In general, induced absorption can occur due to a variety of processes [24]. The theory of TPA fitted well with the experimental curve infers that TPA is the basic mechanism. For 532 nm excitation, we can approximate the nonlinear absorption to an effective



process and evaluate the nonlinear absorption coefficients [25-26].

Table 1 show that high nonlinearity is obtained for 100 MW/cm² and small value for 125 MW/cm². Thus when the incident intensity exceeds the saturation intensity, the nonlinear absorption coefficient of the medium decreases [27]. From these values of β , it is clear that as the input laser intensity I_0 increases, the nonlinear behavior of lead chloride decreases, which is due to the removal of an appreciable fraction of photo carriers from the ground state. Here the TPA technique which is comparatively simpler than the single photon process is more indicative of bulk material characteristics.

Materials that exhibit RSA are currently of interest for use in optical limiting devices for protection of sensors and eyes from energetic light pulses. The maximum criteria identified for a material to act as an effective optical limiter are low limiting threshold, large dynamic range, and longer excited state life time to accumulate the population, high optical damage threshold, broadband response, fast response time and high linear transmittance [28].

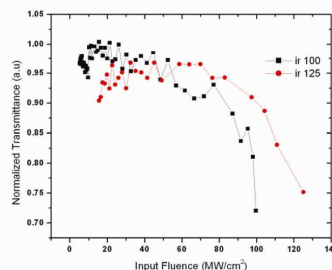


Figure 4. optical limiting response of PbCl₂

In lead chloride samples optical limiting is due to TPA. PbCl₂ is a good optical limiter that transmits light at low input intensity while become opaque at high input fluences. PbCl₂ should have high transmittance for weak incident light and instantaneous response over a broad spectral range [29].

Figure 4 shows the optical limiting response of PbCl₂. The limiting threshold is an important factor which decides the efficiency of optical limiter. It is obvious that lower the optical limiting threshold, better the optical limiting material. The optical limiting property occurs mainly due to absorptive nonlinearity which corresponds to the imaginary part of the third order susceptibility [30]. The optical limiting threshold values at two different laser intensities are shown in table.1. From the table, it is observed that there is a small limiting threshold for low input fluence and limiting threshold increases with increase in I_0 values. From the values of fluence at the focus, the fluence values at other positions could be calculated using the standard equations for Gaussian beam waist [25].

Conclusion

Highly luminescent Lead Chloride crystals were prepared and characterized. Spectrophotometric studies were carried out to evaluate the band gap. Optical nonlinearity in five different PbCl₂ samples were investigated using z-scan technique. Observed nonlinearity is third order and two photon absorption coefficients were tabulated with different types of PbCl₂ samples in solution phase. The nonlinear curves exhibit valleys to show reverse saturable absorption indicating positive nonlinear absorption. RSA nature of the samples makes them suitable for optical limiting applications and the optical limiting threshold of these samples was evaluated. The nonlinear studies on these crystal solutions gave a clear picture that these materials are highly nonlinear due to their high values of nonlinear absorption coefficients. Thus these PbCl₂ crystals prepared by sol-gel technique are

well suited for applications in optoelectronic and non-linear optical devices.

Acknowledgement

I.Rejeena thanks UGC for financial support through Moulana Azad National Fellowship. KSCSTE is also acknowledged for financial assistance

References

- [1] Nisha Santha Kumari.P and Kalainathan .S 2008 *Cryst.Res.Technol.* **43** 4
- [2] Fujita. M, Itoh.M, Bokumoto. Y, Nagakawa. H, Alov.D.L, Kitaura .M 2000 *Phys. Rev. B.* **61** 23
- [3] Alov D. L and Rybchenko S.I 1995 *J.Phys.:Condens.Matter* **7**, 1475
- [4] Zamkov A.V, Kokov. I.T,and Anistratov. A.T 1983 *Phys.Status Solidi A* **79** K177
- [5] Ren.Q, Ding.L, Chen.F, Cheng. R and Xu .D 1997 *J.Mater.Sci.Lett.* **16**,1247
- [6] Plekhanov.V 1973 *Phys.StatusSolidi B* **57** K55
- [7] Nistor.S.V, Goovaerts.E and Schoemaker.D 1993 *Phys.Rev.B* **48** 9575
- [8] Kitaura M, Nakagawa.H 1996 *J.Electron Spectrosc.Relat.Phenom.* **79** 171
- [9] Kitaura.M and Nakagawa.H 1997 *J.Lumin.* **72-74** 883
- [10] Itoh.M, Nakagawa.H, Kitaura. M, Fujita.M and Alov.D.L 1999 *J.Phys.:Condens.Matter* **11** 3003
- [11] Kink.R, Avarmaa.T, Kisand.V. Lohmus.A, Kink.I and Martinson.I 1998 *J.Phys.:Condens.Matter* **10** 693
- [12] Kanbe.J, Takezoe.H,and Onaka.R 1976 *J.Phys.Soc.Jpn.* **41** 942
- [13] Eijkelenkamp A.J.H.and V A.J os.K J.. 1976 *Phys.Status Solidi B* **76** 769
- [14] Beaumont.J.J.H.,Bourdillon .A.J and Bordas.J 1977 *J.Phys.C* **10** 761
- [15] Fujita.M, Nakagawa.H, Fukui.K, Matsumoto.H, Miyanaga.T and Watanabe.M 1991 *J.Phys.Soc.Jpn.* **60** 4393
- [16] Sobolev.V.V, Kalugin.A.I, Smirnov.S.V 2002 *Phys. Solid state* **44** 870
- [17] Kalugin.A.I and Sobolev.V.V 2005 *Phys. Rev. B* **71** 115112
- [18] Timoshkin.A.N, Sobolev.V.Val and Sobolev.V.V 2000 *Phys. Solid state* **42** 37
- [19] Melo.F.E.A, Garret.K.W, Mendis Filho and Moreira.J.E 1979 *Solid state commn.* **31** 29-33
- [20] Kaldor.A and Somorjai.G.A 1966 *J. Phys. Chem.* **70** 11
- [21] Bahae. M.S, Said.A.A, and Van Stryland. E.W 1989 *Opt. Lett.* **14**, 955
- [22] Irimpan.L, Krishnan.B, Deepthy.A, Nampoore.V.P.N and Radhakrishnan.P 2008 *J.Appl. Phys.* **103** 033105
- [23] Irimpan.L, Nampoore.V.P.N and Radhakrishnan.P 2008 *J. Appl. Phys.* **103** 094914
- [24] Santhi.A, Namboodiri.V.V, Radhakrishnan.P and Nampoore.V.P.N 2006 *J. Appl. Phys.* **100** 053
- [25] Litty Irimpan, Nampoore.V.P.N and Radhakrishnan.P 2008 *Chem. Phys. Lett.* **455** 265-269
- [26] Tintu.R.,Nampoore.V.P.N, Radhakrishnan.P and Sheenu Thomas 2010 *J. Appl. Phys.* **108** 073525
- [27] Tintu.R.,Nampoore.V.P.N, Radhakrishnan.P and Sheenu Thomas 2011 *J.Phys.D.Appl.Phys.* **44** 025101
- [28] Premkiran.P, Naga Srinivas.N.K.N, Reghunath Reddy.D and Bhasker G. Maiya 2002 *Opt.Commn.* **202** 347- 352
- [29] Aneeshkumar.B, Gopinath.P, Vallabhan.C.P.G, Nampoore.V.P.N, Radhakrishnan.P and Thomas J 2003 *J. Opt. Soc. America.B* **20** 1486
- [30] Quereshi.F.M, Martin.S.J, Long. X, Bradley.D.O.C, Heneri.F.Z,Balu.W.J, Smith.E.C, Wang.C.H, Kar . A.K and H.C.Anderson 1998 *Chem. Phys.* **237** 87